Tuning and Engineering of ZnO and Cu_xO for Sensor, Solar Cells and Memory Devices

Ahmad Sabirin Zoolfakar

(Doctor of Philosophy)

2013

RMIT

Tuning and Engineering of ZnO and Cu_xO for Sensor, Solar Cells and Memory Devices

A thesis submitted in fulfilment of the requirements for the degree of Doctor of Philosophy

Ahmad Sabirin Zoolfakar

BEng(Electrical) & MSc(Microelectronic Systems and Telecommunications)

School of Electrical and Computer Engineering

RMIT University

December 2013

Declaration

I certify that except where due acknowledgement has been made, the work is that of the author alone; the work has not been submitted previously, in whole or in part, to qualify for any other academic award; the content of this thesis is the result of work which has been carried out since the official commencement date of the approved research program; any editorial work, paid or unpaid, carried out by a third party is acknowledged.

…….

Ahmad Sabirin Zoolfakar

Date:

Acknowledgements

There have been many people whose help has ensured the completion of this dissertation. First and foremost, I would like to express my heartfelt appreciation to my senior supervisor Professor Kourosh Kalantar-zadeh, for his guidance and support throughout the duration of my PhD candidature. His persistent assistance on my experiments and research manuscripts were of great help. Certainly his passion towards research, technical writing skills and persuasion has been inspirational and of great value for my future as a researcher. I would like to thank him for his creative ideas and providing me the opportunity to learn, without which this work would have not been possible. I would also like to extend my gratitude to my secondary supervisors Dr. Anthony O'Mullane and Dr. Vipul Bansal whose supervisory inputs and contributions have been valuable in realizing the goals of this research.

In the course of my PhD candidature, I got the opportunity to collaborate with several researchers from interdisciplinary fields, in particular Dr. Serge Zhuiykov and Mr. Eugene Kats from the Commonwealth Scientific Industrial Research Organisation (CSIRO), Dr. Anthony Morfa from Freie Universität Berlin, Dr. Xinjun Liu from Australian National University, Prof. Suresh Bhargava, Dr. Sharath Sriram, Dr. Madhu Bhaskaran and Dr. Kay Latham from RMIT University. I would like to thank these collaborators for providing their expertise and facilities for the progression of my research.

I also wish to extend my appreciation to the current and former researchers and students within the School of Electrical and Computer Engineering and the School of Applied Sciences: Dr. Jian Zhen Ou, Dr. Haidong Zheng, Dr. Amin Kayani, Dr. Rajesh Ramanathan, Dr. Sumeet Walia, Dr. Sivacarendran Balendhran, Dr.

Muhammad Zamharir Ahmad, Dr. Adam Chrimes, Mr. David Yao, Mrs. Rozina Abdul Rani, Mrs. Rosmalini Ab Kadir, Mr. Majid Nour, Mr. Kyle Berean, Ms. Physhar Yi, Mrs. Yusnira Husaini, Mrs. Norhazlin Khairudin, Mrs. Robiatun Adayiah Awang, Mrs. Syazilawati Mohamed, Mr. Muhammad Farid Abdul Khalid, Mr. Wei Zhang, Mr. Yichao Wang, Ms. Manal Alsaif and Ms. Emily Nguyen for their support and for providing an excellent research atmosphere.

The state-of-the-art equipment and facilities provided by RMIT University, has played a major part in achieving my research goals. As such, I would like to thank the people and technical staff who work hard to keep these facilities operational. Specifically, Mr. Yuxun Cao, Mr. Paul Jones and Chiping Wu of the Microelectronics and Materials Technology Centre, RMIT University and Mr. Philip Francis, Mr Peter Rummel and Dr. Matthew Field from the RMIT Microscopy and Microanalysis facility for their technical expertise and assistance throughout the duration of my candidature.

My research work would not have been possible without the financial support by the Ministry of Science, Technology and Innovation of Malaysia and Universiti Teknologi MARA. I would also like to acknowledge the additional financial support and conference funding from the School of Electrical and Computer Engineering and School of Graduate Research.

Finally, special thanks to my gorgeous wife Mrs. Rozina Abdul Rani, my beautiful daughter Ms. Nurqaisara Nasreen and my understanding father & parent-in-law Mr. Zoolfakar Ismail, Mr Abdul Rani Dahalan and Mrs Asmah Yusop as well as my family for their endless encouragement, prayers and support in the time of need.

Dedication

To Ina, Sara, Ayah and Emak, for their love and support.

Abstract

In this thesis, the PhD candidate pursued the development of model sensors, solar cells and memory devices based on transition metal oxides, which are tuned and engineered in order to obtain enhanced properties. The author made informed choices regarding the incorporation of zinc oxide (ZnO) and copper oxides (Cu_xO) (cuprous oxide (Cu_2O) and cupric oxide (CuO)) as the model transition metal oxides. ZnO and Cu_xO are well investigated metal oxides, and a broad range of information regarding their fundamental properties, synthesis methods and applications is available. Their complimentary electronic nature is also required for the proposed studies in this dissertation: ZnO and Cu_xO are intrinsically *n*- and *p*-type semiconductors, respectively.

This PhD research focuses on the engineering and tuning the morphology, crystallinity and stoichiometry of transition metal oxides in order to investigate and devise scenarios that result in the highest efficiencies for the abovementioned model devices. The author of this thesis thoroughly reviewed the physical and chemical properties, as well as methods of synthesis of Cu_xO and ZnO. Additionally, he also studied factors that have been previously employed for enhancing the targeted materials functionalities. This includes tuning the synthesis' parameters such as changes in temperature and pressure, the incorporation of seed layers or templates, nanostructuring and introducing foreign atoms or molecules *via* doping or intercalation as well as applying electric, mechanical, optical and/or electromagnetic fields.

In order to realize the aforementioned goals and create new knowledge, the author implemented his research work in three distinct models:

The first model involved enhancing the performance of semiconducting transition metal oxide vapour sensors by using the nano morphologies of such materials. At the time when this PhD research commenced, the majority of work in the field of metal oxide vapour sensors had been devoted to *n*-type semiconductors, whilst the number of reports on the sensing properties of *p*-type metal oxide semiconductors, such as nanostructured Cu_xO, was significantly lower. As a result, the PhD candidate studied ethanol (C_2H_5OH) vapour sensing devices based on *p*-type nanostructured CuO and Cu_2O thin films, using RF sputtering at relatively low temperature and power conditions. As the aim of this PhD thesis, the author demonstrated control over stoichiometry and grain sizes of the films by altering the sputtering parameters. Single stoichiometry CuO and Cu_2O films were deposited using sputtering power of 200 and 250 W, respectively. CuO films exhibited smaller nanocrystallite base dimensions (~30 nm), in comparison to Cu_2O films (~85 nm), which significantly enhanced surface-to-volume ratio. Consequently, the PhD candidate demonstrated that CuO had a relatively high sensing response of 2.2 at an optimum operating temperature of 180 $^{\circ}$C for 12.5 ppm concentration of ethanol in ambient air.

In the second model, the author expanded his research work on ZnO-Cu_2O heterojunction solar cells. After a comprehensive literature review, the PhD candidate identified several key issues that caused the deterioration of the ZnO-Cu_2O heterojunction based solar cells' performance. Despite their theoretical power conversion efficiency (PCE) of 18 %, in practice ZnO-Cu_2O solar systems had never reached expected high efficiencies. The PhD candidate introduced seed layers for engineering the heterointerface quality of the electrodeposited ZnO for forming ZnO-Cu_2O solar cells. These ZnO seed layers were employed to control the growth,

crystallinity and to augment the surface area of the electrodeposited ZnO films thereby tuning the quality of the ZnO-Cu_2O heterointerface. The PhD candidate was able to obtain a current density of 12.7 mA cm^{-2} which is the highest ever reported.

In the third and final model, the author of this thesis demonstrated his work on the development of ZnO memristive switching devices. Prior to work conducted by the PhD candidate, electrodeposition had not been investigated for ZnO based memristive switching systems. Considering this, the PhD candidate demonstrated the effect of ZnO seed layers on the electrodeposited ZnO films towards their memristive switching performances. By incorporating RF sputtered ZnO seed layers he was able to tune the composition and the grain boundary densities of the deposited films. Consequently, ZnO memristive devices incorporating seed layers demonstrated high switching ratios as well as stable and reliable memristive switching behaviours under continuous cycling conditions.

In summary, the author strongly believes that this PhD thesis provides the readers with an in-depth knowledge of the capabilities that tuning and engineering transition metal oxides provide in enhancing the performance of such materials for specific applications. The author also believes that this study has contributed significantly to the advancement of the field of transition metal oxides as well as creating exciting new knowledge.

List of symbols

E_g	band gap
α	absorption coefficient
E	photon energy
ε	dielectric function
$R(E)$	normal−incident reflectivity
$I–V$	current-voltage
C_p	heat capacity
High−T_C	high transition temperature
C_2H_5OH	ethanol
T	temperature
μ	carrier mobility
Zn_i	Zn interstitials
V_o	oxygen vacancies
V_{OC}	open circuit voltage
J_{sc}	short circuit current density
FF	fill factor
$V_O^{\bullet}$	oxygen vacancies with single positive charge
$V_O^{\bullet\bullet}$	oxygen vacancies with double positive charges
O_O^x	neutral oxygen ion in the lattice
$V_{Zn}^{''}$	zinc vacancy with a double negative charge

List of abbreviations

AFM	atomic force microscopy
ALD	atomic layer deposition
Cu_xO	copper oxides
c−AFM	conductive atomic force microscopy
CVD	chemical vapor deposition
DC	direct current
DFT	density functional theory
DSSC	dye-sensitized solar cells
EBE	electron beam evaporation
FET	field effect transistor
FTO	fluorine doped tin oxide
GGA	generalized gradient approximation
HOMO	highest occupied molecular orbital
HER	hydrogen evolution reaction
HIL	hole injection layers
IDT	interdigitated transducers
IR	infra−red
LDA	local density approximation
LED	light emitting diode
LIB	lithium ion battery
MBE	molecular beam epitaxy
NTE	negative thermal expansion
OLED	organic light emitting diodes
PCE	power conversion efficiency

PL	photo luminescence
PLD	pulsed laser deposition
RF	radio frequency
ROS	reactive oxygen species
SEM	scanning electron microscopy
TEM	transmission electron microscopy
UV	ultra violet
XRD	x-ray diffraction
XPS	x-ray photoemission spectroscopy

List of figures

Table of contents

Chapter 1

Introduction

1.1 Motivation

Transition metal oxides are functional materials that offer a large number of applications in various areas, owing to their diverse properties including their versatile electronic band structure, optical, electrical, magnetic, mechanical and thermal specifications. However, these properties should be adjusted to enhance functionalities of such transition metal oxides for each specific application. Engineering and tuning transition metal oxides syntheses' parameters such as changes in the temperature and pressure, the incorporation of seeds or templates, nanostructuring and introducing foreign atoms or molecules *via* doping or intercalation as well as applying electric, mechanical, optical and/or magnetic fields, provide pathways for the enhancement in their functionalities.[1]

The interest in engineering and tuning procedures has been fuelled by the recent advances in advanced synthesis processes, which now allow better control over the electronic structure, crystallinity, morphology, and stoichiometry of the transition metal oxides.[2-7] Such abilities have led to newer opportunities in disciplines as diverse as physics, chemistry, biology, medicine and engineering.[4-7]

In this PhD research, the PhD candidate made an informed decision to use "nanostructuring" as the core method for tuning and engineering transition metal oxides which he uses for the development of model sensors, solar cells and memory devices with enhanced properties. Nanostructured transition metal oxides can potentially offer remarkable mechanical, electrical, magnetic, thermal and optical

properties, in comparison to their bulk counterparts, endowed by confining the dimensions to nano size ranges.[5, 8]

As the foci of this PhD thesis, exceptional qualities of nanostructured metal oxides that can be engineered using various tuning processes will be implemented for developing advanced sensing, energy conversion and memory devices using engineering processes that result in:

(i) increased surface-to-volume ratio, which provides more surface area for both chemical and physical interactions;

(ii) altered stoichiometry as well as engineered crystallite boundaries and morphologies in a way that suits the specific application,

(iii) desired surface energies for adjusting the targeted physiochemical reactions on the boundaries and properties of interfaces, and

(iv) quantum confinement effects, due to the inherently small size of nanostructured materials, that significantly influences charge transport, electronic band structures, phonon transport and optical properties.

In the next section, the main objectives of this PhD research and the justifications regarding the methods to be used in the process are presented.

1.2 Objectives

In this research, the PhD candidate first focuses on developing high performance gas sensors, then $p-n$ heterojunction based solar cells and finally memristors. The PhD candidate chooses transition metal oxides as the core materials for these devices, and as suggested in the Motivation section, concentrates on engineering and tuning morphologies, crystallinity and stoichiometry of these transition metal oxides in order to investigate and devise scenarios that result in the highest efficiencies.

In order to realize the objectives of this PhD research, the author made informed choices regarding the incorporation of zinc oxide (ZnO) and copper oxides (Cu_xO) as the model transition metal oxides. ZnO and Cu_xO are intrinsically *n*− and *p*−type transition metal oxides, respectively and as a result, exhibit complementary properties. Additionally both ZnO and Cu_xO are well investigated metal oxides, and consequently, a broad range of information regarding their fundamental properties, synthesis methods and applications is available.

In the past two decades, tremendous efforts have been placed for enhancing the performance of semiconducting transition metal oxides gas sensors by using the nano morphologies of such materials.[9-16] Nanostructured transition metal oxides are favorable as sensitive elements for gas sensing due to their increased surface-to-volume ratio, structural dimensions comparable to their Debye length, and their tunable surface energies. These nanostructures are used with the aim of obtaining improved gas sensitivity, stability and rapid responses.[7, 13, 17, 18]

To date, the majority of works in the field of metal oxide gas and vapour sensors have been devoted to *n*-type semiconductors such as ZnO, SnO_2, In_2O_3, WO_3, V_2O_5 and TiO_2 [19, 20], whilst the number of reports on the sensing properties of *p*-type metal oxide semiconductors, such as nanostructured Cu_xO, are significantly lower. [7, 17, 21] This may be due to the higher carrier mobilities of *n*-type metal oxides (e.g. SnO_2 ~160 $cm^2 V^{-1} s$ and ZnO ~200 $cm^2 V^{-1} s$) in comparison to *p*-type metal oxides (e.g. Cu_2O ~10 $cm^2 V^{-1} s$).[22] However, *p*-type metal oxides, including Cu_xO which is the focus of this PhD research, still have great merits for gas sensing applications. Cu_xO is a remarkable catalytic material that can operate at relatively low temperatures in comparison to many *n*-type metal oxides. Additionally, the Cu_xO low bandgaps (less than 2 eV) help in designing and implementing visible−light

optoelectronically−tunable semiconducting sensors. On the contrary, the large bandgap of many *n*-type semiconducting metal oxides can only be tuned in the UV range, which is not practical for many safe sensing applications. Therefore, it is imperative to further develop efficient nanostructured *p*-type gas sensors based on a clear understanding from the experimental explorations. One of the objectives of this PhD project is to address the current problems of *p*-type gas sensors and increase their sensing performance *via* nanostructuring processes. The Cu_xO nanostructured films, which are selected as the model *p*-type metal oxide material by the PhD candidate, are formed by RF sputtering. The sputtering parameters are altered to tune the parameters which affect the stoichiometry and morphology of the obtained films. As the parameter of choice, the PhD candidate altered the sputtering power, as this factor has the strongest effect on both stoichiometry and morphology of the films. The details will be presented in this thesis.

The development of low cost, efficient and reliable solar cells is an important goal for managing the growing global energy demands, and reducing greenhouse gas emissions.[23] Transition metal oxide semiconductors are ideal for thin film based solar cells, as many of them are thermally- and photo-stable, earth-abundant, have tuneable electronic properties, can be structurally adjusted, and offer excellent characteristics for forming a wide range of heterojunction based devices.[24, 25]

The PhD candidate chose to use *n*-type ZnO/*p*-type Cu_2O heterojunction as the model for investigating the effect of engineering and nanostructuring of metal oxide thin films on the solar cell efficiency. The knowledge obtained regarding Cu_xO in the first part of this PhD research is used in this section. As previously mentioned, in this PhD research, ZnO will be used as the model *n*-type material for establishing these

heterojunctions, as a wide range of information is available regarding its properties and synthesis methods.

Thin film photovoltaic devices made of ZnO-Cu_2O heterojunctions have attracted increasing interest due to their theoretical power conversion efficiency (PCE) of 18% and an absorption coefficient higher than single crystalline Si.[26, 27] Despite such advantages, in practice the ZnO-Cu_2O solar systems have never exceeded desirable solar conversion efficiencies.[28-30] In this PhD investigation, the PhD candidate will focus on finding methods based on engineering and tuning the ZnO nanostructures and the Cu_2O-ZnO heterojunction interfaces for increasing the efficiency.

Increasing the crystallinity of the thin films and at the same time the roughness of the heterojunction are two of the key factors to enhance the efficiency of ZnO-Cu_2O heterojunction solar cells. However, obtaining rough surfaces that increase the surface-to-volume ratio, hence increasing the heterointerface and solar cell current density, has been a challenge.

In this research, the PhD candidate uses electrodeposition for forming tuneable ZnO layers for developing ZnO-Cu_2O heterojunction solar cells. The PhD candidate made an informed choice about using electrodeposition as it is one of the more versatile methods for forming ZnO thin films that allows the highest possibility of change in the parameters of thin films. Many conventional electrodeposition methods of ZnO produce highly crystalline films which is the parameter that is highly sought after in heterojuntion solar cells but often result in low surface roughness.[30, 31] The electrodeposited ZnO crystallites generally follow the topography of the substrates and well−engineered tuning methods are required to modify their morphologies into nanocrystallites with low dimensions.[32-34] Knowing that RF

sputtered seed layers are result in small crystallites, the PhD candidate will use seed layer to tune the electrodeposited films in process, which will be detailed in this PhD thesis.

In the last part of this PhD research, the PhD candidate focuses on developing memristors using metal oxides. Transition metal oxides have attracted significant attention as the core in metal/semiconductor/metal structures for memory devices because of their electronics and electrical structural simplicity, low power consumption, fast switching, high density integration and process compatibility with CMOS technologies.[35-39] Memristive switching involves a “switch” from a high resistance state (HRS, or “OFF” state) to a low resistance state (LRS, or “ON” state) and *vice versa*. Generally, such a switching mechanism can be classified according to the dominant contribution to this effect including thermal, electronic or ionic effect during the ON/OFF process.[40, 41]

Based on the knowledge achieved regarding the tuning of ZnO thin films in the previous sections, in the continuation of this PhD research, the candidate draws his attention to the development of memristors using ZnO. ZnO-based memristors can be prepared using several techniques such as pulsed laser deposition [42], sputtering [39, 43-46], electrodeposition [47], metal organic chemical vapour deposition [48] and spin coating [49]. However, among these methods, electrodeposition has several advantages such as control over crystallinity, stoichiometry, nanostructure morphologies and doping concentration, which are all favourable for this PhD research. So far there has been no report on ZnO thin film based memristive switching devices formed using an electrodeposition approach. As such, the final objective of this PhD project is to demonstrate that electrodeposition can be applied as a highly tuneable deposition process for fabricating ZnO based

memristive switching devices and investigate their operation, which will be comprehensively presented in this PhD thesis.

1.3 Thesis organisation

This dissertation presents details of the work that is carried out and outcomes that are produced by the PhD candidate regarding tuning and engineering of ZnO and Cu_xO into desired nano−architectures that provide remarkable enhancement for developing advanced sensing, energy conversion and memory devices. Based on the motivation and objectives highlighted by the author, this thesis consists of six chapters, which are presented as follows:

In Chapter 2, the author will provide the literature review. The chapter will discuss the fundamental properties, variety of synthesis techniques and applications associated with nanostructured Cu_xO and ZnO. Particular emphasis is placed on the enhancements that can be achieved by exploiting the effects of nanostructured forms of Cu_xO and ZnO.

In Chapter 3, the author will cover his work on synthesizing and characterising the RF sputtered Cu_xO films and the investigations on their ethanol vapour sensing performance. The author will demonstrate the tenability that can be achieved by changing the parameters of a RF sputtering system to alter the stoichiometry of Cu_xO with the aim of producing nanostructures with well-engineered morphological sizes.

In Chapter 4, the author will deliver his research work on ZnO-Cu_2O heterojunction solar cells. The author will introduce sputtered ZnO seed layers followed by the

sequential electrodeposition of ZnO and Cu_2O films. The seed layer is employed to control the growth and crystallinity and to augment the surface area of the electrodeposited ZnO films, thereby tuning the quality of the ZnO-Cu_2O heterointerface. The author will present the outcomes of thorough characterization the synthesized material and demonstrate their effect towards photovoltaic performance.

In Chapter 5, the author of this thesis will present his work conducted on the development of ZnO memristive switching which is fabricated using an electrodeposition approach. The author employs seed layer to tune the morphology of the electrodeposited ZnO films in order to adjust the grain boundary density as well as their stoichiometry. The author will also provide detailed insights into the enhancement of the memristive switching performance contribute by the seed layers.

Finally, in Chapter 6, the author will present the concluding remarks and the future outlook of the research work relevant to this thesis.

References

[1] J. Wu, J. Cao, W.-Q. Han, A. Janotti, and H.-C. Kim, *Functional Metal Oxide Nanostructures.* New York: Springer 2012.

[2] H. Gleiter, J. Weissmuller, O. Wollersheim, and R. Wurschum, "Nanocrystalline Materials: A Way to Solids With Tunable Electronic Structures And Properties?," *Acta Mater.*, vol. 49, pp. 737-745, 2001.

[3] J. Z. Ou, R. A. Rani, M.-H. Ham, M. R. Field, Y. Zhang, H. Zheng, *et al.*, "Elevated Temperature Anodized Nb_2O_5: A Photoanode Material with Exceptionally Large Photoconversion Efficiencies," *ACS NANO*, vol. 6, pp. 4045-4053, 2012.

[4] S. Balendhran, J. Deng, J. Z. Ou, S. Walia, J. Scott, J. Tang, *et al.*, "Enhanced Charge Carrier Mobility in Two-Dimensional High Dielectric Molybdenum Oxide," *Adv. Mater.*, vol. 25, pp. 109-114, 2013.

[5] H. D. Zheng, J. Z. Ou, M. S. Strano, R. B. Kaner, A. Mitchell, and K. Kalantar-Zadeh, "Nanostructured Tungsten Oxide - Properties, Synthesis, and Applications," *Adv. Funct. Mater.*, vol. 21, pp. 2175-2196, 2011.

[6] G. I. N. Waterhouse, A. K. Wahab, M. Al-Oufi, V. Jovic, D. H. Anjum, D. Sun-Waterhouse, *et al.*, "Hydrogen Production by Tuning The Photonic Band Gap with the Electronic Band Gap of TiO_2," *Scientific Reports*, vol. 3, pp. 2849-2849, 2013.

[7] D. P. Volanti, A. A. Felix, M. O. Orlandi, G. Whitfield, D.-J. Yang, E. Longo, *et al.*, "The Role of Hierarchical Morphologies in the Superior Gas Sensing Performance of CuO-Based Chemiresistors," *Adv. Funct. Mater.*, vol. 23, pp. 1759-1766, 2013.

[8] A. S. Arico, P. Bruce, B. Scrosati, J. M. Tarascon, and W. Van Schalkwijk, "Nanostructured Materials for Advanced Energy Conversion and Storage Devices," *Nat. Mater.*, vol. 4, pp. 366-377, 2005.

[9] C. Wang, L. Yin, L. Zhang, D. Xiang, and R. Gao, "Metal oxide gas sensors: Sensitivity and influencing factors," *Sensors*, vol. 10, pp. 2088-2106, 2010.

[10] G. Eranna, B. C. Joshi, D. P. Runthala, and R. P. Gupta, "Oxide materials for development of integrated gas sensors - A comprehensive review," *Crit. Rev. Solid State*, vol. 29, pp. 111-188, 2004.

[11] N. Barsan, D. Koziej, and U. Weimar, "Metal oxide-based gas sensor research: How to?," *Sensor Actuat. B-Chem.*, vol. 121, pp. 18-35, 2007.

[12] N. Barsan and U. Weimar, "Conduction model of metal oxide gas sensors," *J. Electroceram.*, vol. 7, pp. 143-167, 2001.

[13] E. Comini, "Metal oxide nano-crystals for gas sensing," *Anal. Chim. Acta*, vol. 568, pp. 28-40, 2006.

[14] M. H. Yaacob, M. Breedon, K. Kalantar-zadeh, and W. Wlodarski, "Absorption spectral response of nanotextured WO_3 thin films with Pt catalyst towards H_2," *Sensor Actuat. B-Chem.*, vol. 137, pp. 115-120, 2009.

[15] M. Shafiei, J. Yu, R. Arsat, K. Kalantar-zadeh, E. Comini, M. Ferroni, *et al.*, "Reversed bias Pt/nanostructured ZnO schottky diode with enhanced electric field for hydrogen sensing," *Sensor Actuat. B-Chem.*, vol. 146, pp. 507-512, 2010.

[16] A. Z. Sadek, V. Bansal, D. G. McCulloch, P. G. Spizzirri, K. Latham, D. W. M. Lau, *et al.*, "Facile, size-controlled deposition of highly dispersed gold nanoparticles on nitrogen carbon nanotubes for hydrogen sensing," *Sensor Actuat. B-Chem.*, vol. 160, pp. 1034-1042, 2011.

[17] D. Barreca, E. Comini, A. Gasparotto, C. Maccato, C. Sada, G. Sberveglieri, *et al.*, "Chemical vapor deposition of copper oxide films and entangled quasi-1D nanoarchitectures as innovative gas sensors," *Sensor Actuat. B-Chem.*, vol. 141, pp. 270-275, 2009.

[18] E. Comini, G. Faglia, G. Sberveglieri, Z. W. Pan, and Z. L. Wang, "Stable and highly sensitive gas sensors based on semiconducting oxide nanobelts," *Appl. Phys. Lett.*, vol. 81, pp. 1869-1871, 2002.

[19] A. Tricoli, M. Righettoni, and A. Teleki, "Semiconductor Gas Sensors: Dry Synthesis And Application," *Angew. Chem. Int. Edit.*, vol. 49, pp. 7632-7659, 2010.

[20] A. Tricoli, M. Graf, and S. E. Pratsinis, "Optimal doping for enhanced SnO_2 sensitivity and thermal stability," *Adv. Funct. Mater.*, vol. 18, pp. 1969-1976, 2008.

[21] X. Gou, G. Wang, J. Yang, J. Park, and D. Wexler, "Chemical Synthesis, Characterisation and Gas Sensing Performance of Copper Oxide Nanoribbons," *J. Mater. Chem.*, vol. 18, pp. 965-969, 2008.

[22] X.-W. Liu, F.-Y. Wang, F. Zhen, and J.-R. Huang, "In situ growth of Au nanoparticles on the surfaces of Cu_2O nanocubes for chemical sensors with enhanced performance," *RSC Advances*, vol. 2, pp. 7647-7651, 2012.

[23] V. Fthenakis, J. E. Mason, and K. Zweibel, "The technical, geographical, and economic feasibility for solar energy to supply the energy needs of the US," *Energ. Policy*, vol. 37, pp. 387-399, 2009.

[24] K. L. Chopra, P. D. Paulson, and V. Dutta, "Thin-film solar cells: An overview," *Prog. Photovoltaics*, vol. 12, pp. 69-92, 2004.

[25] J. Jasieniak, B. I. MacDonald, S. E. Watkins, and P. Mulvaney, "Solution-Processed Sintered Nanocrystal Solar Cells via Layer-by-Layer Assembly," *Nano Lett.*, vol. 11, pp. 2856-2864, 2011.

[26] B. M. Fariza, J. Sasano, T. Shinagawa, H. Nakano, S. Watase, and M. Izaki, "Electrochemical Growth of (0001)-n-ZnO Film on (111)-p-Cu_2O Film and the Characterization of the Heterojunction Diode," *J. Electrochem. Soc.*, vol. 158, pp. 621-625, 2011.

[27] S. M. Sze and K. K. Ng, *Physics of Semiconductor Devices*. New Jersey: John Wiley and Sons, 2007.

[28] K. P. Musselman, A. Marin, A. Wisnet, C. Scheu, J. L. MacManus-Driscoll, and L. Schmidt-Mende, "A Novel Buffering Technique for Aqueous Processing of Zinc Oxide Nanostructures and Interfaces, and Corresponding Improvement of Electrodeposited ZnO-Cu_2O Photovoltaics," *Adv. Funct. Mater.*, vol. 21, pp. 573-582, 2011.

[29] K. P. Musselman, A. Wisnet, D. C. Iza, H. C. Hesse, C. Scheu, J. L. MacManus-Driscoll, *et al.*, "Strong Efficiency Improvements in Ultra-low-Cost Inorganic Nanowire Solar Cells," *Adv. Mater.*, vol. 22, pp. E254-E285, 2010.

[30] H. Wei, H. Gong, Y. Wang, X. Hu, L. Chen, H. Xu, *et al.*, "Three Kinds of Cu_2O/ZnO Heterostructure Solar Cells Fabricated With Electrochemical Deposition And Their Structure-Related Photovoltaic Properties," *Crystengcomm*, vol. 13, pp. 6065-6070, 2011.

[31] J. B. Cui and U. J. Gibson, "A Simple Two-Step Electrodeposition of Cu_2O/ZnO Nanopillar Solar Cells," *J. Phys. Chem. B*, vol. 114, pp. 6408-6412, 2010.

[32] V. Donderis, M. A. Hernández-Fenollosa, L. C. Damonte, B. Marí, and J. Cembrero, "Enhancement of surface morphology and optical properties of nanocolumnar ZnO films," *Superlattice. Micros.*, vol. 42, pp. 461-467, 2007.

[33] X. J. Huang, O. Yarimaga, J. H. Kim, and Y. K. Choi, "Substrate surface roughness-dependent 3-D complex nanoarchitectures of gold particles from directed electrodeposition," *J. Mater. Chem.*, vol. 19, pp. 478-483, 2009.

[34] A. I. Inamdar, S. H. Mujawar, S. B. Sadale, A. C. Sonavane, M. B. Shelar, P. S. Shinde, *et al.*, "Electrodeposited zinc oxide thin films: Nucleation and growth mechanism," *Sol. Energ. Mater. Sol. C.*, vol. 91, pp. 864-870, 2007.

[35] J. J. Yang, M. D. Pickett, X. Li, D. A. A. Ohlberg, D. R. Stewart, and R. S. Williams, "Memristive switching mechanism for metal/oxide/metal nanodevices," *Nat. Nanotechnol.*, vol. 3, pp. 429-433, 2008.

[36] K. Szot, W. Speier, G. Bihlmayer, and R. Waser, "Switching the electrical resistance of individual dislocations in single-crystalline SrTiO3," *Nat. Mater.*, vol. 5, pp. 312-320, 2006.
[37] Y. Watanabe, "Review of resistance switching of ferroelectrics and oxides in quest for unconventional electronic mechanisms," *Ferroelectrics*, vol. 349, pp. 190-209, 2007.
[38] R. Waser, R. Dittmann, G. Staikov, and K. Szot, "Redox-Based Resistive Switching Memories - Nanoionic Mechanisms, Prospects, and Challenges," *Adv. Mater.*, vol. 21, pp. 2632-2663, 2009.
[39] N. Xu, L. F. Liu, X. Sun, C. Chen, Y. Wang, D. D. Han, *et al.*, "Bipolar Switching Behavior in TiN/ZnO/Pt Resistive Nonvolatile Memory With Fast Switching And Long Retention," *Semicon. Sci. Tech.*, vol. 23, p. 075019, 2008.
[40] R. Waser and M. Aono, "Nanoionics-based resistive switching memories," *Nat. Mater.*, vol. 6, pp. 833-840, 2007.
[41] L. Chua, "Resistance switching memories are memristors," *Appl. Phys. A-Mater.*, vol. 102, pp. 765-783, 2011.
[42] L. M. Kukreja, A. K. Das, and P. Misra, "Studies on Nonvolatile Resistance Memory Switching in ZnO Thin Films," *B. Mater. Sci.*, vol. 32, pp. 247-252, 2009.
[43] Y. C. Yang, F. Pan, Q. Liu, M. Liu, and F. Zeng, "Fully Room-Temperature-Fabricated Nonvolatile Resistive Memory for Ultrafast and High-Density Memory Application," *Nano Lett.*, vol. 9, pp. 1636-1643, 2009.
[44] W.-Y. Chang, Y.-C. Lai, T.-B. Wu, S.-F. Wang, F. Chen, and M.-J. Tsai, "Unipolar resistive switching characteristics of ZnO thin films for nonvolatile memory applications," *Appl. Phys. Lett.*, vol. 92, p. 022110, 2008.
[45] Z. Ji, Q. Mao, and W. Ke, "Effects of oxygen partial pressure on resistive switching characteristics of ZnO thin films by DC reactive magnetron sputtering," *Solid State Commun.*, vol. 150, pp. 1919-1922, 2010.
[46] S. Lee, H. Kim, D.-J. Yun, S.-W. Rhee, and K. Yong, "Resistive switching characteristics of ZnO thin film grown on stainless steel for flexible nonvolatile memory devices," *Appl. Phys. Lett.*, vol. 95, p. 262113, 2009.
[47] P. Liu, G. She, W. Shi, and D. Chen, "Electric-pulse-induced resistance switching observed in ZnO nanotube point contact system," *Physica E*, vol. 42, pp. 791-794, 2010.
[48] J. W. Seo, J.-W. Park, K. S. Lim, J.-H. Yang, and S. J. Kang, "Transparent resistive random access memory and its characteristics for nonvolatile resistive switching," *Appl. Phys. Lett.*, vol. 93, p. 223505, 2008.
[49] S. Kim, H. Moon, D. Gupta, S. Yoo, and Y.-K. Choi, "Resistive, Switching Characteristics of Sol-Gel Zinc Oxide Films for Flexible Memory Applications," *IEEE T. Electron Dev.*, vol. 56, pp. 696-699, 2009.

Chapter 2

Literature Review

2.1 Introduction

In the previous Chapter, the author highlighted the importance of tuning and engineering transition metal oxides for the development of systems which will be presented in this PhD thesis including sensors, solar cells and memory devices with enhanced properties. In order to realize the “motivation” and “objectives” of this PhD research, the author chose to conduct a thorough literature review on the properties of Cu_xO and ZnO in order to make informed choices and to gain necessary knowledge prior the development of the model systems.

In this Chapter, the author will present a general, yet complete, review of nanostructured Cu_xO. He will discuss the fundamental chemical and physical properties of nanostructured Cu_xO and summarize the different methods of synthesis that have been reported. Finally the author will present a selection of interesting applications that exploit Cu_xO and illustrate the enhancements made possible by using the nanostructured form of Cu_xO.

This Chapter also includes some of the fundamental properties of nanostructured ZnO. The presentation is much more concise than that of the Cu_xO section. The reason is that plenty of great reviews are available on different aspects of nanostructured ZnO. As such, the author only focuses on nanostructured ZnO in the context which is relevant to this PhD thesis. He will discuss the fundamental properties including crystal structure, electronic band structure and optical characteristics as well as electrical behaviour of ZnO. In addition, the author presents

a discussion on electrodeposition of ZnO and the usage of nanostructured ZnO with foci on ZnO/Cu_xO heterostructures and memristors applications.

A comprehensive review covering the nanostructured Cu_xO properties, synthesis methods and applications does not exist in literature. As such, a major portion of this chapter was organized as a review paper was submitted to the *Journal of Materials Chemistry C.*

2.2 Fundamental Properties of Cu_xO

In this section, the fundamental properties such as crystal structures, electronic band structures, optical and electrical as well as transport properties of nanostructured Cu_xO are discussed. This section also describes the effect of doping or the presence of impurities on the properties of nanostructured Cu_xO.

2.2.1 Crystal Structure

CuO which has a black colour belongs to the monoclinic crystal system, with a crystallographic space group for the unit cell of C2/c. The crystallographic properties of CuO are tabulated in Table 2.1.[1-4] The copper atom is coordinated to four coplanar oxygen atoms situated at the corners of a rectangular parallelogram, which form chains by sharing edges. The oxygen atom is coordinated to four copper atoms situated at the corners of a distorted tetrahedron. The chains traverse the structure in the [110] and [$\bar{1}$10] directions. The two types of chains alternate in the [001] direction and each type is stacked in the [010] direction with a separation between the chains of about 2.7 Å.[1, 2, 5]. Figure 2.1a demonstrates the crystal structure of CuO.

Cu_2O is the second stable phase of copper-oxide compounds which is reddish in colour. Cu_2O belongs to the cubic structure (space group, O_h^4 or $Pn\bar{3}m$) with a lattice constant of 4.2696 Å. Each Cu atom in the unit cell is coordinated by two oxygen atoms.[5] The crystallographic properties of CuO are tabulated in table 2.1. [1-4] Figure 2.1b demonstrates the crystal structure of Cu_2O.

The third stable phase of copper-oxide with an atomic ratio of 1.33 is Cu_4O_3.[6] Cu_4O_3 is an intermediate between Cu_2O and CuO due to its similar crystal structure.[7] This less studied compound of the Cu_xO family was first discovered in 1870 as a mineral in the Copper Queen mine (Arizona, US). [4] Cu_4O_3 belongs to the tetragonal structure (space group, $I4_1/amd$) with a lattice constant of a = 5.837 Å and c = 9.932 Å. [7] Figure 2.1c demonstrates the crystal structure of Cu_4O_3. From the crystal structure, one can observe that there are two types of copper ion which are Cu^+ and Cu^{2+}. The Cu^+ has two oxygen atoms nearest neighbours forming collinear bonds of length 1.87 Å which is similar to cuprite (Cu_2O ~ 1.85 Å). Similarly, the Cu^{2+} is surrounded by four oxygen atoms with bond lengths and angles being very close to those observed in tenorite (CuO).[1, 5, 7] The crystallographic properties of Cu_4O_3 are tabulated in table 2.1.[4, 7, 8]

Table 2.1 Crystallographic properties of CuO, Cu_2O and Cu_4O_3 [1-4, 7, 8]

	CuO	**Cu_2O**	**Cu_4O_3**
Lattice parameters	Monoclinic a = 4.6837 Å b = 3.4226 Å c = 5.1288 Å β = 99.54° α = γ = 90°	Cubic a = 4.2696 Å	Tetragonal a = 5.837 Å b = 9.932 Å
Shortest distance			
bond length Cu — O	1.95 Å	1.84 Å	1.87 Å
separation O — O	2.62 Å	3.68 Å	2.56 Å
separation Cu — Cu	2.90 Å	3.01 Å	2.92 Å
Formula weight	79.57	143.14	302.18
Density	6.52 gcm^{-3}	5.75 gcm^{-3}	5.93 gcm^{-3}
Melting point	1201 ºC	1235 ºC	400 ºC
Cell volume	81.08 $Å^3$	77.833 × 10^{-24} cm^{-3}	338 $Å^3$

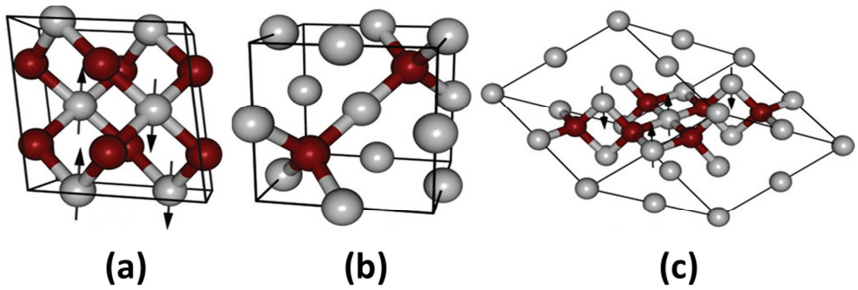

Figure 2.1 Monoclinic, cubic and tetragonal crystal structure of the copper oxide compounds (a) CuO, (b) Cu_2O and (c) Cu_4O_3 (gray and red spheres represent copper and oxygen atoms, respectively). For the antiferromagnetic CuO and Cu_4O_3 the arrows on the copper ions indicate the orientation of local magnetic moments. Reprinted with permission from ref 5. Copyright (2013) by the American Physical Society.

2.2.2 Electronic Band Structure

The reported band gap (E_g) values for CuO, which is a *p*-type semiconductor, are generally in the range of 1.2 to 2.16 eV.[9-13] This wide range is attributed to two factors: interpretation of the nature of the gap (i.e. direct or indirect) and annealing treatment.[11, 14-16] According to the Tauc relationship, for photon energies (E) greater than the band gap energy, the light absorption can be approximated using:[17]

$$\alpha E = \alpha_o \left(E - E_g\right)^{\eta} \qquad (2.1)$$

where α is the absorption coefficient, α_o is a constant, E_g is the band gap energy and η is an exponent that depends on the type of transition involved. The value of η is $\frac{1}{2}$ or 2 for direct or indirect transitions, respectively. Rakhshani *et al*. have reported detailed studies of band gap determination of RF sputtered CuO films.[9] They found that their CuO films exhibited an indirect transition with a band gap of 1.21 eV. In contrast, Pierson *et al.* while reporting the same deposition technique (RF sputtering), determined their CuO films exhibited a direct band gap with a value of 1.71 eV.[18] The different values of E_g were due to different models $(\alpha E)^2$ or $(\alpha E)^{\frac{1}{2}}$ being used to determine the band gap value. The other significant factor that contributes to the variation of band gap values of CuO films is related to the heat treatment of the films.[15, 16] Izaki *et al.* demonstrated that annealing electrodeposited CuO films altered the E_g value.[15] They reported a reduction of 7.5% in E_g after annealing the as-deposited CuO at 773 K. They suggested that the changes in the composition and lattice constant were induced by the annealing process, altering the CuO band gap. [15]

Cu_2O is also a *p*-type semiconductor material due to the presence of copper vacancies.[4, 19] It is a direct band gap material with E_g > 2.1 eV, however the band gap can be tuned *via* engineering the grains dimensions.[10, 14, 16, 20, 21] In nanostructured Cu_2O films, the band gap generally increases upon reducing the grain size. [20, 21] This observation is widely attributed to the quantum confinement effect in smaller grains, causing a blue shift in the band gap.[22-24] The effect occurs when nanograins are reduced to a size that is smaller than the Bohr radius.[23, 24] In a recent study conducted by Poulopoulos *et al.*,[24] on Cu_2O thin films with thicknesses ranging from 0.75 to 5.4 nm the E_g value increased significantly from ~ 2.6 eV (5.4 nm film thickness) to ~ 3.8 eV (0.75 nm film thickness) due to quantum confinement effects. In addition, Balamurugan *et al* [21] and Chang Y *et al*.[20] also reported on the observation of quantum confinement effects in Cu_2O. They further studied the effect of temperature [21] and annealing duration [20] on manipulating the crystallite sizes and hence altering the band gap of Cu_2O.

Similar to CuO, the optical band gap of Cu_4O_3 has also been reported with a wide range of values from 1.34 to 2.47 eV which can also be attributed to the interpretation of the type of band gap and whether direct or indirect transitions are allowed. [6, 18, 25, 26]

A good comparison between the electronic properties of the three types of Cu_xO is presented via the band structure density functional theory (DFT) calculations by Heinemann *et al.* (Figure 2.2i).[5] Figure 2.2ii illustrates the Brillouin zones with special high symmetry *k* points of the three copper oxide compounds, which were used for the band structures DFT calculations.[5]

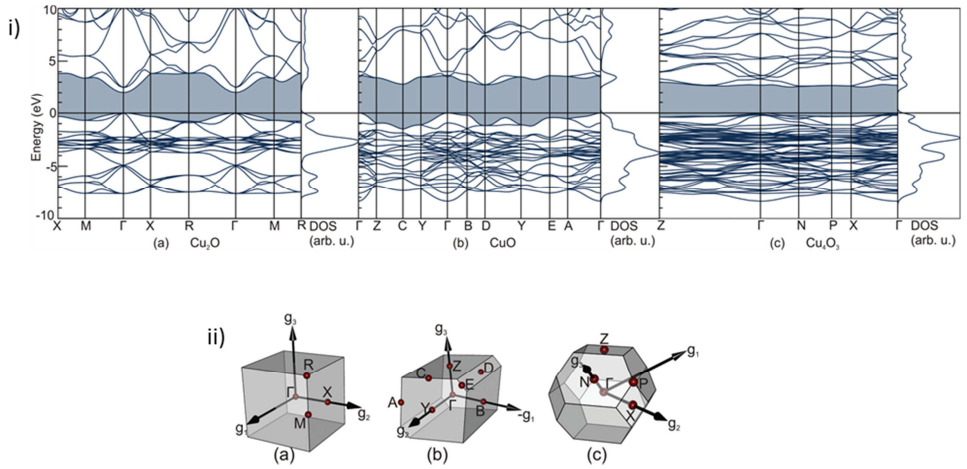

Figure 2.2 (i) Electronic band structure and density of states from hybrid functional DFT calculations and (ii) Brillouin zones with special high symmetry *k* points of the three copper oxide compounds to: (a) Cu_2O, (b) CuO and (c) Cu_4O_3. Reprinted with permission from ref 5. Copyright (2013) by the American Physical Society.

2.2.3 Optical Properties

The optical behaviours of Cu_xO films have been experimentally studied, in particular the complex dielectric function ($\varepsilon(E)=\varepsilon_1(E)+i\varepsilon_2(E)$) was determined *via* spectroscopic ellipsometry.[4, 27, 28] For comparison, the imaginary part (ε_2) of the dielectric function for CuO, Cu_2O and Cu_4O_3 are shown in Figure 2.3a,b with Gaussians fitting marked with numbers 1 to 7. For Cu_2O the peaks originate from the various band gaps corresponding to 2.59 eV (1), 2.71 eV (2),…and 5.24 eV (7).[4] The difference in energy between these two first peaks is attributed to the spin–orbit–splitting energy of ~0.12 eV for Cu_2O.[27] The absence of any sharp peaks for the CuO (ε_2) spectrum is due to low symmetry of this crystal. Similarly no sharp peak is seen for Cu_4O_3 for energies of less than 3.7 eV.

There are many reports regarding the absorption coefficient $\alpha(E)$ and normal–incidence reflectivity $R(E)$ of Cu_xO films in optical ranges.[4, 27-29] A detailed analysis of the absorption coefficient obtained on bulk and thin film Cu_2O can be found in the report by Marleba *et al*.[29]

Mayer *et al.* have reported that CuO is nonluminescent.[4] This is despite a few reports demonstrating the photoluminescence of CuO films, however the purity of such films is questionable (the presence of Cu_2O is a possibility). On the other hand, Cu_2O shows a weak photoluminescence effect due to the fact that optical transitions require parity change, which does not exist between the energetically highest valence band and lowest conduction band of the Cu_2O direct transition band.[4]

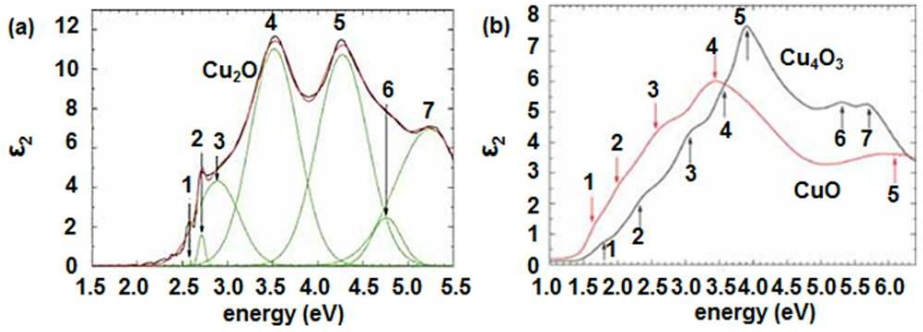

Figure 2.3 Gaussian fit to the imaginary part of the dielectric ε_2 for (a) Cu_2O, (b) CuO and Cu_4O_3. Reprinted with permission from ref 4. Copyright (2012) by WILEY-VCH Verlag GmbH & Co. KGaA, Weinheim.

2.2.4 Vibrational Properties

The lattice dynamics of Cu_xO materials have been studied using infrared (IR), Raman and photoluminescence spectroscopy.[30-34] These studies provided insight into the nature of the electron phonon interaction and the negative thermal expansion (NTE) in Cu_xO. These methods also provided information about spin–phonon interaction and size dependent electron phonon scattering.[34] Debbichi *et al.* reported an extensive study of vibrational properties of Cu_xO *via* Raman spectroscopy where they clearly distinguished the different types of vibrational modes either by Raman and IR spectroscopy.[34] The IR spectroscopy modes are associated with the relative motion of both copper and oxygen atoms which consist of asymmetric Cu–O stretching and asymmetric O–Cu–O bending modes. In contrast, Raman active modes only involve the relative motion of oxygen atoms.[35] Figure 2.4 shows Raman spectra of Cu_xO with calculated frequencies of Raman active vibrational modes.[34] The symmetries of the zone–center modes are given by the following representations:[4, 34]

$$\Gamma_{Cu_2O} = A_{2u} + E_u + 3T_{1u} + T_{2u} + T_{2g} \quad (2.2)$$

$$\Gamma_{CuO} = A_g + 2B_g + 4A_u + 5B_u \quad (2.3)$$

$$\Gamma_{Cu_4O_3} = 3E_g + A_{1g} + 2B_{1g} + 9E_u + 6A_{2u} + 5B_{2u} + 2B_{1u} + 2A_{1u} \quad (2.4)$$

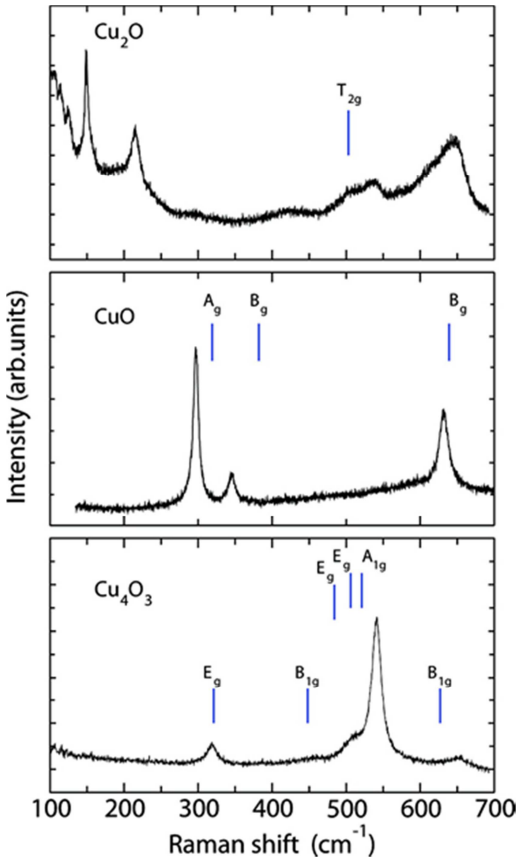

Figure 2.4 Experimental Raman spectra of Cu_2O, CuO and Cu_4O_3. The calculated frequencies of Raman active vibrational modes are indicated by vertical bars. Reprinted with permission from ref 34. Copyright (2012) by American Chemical Society.

2.2.5 Electrical Properties

The electrical conductivity and hole density of *p*-type Cu_2O films vary with copper vacancy density, which act as shallow acceptors.[4] Similarly in CuO, copper deficiencies account for the intrinsic *p*-type semiconducting behaviour.[36] Suda *et al.* and Young *et al.* have studied the effect of temperature on electrical conductivity of CuO and Cu_2O films, respectively (Figure 2.5 a,b).[37, 38] They have shown that an increase in temperature increases the conductivity of CuO and Cu_2O due to an increase in hole concentration.[37] It is possible to tune the electrical properties

(resistivity, carrier concentration and mobility) of Cu_xO by changing the stoichiometry and crystallinity of the Cu_xO films during the deposition process. Deposition parameters, such as pH of the solution in electrodeposition and hydrothermal methods and ion pressure and concentration in RF sputtering techniques, significantly contribute to changes in stoichiometry and crystallinity.[39-41]

2.2.6 Thermal Properties

A limited number of studies have been carried out on the thermal properties of pristine copper oxides films. However, great interest has been shown for the development of nanoparticles of Cu_xO suspensions in fluids (nanofluids) due to the significant enhancement of thermal conductivity that they grant to the fluid in which they are suspended.[42-45] The relatively high thermal conductivity of the CuO (76.5 W mK^{-1})[44], makes it an excellent candidate for enhancing the efficiency and reliability of refrigeration and air conditioning systems.[46, 47] In contrast, Cu_2O has a rather low thermal conductivity of the order of 4.5 W mK^{-1}.[48, 49] It has been shown that the thermal conductivity enhancement of both CuO and Cu_2O nanofluids correspond to an increased particle volume fraction and temperature.[50-53]

The variations in the Seebeck coefficient (*S*) of CuO and Cu_2O as a function of temperature are shown in Figure 2.5a,c for which both oxides show decreasing trends. It has been shown that at 500 K, CuO and Cu_2O exhibit a maximum value of 200 μV K^{-1} and 1050 μV K^{-1}, respectively.[37, 38]

The presence of a wide gap in the phonon spectra between low frequency (due to acoustic and optical phonon modes that involve the motion of Cu atoms) and high

frequency (due to the optical modes of oxygen vibrations) bands are reflected in the temperature dependence of heat capacity.[54] The calculated and experimental heat capacities (C_p) of CuO and Cu_2O as a function of temperature are shown in Figure 2.5d,e.[54-59] As seen from the Figure, the shape of C_p *vs* temperature curves for both CuO (for temperatures below 800 K) and Cu_2O (for temperatures below 500 K) are accurately accounted for by the calculations that employ the quasi–harmonic approximation.[54]

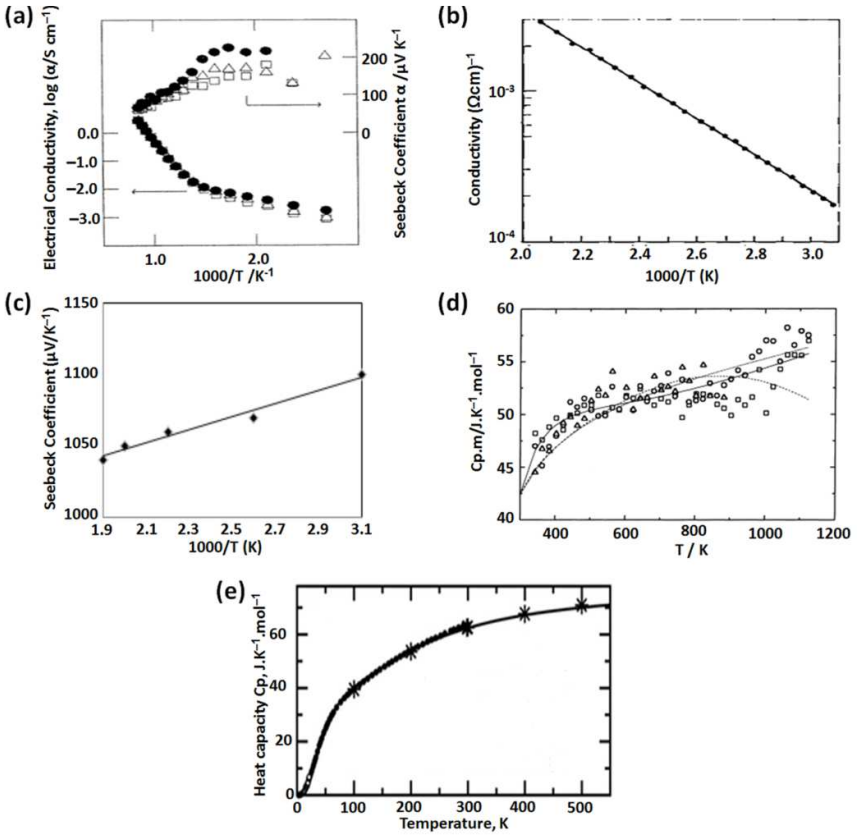

Figure 2.5 (a) Temperature dependence for electrical conductivity and Seebeck coefficient of CuO in oxygen (●), in air (Δ) and in 3% O_2–Ar (□), (b) Electrical conductivity of Cu_2O single crystal *vs* 1/*T*, (c) Seebeck coefficient of Cu_2O single crystal *vs* 1/*T*, calculated and experimental heat capacities, C_p of (d) CuO: (□ Δ ○) ref 55, (· · ·) ref 56, (---) ref 57, and (e) Cu_2O: (—) ref 54, (○) ref 58 (●) ref 59. Reprinted with permission from (a) ref 38 copyright (1992) by The Japan Society of Applied Physics, (b and c) ref 37 copyright (1969) by Elsevier, (d) ref 55 copyright (2000) by Elsevier, (e) ref 54 copyright (2012) National Academy of Science, USA.

2.2.7 Magnetic Properties and Superconductivity

The copper–oxygen covalent bond is the prominent factor governing the properties of high transition temperature (High–T_c) superconducting Cu_xO compounds.[60] Both CuO and Cu_4O_3 have an antiferromagnetic ground state. For CuO the antiferromagnetic unit cell has twice the size of the primitive unit cell of the crystal.[5] In the case of Cu_4O_3, it was suggested that the antiferromagnetic unit cell doubles the crystallographic unit cell in all three special directions.[5, 61-63] The CuO antiferromagnetic transition takes place in two stages: near 230 K it leads to incommensurate antiferromagnetic order and near 210 K by a first order transition to a commensurate antiferromagnetic order.[60] As mentioned in section 2.1, the copper atom of CuO is surrounded by four coplanar oxygen atoms, resulting in two sets of one dimensional Cu–O chains. The magnetic interaction due to super exchange leads to antiferromagnetic order in the Cu–O–Cu chains along the $[10\bar{1}]$ direction with a bond angle of 146°.[60]

A neutron diffraction study revealed that Cu_4O_3 undergoes a magnetic phase transition below 42.3 K leading to a pyrochlore lattice.[61, 62] The amplitude of the magnetic moment carried by Cu^{2+} is $\sim 0.46\,\mu_\beta$ which indicates the strong covalent character of the Cu–O bonds and the presence of strong fluctuations even at low temperatures.[61]

Compounds made of Cu and O are the base of a famous class of high–T_c superconductors.[60] Superconductivity in these materials is observed when they are strongly doped away from their ideal stoichiometry. It has been shown that spatial changes in carrier density and superconducting gap produce local inhomogeneity, which strongly affects their superconductivity.[64]

High–T_c was first discovered by Bednorz and Müller in 1986 using Cu and O compounds such as La_2CuO_4 doped with Ba.[65] A few months later it was found that doping the same material with Sr raised the superconducting critical temperature to nearly 40 K.[65] Recently, the performance of high−T_c copper and oxygen based materials were further enhanced with the inclusion of extra oxygen atoms as mobile "holes" into the copper oxide planes as illustrated in the $Bi_2Sr_2CaCu_2O_{8+x}$ and $YBa_2Cu_3O_{6+x}$ systems.[64, 66] Apart from providing charge carriers, the role of oxygen dopants is still debatable and being investigated.[64, 66-68]

2.2.8 Doping

It is possible to modify the chemical and physical properties of Cu_xO through doping. It has been shown that doping has the capability to alter the conduction type of Cu_2O (from *p* to *n*). Based on the valence of Cu and O, which are +1 and –2 in Cu_2O, some *n*-type dopants including group VII elements such as halogens (O sites) (and possibly group II elements (Cu sites)) allow this transition to occur.[69] The typical reported halogen dopants include flourine (F), chlorine (Cl) and bromine (Br) which can be intercalated into the structure of Cu_2O during the synthesis process.[69-72] Theoretically, F is the best match for O given the similarity in size; however, CuF is soluble in water.[69] Recently, Scanlon *et al.* have demonstrated that intrinsic *n*-type defects or defects complexes in Cu_2O created during an electrodeposition process cannot be the source of any *n*-type behaviour.[41] They have suggested that the *n*-type conduction is due to an inversion layer which was attributed to a shallow donor level being formed during the electrodeposition process or due to external impurities (dopants).[41]

Generally, the hole density of native *p*–type Cu_xO films are poor, uncontrollable and sensitive to the preparation methods and experimental conditions. It has been reported that nitrogen (N) and silicon (Si) doped Cu_2O *via* a RF sputtering process can significantly reduce such instabilities.[73-76] These dopants were found to act as acceptors, which are incorporated into the oxygen lattice without converting the conduction type of Cu_2O.[75, 76] To further stabilize the films Ishizuka *et al.* and Okamoto *et al.* investigated the effect of passivation using hydrogen (H) and crown–ether cyanide of the N doped Cu_2O films.[73, 77] The improvement after the treatment indicates that hole traps are passivated by the cyanide or protons. These holes traps are generally due to oxygen vacancies or dangling bonds of Cu.[73]

For solar cells applications, the intrinsic photoconductivity of Cu_2O can be limited by minority charge carrier recombination caused by native defects acting as trap states. Isseroff *et al*. used first principles DFT calculations to study these trap states and demonstrated that substitutional cation doping reduces the recombination effect.[19] They found that split vacancies are the source of trap states that inhibit the minority carrier diffusion in Cu_2O. Dopants such as lithium (Li), magnesium (Mg), manganese (Mn), and zinc (Zn) prevent the formation of the split vacancies for a single cation vacancy which resulted in an electronic structure that exhibited no trap states within the band gap.[19]

2.3 Nanostructured Cu_xO Synthesis Methods

Many different approaches for the synthesis of nanostructured Cu_xO have been implemented using both vapour and liquid-phase-based methods. In this section, the author presents the most common synthesis methods and describe how they can be employed for engineering and tuning the morphologies and properties of Cu_xO.

2.3.1 Vapour phase Synthesis

Vapour phase synthesis methods can be divided into two different categories: (i) physical vapour deposition (PVD) and (ii) chemical vapour deposition (CVD). The main difference between them is the process they employ, in which PVD uses physical forces to deposit films, while CVD uses chemical processes. Many of the common PVD synthesis techniques such as RF sputtering, direct current (DC) sputtering, thermal evaporation, thermal oxidation, molecular beam epitaxy (MBE), pulse vapour deposition (PLD) and electron beam epitaxy (EBE) have been used for the deposition of nanostructured Cu_xO. A PVD process is purely physical, starting with either Cu_xO or Cu as the source material in the form of a solid target or powder, which is evaporated or sputtered with the application of ion bombardment, thermal heating, electron beam impingement or laser irradiation.

2.3.1.1 Sputtering

Amongst the PVD techniques, sputtering has, thus far been the most common technique to synthesize Cu_xO, due to the ease of control over the deposition parameters. Sputtering is a process in which atoms are ejected from a solid target material by bombarding it with energetic particles. It offers a high degree of control

over a film's crystallinity and stoichiometry. The crystallinity and stoichiometry of the copper oxides films can be controlled by varying the sputtering parameters such as applied power, oxygen flow rate and concentration as well as annealing temperature.[18, 78-80]

Generally in an oxygen rich sputtering chamber, at relatively low sputtering powers, only a small number of Cu atoms are sputtered, which effectively react with oxygen in the plasma, resulting in the deposition of films with high oxygen content such as CuO films. Conversely, Cu_2O films are formed at high sputtering powers, due to a large number of sputtered Cu atoms.[78] However, relatively high sputtering powers can also adversely affect the stoichiometry of the films, resulting in presence of unreacted metallic copper and undesirable stoichiometric ratios between copper and oxygen.[78]

Although Cu_4O_3 was discovered during the late 1870s, the synthesis of single phase Cu_4O_3 thin films has rarely been reported. Pierson *et al.* and Richthofen *et al.* have successfully demonstrated the synthesis of single CuO, Cu_2O and Cu_4O_3 phases by varying the oxygen flow rate using a reactive magnetron sputtering technique.[18, 80] They used a Cu target with the RF power maintained at 600 W. It was suggested that conductive Cu−rich copper oxide (Cu_4O_3) thin films tended to form with an oxygen flow rate $R(O_2) < 30\%$, whereas insulator O−rich copper oxide (CuO) thin films tended to form at $R(O_2) \geq 30\%$.[81] This is in contrast to the work of Blobaum *et al.* whom also successfully synthesized Cu_4O_3 films *via* the sputtering, but with a CuO target and at a lower sputtering power of 200 W.[79]

The PhD candidate chose RF sputtering for the fabrication of the vapor sensors in the course of this PhD research. This is due to the high flexibility that this

technique offers for the formation of highly crystalline and granular Cu_xO films with a great control over their stoichiometry.

2.3.1.2 Thermal Evaporation

Deposition of Cu_xO using thermal evaporation is achieved by vaporizing a source material of Cu or Cu_xO (in either powder or condensed form) using heat either in a vacuum or in a controlled gaseous environment at a low pressure.[11, 21, 82-85] The vaporized Cu or Cu_xO that emanates from the material source interacts with the gas molecules in the environment of the deposition chamber before condensing onto a substrate. Processing parameters such as evaporation temperature, substrate temperature, substrate type, gas environment and pressure all play important roles in achieving the desirable nanostructured Cu_xO thin films.[11, 84, 86, 87] Generally, the nanostructured morphology can be controlled by tuning the deposition parameters. For instance, the diameter and density of Cu_xO nanowires can be altered by changing the evaporation temperature.[86] However, very high evaporation temperatures (>900º C) are not suitable for nanowire formation as Cu_xO nanostructures can be fused together, as observed by Huang *et al.*[82]

2.3.1.3 Other PVD methods

Apart from the aforementioned vapour phase methods, PLD [88-92] and EBE [93-96] deposition techniques are the other alternatives available for synthesizing Cu_xO films. It has been reported that the as-synthesized Cu_xO from these methods are usually compact thin films, which are textured by nanocrystallites (10−800 nm). The dimensions of the crystallites are significantly affected by the oxygen pressure and

substrate temperature which were identified as being the two most important parameters.[89, 90]

2.3.1.4 CVD methods

CVD processes have become popular deposition techniques owing to their inherent flexibility and potential to tailor the Cu_xO phase composition by simply varying the operating conditions and precursors. Many forms of CVD have been used for depositing different Cu_xO stoichiometries, including atmospheric pressure CVD [97-99], aerosol assisted CVD [100-103] and plasma assisted CVD.[104]

Generally, precursors such as bis–(2,4–pentanedionato) copper (II) or $Cu(acac)_2$ (acac = acetylacetonate) are used due to their high sublimation rate (activation energy of 105.6 kJ mol^{-1}) and low sublimation temperature between 140 to 190 ºC.[97] Valtierra *et al.* have demonstrated the synthesis of Cu_4O_3 and CuO thin films on fiberglass substrates using $Cu(acac)_2$ as a precursor and oxygen as a carrier-reactant gas *via* atmospheric pressure CVD. [97] The deposition temperature of CuO and Cu_4O_3 were recorded at 315 ºC and 345 ºC, respectively. In addition, thin films of Cu_2O have also been synthesized on fiberglass substrates using a similar technique and precursors by Ortiz *et al.* at a deposition temperature of 320 ºC.[99]

However, precursors such as $Cu(acac)_2$, $Cu(dpm)_2$ (dpm = dipivaloylmethanate) and $Cu(hfa)_2$ (hfa = hexafluoroacetylacetonate) may present drawbacks in terms of poor thermal characteristics, reduced shelf life, halide incorporation or instability upon prolonged utilization due to aging phenomena.[105] Therefore, a second generation of adducts of the type $M(hfa)_2$• tetramethylethylenediamine(TMEDA) (M = Cu(I) or Cu(II)) have been successfully

adopted as alternative precursors.[105] They have favourable properties in terms of improved long–term stability and volatility with respect to conventional β–diketonate.[98, 105] Barreca *et al.* were the first group to successfully demonstrate the deposition of nanostructured CuO and Cu_2O using $Cu(hfa)_2$ adduct with TMEDA *via* CVD.[105]

Spray pyrolysis is a typical aerosol-assisted chemical vapour deposition, which is utilized in the glass industry and in solar cell production to deliver film coatings of various thicknesses.[23] This method has the benefit of forming large-scale thin films by using a simple apparatus that can lead to increase productivity. Moreover, the film thickness and stoichiometry are easy to control and the resulting films are generally dense.[101, 102] During film deposition, the precursor's solution is pumped to an atomizer, and then sprayed onto heated substrates. Subsequently the droplets undergo evaporation, solute condensation and thermal decomposition, which results in film formation.[23] The composition of these thin films is highly dependent on the solvent, morphology of the substrate as well as the deposition temperatures.[100, 106]

Cu_xO films generated by the spray pyrolysis method are generally produced from copper acetate or copper nitrate as precursors dissolved in alcohol based solutions such as ethanol, propanol or methanol.[100, 102, 106] Alcohols are used to increase the wettability of the sprayed solution on the substrate and to improve the homogeneity of the deposited films.[101] It has been reported that Cu_xO nanostructures form with the addition of glucose or sucrose to the solution.[101, 103] These sugars are used as reducing agents in the precipitation of the Cu_xO nanostructures.[101]

Apart from CuO and Cu_2O films, Cu_4O_3 films can also be obtained *via* spray pyrolysis techniques. Albores *et al.* have successfully demonstrated the deposition of Cu_4O_3 films on ZnO nanorods.[106] The formation of Cu_4O_3 films is a gradual process. Initially, the possible lattice matching of ZnO and CuO promotes the growth of CuO. In the presence of methanol, at elevated temperatures, the Cu^{2+} in CuO is reduced to Cu^{1+} forming Cu_2O as:[106]

$$CH_3OH_{(g)} + 6CuO \rightarrow 3Cu_2O + CO_{2(g)} + 2H_2O_{(g)} \quad (2.5)$$

Then at these elevated temperatures, the solid reaction between CuO and Cu_2O results in paramelaconite phase formation which can be described by:[106]

$$2CuO + Cu_2O \rightarrow Cu_4O_3 \quad (2.6)$$

2.3.2 Liquid phase Synthesis

Liquid phase techniques include methods such as electrodeposition, hydrothermal and sol–gel. These methods are generally chosen due to their low capital cost and better control of the material's morphology in comparison to vapour phase deposition techniques as well as the deposition at relatively low temperatures, which is crucial for low-heat-tolerant substrates.

2.3.2.1 Electrodeposition

Electrodeposition is a process in which metal ions in an electrolyte are reduced at a conducting electrode under potential control. The process uses electrical current to reduce Cu^{2+} ions from an aqueous solution. The electrolyte generally contains a

mixture of a Cu salt such as copper sulphate, copper acetate or copper nitrate and a chelating agent such as lactic acid, ammonium nitrate, amino acids or tartaric acids.[15, 107-110] The deposition is carried out in alkaline environment with the addition of sodium hydroxide or ammonia to control the pH level. The electrodeposition technique is commonly used for depositing CuO and Cu_2O films.[15, 107, 108, 110-114] The stoichiometry of the electrodeposited films is very much dependent on the type of the chelating agent and applied potential used during the electrodeposition process. Generally, CuO films are obtained upon the application of a positive voltage/current bias, where oxidation of Cu is expected and this process is well known as anodic electrodeposition. Inversely, Cu_2O films are deposited at a negative bias, in which the reduction process occurs (cathodic electrodeposition).[107, 115]

Synthesis of CuO films *via* anodic electrodeposition in an alkaline solution containing copper (II) nitrate, ammonium nitrate and ammonia has been reported by Izaki *et al.* at +0.9 V *vs* Ag/AgCl.[107] Sasano *et al.* demonstrated that CuO films formed by applying potential pulses are more crystalline than the ones deposited using a constant potential.[109] The mechanism for the electrodeposition of CuO films is outlined in equations (2.7)–(2.10). The reaction starts *via* electrolysis of water to generate oxygen and protons (reaction 2.7). Consequently, these protons react with ammonia Cu(II) complexes to yield free Cu(II) ions in the vicinity of a substrate's surface (reaction 2.8). The free Cu(II) ions are then hydrolyzed to form CuO films on the substrate (reactions 2.9 and 2.10).[107, 115]

$$2H_2O \rightarrow O_2 + 4H^+ 4e^- \qquad (2.7)$$

$$Cu(NH_3)_4^{2+} + 4H^+ \rightarrow Cu^{2+} + 4NH_4^+ \quad (2.8)$$

$$Cu^{2+} + 2OH^- \rightarrow Cu(OH)_2 \quad (2.9)$$

$$Cu(OH)_2 \rightarrow CuO + H_2O \quad (2.10)$$

Similarly, syntheses of Cu_2O films have been reported *via* cathodic electrodeposition using an alkaline aqueous solution containing copper (II) sulphate or copper (II) acetate and lactic acid as the chelating agent.[108, 112, 114, 116, 117] Izaki *et al.* have demonstrated the electrodeposition of Cu_2O films onto ZnO for forming heterojunction solar cells.[108] The electrodeposition process was carried out at –4.0 mA cm^{-2}. Cu_2O was formed according to the following electrochemical reaction.[108]

$$2Cu^{2+} + 2e^- + 2OH^- \rightarrow Cu_2O + H_2O \quad (2.11)$$

Due to the distinct advantages of electrodeposition in obtaining highly crystalline films with no defects using this method, the PhD candidate has chosen this technique in the formation of the ZnO-Cu_xO heterostructures which will be explained in the course of this dissertation.

2.3.2.2 Hydrothermal and Solvothermal

Hydrothermal and solvothermal processes are facile and cost-effective deposition techniques. They have the capability of producing Cu_xO of different morphologies including nanodendrites [118], nanowires [119], nanorings [120], nanorods [121-124], nanoribbons [120, 123], nanotubes [121], microspheres [123, 125] and macrowhiskers.[126] (Figure 2.6)

The synthesis of Cu_xO has been hydrothermally achieved using various precursors such as copper (II) chloride, copper (II) acetate or copper (II) sulphate.

Generally, a lower concentration of $Cu(OH)_4^{2-}$ precursors favours tubular formation, whereas a higher concentration leads to rodlike morphologies.[121, 123] In most cases, the hydrothermal synthesis of Cu_xO starts with the preparation of a solution that contains copper salts, sodium hydroxide and solvents, typically deionized water. Such a solution is then kept at an elevated temperature (100 – 300 ºC) for a certain period of time, allowing the nucleation and growth of Cu_xO crystallites.

Solvothermal methods are almost identical to hydrothermal methods except that organic solvents are used instead of water.[127, 128] In comparison with the hydrothermal method, the solvothermal method exhibits many advantages such as easier morphological control, free foreign anions and macroscopic quantity.[129, 130] Recent reports have shown that high-aspect-ratio of Cu_xO nanostructures can be synthesized *via* solvothermal methods.[131-134] Zhao *et al*. have demonstrated a facile method to synthesize pure polycrystalline Cu_4O_3 microspheres using copper (II) nitrate as the precursor in the presence of *N*,*N*−dimethylformamide and ethanol.[130] They have successfully manipulated the CuO/Cu_2O stoichiometry ratio to generate Cu_4O_3 films with the reaction of $(2CuO + Cu_2O \rightarrow Cu_4O_3)$ in a closed system. [130]

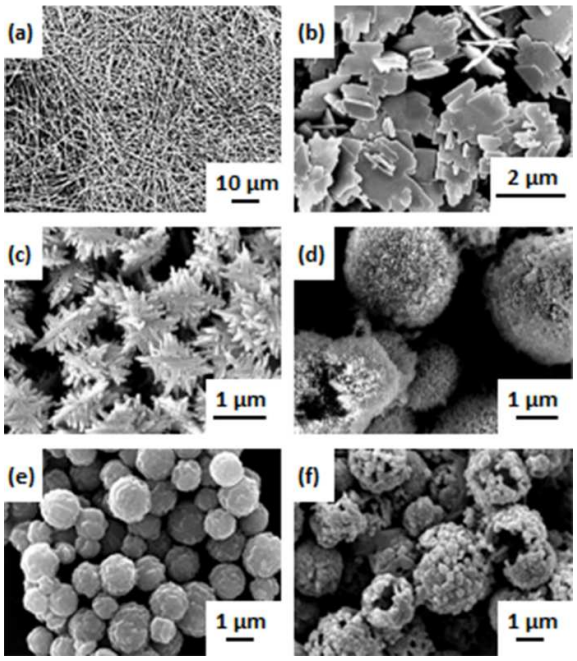

Figure 2.6 SEM images of various morphologies *via* hydrothermally/solvothermally synthesized of (a) Cu_2O nanowires synthesized at 180 °C in Copper (II) acetate aqueous solution with pyrrole, (b) CuO flake–like synthesized at 200 °C in Copper (II) sulphate aqueous, (c) CuO/Cu_2O dendrite–like synthesized at 200 °C in Copper (II) sulphate aqueous with 10 ml ethylene glycol (EG), (d) CuO/Cu_2O flower–like synthesized at 200 °C in Copper (II) sulphate aqueous with 20 ml EG, and CuO/Cu_2O composite hollow microspheres obtained in a Copper (II) acetate aqueous solution at 200 °C for (e) 1 hour and (f) 5 hours. Reprinted with permission from (a) ref 119 copyright (2007) American Chemical Society, (b,c,d) ref (118) copyright (2004) by IOP Publishing Ltd, (e,f) ref 125 copyright (2007) American Chemical Society.

2.3.2.3 Other film formation methods

Thermal oxidation techniques offer a simple, convenient and fast method to synthesize nanostructured Cu_xO with various morphologies including nanowires, nanoribbons and nanorods.[135-138] In this method nanostructured Cu_xO is directly grown on the surface of a Cu substrate.[137-139] Thermal oxidation is performed by

simply heating a Cu substrate to a high temperature (typically between 400 and 800 °C) in an oxygen rich environment.[135, 137, 138, 140]

A sol–gel process involves the formation of a colloidal solution (sol) from selected chemicals that acts as a precursor for an integrated network (gel) of either discrete particles or connected networks. During the gelation (aging process), various forms of hydrolysis and polycondensation processes can take place. Film deposition is generally carried out during the gelation process *via* dip-coating, spin coating or drop–casting onto the substrates. Armelao *et al.* have reported Cu_xO thin films *via* sol–gel synthesis, using ethanolic solutions of copper (II) acetate.[141] Films were obtained by dip–coating at room temperature in air and were subsequently heat−treated at different temperature (100–900 ºC) in oxidizing (air), inert (N_2) or reducing (4% H_2 in N_2) atmospheres to observe different crystalline phases of Cu_xO as a function of the annealing conditions.[141] Ray has also reported a similar technique, however he experimented with methanolic solutions of cupric chloride.[142] Under an atmospheric heat-treatment condition, Armelao *et al.* have only managed to observe the CuO phase with 900 ºC annealing, while Ray has successfully demonstrated the deposition of CuO and Cu_2O at 360 ºC and 400-500 ºC, respectively.[141, 142]

Templating is a modification of the sol−gel synthesis technique and can be very effective for the preparation of Cu_xO nanowires.[140] Nanostructured Cu_xO is deposited onto porous templates such as anodic alumina membranes and polycarbonate membranes.[143-145] Generally, templates are used for assisting the growth of the Cu_xO by controlling the diameters, lengths and densities of the nanowires.[143] At the end of the deposition process, the templates must be removed either by chemical reactions[145] or a selective burn-away at high

temperatures[146]. Consequently, this procedure may prolong the process as well as degrade the quality of the Cu_xO. [140]

2.4 Applications Cu_xO

Cu_xO has been employed for a variety of applications ranging from optical devices to high thermal conductivity systems. In this section, some of the most common applications of Cu_xO materials are presented. Particular emphasis is placed on the enhancements that can be achieved by exploiting the nanostructured forms of Cu_xO.

2.4.1 Solar Cells and Light Emitting Diodes

Cu_xO films are possible candidates for developing different types of optical devices, including solar cells based on dye-sensitized and heterojunction architectures as well as organic light emitting diodes.

The quest and need for a clean and economical energy source have increased interest in the development of solar applications. Amongst various metal oxide materials for solar energy applications, Cu_xO has attracted increasing interest due to its theoretical power conversion efficiency (PCE) of 18% and an absorption coefficient higher than single crystalline Si.[147]

As described previously Cu_xO is an intrinsically *p*-type material. However, self−compensation problems and dopant solubility have inhibited the synthesis of *n*−type Cu_xO to produce efficient homojunctions for photovoltaic applications.[113, 148, 149] Therefore, heterojunction architectures have been employed with other *n*−type semiconductors such as ZnO [108, 116], CdO [150], TiO_2 [151-153], Ga_2O_3 [154] and GaN. [4] Amongst the aforementioned *n*-type semiconductors, ZnO has been found to be the most stable and exhibit relatively low lattice mismatch of 7.6% between the (002) ZnO and (111) Cu_2O phase.[108, 110, 113] Despite the predicted

PCE value of 18%, in practice the ZnO−Cu_2O solar systems have yet to reach high efficiencies.[113, 116, 155] To date, the highest efficiency ever reported for bilayer ZnO-Cu_2O heterojunction solar cells has been 3.83%.[156] This is due to the fact that theoretically their intrinsic electronic band structures do not permit an open circuit voltages larger than 0.7 V.[155]

Apart from heterojunction cells, Cu_xO has also been widely used in dye−sensitized solar cell (DSSC) technology. CuO is commonly used as a blocking layer that prevents recombination reactions by forming a potential barrier between the anode and the electrolyte which enhances the PCE of the device.[157-160] Yet in other experiments, the use of Cu_2O at the photoanode of a DSSC was found to decrease the overall PCE.[161] This is due to dissociation of copper in liquid−based electrolytes, inducing numerous extrinsic defects that increases carrier recombination, resulting in photovoltaic performance degradation.[161]

Cu_xO has also been used in organic light emitting diodes (OLEDs).[87, 162] In order to construct efficient OLEDs, it is important to optimize the carrier injection ability at the interface of the active layer and anode materials. The Cu_xO films are commonly used as hole injection layers (HILs) to lower the hole injection barrier.[87, 163, 164] Kim *et al.* have reported the advantage of using a mixed stoichiometry of CuO and Cu_2O for increasing the performance of OLEDs.[87] Mixed stoichiometry of Cu_xO contains high density of defects such as oxygen vacancies or unbonded oxygen atoms, which act as an extra energy state within the energy gap of the Cu_xO layer. Interestingly, when the energy levels of these gap states are aligned with the highest occupied molecular orbital (HOMO) level of the hole transporting layer, no potential barrier is produced at the anode interfaces, which can lead to an increase in the hole injection efficiency.[87]

Based on the aforementioned suitable properties of Cu_xO for establishing heterojunction solar cells, the author of this PhD thesis made an informed decision to choose Cu_2O as the material for investigating model heterojunction solar cells which will comprehensively presented in this PhD dissertation.

2.4.2 Photo–catalytic Applications

Cu_xO is a promising photo–catalyst that is used in many chemical processes, such as organic contamination degradation and water splitting under visible–light irradiation owing to their small band gap and low cost.[98, 165-172] Under illumination, Cu_xO produces electron/hole pairs that can generate hydroxyl radicals ($^{\bullet}HO$) from water. This radical is capable of mineralizing most organic molecules.[167] For water splitting applications, the majority charge carriers of the Cu_xO (holes) oxidize water to oxygen gas (O_2), while the photo–generated minority charge carriers (electrons) reduce water to hydrogen gas (H_2).[165, 171, 172] Significantly, the Cu_xO conduction band is more negative than the redox potential of H^+/H_2, which allows sunlight to produce H_2 from water. [170]

Unfortunately, the general photo–instability of Cu_xO greatly hinders its direct application in photo–catalysis.[165, 173] To overcome this photo–instability effect, Cu_xO is typically coupled with other semiconductors to form heterojunctions and it has been reported that TiO_2 is one of the best candidates for this purpose.[173, 174] Additionally, nanostructuring of Cu_xO can also significantly improve overall stability.[173] Fortunately, the large surface area to volume ratio, which is provided by nanostructuring, significantly increases the effective surface area available for photo–catalytic reactions.[166, 167, 169]

It has also been reported that the photo–catalytic production rate of H_2 can be significantly improved in the presence of alcohol, which provides suitable electron donors (also known as sacrificial agent/reagent).[175-177] Barreca *et al.* have successfully demonstrated excellent performance of nanostructured Cu_2O photo–catalysis for generating H_2 in the presence of methanol.[98] They have suggested that methanol inhibits electron–hole recombination and acts partially as a hydrogen source.[98] However, efficient photo–catalytic activity of CuO for H_2 production has not been reported. This is despite that fact that the band gap of CuO is 1.2 eV, which makes CuO an efficient material to absorb sunlight. However, the position of the conduction band level limits its activity. Therefore, introducing a sacrificial agent is crucial to enable it to be used as a photo−catalyst. For example, Yao *et al.* have reported that CuO exhibits high photo−catalytic activity in oxalic acid solutions.[170] Oxalic acid, which is a common pollutant in industrial wastewater, is a strong reductive agent and acts as an electron donor. [178, 179]

2.4.3 Antimicrobial Applications

The antimicrobial properties of nanostructured Cu_xO, in particular CuO, have attracted growing research interest. Nanostructured Cu_xO commonly offers a strong degree of chemical and physical stability. Most bacterial cells have cellular membranes that contain pores with minimum diameter of 4.0 to 5.0 nm.[180, 181] Cu_xO, with dimensions less than 20 nm, have shown antibacterial properties.[182, 183] The antimicrobial activity of CuO has been attributed to the production of reactive oxygen species (ROS) such as $^{\bullet}O_2^-$, $^{\bullet}HO_2$, $^{\bullet}OH$ and H_2O_2 which can also occur without exposure to any visible light owing to the small band gap of CuO.[184, 185] The generated ROS interact with outer cell walls to generate free radicals. The

radicals penetrate into the inner cell membranes which lead to the disruption of the internal contents of the cell.[184, 185] The effectiveness of the antimicrobial agent appears to be related to the nature of the cell wall structures.[183, 185-187] *S. aureus* is composed of multiple layers of peptidoglycan with numerous pores, which are suggested to be more susceptible to intracellular transductions. In contrast, the cell walls of *E. coli* are relatively thin, mainly consisting of peptidoglycan and outer layers of lipopolysaccharide, lipoprotein and phospholipids, which are less prone to being attacked by CuO nanoparticles. As a result, CuO has a higher antimicrobial activity against *S. aureus* than *E. coli.*[183, 184] In addition, greater sensitivity of *S. aureus* to the CuO nanoparticles has been attributed to the greater abundance of amines and carboxyl groups on their outer cells surface and which possesses greater affinity to antimicrobial agents.[183]

It has been demonstrated that CuO antimicrobial activity can be enhanced by exposing it to light.[182, 184, 188] As described in section 4.2, light irradiation generates excited electron–hole pairs in the CuO and deactivation of the bacteria is possible *via* a photo–catalytic process.[182, 188] Akhavan *et al.* have reported an improvement of 22% of CuO antibacterial activity under illumination.[182]

2.4.4 Electrochemical Applications

The electrochemical properties of nanostructured Cu_xO as electrodes for lithium ion batteries (LIB) have also been of growing research interest. Cu_xO has many attractive advantages over conventional materials including high theoretical capacity (>600 and >350 $mAhg^{-1}$ for CuO and Cu_2O, respectively) and low cost.[189-191] One of the major issues with the use of Cu_xO in LIBs is its large volume variation during the Li^+

ion insertion/extraction processes, which leads to severe mechanical strains and a rapid decay in capacity.[189] Recently, there have been various reports demonstrating LIBs with high reversible capacity and cycling stability by synthesising Cu_xO/graphene nanocomposites.[189, 192, 193] Mai *et al.* reported an excellent reversible capacity of 583.5 $mAhg^{-1}$ with high cycling stability by incorporating CuO nanoparticles (~30 nm) onto graphene sheets (Figure 2.7a). The graphene sheets serve as a conductive network for fast electron transfer as well as buffered spaces to accommodate the CuO volume expansion/contraction during Li^+ insertion/extraction process.[192]

Nanostructuring Cu_xO into hollow nano/microstructures such as spheres, cubes or urchin–like structures increases its LIB performance.[130, 193-195] For example, Park *et al.* have successfully demonstrated that hollow CuO urchin–like nanoparticles possess a charge capacity above 560 $mAhg^{-1}$ (Figure 2.7b).[194] Wei *et al.* have discussed and listed three main advantages of hollow structures as anode materials for LIBs.[195] Zhou *et al.* have reported excellent LIB performance by integrating hollow nanostructures of CuO with graphene.[193] The composites exhibited a durable lifetime with reversible capacities as large as 640 $mAhg^{-1}$ (Figure 2.7c).[193]

2.4.5 Electrochromic Devices

Nanostructured Cu_2O electrochromic based systems, such as smart windows and optical displays, have been studied since the 1990s.[83] It has been found that Cu_2O exhibits cathodic electrochromism, being transparent under visible illumination in their oxidized state and almost black when switched to their reduced state in the presence of an electrolyte containing positive ions such as H^+, Li^+ and Na^+.[83, 196-

199] Generally, it has been found that the electrochromic process corresponds to the conversion of Cu_2O (transparent) to CuO (black) in a reversible reduction–oxidation process (redox).[196, 199] To date, the best coloration efficiency obtained by Cu_2O nanostructures has been up to 37 cm^2C^{-1}, which is only one–fourth of the best of those made from WO_3 nanoporous structures (141.5 cm^2C^{-1}).[196, 200] Unfortunately, nanostructured Cu_2O requires high coloration voltage and shows poor stability[197], and further work should be carried out to solve such important issues.

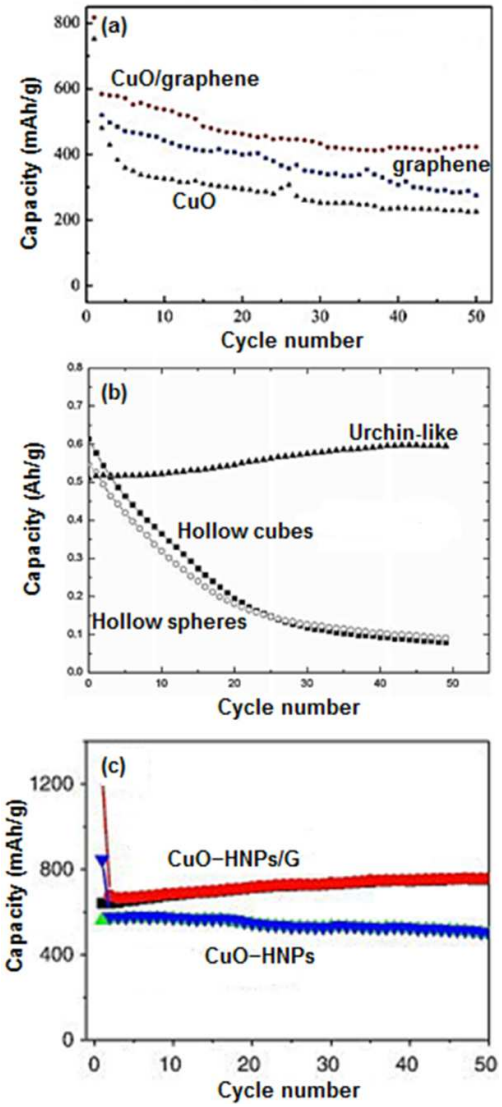

Figure 2.7 Cycling profile of (a) bare CuO, graphene and CuO/graphene electrode at current density of 67 mAg^{-1}, (b) CuO nanoparticles with three types morphologies (urchin−like, hollow cubes and hollow spheres) at a current density of 150 mAg^{-1}, (c) CuO hollow nanoparticles/graphene (CuO−HNPs/G) and CuO hollow nanoparticles (CuO−HNPs) at 50 mAg^{-1}. Reprinted with permission from (a) ref 192 copyright (2011) by Elsevier, (b) ref 194 copyright (2009) by WILEY-VCH Verlag GmbH & Co. KGaA, Weinheim, (c) ref 193 copyright (2011) by Elsevier.

2.4.6 Sensing Applications

Cu_xO offers great potential for the development of highly sensitive, yet low cost sensors. This includes optical, gas and bio sensors. Photodetectors are important devices that can be used in various applications, including thermal imaging systems, free-space communications, navigator aids and ozone-layer monitoring.[201, 202] Among the semiconductor materials, Cu_xO has proven an attractive material for making photodetectors due to its relatively low band gap and remarkable optoelectronics properties.[202-204]

Cu_xO also offers a great possibility for developing highly sensitive semiconductor-based gas sensors. The sensing properties of Cu_xO can be improved by decreasing its size to nanoscale dimensions (comparable to twice of the Debye length) and by adding appropriate dopants.[205] Catalytic nanoparticles such as Pd,[206] Pt,[207] Ag[208] and Au[207, 209, 210] attached to the Cu_xO surface, further increases its sensitivity, mainly due to spill−over effects.[205] Cu_xO thin films have been demonstrated to be highly sensitive towards various gas species including C_2H_5OH,[210-214] CO,[213, 215, 216] NO_2 [212, 216] and H_2S[206, 217, 218].

The ability to tune the shape and dimensions of Cu_xO thereby creating superior chemical and physical properties can be exploited for chemosensors and biosensors. They also show unique surface chemistry, thermal and electrical properties and high surface-to-volume ratio which enhance the sensitivity and response of electrochemical sensors.[219]

Cu_xO has been used as a working electrode in electrochemical based biosensors including in glucose sensors.[220] Most electrochemical glucose sensors involve the use of the enzyme glucose oxidase. However, the greatest drawback of enzymatic sensors is their lack of stability due to the intrinsic nature of enzymes.[221, 222] Development of non-enzymatic sensors, using Cu_xO as the working electrode, has been reported.[222-224] Though non-enzymatic sensors are, by design, quite selective, CuO-based glucose sensors have a fast response times, possess a high degree of repeatability and are extremely stable.[220]

The author of this PhD thesis will use Cu_xO at different states of stoichiometry to develop model alcohol vapour sensors. The process of engineering these Cu_xO films will be comprehensively presented in this thesis.

2.4.7 Tribology and Refrigeration Applications

A large number of studies have reported that adding metal oxides such as Cu_xO in the form of nanoparticles to lubricants is an effective means to reduce wear and friction.[46, 225-228] The friction–reduction and anti–wear behaviours are dependent on the characteristics of the nanoparticles including size (mostly in the range of 2 – 120 nm), morphology and concentration.[225] The colloidal effect, rolling friction effect, third body generation with nanomaterials and protective thin films formation mechanism have been proposed to justify the role of nanomaterials' anti–wear and friction–reduction properties.[46]

Wu *et al.* have compared the tribological properties of two lubricating oils (API–SF engine oil and Base oil) with CuO, TiO_2 and diamond nanoparticles used as additives. They found that CuO suspensions showed the highest reduction of friction

coefficient (due to viscosity and rolling effect) and worn scar depth (owing to reduction of shearing stress) as compared to standard oils without nanoparticles.[225] The shapes of nanoparticles such as sphere, rods, sheets and wires play crucial roles in tribology in monitoring the friction and anti–wear properties. Recently, Gausian *et al.* have revealed that lubricity enhancement is attributed to the synergistic effect of uninterrupted supplies of CuO nanorods under contact surfaces and their rolling mechanism.[46]

In addition to the enhancement of tribological properties, nanofluids with dispersed Cu_xO nanoparticles have great potential for improving heat transfer especially in improving the efficiency of chillers, refrigerators and air–conditioners.[47, 228, 229] Many studies have reported that mixtures with suspended CuO nanoparticles have higher thermal conductivity than the conventional host fluid.[47] This is due to the thermal conductivity of CuO (76.5 W mK^{-1} which is much higher than ethylene glycol that has a value of 0.26 W mK^{-1}). Lee *at al.* have compared the thermal conductivity of CuO and Al_2O_3 nanoparticles suspended in ethylene glycol and found that the thermal conductivity of the CuO suspensions is 7% higher than the Al_2O_3 system.[230]

2.4.8 Field Emission Applications

The field emission (FE) properties of nanostructured Cu_xO are far less reported than other oxides materials such as ZnO, SnO_2 and In_2O_3. Due to its relatively narrow band gap, Cu_xO offers an attractive alternative to serve as a FE emitter.[231-233] In a FE system the emitting capability is believed to be highly dependent on both the properties of the material and configuration of the cathode.[23] It is known that

materials with higher aspect ratios and sharp edges generally produce higher FE currents.[231, 233, 234] Zhu *et al.* have reported FE measurements of CuO nanowire films with a low turn−on field of 3.5−4.5 V μm^{-1}. They obtained a large current density of 0.45 mA cm^{-2} at an applied electric field of 7 V μm^{-1}.[232] Nanostructured Cu_2O also exhibits relatively high FE performance. Shi *et al.* have demonstrated Cu_2O micro−porous cubes with a low turn−on field of 3.1 V μm^{-1}. They showed a high current density of 1 mA cm^{-2} at an applied electric field of 11 V μm^{-1}.[234] It has also been reported that Cu_2O can be coupled with other metal oxides such as ZnO or TiO_2 to enhance its FE performance (Figure 2.8).[233, 235, 236] This enhanced FE is attributed to the alteration in electron affinity of Cu_xO by the other metal oxides forming a nano−heterojunction.[236] Additionally, the presence of the heterojunctions promotes charge separation, where the electrons move to ZnO or TiO_2 and the holes move to Cu_2O, which reduces the recombination of electron−hole pairs.[236]

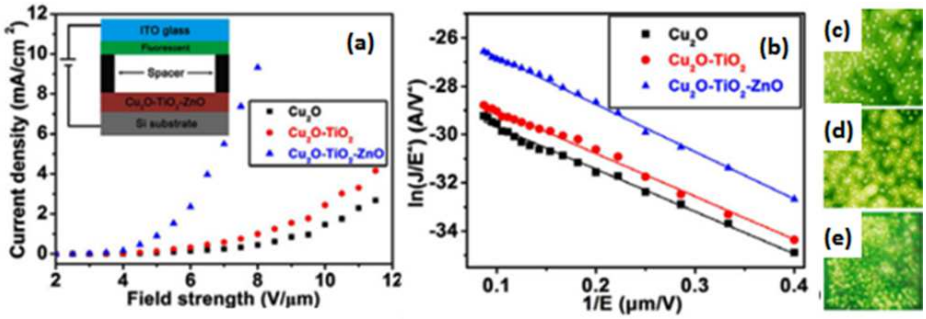

Figure 2.8 (a) Field emission *J*−*E* curves, (b) corresponding F−N plots of the samples. (c)−(e) Electron emission images of the pure Cu_2O nanopines, Cu_2O−TiO_2−ZnO composite samples, respectively. Reprinted with permission from ref 236. Copyright (2013) by IOP Publishing Ltd.

2.4.9 Other Applications

Nanostructured Cu_xO has also been reported for many applications other than those presented in sections 4.1 to 4.8. Of note, nanostructured CuO has been used in ceramic resistors[237] and supercapacitors.[238, 239] Nanostructured Cu_2O has also been incorporated in memristors,[240-242] heterogeneous catalysis,[243-247] anti−fouling [248-250] and thin−film transistors.[4, 251, 252] Of course, there are other applications for which Cu_xO has been used, but these are beyond the scope of this research.

2.5 Fundamental Properties of ZnO

2.5.1 Crystal Structure

ZnO has three types of crystal structures including wurtzite, zinc blende and rocksalt as shown in Figure 2.9. Under ambient conditions, the thermodynamically stable phase is wurtzite. The wurtzite structure has a hexagonal unit cell with two lattice parameters *a* and *c* in the *c/a* = 1.633 ratio and belongs to the space group $P6_3mc$.[253] The wurtzite structure of ZnO can be simply described as a number of alternating planes composed of tetrahedrally coordinated O^{2-} and Zn^{2+} ions, stacked alternately along the *c*–axis (Figure 2.9a).[254, 255]

The symmetry of the zinc–blende structure is given by the space group $F\bar{4}3m$ and composed of two interpenetrating face–cantered–cubic (fcc) sublattices shifted along the body diagonal by one–quarter of a body diagonal. There are four atoms per unit cell and every atom of one type (group II) is tetrahedrally coordinated with four atoms of the other type (group VI) (Figure 2.9b).[256]

The space group symmetry of the rocksalt type of structure is $Fm3m$ and the structure is sixfold coordinated with two lattice parameters *a* and *c* in the ratio of *c/a* = 1.00 (Figure 2.9c).[257] However, stable rocksalt structure cannot be obtained using conventional growth methods. Generally, the pressure–induced phase transition from wurtzite to the rocksalt phase occurs at approximately 9.1 GPa together with a large volume decrease of about 17%.[256, 257] In addition, Aoumeur *et al.* revealed that at 8.9 GPa, the ZnO zinc–blende structure exhibit unstable characteristic and converted into rocksalt structure.[258]

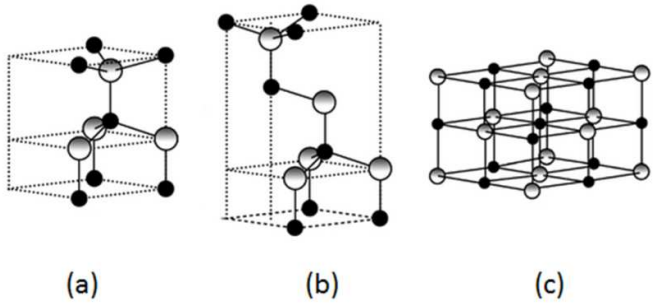

Figure 2.9 ZnO crystal structure: (a) hexagonal wurtzite, (b) cubic zinc−blende and (c) cubic rocksalt. Shaded gray and black spheres denote ZnO and O atoms, respectively. Reprinted with permission from ref 256. Copyright (2005) by American Institute of Physics.

2.5.2 Electronic Band Structure and Optical Properties

The electronic band structure of ZnO has been comprehensively studied by a number of researchers.[256, 259-261] Several theoretical approaches of varying degrees of complexity have been employed to calculate the band structures of ZnO, in particular the wurtzite structure.[262-264] Mostly these theories use local−density approximation (LDA), which is complicated because of the cationic *d* electrons. If the *d* electrons are treated as the core electrons, the calculated lattice constant underestimates the experimental values by as much as 18% for wurtzite ZnO.[256]

For example, the LDA underestimates the ZnO E_g to be as low as 0.23 eV, contradict to the experimental value of 3.37 eV.[256] This deviation is attributed to the measured exciton energies influenced by electronics relaxations, which is expected to be mostly pronounced for the highly localized cationic semicore *d* states.[256] Jaffe *et al.* have demonstrated electronic band structure calculations for the other phases of ZnO using combination of LDA and generalized gradient approximation (GGA) with optimized Gaussian basis sets to expand the crystal orbitals and periodic electron density.[259]

Optical properties of nanostructured ZnO have been studied by a variety of experimental techniques such as optical absorption, transmission, reflection, photoreflection, spectroscopic ellipsometry, photoluminescence, cathodoluminescence and calorimetric spectroscopy.[265-269] Mostly, these experimental techniques have demonstrated that nanostructured ZnO has a direct transition with E_g of ~ 3.37 eV and a large exciton binding energy of ~ 60 meV.[256, 265, 268] This large exciton binding energy means that the excitation of electrons at room temperature is stable, resulting in efficient excitonic recombination.[256]

2.5.3 Electrical Properties

ZnO is naturally a *n*-type semiconductor because of a deviation from stoichiometry due to the presence of intrinsic defects such as O vacancies (V_o) and Zn interstitials (Z_{n_i}).[256, 270] Using Monte Carlo simulations, Albrecht *et al.* have predicted a room temperature electron mobility of ZnO as large as 300 $cm^2/V{\cdot}s$. [271] The highest room−temperature electron mobility for a bulk ZnO single crystal, grown by an evaporation method, has been reported to be about ~200 $cm^2/V{\cdot}s$ with a carrier concentration of 6.0×10^{16} cm^{-3}.[272] Recently, Shinagawa *et al.* have reported a

comprehensive study of electrical properties of nanostructured ZnO films prepared by an electrodeposition technique.[273] They found that the resistivity changes about 5 and 6 orders of magnitude with the applied current density and the deposition temperature, respectively.[273] Reviews on the electrical properties of ZnO *via* other methods are found elsewhere.[274]

2.6 Nanostructured ZnO Synthesis methods

Similar to nanostructured Cu_xO, there are many different techniques for synthesizing nanostructured ZnO using both vapour and liquid−phase−based methods. Most of these techniques have been discussed comprehensively in the literature.[254, 255, 275, 276] This PhD dissertation only focuses the electrodeposition technique as it is the main method that will be used for the formation of the ZnO films by the author. The PhD candidate also used RF magnetron sputtering for the formation of ZnO seed layers, which the readers can find a large number of reviews including the ones written by Ellmer [277] and Triboulet *et al.*[278]

Since the first reports on ZnO electrodeposition by Izaki *et al.*[279] and Lincot *et al.*[280] in 1996, a wide range of studies regarding the electrodepostion of ZnO have been published. The emerging popularity is due to their significant advantages over vacuum deposition techniques. Electrodeposition has shown to be a powerful technique to control the crystallization and engineering of the nanostructured thin films.[281, 282] Additionally, electrodeposition presents several other advantages such as low fabrication costs, facile control over film thickness, morphology and doping concentration as well as low temperature and low ambient pressure processing.[111, 273, 283]

Solutions that contains $Zn(NO_3)_2$ are amongst the most common aqueous electrolytes that are used in electrodeposition.[111, 279, 284] A reaction mechanism of the cathodic ZnO electrodeposition from $Zn(NO_3)_2$ aqueous solutions start *via* the reduction of nitrate ions on the substrate. This produces hydroxide ions and the process raises the electrolyte pH near the solid-solution interface. In the presence of zinc ions in the electrolyte, $Zn(OH)_4^{2-}$ is formed that eventually converts to ZnO *via* a dehydration process.[279, 285] The formation rate of the ZnO films is affected by the applied current density and Zn^{2+} concentration, and the crystallization accompanied by dehydration may depend on the deposition temperature.[273, 286] In order to ensure that the formation of ZnO occurs, the electrodeposition process needs to be carried out at temperatures equal or greater than 50 ºC otherwise metallic Zn is deposited instead.[287] Additionally, hydrogen evolution, which is detrimental to the quality of the electrodeposited films, can be avoided by choosing the right deposition potential. It has been demonstrated that different morphologies of ZnO *via* electrodeposition technique can be obtained such as nanorods,[284, 288] nanosheets,[288] nanoneedles,[288] nanowires,[113, 116, 289] and nanotubes[286].

2.7 Applications ZnO

As presented in the previous section, ZnO is a wide bandgap semiconductor with high electron mobility. It has a high stability, is facile to synthesis and can be synthesized into many different nano morphologies. ZnO is an integral component of many emerging technologies in areas such as optoelectronics, energy harvesting, sensing and catalyst. In this PhD work, only two of the ZnO applications are investigated focused including solar cells and memristive switching. As a result, the

PhD candidate only focuses on presenting his views on these two. The readers can refer to comprehensive reviews such as the manuscripts by Wang *et al.*[254] and Ahmad *et al.*[290] for obtaining an overall view regarding a wide range of ZnO applications.

2.7.1 Solar Cells

ZnO has been used as a hole charge blocking as well as electron charge transport layer in organic solar cells[291, 292], ZnO nanowires have been used as the charge scavenger in dye−sensitized and hybrid solar cells,[293-297] and heterojunction solar cells with structures based on ZnO−CdSe−CuSCN [298] and ZnO−Cu_2O [113, 116, 155] have been developed using ZnO films. This PhD thesis only focuses on ZnO−Cu_2O heterojunction solar cells. For brevity, only a background regarding this structure is discussed by the author of this thesis. The readers can refer to review papers written by Xu *et al.*[281] and Zhang *et al.*[299] for further information regarding ZnO based solar cells.

In the past decade, the curiosity regarding ZnO−Cu_2O heterojunctions has increased exponentially due to its prospect in green energy harvesting and photocatalysis. When a junction forms between ZnO and Cu_2O, it can help to facilitate the separation and transportation of the photoinduced charge carriers in ZnO-Cu_2O structures that decreases the possibility of election-hole recombination, enhancing the photovoltaic efficiency.[300]

ZnO and Cu_2O can be prepared using different methods such as thermal oxidation,[301] electrodeposition,[108, 111, 112, 281, 302] anodic oxidation,[303] PLD,[304] spraying,[305] thermal evaporation[82, 137], nanoparticle inks[306], DC sputtering[307] and RF sputtering.[308-310] Sections 2.3.2.1 and 2.6 were devoted

to the advantages of electrodeposition for the formation of Cu_xO and ZnO, respectively, explaining the motivation of the PhD candidate in implementing this method in the course of his research. As a result, ZnO−Cu_2O heterojunction solar cells based on electrodeposition methods have attracted significant attention.[108, 112, 114, 311] However, obtaining rough surfaces that increase the surface-to-volume ratio, hence increasing the heterointerface and solar cell current density, has been a challenge. Many conventional electrodeposition methods of ZnO produce highly crystalline films which is the parameter that is highly sought after in heterojuntion solar cells but often have low surface roughness.[112, 114] The electrodeposited ZnO crystallites generally follow the topography of the substrates and well-engineered tuning methods are required to modify their morphologies into nanocrystallites with low dimensions.[312-314] There are recent reports by Cui *et. al*.[112] and Musselman *et. al.[155]* describing the use of growth directing agents such as hexamethylenetetramine (HMT) and potassium chloride (KCl) to reduce the radius of the electrodeposited nanowires. However in their ZnO films, the spacing between the nanowires was still more than ideal and many of the nanowires were criss-crossed as they were not all grown normal to the heterojunction surface.

It has been previously demonstrated that the application of a ZnO seed layer can significantly enhance the surface-to-volume ratio of hydrothermally deposited ZnO films.[310, 315-319] Peterson *et. al.* were among the first to exploit the advantages of RF sputtered ZnO seed layers. They have reported that a seeding layer on substrates can significantly affect the nucleation and growth of ZnO nanowires in a hydrothermal process.[317] They believed that the interfacial tension between solution species and crystal nucleation sites depend on the degree of structural fits, the same crystal type having the best fit and lowest energy barrier.[317] As a result,

the author of this PhD thesis draws his attention to employ similar concept for developing high performance of electrodeposited ZnO−Cu_2O based heterojunction solar cells using seed layers of ZnO.

2.7.2 Memristors

In 1971, Lean Chua, a professor from University of California, published a paper in *IEEE Transactions on Circuits Theory*[320], postulating the existence of a fourth circuit element, in addition to resistors, inductors and capacitors.[321] Chua named the element as memristors.[320] No one actually paid any serious attention to this basic circuit element until 2008 when a group of scientist from Hewlett−Packard lead by Stanley Williams published an article in *Nature*[322] and successfully built a memristor prototype to understand its operations.[321] Stanley Williams *et al.* defined memristance as a property of the electronic component. If charge flows in one direction, the resistance of this component will increase and if a charge flows in the opposite direction, the resistance will decrease. If the flow of charge is stopped by turning off the applied voltage, the component will "remember" the last resistance that it had, and when the flow of charge starts again the resistance of the circuit will be what it was last active.[321]

Memristive switching phenomena in various metal oxides have attracted considerable attention due to their potential applications in future non−volatile memory devices. Memristive switching involves a "switch" from a high resistance state (HRS, or "OFF" state) to a low resistance state (LRS, or "ON" state) and *vice versa*. Generally, such a switching mechanism can be classified according to the dominant contribution to this effect including thermal, electronic or ionic effect

during the ON/OFF process. [323, 324] Transition metal oxide based memristive devices have attracted considerable attention due to their electronic and electrical properties such as wide band gaps, structural simplicity, low power consumption, fast switching, high density integration and process compatibility with CMOS technologies. [325-329] Transition metal oxides such as TiO_2 [327, 330, 331], NiO [332, 333], Al_2O_3 [334], HfO_2 [335], ZrO_2 [336], Ta_2O_5 [337], SnO_2 [338] and ZnO [329, 339, 340] are some of the promising materials for memristive applications.

Amongst the various transition metal oxides being investigated for memristor applications, ZnO possesses several advantages. ZnO has favourable properties including wide band gap, high electron mobility, and large excitation binding energy. [114, 341] It is also inexpensive and abundant. For memristive devices, a wide band gap metal oxide is favourable due to susceptibility to doping by incorporating a variety of defects and impurities. Typically, as synthesized ZnO is intrinsically "self−doped" by native interstitial, vacancy point defects, and substituting cations of various valence states which introduce oxygen vacancies into the crystal lattice. [323, 327, 342]

ZnO−based memristors can be prepared by several techniques such as PLD [339], sputtering [329, 343-346], electrodeposition [347], MOCVD [348] and spin coating [349]. Highly promising performance characteristics, including relatively high programming speed (<20 ns), long retention time (~10^5 s) and R_{OFF}/R_{ON} in the range of 10 – 20 000, have been demonstrated and most of the devices were fabricated in vacuum environment.[329, 339, 340]

In this PhD project, the researcher investigates model memristive devices based on electrodeposited ZnO films.

2.8 Summary

In this chapter, the author presented a comprehensive review of nanostructured Cu_xO focusing on their properties, preparation, processing and device applications. An overview of the material properties, including crystal structures, electronic band structures, optical, vibrational, electrical, thermal and magnetic as well as superconductivity were presented. Numerous synthesis techniques were reviewed, focusing on methods that produce nanostructured Cu_xO. Different synthesis techniques provide flexibility within the constraints of any particular applications needs. Additionally, the author discussed the major applications of nanostructured Cu_xO including in optics, sensing, tribology, refrigeration, electrochemistry, photocatalysis, High–T_C superconductivity, electrochromics and antimicrobial devices. A major portion of this Chapter was submitted for publication consideration as a review paper in the journal of *Crystal Growth & Design.*

The author also reviewed some of the fundamental properties of nanostructured ZnO, including its crystal structures, electronic band structures, optical characteristics and electrical behaviours. In addition, the author also presented a review on electrodeposition of ZnO and the usage of nanostructured ZnO for solar cells and memristor switching applications.

In the next Chapter, the author will present his achievements in the development of nanostructured Cu_xO semiconducting gas sensors. The author will discuss in detail, the fabrication process, characterization and the investigation of tuning and engineering of Cu_xO in enhancing the performance of such sensors.

References

[1] S. Asbrink and L. J. Norrby, "A Refinement Of Crystal Structure of Copper(II) Oxide With A Discussion of Some Exceptional ESDS," *Acta Crystall. B-Stru.,* vol. B 26, pp. 8-&, 1970.

[2] W. Y. Ching, Y. N. Xu, and K. W. Wong, "Ground-State And Optical-Properties of Cu_2O And CuO Crystals," *Phys. Rev. B,* vol. 40, pp. 7684-7695, 1989.

[3] T. Ito, H. Yamaguchi, K. Okabe, and T. Masumi, "Single-Crystal Growth and Characterization of Cu_2O and CuO," *J. Mater. Sci.,* vol. 33, pp. 3555-3566, 1998.

[4] B. K. Meyer, A. Polity, D. Reppin, M. Becker, P. Hering, P. J. Klar, *et al.*, "Binary Copper Oxide Semiconductors: From Materials Towards Devices," *Phys. Status Solidi B,* vol. 249, pp. 1487-1509, 2012.

[5] M. Heinemann, B. Eifert, and C. Heiliger, "Band Structure and Phase Stability of the Copper Oxides Cu_2O, CuO, and Cu_4O_3," *Phys. Rev. B,* vol. 87, 2013.

[6] J. F. Pierson, E. Duverger, and O. Banakh, "Experimental And Theoretical Contributions To The Determination of Optical Properties of Synthetic Paramelaconite," *J. Solid State Chem.,* vol. 180, pp. 968-973, 2007.

[7] M. Okeeffe and J. O. Bovin, "Crystal-Structure of Paramelaconite, Cu_4O_3," *Am. Mineral.,* vol. 63, pp. 180-185, 1978.

[8] C. Frondel, "Paramelaconite a Tetragonal Oxide of Copper," *Am. Mineral.,* vol. 26, pp. 657-672, 1941.

[9] A. E. Rakhshani and F. K. Barakat, "Optical Constants of Reactively Sputtered Cupric Oxide Films," *Mater. Lett.,* vol. 6, pp. 37-40, 1987.

[10] M. T. S. Nair, L. Guerrero, O. L. Arenas, and P. K. Nair, "Chemically Deposited Copper Oxide Thin Films: Structural, Optical And Electrical Characteristics," *Appl. Surf. Sci.,* vol. 150, pp. 143-151, 1999.

[11] M. F. Al-Kuhaili, "Characterization of Copper Oxide Thin Films Deposited by The Thermal Evaporation of Cuprous Oxide (Cu_2O)," *Vacuum,* vol. 82, pp. 623-629, 2008.

[12] A. Chen, G. Yang, H. Long, F. Li, Y. Li, and P. Lu, "Nonlinear Optical Properties of Laser Deposited CuO Thin Films," *Thin Solid Films,* vol. 517, pp. 4277-4280, 2009.

[13] J. Ghijsen, L. H. Tjeng, J. Vanelp, H. Eskes, J. Westerink, G. A. Sawatzky, *et al.*, "Electronic-Structure of Cu_2O and CuO," *Phys. Rev. B,* vol. 38, pp. 11322-11330, 1988.

[14] A. A. Ogwu, E. Bouquerel, O. Ademosu, S. Moh, E. Crossan, and F. Placido, "The Influence of RF Power And Oxygen Flow Rate During Deposition on The Optical Transmittance of Copper Oxide Thin Films Prepared by Reactive Magnetron Sputtering," *J. Phys. D Appl. Phys.,* vol. 38, pp. 266-271, 2005.

[15] M. Izaki, "Effects of Annealing on Optical and Electrical Characteristics of P-Type Semiconductor Copper (II) Oxide Electrodeposits," *Thin Solid Films,* vol. 520, pp. 2434-2437, 2012.

[16] K. Nakaoka, J. Ueyama, and K. Ogura, "Photoelectrochemical Behavior of Electrodeposited CuO and Cu_2O Thin Films on Conducting Substrates," *J. Electrochem. Soc.,* vol. 151, pp. C661-C665, 2004.

[17] J. C. Tauc, *Optical Properties of Solids.* Amsterdam: North-Holland, 1972.

[18] J. F. Pierson, A. Thobor-Keck, and A. Billard, "Cuprite, Paramelaconite And Tenorite Films Deposited by Reactive Magnetron Sputtering," *Appl. Surf. Sci.,* vol. 210, pp. 359-367, 2003.

[19] L. Y. Isseroff and E. A. Carter, "Electronic Structure of Pure and Doped Cuprous Oxide with Copper Vacancies: Suppression of Trap States," *Chem. Mater.,* vol. 25, pp. 253-265, 2013.

[20] Y. Chang, J. J. Teo, and H. C. Zeng, "Formation of Colloidal CuO Nanocrystallites And Their Spherical Aggregation And Reductive Transformation to Hollow Cu_2O Nanospheres," *Langmuir,* vol. 21, pp. 1074-1079, 2005.

[21] B. Balamurugan and B. R. Mehta, "Optical and Structural Properties of Nanocrystalline Copper Oxide Thin Films Prepared by Activated Reactive Evaporation," *Thin Solid Films,* vol. 396, pp. 90-96, 2001.

[22] A. D. Yoffe, "Low-Dimensional Systems - Quantum-Size Effects And Electronic-Properties Of Semiconductor Microcrystallites (Zero-Dimensional Systems) And Some Quasi-2-Dimensional Systems," *Adv. Phys.,* vol. 42, pp. 173-266, 1993.

[23] H. D. Zheng, J. Z. Ou, M. S. Strano, R. B. Kaner, A. Mitchell, and K. Kalantar-Zadeh, "Nanostructured Tungsten Oxide - Properties, Synthesis, and Applications," *Adv. Funct. Mater.,* vol. 21, pp. 2175-2196, 2011.

[24] P. Poulopoulos, S. Baskoutas, S. D. Pappas, C. S. Garoufalis, S. A. Droulias, A. Zamani, *et al.,* "Intense Quantum Confinement Effects in Cu_2O Thin Films," *J. Phys. Chem. C,* vol. 115, pp. 14839-14843, 2011.

[25] A. Thobor and J. F. Pierson, "Properties And Air Annealing of Paramelaconite Thin Films," *Mater. Lett.,* vol. 57, pp. 3676-3680, 2003.

[26] J. F. Pierson, D. Wiederkehr, and A. Billard, "Reactive Magnetron Sputtering of Copper, Silver And Gold," *Thin Solid Films,* vol. 478, pp. 196-205, 2005.

[27] T. Ito, T. Kawashima, H. Yamaguchi, T. Masumi, and S. Adachi, "Optical Properties of Cu_2O Studied by Spectroscopic Ellipsometry," *J. Phys. Soc. Jpn.,* vol. 67, pp. 2125-2131, 1998.

[28] T. Ito, H. Yamaguchi, T. Masumi, and S. Adachi, "Optical Properties of CuO Studied by Spectroscopic Ellipsometry," *J. Phys. Soc. Jpn.,* vol. 67, pp. 3304-3309, 1998.

[29] C. Malerba, F. Biccari, C. Leonor Azanza Ricardo, M. D'Incau, P. Scardi, and A. Mittiga, "Absorption Coefficient of Bulk and Thin Film Cu_2O," *Sol. Energ. Mat. Sol. C.,* vol. 95, pp. 2848-2854, 2011.

[30] M. M. Beg and S. M. Shapiro, "Study of Phonon Dispersion-Relations in Cuprous-Oxide by Inelastic Neutron-Scattering," *Phys. Rev. B,* vol. 13, pp. 1728-1734, 1976.

[31] M. Ivanda, D. Waasmaier, A. Endriss, J. Ihringer, A. Kirfel, and W. Kiefer, "Low-Temperature Anomalies of Cuprite Observed by Raman Spectroscopy And X-Ray Powder Diffraction," *J. Raman Spectrosc.,* vol. 28, pp. 487-493, 1997.

[32] R. Mittal, S. L. Chaplot, S. K. Mishra, and P. P. Bose, "Inelastic Neutron Scattering and Lattice Dynamical Calculation of Negative Thermal Expansion Compounds Cu_2O and Ag_2O," *Phys. Rev. B,* vol. 75, 2007.

[33] W. Reichardt, F. Gompf, M. Ain, and B. M. Wanklyn, "Lattice-Dynamics of Cupric Oxide," *Z. Phys. B Con. Mat.,* vol. 81, pp. 19-24, 1990.

[34] L. Debbichi, M. C. M. de Lucas, J. F. Pierson, and P. Kruger, "Vibrational Properties of CuO and Cu_4O_3 From First-Principles Calculations, and Raman

and Infrared Spectroscopy," *J. Phys. Chem. C,* vol. 116, pp. 10232-10237, 2012.
[35] R. J. Elliott, "Symmetry of Excitons in Cu_2O," *Phys. Rev.,* vol. 124, pp. 340-&, 1961.
[36] Y. K. Jeong and G. M. Choi, "Nonstoichiometry and Electrical Conduction of CuO," *J. Phys. Chem. Solids,* vol. 57, pp. 81-84, 1996.
[37] A. P. Young and C. M. Schwartz, "Electrical Conductivity And Thermoelectric Power of Cu_2O," *J. Phys. Chem. Solids,* vol. 30, pp. 249-252, 1969.
[38] S. Suda, S. Fujitsu, K. Koumoto, and H. Yanagida, "The Effect of Atmosphere And Doping On Electrical-Conductivity of CuO," *Jpn. J. Appl. Phys. 1,* vol. 31, pp. 2488-2491, 1992.
[39] K. Mizuno, M. Izaki, K. Murase, T. Shinagawa, M. Chigane, M. Inaba, *et al.*, "Structural and Electrical Characterizations of Electrodeposited P-Type Semiconductor Cu_2O Films," *J. Electrochem. Soc.,* vol. 152, pp. C179-C182, 2005.
[40] P. Thien Viet, M. Rao, P. Andreasson, Y. Peng, J. Wang, and K. B. Jinesh, "Photocarrier Generation in Cu_xO Thin Films Deposited by Radio Frequency Sputtering," *Appl. Phys. Lett.,* vol. 102, 2013.
[41] D. O. Scanlon and G. W. Watson, "Undoped n-Type Cu_2O: Fact or Fiction?," *J. Phys. Chem. Lett.,* vol. 1, pp. 2582-2585, 2010.
[42] L. Q. Wang and J. Fan, "Nanofluids Research: Key Issues," *Nanoscale Res. Lett.,* vol. 5, pp. 1241-1252, 2010.
[43] X. Wei, H. Zhu, T. Kong, and L. Wang, "Synthesis And Thermal Conductivity of Cu_2O Nanofluids," *Int. J. Heat Mass Tran.,* vol. 52, pp. 4371-4374, 2009.
[44] Y. J. Hwang, Y. C. Ahn, H. S. Shin, C. G. Lee, G. T. Kim, H. S. Park, *et al.*, "Investigation on Characteristics of Thermal Conductivity Enhancement of Nanofluids," *Curr. Appl. Phys.,* vol. 6, pp. 1068-1071, 2006.
[45] S. Walia, S. Balendhran, H. Nili, S. Zhuiykov, G. Rosengarten, Q. H. Wang, *et al.*, "Transition Metal Oxides – Thermoelectric Properties," *Prog. Mater. Sci.,* vol. 58, pp. 1443-1489, 2013.
[46] R. Gusain and O. P. Khatri, "Ultrasound Assisted Shape Regulation of CuO Nanorods in Ionic Liquids and Their Use as Energy Efficient Lubricant Additives," *J. Mater. Chem. A,* vol. 1, pp. 5612-5619, 2013.
[47] R. Saidur, S. N. Kazi, M. S. Hossain, M. M. Rahman, and H. A. Mohammed, "A Review On The Performance of Nanoparticles Suspended With Refrigerants And Lubricating Oils in Refrigeration Systems," *Renew. Sust. Energ. Rev.,* vol. 15, pp. 310-323, 2011.
[48] H. Timm and J. Janek, "On the Soret Effect in Binary Nonstoichiometric Oxides—Kinetic Demixing of Cuprite in A Temperature Gradient," *Solid State Ionics,* vol. 176, pp. 1131-1143, 2005.
[49] X. Chen, D. Parker, M. H. Du, and D. J. Singh, "Potential Thermoelectric Performance of Hole-Doped Cu_2O," *New J. Phys.,* vol. 15, 2013.
[50] H. A. Mintsa, G. Roy, C. T. Nguyen, and D. Doucet, "New Temperature Dependent Thermal Conductivity Data for Water-Based Nanofluids," *Int. J. Therm. Sci.,* vol. 48, pp. 363-371, 2009.
[51] C. H. Li and G. P. Peterson, "Experimental Investigation of Temperature And Volume Fraction Variations on The Effective Thermal Conductivity of Nanoparticle Suspensions (Nanofluids)," *J. Appl. Phys.,* vol. 99, 2006.

[52] M. J. Nine, B. Munkhbayar, M. S. Rahman, H. Chung, and H. Jeong, "Highly Productive Synthesis Process of Well Dispersed Cu_2O and Cu/Cu_2O Nanoparticles And Its Thermal Characterization," *Mater. Chem. Phys.*, vol. 141, pp. 636-642, 2013.

[53] H. Zhu, D. Han, Z. Meng, D. Wu, and C. Zhang, "Preparation And Thermal Conductivity of CuO Nanofluid Via A Wet Chemical Method," *Nanoscale Res. Lett.*, vol. 6, 2011.

[54] P. A. Korzhavyi, I. L. Soroka, E. I. Isaev, C. Lilja, and B. Johansson, "Exploring Monovalent Copper Compounds With Oxygen And Hydrogen," *P. Natl. Acad. Sci. USA*, vol. 109, pp. 686-689, 2012.

[55] J. Leitner, D. Sedmidubský, B. Doušová, A. Strejc, and M. Nevřiva, "Heat Capacity of CuO in The Temperature Range of 298.15–1300 K," *Thermochim. Acta*, vol. 348, pp. 49-51, 2000.

[56] M. W. Chase, C. A. Davies, J. R. Downey, D. J. Frurip, R. A. McDonald, and A. N. Syverud, "Janaf Thermochemical Tables," *J. Phys. Chem. Ref. Data*, vol. 14, pp. 1-926, 1985.

[57] E. Gmelin, "Cupric Oxide CuO - Its Structural, Electrical, Thermal And Magnetic-Properties," *Indian J. Pure Ap. Phys.*, vol. 30, pp. 596-608, 1992.

[58] L. V. Gregor, "Heat Capacity of Cuprous Oxide from 2.8 to 21 ^{o}K," *J. Phys. Chem.*, vol. 66, pp. 1645-&, 1962.

[59] J. H. Hu and H. L. Johnston, "Low Temperature Heat Capacities of Inorganic Solids .IX. Heat Capacity and Thermodynamic Properties of Cuprous Oxide from 14^{o}K to 300^{o}K," *J. Am. Chem. Soc.*, vol. 73, pp. 4550-4551, 1951.

[60] D. D. Lawrie, J. P. Franck, and C.-T. Lin, "Search for An Isotope Effect in The Antiferromagnetic Transitions of Cupric Oxide CuO," *Physica C*, vol. 297, pp. 59-63, 1998.

[61] L. Pinsard-Gaudart, J. Rodriguez-Carvajal, A. Gukasov, and P. Monod, "Magnetic Properties of Paramelaconite (Cu_4O_3): A pyrochlore lattice with $S_{1/2}$," *Phys. Rev. B*, vol. 69, 2004.

[62] M. H. Whangbo and H. J. Koo, "Spin Dimer Analysis of The Spin Exchange Interactions in Paramelaconite Cu_4O_3 And Its Analogue $Ag_2Cu_2O_3$ And The Spin Ordering of The Cu_2O_3 Spin Lattice Leading To Their Magnetic Phase Transitions," *Inorg. Chem.*, vol. 41, pp. 3570-3577, 2002.

[63] B. X. Yang, J. M. Tranquada, and G. Shirane, "Neutron-Scattering Studies of The Magnetic-Structure Of Cupric Oxide," *Phys. Rev. B*, vol. 38, pp. 174-178, 1988.

[64] S. H. Pan, J. P. O'Neal, R. L. Badzey, C. Chamon, H. Ding, J. R. Engelbrecht, *et al.*, "Microscopic Electronic Inhomogeneity in The High-Tc Superconductor $Bi_2Sr_2CaCu_2O_{8+x}$," *Nature*, vol. 413, pp. 282-285, 2001.

[65] M. A. Kastner, R. J. Birgeneau, G. Shirane, and Y. Endoh, "Magnetic, Transport And Optical Properties of Monolayer Copper Oxides," *Rev. Mod. Phys.*, vol. 70, pp. 897-928, 1998.

[66] J. M. Tranquada, H. Woo, T. G. Perring, H. Goka, G. D. Gu, G. Xu, *et al.*, "Quantum Magnetic Excitations From Stripes in Copper Oxide Superconductors," *Nature*, vol. 429, pp. 534-538, 2004.

[67] M. Karppinen and H. Yamauchi, "The Doping Routes and Distribution of Holes in Layered Cuprates: A Novel Bond-Valence Approach," *Philos. Mag. B*, vol. 79, pp. 343-366, 1999.

[68] H. Yamauchi and M. Karppinen, "Hole-Doping of The CuO_2 Planes in High T_c Superconductors," *Mat. Sci. Eng. B-Solid*, vol. 54, pp. 92-97, 1998.

[69] X. Han, K. Han, and M. Tao, "n-Type Cu_2O by Electrochemical Doping with Cl," *Electrochem. Solid Lett.*, vol. 12, pp. H89-H91, 2009.

[70] K. Han and M. Tao, "N-Type Doping in Electrodeposited Cu_2O by Cu Diffusion," in *Photovoltaics for the 21st Century 5*. vol. 25, M. Tao, P. Chang, K. Kakimoto, M. Sunkara, J. Brownson, C. Claeys, *et al.*, Eds., ed, 2010, pp. 103-109.

[71] X. Han, K. Han, and M. Tao, "Characterization of Cl-doped n-type Cu_2O Prepared by Electrodeposition," *Thin Solid Films*, vol. 518, pp. 5363-5367, 2010.

[72] C. A. N. Fernando and S. K. Wetthasinghe, "Investigation of Photoelectrochemical Characteristics of n-type Cu_2O Films," *Sol. Energ. Mat. Sol. C.*, vol. 63, pp. 299-308, 2000.

[73] Y. Okamoto, S. Ishizuka, S. Kato, T. Sakurai, N. Fujiwara, H. Kobayashi, *et al.*, "Passivation of Defects in Nitrogen-Doped Polycrystalline Cu_2O Thin Films by Crown-Ether Cyanide Treatment," *Appl. Phys. Lett.*, vol. 82, pp. 1060-1062, 2003.

[74] B. B. Li, L. Lin, H. L. Shen, F. E. Boafo, Z. F. Chen, B. Liu, *et al.*, "Effect of N Doping on Hole Density of Cu_2O:N Films Prepared by The Reactive Magnetron Sputtering Method," *Eur. Phys. J-Appl. Phys.*, vol. 58, 2012.

[75] K. Akimoto, S. Ishizuka, M. Yanagita, Y. Nawa, G. K. Paul, and T. Sakurai, "Thin Film Deposition of Cu_2O and Application For Solar Cells," *Sol. Energy*, vol. *80*, pp. 715-722, 2006.

[76] S. Ishizuka, S. Kato, Y. Okamoto, and K. Akimoto, "Control of Hole Carrier Density of Polycrystalline Cu_2O Thin Films by Si Doping," *Appl. Phys. Lett.*, vol. 80, pp. 950-952, 2002.

[77] S. Ishizuka, S. Kato, Y. Okamoto, and K. Akimoto, "Hydrogen Treatment for Polycrystalline Nitrogen-Doped Cu_2O Thin Film," *J. Cryst. Growth*, vol. 237–239, Part 1, pp. 616-620, 2002.

[78] A. S. Reddy, H.-H. Park, V. S. Reddy, K. V. S. Reddy, N. S. Sarma, S. Kaleemulla, *et al.*, "Effect of Sputtering Power on The Physical Properties of DC Magnetron Sputtered Copper Oxide Thin Films," *Mater. Chem. Phys.*, vol. 110, pp. 397-401, 2008.

[79] K. J. Blobaum, D. Van Heerden, A. J. Wagner, D. H. Fairbrother, and T. P. Weihs, "Sputter-Deposition and Characterization of Paramelaconite," *J. Mater. Res.*, vol. 18, pp. 1535-1542, 2003.

[80] A. V. Richthofen, R. Domnick, and R. Cremer, "Preparation of Cuprite (Cu_2O), Paramelaconite ($Cu_3^{2+}Cu_2^{1+}O_4$) And Tenorite (CuO) With Magnetron Sputtering Ion Plating: Characterization by EPMA, XRD, HEED and SEM," *Fresen. J. Anal. Chem.*, vol. 358, pp. 312-315, 1997.

[81] P. K. Ooi, S. S. Ng, M. J. Abdullah, H. Abu Hassan, and Z. Hassan, "Effects of Oxygen Percentage on The Growth of Copper Oxide Thin Films by Reactive Radio Frequency Sputtering," *Mater. Chem. Phys.*, vol. 140, pp. 243-248, 2013.

[82] L. S. Huang, S. G. Yang, T. Li, B. X. Gu, Y. W. Du, Y. N. Lu, *et al.*, "Preparation of Large-Scale Cupric Oxide Nanowires by Thermal Evaporation Method," *J. Cryst. Growth*, vol. 260, pp. 130-135, 2004.

[83] N. Özer and F. Tepehan, "Structure and Optical Properties of Electrochromic Copper Oxide Films Prepared by Reactive And Conventional Evaporation Techniques," *Sol. Energ. Mat. Sol. C.*, vol. 30, pp. 13-26, 1993.

[84] K. Santra, C. K. Sarkar, M. K. Mukherjee, and B. Ghosh, "Copper-Oxide Thin-Films Grown by Plasma Evaporation Method," *Thin Solid Films,* vol. 213, pp. 226-229, 1992.

[85] B. Balamurugan, B. R. Mehta, D. K. Avasthi, F. Singh, A. K. Arora, M. Rajalakshmi, *et al.*, "Modifying the Nanocrystalline Characteristics-Structure, Size, and Surface States of Copper Oxide Thin Films by High-Energy Heavy-Ion Irradiation," *J. Appl. Phys.*, vol. 92, pp. 3304-3310, 2002.

[86] X. Jiang, T. Herricks, and Y. Xia, "CuO Nanowires Can Be Synthesized by Heating Copper Substrates in Air," *Nano Lett.*, vol. 2, pp. 1333-1338, 2002.

[87] S. Kim, K. Hong, K. Kim, I. Lee, and J.-L. Lee, "Phase-Controllable Copper Oxides for An Efficient Anode Interfacial Layer in Organic Light-Emitting Diodes," *J. Mater. Chem.*, vol. 22, pp. 2039-2044, 2012.

[88] Y. Fu, H. Lei, X. Wang, D. Yan, L. Cao, G. Yao, *et al.*, "Fabrication of Two Domain Cu_2O(011) Films on MgO(001) by Pulsed Laser Deposition," *Appl. Surf. Sci.*, vol. 273, pp. 19-23, 2013.

[89] A. Chen, H. Long, X. Li, Y. Li, G. Yang, and P. Lu, "Controlled Growth and Characteristics of Single-Phase Cu_2O and CuO Films by Pulsed Laser Deposition," *Vacuum,* vol. 83, pp. 927-930, 2009.

[90] M. Kawwam, F. Alharbi, A. Aldwayyan, and K. Lebbou, "Morphological Study of PLD Grown CuO films on $SrTiO_3$, Sapphire, Quartz and MgO Substrates," *Appl. Surf. Sci.*, vol. 258, pp. 9949-9953, 2012.

[91] W. Seiler, E. Millon, J. Perrière, R. Benzerga, and C. Boulmer-Leborgne, "Epitaxial Growth of Copper Oxide Films by Reactive Cross-Beam Pulsed-Laser Deposition," *J. Cryst. Growth,* vol. 311, pp. 3352-3358, 2009.

[92] M. Kawwam, F. H. Alharbi, T. Kayed, A. Aldwayyan, A. Alyamani, N. Tabet, *et al.*, "Characterization of CuO(111)/MgO(100) Films Grown Under Two Different PLD backgrounds," *Appl. Surf. Sci.*, vol. 276, pp. 7-12, 2013.

[93] K. P. Muthe, J. C. Vyas, S. N. Narang, D. K. Aswal, S. K. Gupta, D. Bhattacharya, *et al.*, "A Study of The CuO Phase Formation During Thin Film Deposition by Molecular Beam Epitaxy," *Thin Solid Films,* vol. 324, pp. 37-43, 1998.

[94] K. Kawaguchi, R. Kita, M. Nishiyama, and T. Morishita, "Molecular Beam Epitaxy Growth of CuO and Cu_2O Films with Controlling The Oxygen Content by The Flux Ratio of Cu/O^+," *J. Cryst. Growth,* vol. 143, pp. 221-226, 1994.

[95] J. Li, Z. Mei, D. Ye, H. Liang, Y. Liu, and X. Du, "Growth of Single-Crystalline Cu_2O (111) Film on Ultrathin MgO Modified Alpha-Al_2O_3 (0001) Substrate by Molecular Beam Epitaxy," *J. Cryst. Growth,* vol. 353, pp. 63-67, 2012.

[96] D. S. Darvish and H. A. Atwater, "Epitaxial Growth of Cu_2O and ZnO/Cu_2O Thin Films on MgO by Plasma-Assisted Molecular Beam Epitaxy," *J. Cryst. Growth,* vol. 319, pp. 39-43, 2011.

[97] J. Medina-Valtierra, C. Frausto-Reyes, G. Camarillo-Martinez, and J. A. Ramirez-Ortiz, "Complete Oxidation of Isopropanol Over Cu_4O_3 (Paramelaconite) Coating Deposited on Fiberglass by CVD," *J. A. Appl. Catal.*, vol. 356, pp. 36-42, 2009.

[98] D. Barreca, P. Fornasiero, A. Gasparotto, V. Gombac, C. Maccato, T. Montini, *et al.*, "The Potential of Supported Cu_2O and CuO Nanosystems in Photocatalytic H_2 Production," *Chemsuschem,* vol. 2, pp. 230-233, 2009.

[99] J. Ramirez-Ortiza, T. Ogura, J. Medina-Valtierra, S. E. Acosta-Ortiz, P. Bosch, J. A. de los Reyes, *et al.*, "A Catalytic Application of Cu_2O And CuO Films Deposited Over Fiberglass," *Appl. Surf. Sci.,* vol. 174, pp. 177-184, 2001.

[100] C. R. Crick and I. P. Parkin, "CVD of Copper And Copper Oxide Thin Films via The in Situ Reduction of Copper (II) Nitrate-A Route to Conformal Superhydrophobic Coatings," *J. Mater. Chem.,* vol. 21, pp. 14712-14716, 2011.

[101] T. Kosugi and S. Kaneko, "Novel Spray-Pyrolysis Deposition of Cuprous Oxide Thin Films," *J. Am. Ceram. Soc.,* vol. 81, pp. 3117-3124, 1998.

[102] J. Morales, L. Sanchez, F. Martin, J. R. Ramos-Barrado, and M. Sanchez, "Nanostructured CuO Thin Film Electrodes Prepared by Spray Pyrolysis: A Simple Method for Enhancing The Electrochemical Performance of CuO in Lithium Cells," *Electrochim. Acta,* vol. 49, pp. 4589-4597, 2004.

[103] G. Q. Jian, L. Liu, and M. R. Zachariah, "Facile Aerosol Route to Hollow CuO Spheres and its Superior Performance as an Oxidizer in Nanoenergetic Gas Generators," *Adv. Funct. Mater.,* vol. 23, pp. 1341-1346, 2013.

[104] T. Ghodselahi, M. A. Vesaghi, A. Shafiekhani, A. Baghizadeh, and M. Lameii, "XPS Study of The Cu@Cu_2O Core-Shell Nanoparticles," *Appl. Surf. Sci.,* vol. 255, pp. 2730-2734, 2008.

[105] D. Barreca, A. Gasparotto, C. Maccato, E. Tondello, O. I. Lebedev, and G. Van Tendeloo, "CVD of Copper Oxides From a Beta-Diketonate Diamine Precursor: Tailoring the Nano-Organization," *Cryst. Growth Des.,* vol. 9, pp. 2470-2480, 2009.

[106] F. Pola-Albores, W. Antunez-Flores, P. Amezaga-Madrid, E. Rios-Valdovinos, M. Valenzuela-Zapata, F. Paraguay-Delgado, *et al.*, "Growth And Microstructural Study of CuO Covered ZnO Nanorods," *J. Cryst. Growth,* vol. 351, pp. 77-82, 2012.

[107] M. Izaki, M. Nagai, K. Maeda, F. B. Mohamad, K. Motomura, J. Sasano, *et al.*, "Electrodeposition of 1.4-eV-Bandgap P-Copper (II) Oxide Film With Excellent Photoactivity," *J. Electrochem. Soc.,* vol. 158, pp. D578-D584, 2011.

[108] M. Izaki, T. Shinagawa, K.-T. Mizuno, Y. Ida, M. Inaba, and A. Tasaka, "Electrochemically Constructed P-Cu_2O/N-ZnO Heterojunction Diode for Photovoltaic Device," *J. Phys. D Appl. Phys.,* vol. 40, pp. 3326-3329, 2007.

[109] J. Sasano, K. Motomura, M. Nagai, F. B. Mohamad, and M. Izaki, "Pulse Electrodeposition of CuO Thin Films to Improve Crystallinity for the Enhancement of Photoelectrochemical Response," *Electrochemistry,* vol. 79, pp. 831-837, 2011.

[110] B. M. Fariza, J. Sasano, T. Shinagawa, S. Watase, and M. Izaki, "Light-Assisted Electrochemical Construction of (111)Cu_2O/(0001)ZnO Heterojunction," *Thin Solid Films,* vol. 520, pp. 2261-2264, 2012.

[111] B. M. Fariza, J. Sasano, T. Shinagawa, H. Nakano, S. Watase, and M. Izaki, "Electrochemical Growth of (0001)-n-ZnO Film on (111)-p-Cu_2O Film and the Characterization of the Heterojunction Diode," *J. Electrochem. Soc.,* vol. 158, pp. 621-625, 2011.

[112] J. B. Cui and U. J. Gibson, "A Simple Two-Step Electrodeposition of Cu_2O/ZnO Nanopillar Solar Cells," *J. Phys. Chem. B,* vol. 114, pp. 6408-6412, 2010.

[113] K. P. Musselman, A. Marin, L. Schmidt-Mende, and J. L. MacManus-Driscoll, "Incompatible Length Scales in Nanostructured Cu_2O Solar Cells," *Adv. Funct. Mater.*, vol. 22, pp. 2202-2208, 2012.
[114] H. Wei, H. Gong, Y. Wang, X. Hu, L. Chen, H. Xu, *et al.*, "Three Kinds of Cu_2O/ZnO Heterostructure Solar Cells Fabricated With Electrochemical Deposition And Their Structure-Related Photovoltaic Properties," *Crystengcomm*, vol. 13, pp. 6065-6070, 2011.
[115] P. Poizot, C. J. Hung, M. P. Nikiforov, E. W. Bohannan, and J. A. Switzer, "An Electrochemical Method For CuO Thin Film Deposition From Aqueous Solution," *Electrochem. Solid St.*, vol. 6, pp. C21-C25, 2003.
[116] K. P. Musselman, A. Marin, A. Wisnet, C. Scheu, J. L. MacManus-Driscoll, and L. Schmidt-Mende, "A Novel Buffering Technique for Aqueous Processing of Zinc Oxide Nanostructures and Interfaces, and Corresponding Improvement of Electrodeposited ZnO-Cu_2O Photovoltaics," *Adv. Funct. Mater.*, vol. 21, pp. 573-582, 2011.
[117] W. Y. Zhao, W. Y. Fu, H. B. Yang, C. J. Tian, M. H. Li, Y. X. Li, *et al.*, "Electrodeposition of Cu_2O Films And Their Photoelectrochemical Properties," *Crystengcomm*, vol. 13, pp. 2871-2877, 2011.
[118] S. Z. Li, H. Zhang, Y. J. Ji, and D. R. Yang, "CuO Nanodendrites Synthesized by A Novel Hydrothermal Route," *Nanotechnology*, vol. 15, pp. 1428-1432, 2004.
[119] Y. W. Tan, X. Y. Xue, Q. Peng, H. Zhao, T. H. Wang, and Y. D. Li, "Controllable Fabrication And Electrical Performance of Single Crystalline Cu_2O Nanowires With High Aspect Ratios," *Nano Lett.*, vol. 7, pp. 3723-3728, 2007.
[120] X. Wang, G. Xi, S. Xiong, Y. Liu, B. Xi, W. Yu, *et al.*, "Solution-Phase Synthesis of Single-Crystal CuO Nanoribbons and Nanorings," *Cryst. Growth Des*, vol. 7, pp. 930-934, 2007.
[121] M. H. Cao, C. W. Hu, Y. H. Wang, Y. H. Guo, C. X. Guo, and E. B. Wang, "A Controllable Synthetic Route to Cu, Cu_2O, and CuO Nanotubes and Nanorods," *Chem. Commun.*, pp. 1884-1885, 2003.
[122] C. Yang, X. Su, F. Xiao, J. Jian, and J. Wang, "Gas Sensing Properties of CuO Nanorods Synthesized by A Microwave-Assisted Hydrothermal Method," *Sens. Actuator B Chem.*, vol. 158, pp. 299-303, 2011.
[123] Z. H. Yang, J. Xu, W. X. Zhang, A. P. Liu, and S. P. Tang, "Controlled Synthesis of CuO Nanostructures by A Simple Solution Route," *J. Solid State Chem.*, vol. 180, pp. 1390-1396, 2007.
[124] L. Liu, K. Hong, T. Hu, and M. Xu, "Synthesis of Aligned Copper Oxide Nanorod Arrays by A Seed Mediated Hydrothermal Method," *J. Alloy Comp.*, vol. 511, pp. 195-197, 2012.
[125] H. Yu, J. Yu, S. Liu, and S. Mann, "Template-Free Hydrothermal Synthesis of CuO/Cu_2O Composite Hollow Microspheres," *Chem. Mater.*, vol. 19, pp. 4327-4334, 2007.
[126] Z. Z. Chen, E. W. Shi, Y. Q. Zheng, W. J. Li, B. Xiao, and J. Y. Zhuang, "Growth of Hex-Pod-Like Cu_2O Whisker Under Hydrothermal Conditions," *J. Cryst. Growth*, vol. 249, pp. 294-300, 2003.
[127] S. M. Gupta and M. Tripathi, "A review on The Synthesis of TiO_2 Nanoparticles by Solution Route," *Cent. Eur. J. Chem.*, vol. 10, pp. 279-294, 2012.

[128] M. Rajamathi and R. Seshadri, "Oxide And Chalcogenide Nanoparticles From Hydrothermal/Solvothermal Reactions," *Curr. Opin. Solid St. M.*, vol. 6, pp. 337-345, 2002.
[129] G.-D. Yao, Z.-B. Huo, and F.-M. Jin, "Direct Reduction of Copper Oxide Into Copper Under Hydrothermal Conditions," *Res. Chem. Intermediat.*, vol. 37, pp. 351-358, 2011.
[130] L. Zhao, H. Chen, Y. Wang, H. Che, P. Gunawan, Z. Zhong, *et al.*, "Facile Solvothermal Synthesis of Phase-Pure Cu_4O_3 Microspheres and Their Lithium Storage Properties," *Chem. Mater.*, vol. 24, pp. 1136-1142, 2012.
[131] A. Aslani and V. Oroojpour, "CO Gas Sensing of CuO Nanostructures, Synthesized by an Assisted Solvothermal Wet Chemical Route," *Physica B*, vol. 406, pp. 144-149, 2011.
[132] A. Aslani, "Controlling The Morphology And Size of CuO Nanostructures With Synthesis by Solvo/Hydrothermal Method Without Any Additives," *Physica B*, vol. 406, pp. 150-154, 2011.
[133] X.-Y. Yu, R.-X. Xu, C. Gao, T. Luo, Y. Jia, J.-H. Liu, *et al.*, "Novel 3D Hierarchical Cotton-Candy-Like CuO: Surfactant-Free Solvothermal Synthesis and Application in As(III) Removal," *ACS Appl. Mater. Interfaces*, vol. 4, pp. 1954-1962, 2012.
[134] S. J. Chen, X. T. Chen, Z. L. Xue, L. H. Li, and X. Z. You, "Solvothermal Preparation of Cu_2O Crystalline Particles," *J. Cryst. Growth*, vol. 246, pp. 169-175, 2002.
[135] M. Vila, C. Diaz-Guerra, and J. Piqueras, "Optical And Magnetic Properties of CuO Nanowires Grown by Thermal Oxidation," *J. Phys. D Appl. Phys.*, vol. 43, 2010.
[136] M. Kaur, K. P. Muthe, S. K. Despande, S. Choudhury, J. B. Singh, N. Verma, *et al.*, "Growth and Branching of CuO Nanowires by Thermal Oxidation of Copper," *J. Cryst. Growth*, vol. 289, pp. 670-675, 2006.
[137] A. H. Jayatissa, K. Guo, and A. C. Jayasuriya, "Fabrication of Cuprous and Cupric Oxide Thin Films by Heat Treatment," *Appl. Surf. Sci.*, vol. 255, pp. 9474-9479, 2009.
[138] J. Liang, N. Kishi, T. Soga, and T. Jimbo, "Cross-Sectional Characterization of Cupric Oxide Nanowires Grown by Thermal Oxidation of Copper Foils," *Appl. Surf. Sci.*, vol. 257, pp. 62-66, 2010.
[139] A. O. Musa, T. Akomolafe, and M. J. Carter, "Production of Cuprous Oxide, A Solar Cell Material, by Thermal Oxidation And A Study of Its Physical And Electrical Properties," *Sol. Energ. Mat. Sol. C.*, vol. 51, pp. 305-316, 1998.
[140] G. Filipic and U. Cvelbar, "Copper Oxide Nanowires: A Review of Growth," *Nanotechnology*, vol. 23, 2012.
[141] L. Armelao, D. Barreca, M. Bertapelle, G. Bottaro, C. Sada, and E. Tondello, "A Sol-Gel Approach to Nanophasic Copper Oxide Thin Films," *Thin Solid Films*, vol. 442, pp. 48-52, 2003.
[142] S. C. Ray, "Preparation of Copper Oxide Thin Film by The Sol-Gel-Like Dip Technique And Study of Their Structural And Optical Properties," *Sol. Energ. Mat. Sol. C.*, vol. 68, pp. 307-312, 2001.
[143] C.-T. Hsieh, J.-M. Chen, H.-H. Lin, and H.-C. Shih, "Synthesis of Well-Ordered CuO Nanofibers by a Self-Catalytic Growth Mechanism," *Appl. Phys. Lett.*, vol. 82, pp. 3316-3318, 2003.

[144] Y.-k. Su, C.-m. Shen, H.-t. Yang, H.-l. Li, and H.-j. Gao, "Controlled Synthesis of Highly Ordered CuO Nanowire Arrays by Template-Based Sol-Gel Route," *T. Nonferr. Metal Soc.,* vol. 17, pp. 783-786, 2007.
[145] X. Hong, G. Wang, W. Zhu, X. Shen, and Y. Wang, "Synthesis of Sub-10 nm Cu_2O Nanowires by Poly(vinyl pyrrolidone)-Assisted Electrodeposition," *J. Phys. Chem. C,* vol. 113, pp. 14172-14175, 2009.
[146] H. Wu, D. Lin, and W. Pan, "Fabrication, Assembly, And Electrical Characterization of CuO Nanofibers," *Appl. Phys. Lett.,* vol. 89, pp. 133125-133123, 2006.
[147] S. M. Sze and K. K. Ng, *Physics of Semiconductor Devices*. New Jersey: John Wiley and Sons, 2007.
[148] S. Ishizuka and K. Akimoto, "Control of The Growth Orientation And Electrical Properties of Polycrystalline Cu_2O Thin Films by Group-IV Elements Doping," *Appl. Phys. Lett.,* vol. 85, pp. 4920-4922, 2004.
[149] R. P. Wijesundera, "Fabrication of The CuO/Cu_2O Heterojunction Using An Electrodeposition Technique For Solar Cell Applications," *Semicond. Sci. Tech.,* vol. 25, 2010.
[150] Y. Hames and S. E. San, "CdO/Cu_2O Solar Cells by Chemical Deposition," *Sol. Energy,* vol. 77, pp. 291-294, 2004.
[151] D. Li, C.-J. Chien, S. Deora, P.-C. Chang, E. Moulin, and J. G. Lu, "Prototype of a Scalable Core-Shell Cu_2O/TiO_2 Solar Cell," *Chem. Phys. Lett.,* vol. 501, pp. 446-450, 2011.
[152] A. R. Zainun, S. Tomoya, U. Mohd Noor, M. Rusop, and I. Masaya, "New Approach For Generating Cu_2O/TiO_2 Composite Films For Solar Cell Applications," *Mater. Lett.,* vol. 66, pp. 254-256, 2012.
[153] M. Wang, L. Sun, Z. Lin, J. Cai, K. Xie, and C. Lin, "P-N Heterojunction Photoelectrodes Composed of Cu_2O-Loaded TiO_2 Nanotube Arrays With Enhanced Photoelectrochemical And Photoelectrocatalytic Activities," *Energ. Environ. Sci.,* vol. 6, pp. 1211-1220, 2013.
[154] T. Minami, Y. Nishi, and T. Miyata, "High-Efficiency Cu_2O-Based Heterojunction Solar Cells Fabricated Using a Ga_2O_3 Thin Film as N-Type Layer," *Appl. Phys. Express,* vol. 6, 2013.
[155] K. P. Musselman, A. Wisnet, D. C. Iza, H. C. Hesse, C. Scheu, J. L. MacManus-Driscoll, *et al.*, "Strong Efficiency Improvements in Ultra-low-Cost Inorganic Nanowire Solar Cells," *Adv. Mater.,* vol. 22, pp. E254-E285, 2010.
[156] T. Minami, Y. Nishi, T. Miyata, and J. Nomoto, "High-Efficiemcy Oxide Solar Cells with ZnO/Cu_2O Heterjunction Fabricated on Thermally Oxidized Cu_2O sheets," *Appl. Phys. Express,* vol. 4, p. 62301, 2011.
[157] P. Raksa, S. Nilphai, A. Gardchareon, and S. Choopun, "Copper Oxide Thin Film and Nanowire As A Barrier in ZnO Dye-Sensitized Solar Cells," *Thin Solid Films,* vol. 517, pp. 4741-4744, 2009.
[158] M. H. Kim and Y. U. Kwon, "Semiconducting Divalent Metal Oxides as Blocking Layer Material for SnO_2-Based Dye-Sensitized Solar Cells," *J. Phys. Chem. C,* vol. 115, pp. 23120-23125, 2011.
[159] R. Sahay, J. Sundaramurthy, P. S. Kumar, V. Thavasi, S. G. Mhaisalkar, and S. Ramakrishna, "Synthesis And Characterization of CuO Nanofibers, And Investigation For Its Suitability As Blocking Layer in ZnO NPs Based Dye Sensitized Solar Cell And As Photocatalyst In Organic Dye Degradation," *J. Solid State Chem.,* vol. 186, pp. 261-267, 2012.

[160] S. Anandan, X. G. Wen, and S. H. Yang, "Room Temperature Growth of CuO Nanorod Arrays on Copper And Their Application As A Cathode In Dye-Sensitized Solar Cells," *Mater. Chem. Phys.*, vol. 93, pp. 35-40, 2005.
[161] H.-S. Koo, D.-T. Wang, Y.-K. Yu, S.-H. Ho, J.-Y. Jhang, M. Chen, *et al.*, "Effect of Cu_2O Doping in TiO_2 Films on Device Performance of Dye-Sensitized Solar Cells," *Jpn. J. Appl. Phys.*, vol. 51, 2012.
[162] G. B. Murdoch, M. Greiner, M. G. Helander, Z. B. Wang, and Z. H. Lu, "A Comparison of CuO and Cu_2O Hole-Injection Layers for Low Voltage Organic Devices," *Appl. Phys. Lett.*, vol. 93, 2008.
[163] W. P. Hu, K. Manabe, T. Furukawa, and M. Matsumura, "Lowering of Operational Voltage of Organic Electroluminescent Devices by Coating Indium-Tin-Oxide Electrodes With a Thin CuO_x Layer," *Appl. Phys. Lett.*, vol. 80, pp. 2640-2641, 2002.
[164] T. Satoh and H. Fujikawa, "Copper-Doped Indium Tin Oxide Electrode For Organic Light-Emitting Devices," *Jpn. J. Appl. Phys. 1*, vol. 46, pp. 1640-1642, 2007.
[165] Z. Zheng, B. Huang, Z. Wang, M. Guo, X. Qin, X. Zhang, *et al.*, "Crystal Faces of Cu_2O and Their Stabilities in Photocatalytic Reactions," *J. Phys. Chem. C*, vol. 113, pp. 14448-14453, 2009.
[166] M. Vaseem, A. Umar, Y. B. Hahn, D. H. Kim, K. S. Lee, J. S. Jang, *et al.*, "Flower-Shaped CuO Nanostructures: Structural, Photocatalytic And XANES Studies," *Catal. Commun.*, vol. 10, pp. 11-16, 2008.
[167] S. P. Meshram, P. V. Adhyapak, U. P. Mulik, and D. P. Amalnerkar, "Facile Synthesis of CuO Nanomorphs And Their Morphology Dependent Sunlight Driven Photocatalytic Properties," *Chem. Eng. J.*, vol. 204–206, pp. 158-168, 2012.
[168] H. Xu, G. Zhu, D. Zheng, C. Xi, X. Xu, and X. Shen, "Porous CuO Superstructure: Precursor-Mediated Fabrication, Gas Sensing and Photocatalytic Properties," *J. Colloid Interf. Sci.*, vol. 383, pp. 75-81, 2012.
[169] J. Liu, J. Jin, Z. Deng, S.-Z. Huang, Z.-Y. Hu, L. Wang, *et al.*, "Tailoring CuO Nanostructures for Enhanced Photocatalytic Property," *J. Colloid Interf. Sci.*, vol. 384, pp. 1-9, 2012.
[170] M.-h. Yao, Y.-g. Tang, L. Zhang, H.-h. Yang, and J.-h. Yan, "Photocatalytic Activity of CuO Towards HER in Catalyst From Oxalic Acid Solution Under Simulated Sunlight Irradiation," *T. Nonferr. Metal Soc.*, vol. 20, pp. 1944-1949, 2010.
[171] M. Hara, T. Kondo, M. Komoda, S. Ikeda, K. Shinohara, A. Tanaka, *et al.*, "Cu_2O as a Photocatalyst for Overall Water Splitting Under Visible Light Irradiation," *Chem. Commun.*, pp. 357-358, 1998.
[172] P. E. de Jongh, D. Vanmaekelbergh, and J. J. Kelly, "Cu_2O: A Catalyst For The Photochemical Decomposition of Water?," *Chem. Commun.*, pp. 1069-1070, 1999.
[173] G. K. Mor, O. K. Varghese, R. H. T. Wilke, S. Sharma, K. Shankar, T. J. Latempa, *et al.*, "P-Type Cu-Ti-O Nanotube Arrays And Their Use in Self-Biased Heterojunction Photoelectrochemical Diodes For Hydrogen Generation," *Nano Lett.*, vol. 8, pp. 1906-1911, 2008.
[174] W. Siripala, A. Ivanovskaya, T. F. Jaramillo, S. H. Baeck, and E. W. McFarland, "A Cu_2O/TiO_2 Heterojunction Thin Film Cathode For Photoelectrocatalysis," *Sol. Energ. Mat. Sol. C.*, vol. 77, pp. 229-237, 2003.

[175] M. Ni, M. K. H. Leung, D. Y. C. Leung, and K. Sumathy, "A Review And Recent Developments in Photocatalytic Water-Splitting Using TiO_2 For Hydrogen Production," *Renew. Sust. Energ. Rev.*, vol. 11, pp. 401-425, 2007.
[176] N. Strataki, V. Bekiari, D. I. Kondarides, and P. Lianos, "Hydrogen Production by Photocatalytic Alcohol Reforming Employing Highly Efficient Nanocrystalline Titania Films," *Appl. Catal. B-Environ.*, vol. 77, pp. 184-189, 2007.
[177] J. Bandara, C. P. K. Udawatta, and C. S. K. Rajapakse, "Highly Stable CuO Incorporated TiO_2 Catalyst for Photocatalytic Hydrogen Production from H_2O," *Photochem. Photobio. S.*, vol. 4, pp. 857-861, 2005.
[178] S. Song, J. Tu, L. Xu, X. Xu, Z. He, J. Qiu, *et al.*, "Preparation of A Titanium Dioxide Photocatalyst Codoped With Cerium And Iodine and Its Performance In The Degradation Of Oxalic Acid," *Chemosphere*, vol. 73, pp. 1401-1406, 2008.
[179] H. Yang, J. Yan, Z. Lu, X. Cheng, and Y. Tang, "Photocatalytic Activity Evaluation of Tetragonal $CuFe_2O_4$ Nanoparticles For the H_2 Evolution Under Visible Light Irradiation," *J. Alloy Compd.*, vol. 476, pp. 715-719, 2009.
[180] P. Demchick and A. L. Koch, "The Permeability of the Wall Fabric of Escherichia Coli and Bacillus Subtilis," *J. Bacteriol.*, vol. 178, pp. 768-773, 1996.
[181] K. A. Brogden, "Antimicrobial Peptides: Pore Formers or Metabolic Inhibitors in Bacteria?," *Nature Reviews Microbiology*, vol. 3, pp. 238-250, 2005.
[182] O. Akhavan and E. Ghaderi, "Cu and CuO Nanoparticles Immobilized by Silica Thin Films as Antibacterial Materials and Photocatalysts," *Surf. Coat. Tech.*, vol. 205, pp. 219-223, 2010.
[183] A. Azam, A. S. Ahmed, M. Oves, M. S. Khan, and A. Memic, "Size-Dependent Antimicrobial Properties of CuO Nanoparticles Against Gram-Positive and -Negative Bacterial Strains," *Int. J. Nanomed.*, vol. 7, pp. 3527-3535, 2012.
[184] N. Ekthammathat, T. Thongtem, and S. Thongtem, "Antimicrobial Activities of CuO Films Deposited on Cu Foils by Solution Chemistry," *Appl. Surf. Sci.*, vol. 277, pp. 211-217, 2013.
[185] M. S. Hassan, T. Amna, O. B. Yang, M. H. El-Newehy, S. S. Al-Deyab, and M.-S. Khil, "Smart Copper Oxide Nanocrystals: Synthesis, Characterization, Electrochemical and Potent Antibacterial Activity," *Colloid Surface B*, vol. 97, pp. 201-206, 2012.
[186] I. Perelshtein, G. Applerot, N. Perkas, E. Wehrschuetz-Sigl, A. Hasmann, G. Guebitz, *et al.*, "CuO–Cotton Nanocomposite: Formation, Morphology, And Antibacterial Activity," *Surf. Coat. Tech.*, vol. 204, pp. 54-57, 2009.
[187] G. Ren, D. Hu, E. W. C. Cheng, M. A. Vargas-Reus, P. Reip, and R. P. Allaker, "Characterisation Of Copper Oxide Nanoparticles For Antimicrobial Applications," *Int. J. Antimicrob. Ag.*, vol. 33, pp. 587-590, 2009.
[188] M. Paschoalino, N. C. Guedes, W. Jardim, E. Mieluarski, J. A. Mielczarski, P. Bowen, *et al.*, "Inactivation of E-Coli Mediated by High Surface Area CuO Accelerated by Light Irradiation > 360 nm," *J. Photoch. Photobio. A*, vol. 199, pp. 105-111, 2008.
[189] B. Wang, X.-L. Wu, C.-Y. Shu, Y.-G. Guo, and C.-R. Wang, "Synthesis of CuO/Graphene Nanocomposite As A High-Performance Anode Material for Lithium-Ion Batteries," *J. Mater. Chem.*, vol. 20, pp. 10661-10664, 2010.

[190] J. Y. Xiang, J. P. Tu, L. Zhang, Y. Zhou, X. L. Wang, and S. J. Shi, "Self-Assembled Synthesis of Hierarchical Nanostructured CuO With Various Morphologies And Their Application as Anodes For Lithium Ion Batteries," *J. Power Sources,* vol. 195, pp. 313-319, 2010.
[191] L. Ji, Z. Lin, M. Alcoutlabi, and X. Zhang, "Recent Developments in Nanostructured Anode Materials for Rechargeable Lithium-Ion Batteries," *Energ. Environ. Sci.,* vol. 4, pp. 2682-2699, 2011.
[192] Y. J. Mai, X. L. Wang, J. Y. Xiang, Y. Q. Qiao, D. Zhang, C. D. Gu, *et al.*, "CuO/Graphene Composite as Anode Materials For Lithium-Ion Batteries," *Electrochim. Acta,* vol. 56, pp. 2306-2311, 2011.
[193] J. Zhou, L. Ma, H. Song, B. Wu, and X. Chen, "Durable High-Rate Performance of CuO Hollow Nanoparticles/Graphene-Nanosheet Composite Anode Material For Lithium-Ion Batteries," *Electrochem. Commun.,* vol. 13, pp. 1357-1360, 2011.
[194] J. C. Park, J. Kim, H. Kwon, and H. Song, "Gram-Scale Synthesis of Cu_2O Nanocubes and Subsequent Oxidation to CuO Hollow Nanostructures for Lithium-Ion Battery Anode Materials," *Adv. Mater.,* vol. 21, pp. 803-+, 2009.
[195] W. Wei, Z. Wang, Z. Liu, Y. Liu, L. He, D. Chen, *et al.*, "Metal Oxide Hollow Nanostructures: Fabrication And Li Storage Performance," *J. Power Sources,* vol. 238, pp. 376-387, 2013.
[196] R. Neskovska, M. Ristova, J. Velevska, and M. Ristov, "Electrochromism of The Electroless Deposited Cuprous Oxide Films," *Thin Solid Films,* vol. 515, pp. 4717-4721, 2007.
[197] M. Ristova, R. Neskovska, and V. Mirčeski, "Chemically Deposited Electrochromic Cuprous Oxide Films For Solar Light Modulation," *Sol. Energ. Mater. Sol. C.,* vol. 91, pp. 1361-1365, 2007.
[198] T. J. Richardson, J. L. Slack, and M. D. Rubin, "Electrochromism in Copper Oxide Thin Films," *Electrochim. Acta,* vol. 46, pp. 2281-2284, 2001.
[199] O. Akhavan, H. Tohidi, and A. Z. Moshfegh, "Synthesis and Electrochromic Study of Sol–Gel Cuprous Oxide Nanoparticles Accumulated on Silica Thin Film," *Thin Solid Films,* vol. 517, pp. 6700-6706, 2009.
[200] J. Z. Ou, S. Balendhran, M. R. Field, D. G. McCulloch, A. S. Zoolfakar, R. A. Rani, *et al.*, "The Anodized Crystalline WO_3 Nanoporous Network With Enhanced Electrochromic Properties," *Nanoscale,* vol. 4, pp. 5980-5988, 2012.
[201] T. Y. Zhai, X. S. Fang, M. Y. Liao, X. J. Xu, H. B. Zeng, B. Yoshio, *et al.*, "A Comprehensive Review of One-Dimensional Metal-Oxide Nanostructure Photodetectors," *Sensors,* vol. 9, pp. 6504-6529, 2009.
[202] S. B. Wang, C. H. Hsiao, S. J. Chang, K. T. Lam, K. H. Wen, S. C. Hung, *et al.*, "A CuO Nanowire Infrared Photodetector," *Sens. Actuator A Phys.,* vol. 171, pp. 207-211, 2011.
[203] L. Liao, B. Yan, Y. F. Hao, G. Z. Xing, J. P. Liu, B. C. Zhao, *et al.*, "P-type Electrical, Photoconductive, and Anomalous Ferromagnetic Properties of Cu_2O Nanowires," *Appl. Phys. Lett.,* vol. 94, 2009.
[204] S. Sahoo, S. Husale, B. Colwill, T.-M. Lu, S. Nayak, and P. M. Ajayan, "Electric Field Directed Self-Assembly of Cuprous Oxide Nanostructures for Photon Sensing," *ACS Nano,* vol. 3, pp. 3935-3944, 2009.
[205] A. Tricoli, M. Righettoni, and A. Teleki, "Semiconductor Gas Sensors: Dry Synthesis And Application," *Angew. Chem. Int. Edit.,* vol. 49, pp. 7632-7659, 2010.

[206] H. Kim, C. Jin, S. Park, S. Kim, and C. Lee, "H_2S Gas Sensing Properties of Bare and Pd-Functionalized CuO Nanorods," *Sens. Actuator B-Chem.*, vol. 161, pp. 594-599, 2012.
[207] X. Gou, G. Wang, J. Yang, J. Park, and D. Wexler, "Chemical Synthesis, Characterisation and Gas Sensing Performance of Copper Oxide Nanoribbons," *J. Mater. Chem.*, vol. 18, pp. 965-969, 2008.
[208] G. X. Zhu, H. Xu, Y. Y. Xiao, Y. J. Liu, A. H. Yuan, and X. P. Shen, "Facile Fabrication and Enhanced Sensing Properties of Hierarchically Porous CuO Architectures," *ACS Appl. Mater. Interfaces*, vol. 4, pp. 744-751, 2012.
[209] M. Ando, T. Kobayashi, and M. Haruta, "Combined Effects of Small Gold Particles on The Optical Gas Sensing by Transition Metal Oxide Films," *Catal. Today*, vol. 36, pp. 135-141, 1997.
[210] X.-W. Liu, F.-Y. Wang, F. Zhen, and J.-R. Huang, "In Situ Growth of Au Nanoparticles on The Surfaces of Cu_2O Nanocubes for Chemical Sensors With Enhanced Performance," *RSC Advances*, vol. 2, pp. 7647-7651, 2012.
[211] H. T. Hsueh, S. J. Chang, F. Y. Hung, W. Y. Weng, C. L. Hsu, T. J. Hsueh, *et al.*, "Ethanol Gas Sensor of Crabwise CuO Nanowires Prepared on Glass Substrate," *J. Electrochem. Soc.*, vol. 158, pp. J106-J109, 2011.
[212] D. D. Li, J. Hu, R. Q. Wu, and J. G. Lu, "Conductometric Chemical Sensor Based on Individual CuO Nanowires," *Nanotechnology*, vol. 21, 2010.
[213] Y. Zhang, X. He, J. Li, H. Zhang, and X. Gao, "Gas-Sensing Properties of Hollow And Hierarchical Copper Oxide Microspheres," *Sens. Actuator B Chem.*, vol. 128, pp. 293-298, 2007.
[214] H. G. Zhang, Q. S. Zhu, Y. Zhang, Y. Wang, L. Zhao, and B. Yu, "One-Pot Synthesis And Hierarchical Assembly of Hollow Cu_2O Microspheres With Nanocrystals-Composed Porous Multishell And Their Gas-Sensing Properties," *Adv. Funct. Mater.*, vol. 17, pp. 2766-2771, 2007.
[215] L. Liao, Z. Zhang, B. Yan, Z. Zheng, Q. L. Bao, T. Wu, *et al.*, "Multifunctional CuO Nanowire Devices: P-type Field Effect Transistors and CO Gas Sensors," *Nanotechnology*, vol. 20, 2009.
[216] Y.-S. Kim, I.-S. Hwang, S.-J. Kim, C.-Y. Lee, and J.-H. Lee, "CuO Nanowire Gas Sensors For Air Quality Control in Automotive Cabin," *Sens. Actuator B-Chem.*, vol. 135, pp. 298-303, 2008.
[217] F. Zhang, A. W. Zhu, Y. P. Luo, Y. Tian, J. H. Yang, and Y. Qin, "CuO Nanosheets for Sensitive and Selective Determination of H_2S with High Recovery Ability," *J. Phys. Chem. C*, vol. 114, pp. 19214-19219, 2010.
[218] J. T. Zhang, J. F. Liu, Q. Peng, X. Wang, and Y. D. Li, "Nearly Monodisperse Cu_2O and CuO Nanospheres: Preparation And Applications For Sensitive Gas Sensors," *Chem. Mater.*, vol. 18, pp. 867-871, 2006.
[219] T. Asefa, C. T. Duncan, and K. K. Sharma, "Recent Advances in Nanostructured Chemosensors and Biosensors," *Analyst*, vol. 134, pp. 1980-1990, 2009.
[220] S. Park, H. Boo, and T. D. Chung, "Electrochemical Non-Enzymatic Glucose Sensors," *Anal. Chim. Acta*, vol. 556, pp. 46-57, 2006.
[221] Z. J. Zhuang, X. D. Su, H. Y. Yuan, Q. Sun, D. Xiao, and M. M. F. Choi, "An Improved Sensitivity Non-Enzymatic Glucose Sensor Based On A CuO Nanowire Modified Cu Electrode," *Analyst*, vol. 133, pp. 126-132, 2008.
[222] L. Zhang, H. Li, Y. H. Ni, J. Li, K. M. Liao, and G. C. Zhao, "Porous Cuprous Oxide Microcubes For Non-Enzymatic Amperometric Hydrogen

Peroxide And Glucose Sensing," *Electrochem. Commun.*, vol. 11, pp. 812-815, 2009.

[223] C. Batchelor-McAuley, Y. Du, G. G. Wildgoose, and R. G. Compton, "The Use of copper(II) Oxide Nanorod Bundles for The Non-Enzymatic Voltammetric Sensing of Carbohydrates and Hydrogen Peroxide," *Sens. Actuators B: Chem.*, vol. 135, pp. 230-235, 2008.

[224] C. Batchelor-McAuley, G. G. Wildgoose, R. G. Compton, L. Shao, and M. L. H. Green, "Copper Oxide Nanoparticle Impurities Are Responsible For The Electroanalytical Detection of Glucose Seen Using Multiwalled Carbon Nanotubes," *Sens. Actuators B: Chem.*, vol. 132, pp. 356-360, 2008.

[225] Y. Y. Wu, W. C. Tsui, and T. C. Liu, "Experimental Analysis of Tribological Properties of Lubricating Oils With Nanoparticle Additives," *Wear*, vol. 262, pp. 819-825, 2007.

[226] A. H. Battez, R. Gonzalez, J. L. Viesca, J. E. Fernandez, J. M. D. Fernandez, A. Machado, *et al.*, "CuO, ZrO_2 and ZnO Nanoparticles as Antiwear Additive in Oil Lubricants," *Wear*, vol. 265, pp. 422-428, 2008.

[227] T. Oishi, M. Goto, A. Kasahara, and M. Tosa, "Low Frictional Copper Oxide Film Prepared With Sodium Hydroxide Solution," *Surf. Interface Anal.*, vol. 36, pp. 1259-1261, 2004.

[228] M. A. Kedzierski, "Viscosity and Density of CuO Nanolubricant," *Int. J. Refrig.*, vol. 35, pp. 1997-2002, 2012.

[229] S.-s. Bi, L. Shi, and L.-l. Zhang, "Application of Nanoparticles in Domestic Refrigerators," *Appl. Therm. Eng.*, vol. 28, pp. 1834-1843, 2008.

[230] S. Lee, S. U. S. Choi, S. Li, and J. A. Eastman, "Measuring Thermal Conductivity of Fluids Containing Oxide Nanoparticles," *J. Heat Trans-T Asme*, vol. 121, pp. 280-289, 1999.

[231] C. T. Hsieh, J. M. Chen, H. H. Lin, and H. C. Shih, "Field Emission From Various CuO Nanostructures," *Appl. Phys. Lett.*, vol. 83, pp. 3383-3385, 2003.

[232] Y. W. Zhu, T. Yu, F. C. Cheong, X. J. Xui, C. T. Lim, V. B. C. Tan, *et al.*, "Large-Scale Synthesis And Field Emission Properties of Vertically Oriented CuO Nanowire Films," *Nanotechnology*, vol. 16, pp. 88-92, 2005.

[233] Y. Wang, S. C. Li, H. Shi, and K. Yu, "Facile Synthesis of P-Type Cu_2O/N-Type ZnO Nano-Heterojunctions With Novel Photoluminescence Properties, Enhanced Field Emission And Photocatalytic Activities," *Nanoscale*, vol. 4, pp. 7817-7824, 2012.

[234] H. Shi, K. Yu, F. Sun, and Z. Zhu, "Controllable Synthesis of Novel Cu_2O Micro/Nano-Crystals And Their Photoluminescence, Photocatalytic And Field Emission Properties," *CrystEngComm*, vol. 14, pp. 278-285, 2012.

[235] R. C. Wang and C. H. Li, "Improved Morphologies and Enhanced Field Emissions of CuO Nanoneedle Arrays by Heating ZnO Coated Copper Foils," *Cryst. Growth Des.*, vol. 9, pp. 2229-2234, 2009.

[236] Y. Wang, K. Yu, H. H. Yin, C. Q. Song, Z. L. Zhang, S. C. Li, *et al.*, "Facile Synthesis, Enhanced Field Emission And Photocatalytic Activities of Cu_2O-TiO_2-ZnO Ternary Hetero-Nanostructures," *J. Phys. D Appl. Phys.*, vol. 46, 2013.

[237] S. Tanaka, Y. Sawai, and A. Chiba, "Electrical Properties And Microstructure of CuO Ceramics Containing Small Amounts of Alkaline Earth Elements," *J. Eur, Ceram. Soc.*, vol. 24, pp. 289-293, 2004.

[238] K. Krishnamoorthy and S.-J. Kim, "Growth, Characterization and Electrochemical Properties of Hierarchical CuO Nanostructures For Supercapacitor Applications," *Mater. Res. Bull.*, vol. 48, pp. 3136-3139, 2013.

[239] D. P. Dubal, G. S. Gund, C. D. Lokhande, and R. Holze, "CuO Cauliflowers For Supercapacitor Application: Novel Potentiodynamic Deposition," *Mater. Res. Bull.*, vol. 48, pp. 923-928, 2013.

[240] B. Singh, B. R. Mehta, D. Varandani, A. V. Savu, and J. Brugger, "CAFM Investigations of Filamentary Conduction in Cu_2O ReRAM Devices Fabricated Using Stencil Lithography Technique," *Nanotechnology,* vol. 23, 2012.

[241] A. Chen, S. Haddad, Y. C. Wu, Z. Lan, T. N. Fang, and S. Kaza, "Switching Characteristics of Cu_2O Metal-Insulator-Metal Resistive Memory," *Appl. Phys. Lett.*, vol. 91, 2007.

[242] W.-Y. Yang, W.-G. Kim, and S.-W. Rhee, "Radio Frequency Sputter Deposition of Single Phase Cuprous Oxide Using Cu_2O As A Target Material And Its Resistive Switching Properties," *Thin Solid Films,* vol. 517, pp. 967-971, 2008.

[243] I. Najdovski, P. Selvakannan, S. K. Bhargava, and A. P. O'Mullane, "Formation of Nanostructured Porous Cu-Au Surfaces: The Influence of Cationic Sites on (Electro)-Catalysis," *Nanoscale,* vol. 4, pp. 6298-6306, 2012.

[244] J. B. Reitz and E. I. Solomon, "Propylene Oxidation on Copper Oxide Surfaces: Electronic and Geometric Contributions to Reactivity and Selectivity," *J. Am. Chem. Soc.*, vol. 120, pp. 11467-11478, 1998.

[245] S. Song, R. Rao, H. Yang, and A. Zhang, "Cu_2O/MWCNTs Prepared by Spontaneous Redox: Growth Mechanism and Superior Catalytic Activity," *J. Phys. Chem. C,* vol. 114, pp. 13998-14003, 2010.

[246] Y. Xu, H. Wang, Y. Yu, L. Tian, W. Zhao, and B. Zhang, "Cu_2O Nanocrystals: Surfactant-Free Room-Temperature Morphology-Modulated Synthesis and Shape-Dependent Heterogeneous Organic Catalytic Activities," *J. Phys. Chem. C,* vol. 115, pp. 15288-15296, 2011.

[247] R. Prucek, L. Kvitek, A. Panacek, L. Vancurova, J. Soukupova, D. Jancik, *et al.*, "Polyacrylate-Assisted Synthesis of Stable Copper Nanoparticles and Copper(I) Oxide Nanocubes with High Catalytic Efficiency," *J. Mater. Chem.*, vol. 19, pp. 8463-8469, 2009.

[248] S. Zhuiykov, E. Kats, D. Marney, and K. Kalantar-zadeh, "Improved Antifouling Resistance of Electrochemical Water Quality Sensors Based on Cu_2O-doped RuO_2 Sensing Electrode," *Prog. Org. Coat.*, vol. 70, pp. 67-73, 2011.

[249] S. Zhuiykov and K. Kalantar-zadeh, "Development of Antifouling of Electrochemical Solid-State Dissolved Oxygen Sensors Based on Nanostructured $Cu_{0.4}Ru_{3.4}O_7$ + RuO_2 sensing electrodes," *Electrochim. Acta*, vol. 73, pp. 105-111, 2012.

[250] S. Zhuiykov, D. Marney, E. Kats, and K. Kalantar-Zadeh, "Potentiometric Solid-State Sensor for DO Measurement in Water Using Sub-Micron $Cu_{0.4}Ru_{3.4}O_7$ + RuO_2 sensing electrode," *Sens. Actuator B Chem.*, vol. 153, pp. 312-320, 2011.

[251] E. Fortunato, V. Figueiredo, P. Barquinha, E. Elamurugu, R. Barros, G. Goncalves, *et al.*, "Thin-Film Transistors Based on P-Type Cu_2O Thin Films Produced At Room Temperature," *Appl. Phys. Lett.*, vol. 96, 2010.
[252] X. Zou, G. Fang, L. Yuan, M. Li, W. Guan, and X. Zhao, "Top-Gate Low-Threshold Voltage P-Cu_2O Thin-Film Transistor Grown on SiO_2/Si Substrate Using a High-kappa HfON Gate Dielectric," *IEEE Electrn Device L.*, vol. 31, pp. 827-829, 2010.
[253] D. R. Sahu, C.-P. Liu, R.-C. Wang, C.-L. Kuo, and J.-L. Huang, "Growth and Application of ZnO Nanostructures," *Int. J. Appl. Ceram. Tec.*, vol. 10, pp. 814-838, 2013.
[254] Z. L. Wang, "Zinc Oxide Nanostructures: Growth, Properties and Applications," *J. Phys-Condens. Mat.*, vol. 16, pp. R829-R858, 2004.
[255] C. Klingshirn, "ZnO: From Basics Towards Applications," *Phys. Status Solidi B*, vol. 244, pp. 3027-3073, 2007.
[256] U. Ozgur, Y. I. Alivov, C. Liu, A. Teke, M. A. Reshchikov, S. Dogan, *et al.*, "A Comprehensive Review of ZnO Materials and Devices," *J. Appl. Phys.*, vol. 98, p. 041301, 2005.
[257] S. Limpijumnong and S. Jungthawan, "First-Principles Study of the Wurtzite-to-Rocksalt Homogeneous Transformation in ZnO: A Case of a Low-Transformation Barrier," *Phys. Rev. B*, vol. 70, 2004.
[258] F. Z. Aoumeur, K. Benkabou, and B. Belgoumène, "Structural and Dynamical Properties of ZnO in Zinc-Blende and Rocksalt Phases," *Physica B*, vol. 337, pp. 292-297, 2003.
[259] J. E. Jaffe, J. A. Snyder, Z. J. Lin, and A. C. Hess, "LDA and GGA Calculations for High-Pressure Phase Transitions in ZnO and MgO," *Phys. Rev. B*, vol. 62, pp. 1660-1665, 2000.
[260] N. A. Hill and U. Waghmare, "First-Principles Study of Strain-Electronic Interplay in ZnO: Stress and Temperature Dependence of the Piezoelectric Constants," *Phys. Rev. B*, vol. 62, pp. 8802-8810, 2000.
[261] J. E. Jaffe, R. Pandey, and A. B. Kunz, "Electronic-Structure of the Rock-Salt-Structure Semiconductors ZnO AND CdO," *Phys. Rev. B*, vol. 43, pp. 14030-14034, 1991.
[262] J. L. Martins, N. Troullier, and S. H. Wei, "Pseudopotential Plane-Wave Calculations For ZNS," *Phys. Rev. B*, vol. 43, pp. 2213-2217, 1991.
[263] S. H. Wei and A. Zunger, "Role of Metal D-States In II-VI Semiconductors," *Phys. Rev. B*, vol. 37, pp. 8958-8981, 1988.
[264] Y. N. Xu and W. Y. Ching, "Electronic, Optical, And Structural-Properties of Some Wurtzite Crystals," *Phys. Rev. B*, vol. 48, pp. 4335-4351, 1993.
[265] J. F. Muth, R. M. Kolbas, A. K. Sharma, S. Oktyabrsky, and J. Narayan, "Excitonic Structure And Absorption Coefficient Measurements of ZnO Single Crystal Epitaxial Films Deposited by Pulsed Laser Deposition," *J. Appl. Phys.*, vol. 85, pp. 7884-7887, 1999.
[266] C. Boemare, T. Monteiro, M. J. Soares, J. G. Guilherme, and E. Alves, "Photoluminescence Studies in ZnO Samples," *Physica B*, vol. 308, pp. 985-988, 2001.
[267] K. Thonke, T. Gruber, N. Teofilov, R. Schonfelder, A. Waag, and R. Sauer, "Donor-Acceptor Pair Transitions in ZnO Substrate Material," *Physica B*, vol. 308, pp. 945-948, 2001.

[268] D. C. Reynolds, D. C. Look, B. Jogai, C. W. Litton, G. Cantwell, and W. C. Harsch, "Valence-Band Ordering in ZnO," *Phys. Rev. B,* vol. 60, pp. 2340-2344, 1999.
[269] P. D. Yang, H. Q. Yan, S. Mao, R. Russo, J. Johnson, R. Saykally, *et al.*, "Controlled Growth of ZnO Nanowires And Their Optical Properties," *Adv. Funct. Mater.*, vol. 12, pp. 323-331, 2002.
[270] C. Y. Zhang, X. M. Li, J. M. Bian, W. D. Yu, and X. D. Gao, "Structural And Electrical Properties of Nitrogen And Aluminum Codoped P-Type ZnO Films," *Solid State Commun.,* vol. 132, pp. 75-78, 2004.
[271] J. D. Albrecht, P. P. Ruden, S. Limpijumnong, W. R. L. Lambrecht, and K. F. Brennan, "High Field Electron Transport Properties of Bulk ZnO," *J. Appl. Phys.,* vol. 86, pp. 6864-6867, 1999.
[272] D. C. Look, D. C. Reynolds, J. R. Sizelove, R. L. Jones, C. W. Litton, G. Cantwell, *et al.*, "Electrical Properties of Bulk ZnO," *Solid State Commun.*, vol. 105, pp. 399-401, 1998.
[273] T. Shinagawa, M. Chigane, K. Murase, and M. Izaki, "Drastic Change in Electrical Properties of Electrodeposited ZnO: Systematic Study by Hall Effect Measurements," *J. Phys. Chem. C,* vol. 116, pp. 15925-15931, 2012.
[274] A. Janotti and C. G. Van de Walle, "Fundamentals of Zinc Oxide as a Semiconductor," *Rep. Prog. Phys.*, vol. 72, 2009.
[275] P. K. Baviskar, P. R. Nikam, S. S. Gargote, A. Ennaoui, and B. R. Sankapal, "Controlled Synthesis of ZnO Nanostructures with Assorted Morphologies via Simple Solution Chemistry," *J. Alloy Compd.,* vol. 551, pp. 233-242, 2013.
[276] Z. Y. Fan and J. G. Lu, "Zinc Oxide Nanostructures: Synthesis and Properties," *J. Nanosci. Nanotechno.*, vol. 5, pp. 1561-1573, 2005.
[277] K. Ellmer, "Magnetron Sputtering of Transparent Conductive Zinc Oxide: Relation Between the Sputtering Parameters and the Electronic Properties," *J. Phys. D Appl. Phys.,* vol. 33, pp. R17-R32, 2000.
[278] R. Triboulet and J. Perrière, "Epitaxial Growth of ZnO films," *Prog. Cryst. Growth Ch.,* vol. 47, pp. 65-138, 2003.
[279] M. Izaki and T. Omi, "Transparent Zinc Oxide films Prepared by Electrochemical Reaction," *Appl. Phys. Lett.,* vol. 68, pp. 2439-2440, 1996.
[280] S. Peulon and D. Lincot, "Cathodic Electrodeposition From Aqueous Solution of Dense or Open-Structured Zinc Oxide Films," *Adv. Mater.,* vol. 8, pp. 166-&, 1996.
[281] S. Xu and Z. L. Wang, "One-Dimensional ZnO Nanostructures: Solution Growth and Functional Properties," *Nano Res.,* vol. 4, pp. 1013-1098, 2011.
[282] I. Gurrappa and L. Binder, "Electrodeposition of Nanostructured Coatings and Their Characterization-A Review," *Sci. Technol. Adv. Mat.,* vol. 9, 2008.
[283] B. J. Plowman, S. K. Bhargava, and A. P. O'Mullane, "Electrochemical Fabrication of Metallic Nanostructured Electrodes for Electroanalytical Applications," *Analyst,* vol. 136, pp. 5107-5119, 2011.
[284] R. Chander and A. K. Raychaudhuri, "Electrodeposition of Aligned Arrays of ZnO Nanorods in Aqueous Solution," *Solid State Commun.,* vol. 145, pp. 81-85, 2008.
[285] A. Chatterjee and J. Foord, "Electrochemical Deposition of Nanocrystalline Zinc Oxide at Conductive Diamond Electrodes," *Diam. Relat. Mater.,* vol. 15, pp. 664-667, 2006.

[286] L. Li, S. Pan, X. Dou, Y. Zhu, X. Huang, Y. Yang, *et al.*, "Direct Electrodeposition of ZnO Nanotube Arrays in Anodic Alumina Membranes," *J. Phys. Chem. C*, vol. 111, pp. 7288-7291, 2007.
[287] J. Cembrero and D. Busquets-Mataix, "ZnO Crystals Obtained by Electrodeposition: Statistical Analysis of Most Important Process Variables," *Thin Solid Films*, vol. 517, pp. 2859-2864, 2009.
[288] L. Xu, Q. Chen, and D. Xu, "Hierarchical ZnO Nanostructures Obtained by Electrodeposition," *J. Phys. Chem. C*, vol. 111, pp. 11560-11565, 2007.
[289] O. Lupan, V. M. Guerin, I. M. Tiginyanu, V. V. Ursaki, L. Chow, H. Heinrich, *et al.*, "Well-Aligned Arrays of Vertically Oriented ZnO Nanowires Electrodeposited on ITO-Coated Glass And Their Integration in Dye Sensitized Solar Cells," *J. Photoch. Photobio. A*, vol. 211, pp. 65-73, 2010.
[290] M. Ahmad and J. Zhu, "ZnO Based Advanced Functional Nanostructures: Synthesis, Properties and Applications," *J. Mater. Chem.*, vol. 21, pp. 599-614, 2011.
[291] M. S. White, D. C. Olson, S. E. Shaheen, N. Kopidakis, and D. S. Ginley, "Inverted Bulk-Heterojunction Organic Photovoltaic Device Using A Solution-Derived ZnO Underlayer," *Appl. Phys. Lett.*, vol. 89, 2006.
[292] A. K. K. Kyaw, X. W. Sun, C. Y. Jiang, G. Q. Lo, D. W. Zhao, and D. L. Kwong, "An Inverted Organic Solar Cell Employing A Sol-Gel Derived ZnO Electron Selective Layer And Thermal Evaporated MoO_3 Hole Selective Layer," *Appl. Phys. Lett.*, vol. 93, 2008.
[293] I. Gonzalez-Valls and M. Lira-Cantu, "Vertically-Aligned Nanostructures Of ZnO For Excitonic Solar Cells: A Review," *Energ. Environ. Sci.*, vol. 2, pp. 19-34, 2009.
[294] L. E. Greene, M. Law, B. D. Yuhas, and P. Yang, "ZnO-TiO2 Core-Shell Nanorod/P_3HT Solar Cells," *J. Phys. Chem. C*, vol. 111, pp. 18451-18456, 2007.
[295] M. Law, L. E. Greene, J. C. Johnson, R. Saykally, and P. D. Yang, "Nanowire Dye-Sensitized Solar Cells," *Nat. Mater.*, vol. 4, pp. 455-459, 2005.
[296] M. Law, L. E. Greene, A. Radenovic, T. Kuykendall, J. Liphardt, and P. Yang, "ZnO-Al_2O_3 and ZnO-TiO_2 Core-Shell Nanowire Dye-Sensitized Solar Cells," *J. Phys. Chem. B*, vol. 110, pp. 22652-22663, 2006.
[297] N. O. V. Plank, H. J. Snaith, C. Ducati, J. S. Bendall, L. Schmidt-Mende, and M. E. Welland, "A Simple Low Temperature Synthesis Route for ZnO-MgO Core-Shell Nanowires," *Nanotechnology*, vol. 19, 2008.
[298] C. Levy-Clement, R. Tena-Zaera, M. A. Ryan, A. Katty, and G. Hodes, "CdSe-Sensitized P-CuSCN/Nanowire N-ZnO Heterojunctions," *Adv. Mater.*, vol. 17, pp. 1512-1515, 2005.
[299] Q. Zhang, C. S. Dandeneau, X. Zhou, and G. Cao, "ZnO Nanostructures for Dye-Sensitized Solar Cells," *Adv. Mater.*, vol. 21, pp. 4087-4108, 2009.
[300] T. Jiang, T. Xie, Y. Zhang, L. Chen, L. Peng, H. Li, *et al.*, "Photoinduced Charge Transfer in ZnO/Cu_2O Heterostructure Films Studied by Surface Photovoltage Technique," *Phys. Chem. Chem. Phys.*, vol. 12, pp. 15476-15481, 2010.
[301] A. Mittiga, E. Salza, F. Sarto, M. Tucci, and R. Vasanthi, "Heterojunction Solar Cell with 2% Efficiency Based on a Cu_2O Substrate," *Appl. Phys. Lett.*, vol. 88, p. 163502, 2006.

[302] E. W. Bohannan, L. Y. Huang, F. S. Miller, M. G. Shumsky, and J. A. Switzer, "In Situ Electrochemical Quartz Crystal Microbalance Study of Potential Oscillations During the Electrodeposition of Cu/Cu_2O Layered Nanostructures," *Langmuir,* vol. 15, pp. 813-818, 1999.
[303] A. Roos and B. Karlsson, "Properties of Oxidized Copper Surfaces for Solar Applications II," *Sol. Energ. Mater.,* vol. 7, pp. 467-480, 1983.
[304] N. Kikuchi and K. Tonooka, "Electrical and Structural Properties of Ni-doped Cu_2O Films Prepared by Pulsed Laser Deposition," *Thin Solid Films,* vol. 486, pp. 33-37, 2005.
[305] D. A. Firmansyah, T. Kim, S. Kim, K. Sullivan, M. R. Zachariah, and D. Lee, "Crystalline Phase Reduction of Cuprous Oxide (Cu_2O) Nanoparticles Accompanied by a Morphology Change during Ethanol-Assisted Spray Pyrolysis," *Langmuir,* vol. 25, pp. 7063-7071, 2009.
[306] A. J. Morfa, G. Beane, B. Mashford, B. Singh, E. Della Gaspera, A. Martucci, *et al.*, "Fabrication of ZnO Thin Films from Nanocrystal Inks," *J. Phys. Chem. C,* vol. 114, pp. 19815-19821, 2010.
[307] C. L. Chu, H. C. Lu, C. Y. Lo, C. Y. Lai, and Y. H. Wang, "Physical Properties of Copper Oxide Thin Films Prepared by DC Reactive Magnetron Sputtering Under Different Oxygen Partial Pressures," *Physica B,* vol. 404, pp. 4831-4834, 2009.
[308] Y. M. Lu, J. Y. Chen, and T. S. Wey, "Nano Cuprous Oxides film Prepared by Magnetron Sputtering," *Mater. Res. Soc. Symp. P,* vol. 822, pp. 55-64, 2004.
[309] Y. M. Lu, W. S. Hwang, W. Y. Liu, and J. S. Yang, "Effect of RF Power on Optical and Electrical Properties of ZnO Thin Film by Magnetron Sputtering," *Mater. Chem. Phys.,* vol. 72, pp. 269-272, 2001.
[310] J. L. Campbell, M. Breedon, K. Latham, and K. Kalantar-zadeh, "Electrowetting of Superhydrophobic ZnO Nanorods," *Langmuir,* vol. 24, pp. 5091-5098, 2008.
[311] S. S. Jeong, A. Mittiga, E. Salza, A. Masci, and S. Passerini, "Electrodeposited ZnO/Cu_2O Heterojunction Solar Cells," *Electrochim. Acta,* vol. 53, pp. 2226-2231, 2008.
[312] V. Donderis, M. A. Hernández-Fenollosa, L. C. Damonte, B. Marí, and J. Cembrero, "Enhancement of Surface Morphology and Optical Properties of Nanocolumnar ZnO films," *Superlattice. Micros.,* vol. 42, pp. 461-467, 2007.
[313] X. J. Huang, O. Yarimaga, J. H. Kim, and Y. K. Choi, "Substrate Surface Roughness-Dependent 3-D Complex Nanoarchitectures of Gold Particles from Directed Electrodeposition," *J. Mater. Chem.,* vol. 19, pp. 478-483, 2009.
[314] A. I. Inamdar, S. H. Mujawar, S. B. Sadale, A. C. Sonavane, M. B. Shelar, P. S. Shinde, *et al.*, "Electrodeposited zinc oxide thin films: Nucleation and growth mechanism," *Sol. Energ. Mater. Sol. C.,* vol. 91, pp. 864-870, 2007.
[315] M. Breedon, J. Yu, W. Wlodarski, and K. Kalantar-Zadeh, "ZnO Nanostructured Arrays Grown from Aqueous Solutions on Different Substrates," presented at the 2008 International Conference on Nanoscience and Nanotechnology, 2008.
[316] S.-J. Park, J. Qiu, W. He, W. Namgung, Y.-D. Kim, J.-H. Lee, *et al.*, "Fabrication of Volmer-Weber Type ZnO Nanorods by Combining RF Sputtering and Hydrothermal Methods," *J. Nanosci. Nanotechno.,* vol. 9, pp. 6993-6997, 2009.

[317] R. B. Peterson, C. L. Fields, and B. A. Gregg, "Epitaxial chemical deposition of ZnO nanocolumns from NaOH," *Langmuir,* vol. 20, pp. 5114-5118, 2004.
[318] H. Zeng, J. Cui, B. Cao, U. Gibson, Y. Bando, and D. Golberg, "Electrochemical Deposition of ZnO Nanowire Arrays: Organization, Doping, and Properties," *Sci. Adv. Mater.,* vol. 2, pp. 336-358, 2010.
[319] H. Zeng, X. Xu, Y. Bando, U. K. Gautam, T. Zhai, X. Fang, *et al.*, "Template Deformation-Tailored ZnO Nanorod/Nanowire Arrays: Full Growth Control and Optimization of Field-Emission," *Adv. Funct. Mater.,* vol. 19, pp. 3165-3172, 2009.
[320] L. O. Chua, "Memristor - Missing Circuit Element," *IEEE T. Circuits Syst.,* vol. CT18, pp. 507-&, 1971.
[321] M. J. Kumar, "Memristor - Why Do We Have to Know About It," *IETE Tech. Rev.,* vol. 26, pp. 3-6, 2009.
[322] D. B. Strukov, G. S. Snider, D. R. Stewart, and R. S. Williams, "The Missing Memristor Found," *Nature,* vol. 453, pp. 80-83, 2008.
[323] R. Waser and M. Aono, "Nanoionics-based Resistive Switching Memories," *Nat. Mater.,* vol. 6, pp. 833-840, 2007.
[324] L. Chua, "Resistance Switching Memories are Memristors," *Appl. Phys. A-Mater.,* vol. 102, pp. 765-783, 2011.
[325] K. Szot, W. Speier, G. Bihlmayer, and R. Waser, "Switching the Electrical Resistance of Individual Dislocations in Single-Crystalline $SrTiO_3$," *Nat. Mater.,* vol. 5, pp. 312-320, 2006.
[326] Y. Watanabe, "Review of Resistance Switching of Ferroelectrics and Oxides in Quest for Unconventional Electronic Mechanisms," *Ferroelectrics,* vol. 349, pp. 190-209, 2007.
[327] J. J. Yang, M. D. Pickett, X. Li, D. A. A. Ohlberg, D. R. Stewart, and R. S. Williams, "Memristive Switching Mechanism for Metal/Oxide/Metal Nanodevices," *Nat. Nanotechnol.,* vol. 3, pp. 429-433, 2008.
[328] R. Waser, R. Dittmann, G. Staikov, and K. Szot, "Redox-Based Resistive Switching Memories - Nanoionic Mechanisms, Prospects, and Challenges," *Adv. Mater.,* vol. 21, pp. 2632-2663, 2009.
[329] N. Xu, L. F. Liu, X. Sun, C. Chen, Y. Wang, D. D. Han, *et al.*, "Bipolar Switching Behavior in TiN/ZnO/Pt Resistive Nonvolatile Memory With Fast Switching And Long Retention," *Semicon. Sci. Tech.,* vol. 23, p. 075019, 2008.
[330] N. Duraisamy, N. M. Muhammad, H.-C. Kim, J.-D. Jo, and K.-H. Choi, "Fabrication of TiO_2 Thin Film Memristor Device using Electrohydrodynamic Inkjet Printing," *Thin Solid Films,* vol. 520, pp. 5070-5074, 2012.
[331] J. J. Yang, F. Miao, M. D. Pickett, D. A. A. Ohlberg, D. R. Stewart, C. N. Lau, *et al.*, "The Mechanism of Electroforming of Metal Oxide Memristive Switches," *Nanotechnology,* vol. 20, p. 215201, 2009.
[332] M.-J. Lee, S. I. Kim, C. B. Lee, H. Yin, S.-E. Ahn, B. S. Kang, *et al.*, "Low-Temperature-Grown Transition Metal Oxide Based Storage Materials and Oxide Transistors for High-Density Non-volatile Memory," *Adv. Func. Mater.,* vol. 19, pp. 1587-1593, 2009.
[333] S. Seo, M. J. Lee, D. H. Seo, S. K. Choi, D. S. Suh, Y. S. Joung, *et al.*, "Conductivity Switching Characteristics and Reset Currents in NiO Films," *Appl. Phys. Lett.,* vol. 86, p. 093509, 2005.

[334] K. M. Kim, B. J. Choi, B. W. Koo, S. Choi, D. S. Jeong, and C. S. Hwang, "Resistive Switching in $Pt/Al_2O_3/TiO_2/Ru$ Stacked Structures," *Electrochem. Solid St.,* vol. 9, pp. G343-G346, 2006.
[335] S. Lee, W.-G. Kim, S.-W. Rhee, and K. Yong, "Resistance Switching Behaviors of Hafnium Oxide Films Grown by MOCVD for Nonvolatile Memory Applications," *J. Electrochem. Soc.,* vol. 155, pp. H92-H96, 2008.
[336] S.-Y. Wang, D.-Y. Lee, T.-Y. Huang, J.-W. Wu, and T.-Y. Tseng, "Controllable Oxygen Vacancies to Enhance Resistive Switching Performance in a ZrO_2-Based RRAM with Embedded Mo Layer," *Nanotechnology,* vol. 21, p. 495201, 2010.
[337] T. Tsuruoka, K. Terabe, T. Hasegawa, and M. Aono, "Forming and Switching Mechanisms of a Cation-Migration-Based Oxide Resistive Memory," *Nanotechnology,* vol. 21, p. 425205, 2010.
[338] K. Nagashima, T. Yanagida, K. Oka, and T. Kawai, "Unipolar Resistive Switching Characteristics of Room Temperature Grown SnO_2 Thin Films," *Appl. Phys. Lett.,* vol. 94, p. 242902, 2009.
[339] L. M. Kukreja, A. K. Das, and P. Misra, "Studies on Nonvolatile Resistance Memory Switching in ZnO Thin Films," *B. Mater. Sci.,* vol. 32, pp. 247-252, 2009.
[340] A. Shih, W. Zhou, J. Qiu, H.-J. Yang, S. Chen, Z. Mi, *et al.*, "Highly Stable Resistive Switching on Monocrystalline ZnO," *Nanotechnology,* vol. 21, p. 125201, 2010.
[341] C. M. Lieber, "One-Dimensional Nanostructures: Chemistry, Physics & Applications," *Solid State Commun.,* vol. 107, pp. 607-616, 1998.
[342] M. Janousch, G. I. Meijer, U. Staub, B. Delley, S. F. Karg, and B. P. Andreasson, "Role of Oxygen Vacancies in Cr-doped $SrTiO_3$ for Resistance-Change Memory," *Adv. Mater.,* vol. 19, pp. 2232-2235, 2007.
[343] Y. C. Yang, F. Pan, Q. Liu, M. Liu, and F. Zeng, "Fully Room-Temperature-Fabricated Nonvolatile Resistive Memory for Ultrafast and High-Density Memory Application," *Nano Lett.,* vol. 9, pp. 1636-1643, 2009.
[344] W.-Y. Chang, Y.-C. Lai, T.-B. Wu, S.-F. Wang, F. Chen, and M.-J. Tsai, "Unipolar Resistive Switching Characteristics of ZnO Thin Films for Nonvolatile Memory Applications," *Appl. Phys. Lett.,* vol. 92, p. 022110, 2008.
[345] Z. Ji, Q. Mao, and W. Ke, "Effects of Oxygen Partial Pressure on Resistive Switching Characteristics of ZnO Thin Films by DC Reactive Magnetron Sputtering," *Solid State Commun.,* vol. 150, pp. 1919-1922, 2010.
[346] S. Lee, H. Kim, D.-J. Yun, S.-W. Rhee, and K. Yong, "Resistive Switching Characteristics of ZnO Thin Film Grown on Stainless Steel for Flexible Nonvolatile Memory Devices," *Appl. Phys. Lett.,* vol. 95, p. 262113, 2009.
[347] P. Liu, G. She, W. Shi, and D. Chen, "Electric-Pulse-Induced Resistance Switching Observed in ZnO Nanotube Point Contact System," *Physica E,* vol. 42, pp. 791-794, 2010.
[348] J. W. Seo, J.-W. Park, K. S. Lim, J.-H. Yang, and S. J. Kang, "Transparent Resistive Random Access Memory and Its Characteristics for Nonvolatile Resistive Switching," *Appl. Phys. Lett.,* vol. 93, p. 223505, 2008.
[349] S. Kim, H. Moon, D. Gupta, S. Yoo, and Y.-K. Choi, "Resistive, Switching Characteristics of Sol-Gel Zinc Oxide Films for Flexible Memory Applications," *IEEE T. Electron Dev.,* vol. 56, pp. 696-699, 2009.

Chapter 3

Nanostructured Copper Oxides as Ethanol Vapour Sensors

3.1 Introduction

In this Chapter the PhD candidate presents the outcomes of his investigations on the development of Cu_xO semiconducting gas sensors. As presented in Chapter 1, the author of this thesis chose Cu_xO as a model *p*-type metal oxide with a plethora of information available regarding its properties and characteristics. The authors uses RF sputtering for depositing Cu_xO films which he will implement for alcohol vapour sensing. The author demonstrates as how changing the RF sputtering parameters including the sputtering power and target to sample distance are used for adjusting the stoichiometry of the deposited films from CuO to Cu_2O and how the grain dimensions can be modified using these tuning processes.

In the past two decades, tremendous efforts have taken place to enhance the performance of gas sensors based on semiconducting metal oxide films *via* incorporating nanomaterial into their structure [1-8]. As described in Chapter 1, the nanostructured metal oxide films are favorable due to their unique properties such as large surface area to volume ratio, presence of size effect (Debye length), and incorporation of various well-controlled dopants at different stoichiometry. These nanostructures are used with the aim of obtaining improved gas sensitivity and a rapid response [5, 9, 10].

In the family of metal oxide semiconductors, copper oxides (Cu_xO - cuprous oxide (Cu_2O) and cupric oxide (CuO)) are amongst the most promising materials for gas sensing due to their high absorption coefficients, favorable electronic structures

and earth-abundance [11, 12]. Copper oxides are intrinsic *p*-type semiconductors with relatively narrow energy band gaps of ~1.2 eV (CuO) and ~2.1 eV (Cu_2O) that exhibit a variety of interesting properties, which can be fully exploited in gas and vapour sensors, including ethanol vapour. Ethanol vapour sensors are extensively used in the fields of wine quality monitoring, breath analysis and food industries [13, 14].

Nanostructures of Cu_xO for ethanol vapour sensing can be prepared by several techniques such as thermal oxidation [15-17], hydrothermal [18-21], chemical vapour deposition [9], DC reactive magnetron sputtering [22, 23] and solvothermal techniques [24, 25]. However, amongst these techniques, RF magnetron sputtering has several advantages such as high control over the deposition parameters (e.g. thickness and uniformity). Additionally, a high degree of film engineering and tuning (crystallinity, morphology of the grains and their stoichiometry) is possible [26-29]. To the best of the author knowledge, to-date there have been no reports on nanostructured Cu_xO films for ethanol vapour sensing formed using the RF magnetron sputtering approach. The goal in this work is to demonstrate that RF magnetron sputtering can be applied as a deposition process for the fabrication of Cu_xO ethanol vapour sensors, and to provide an explanation of their mode of operation.

In this chapter, the author of this PhD thesis presents the synthesis and characterization of the RF sputtered Cu_xO films and investigates their ethanol vapour sensing performance. He will show that relatively low RF powers and substrate temperatures can be used for depositing single stoichiometry Cu_2O and CuO with the aim of producing nanostructures with well-engineered morphological sizes. The characterization analyses will be presented for CuO and Cu_2O films that were

conducted using scanning electron microscopy (SEM), X-ray diffraction (XRD), X-ray photospectroscopy (XPS), conductive atomic force microscopy (c–AFM) and Raman spectroscopy to assess their conditions. For the gas sensing characterizations, the author will present the outcomes using CuO and Cu_2O films based devices that were sputtered onto quartz substrates with pre-patterned gold interdigitated transducers (IDTs) and tested towards ethanol vapour.

The contents of this chapter were published as a full article in the journal *Sensors and Actuators B: Chemical.* [30]

3.2 Experimental

3.2.1 Deposition of nanostructured Cu_2O and CuO films

In the sputtering process, the target was copper of 4 inches diameter and 99.99% purity. The substrates were cleaned using acetone, isopropanol and deionized water to remove any organic contamination. The sputtering chamber was pumped to an ultimate background pressure of 10^{-5} Torr and the sputtering pressure increased to 20×10^{-3} Torr. For comparison, the sputtering RF power was set at different values ranging from 60 to 250 W. The argon and oxygen gas concentration ratio in the chamber was kept constant at 95% and 5%, respectively. The deposition duration was fixed at 9 minutes. The initial substrate temperature was 100 °C and the target to substrate distance was set at 43 mm. The substrates' temperature under this condition, however, gradually increased during the deposition and the final temperature at the end of the process was approximately 120 °C. The increase of the substrates' temperature was due to the relatively small substrate-to-target distance. At such short distances, the energy of the sputtered species, the heat of the plasma

formation and the thermal radiation from the target, may introduce energy flux near the substrates and possibly heat it up during the deposition process. [31]

3.2.2 Structural characterization

The crystallographic properties of the films were studied using XRD (Bruker D8 DISCOVER microdiffractometer fitted with a GADDS (General Area Detector Diffraction System). Data collected at room temperature using CuKα radiation (λ = 1.54178 Å) with a potential of 40 kV and a current of 40 mA, and filtered with a graphite monochromator in the parallel mode (175 mm collimator with 0.5 mm pinholes). In addition, SEM (FEI Nova NanoSEM), c−AFM (Bruker Multimode 8 with PF TUNA), Raman spectroscopy (Renishaw 1000 micro – Raman system) and XPS (VG 310F Scanning Auger Microscope (Nanoprobe)) were utilized to analyze the morphology and structural properties of the films. The thickness measurement of the prepared films was carried out using Ambios Technology XP-2 Stylus Profiler.

3.2.3 Fabrication and characterization of gas sensors

In order to fabricate gas sensors, thin films of copper oxides were sputtered onto quartz substrates (8 × 12 mm) with pre patterned gold interdigitated electrodes (IDTs with 50 μm line/space). Then gold ribbon (99.9 % purity) was attached to the Au pads using silver epoxy and left to dry and solidify in a heated environment of 100 ºC for 15 minutes.

The ethanol (C_2H_5OH) gas sensing experiments were performed in a customized gas sensing chamber equipped with a micro heater (250 Ω, max 10 W) and sealed with a quartz lid. A schematic figure of the Cu_xO based conductometric sensor is shown in Figure 3.1. A DC power supply was connected to the heater to

control the operating temperature. A thermocouple was placed onto the top of the sensors' surfaces for real time temperature monitoring. A gas calibration system was employed in order to deliver specific concentrations of ethanol balanced in synthetic air during the experiments. The developed CuO and Cu_2O based conductometric sensors were initially exposed towards synthetic air of 200 standard cubic centimeters per minutes (sccm). The sensors were then exposed to ethanol vapour of concentrations of 12.5, 31.25, 62.5, 187.5, 250, 375 and 500 ppm at operating temperatures between 25 to 350 ºC. The gas exposure time was fixed at 60 s for each pulse of ethanol vapour and the chamber was purged with synthetic air between each pulse, allowing the sensors to recover to their initial conditions.

The resistance changes of the developed CuO and Cu_2O based conductometric sensors were recorded using a high precision *Keithley 2001* multimeter. A data acquisition system with Labview software (National Instruments) was used in order to collect the data in real time. A detailed schematic diagram of the measurement set-up can be seen in Figure 3.2.

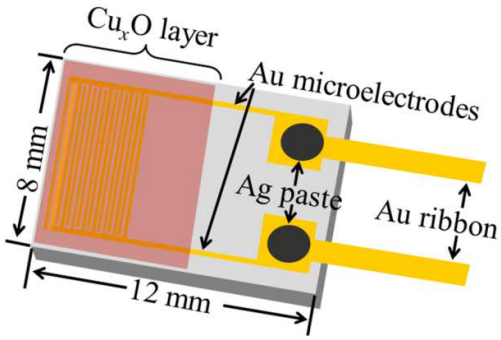

Figure 3.1 Schematic figure of Cu_xO based conductometric sensor.

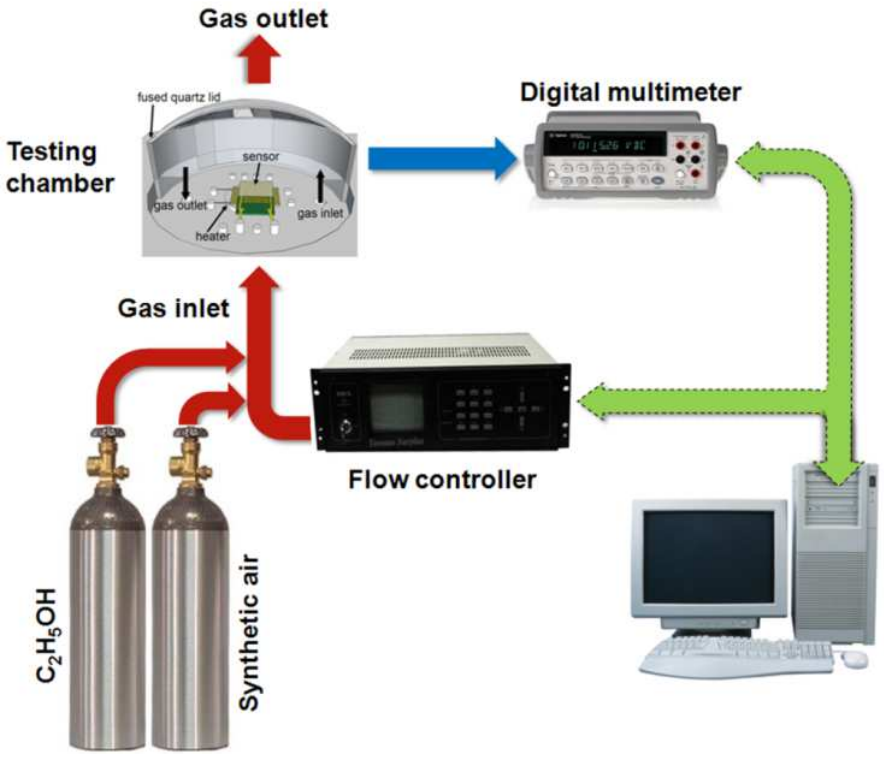

Figure 3.2 Schematic diagram of the measurement set-up.

3.3 Results and Discussions

3.3.1 Cu_2O and CuO films characterizations

Figure 3.3(a) - (d) show the XRD patterns of films resulting from variable sputtering power of 60, 120, 200 and 250 W. The deposited films were crystalline in nature with a cubic structure. As can be seen, Cu_2O (ICDD No. [3-0898], cuprite) of (111) preferred orientation was observed exclusively at a RF sputtering power of 250 W. While CuO (ICDD No. [48-1548], tenorite) of ($\bar{1}11$) was obtained at lower powers of 60, 120 and 200 W. At low sputtering powers, only a small number of Cu atoms are sputtered, which effectively react with oxygen in the plasma, resulting in the deposition of films with high oxygen content, hence CuO was present in the films. [32] Conversely, Cu_2O is formed at high sputtering powers, due to a large number of sputtered Cu atoms. No mixed crystal phase (Cu_2O together with CuO) was observed in any of the films. Based on these results, one can deduce that RF sputtering power plays a significant role in the conversion of CuO to Cu_2O. Additionally, there were no traces of elemental copper observed in the prepared films. The absence of metallic copper during the sputtering processes, implies that the plasma deposition condition is in the reactive mode.[27] It has been suggested that increasing the sputtering power enhances the energy transferred to the sputtered adatom. Hence, it also increases their mobility and surface diffusion length, leading to an increase in the probability of adatom diffusions from the landing sites to the densest lattice plane (111).[33, 34] Therefore, the (111) crystal plane is enhanced. In this work, the target-to-substrate distance was kept at 43 mm, a significantly smaller distance for obtaining Cu_xO than those reported by others, which were in the range of 60 to 70 mm.[32, 35] A closer distance was chosen, as it was assumed that reduction of the target-to-substrate distance plays a significant role in increasing adatom' mobility

and surface diffusion length, which would compensate for the lower substrate temperature and sputtering power in this study.

The thicknesses of the films were ~ 135, 141, 164 and 168 nm (within a ±11% variations) corresponding to the sputtering powers of 60, 120, 200 and 250 W, respectively. The deposition rates of the films were ~ 15.0, 15.7, 18.2 and 18.6 nm/min for sputtering power of 60, 120, 200 and 250 W, respectively.

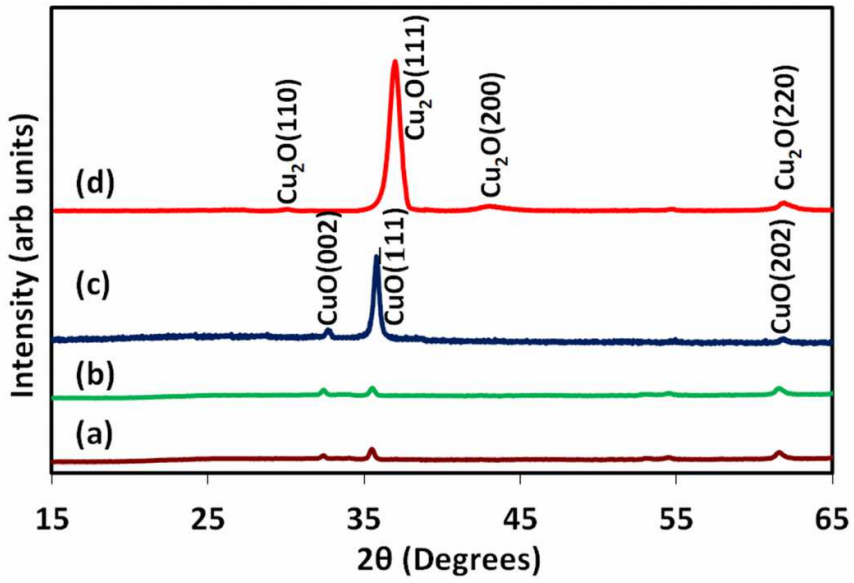

Figure 3.3 XRD patterns of CuO and Cu_2O films deposited at the powers of: (a) 60, (b) 120, (c) 200, and (d) 250 W.

Sheet resistance measurements were carried out on all samples using four probes. These sheet resistances ranged from 5.21×10^6 Ω/□ to 8.2×10^6 Ω/□. According to Zhong *et al.*, when the sheet resistance of Cu_2O reaches 10^6 Ω/□, the copper film is assumed to be fully oxidized,[36] which is also in agreement with the range of values obtained in this experiments as well as the XRD results.

Figure 3.4 shows the SEM top view and the cross-sectional images of films resulting from two sputtering power sets of 200 and 250 W, which corresponds to CuO and Cu_2O, respectively. Both the CuO and Cu_2O nanostructures are composed of compact nanopillar shape crystallites with irregular facades that enhance surface area to volume ratio of the films. It can be seen that grains in CuO films (Figure 3.4a) have significantly smaller dimensions (uniform from top to bottom) than those of grains in Cu_2O films – their base size is 30 nm in comparison to 85 nm, respectively (Figure 3.4b). The size of the nanocrystallites increased when the power was elevated to 250 W. The increase in nanocrystallites size may be due to the fact that at higher powers, ions have more energy at the time of collision with the substrate.[37] Such high energy ions are capable of adjusting their bond direction and length in order to obtain optimum bonding to adjacent atoms, promoting vigorous nucleation that contributes to larger nanocrystallites dimensions [37] as well as conversion from CuO to Cu_2O films. As a result, the Cu_2O films (Figure 3.4b) comprised of relatively larger nanocrystallites.

In order to obtain a better understanding of the deposited materials' elemental composition, XPS analysis was performed for samples obtained at 200 and 250 W. The Cu $2p_{3/2}$ and Cu $2p_{1/2}$ core levels were employed to investigate the Cu surface oxidation. Figure 3.5 shows the photoelectron spectrum of Cu 2p for the films. It illustrates the main and the satellite peaks of Cu $2p_{3/2}$ and Cu $2p_{1/2}$ of the samples.

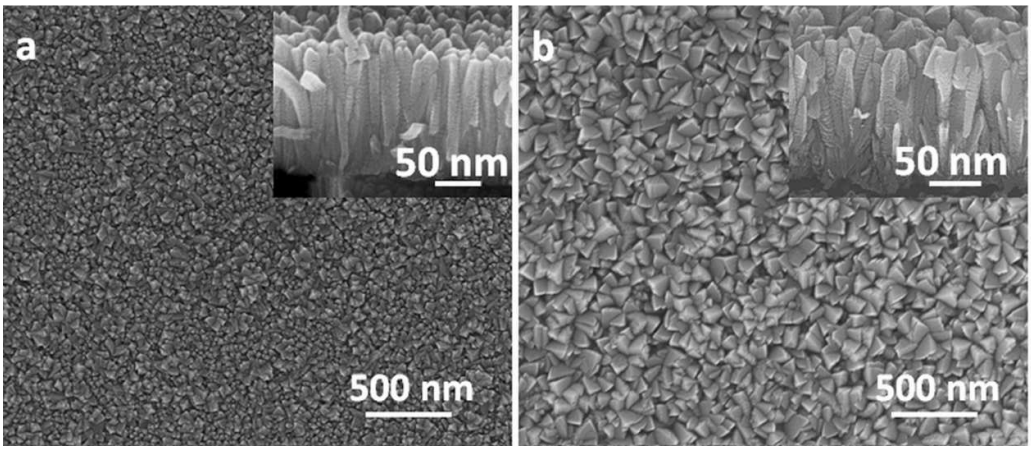

Figure 3.4 Top view SEM images of the RF sputtered (a) CuO deposited at 200 W and (b) Cu_2O deposited at 250 W for 9 minutes duration. Inset: SEM cross section image of the Cu_xO films.

The peaks at 933.6 and 953.6 eV correspond to the binding energies of Cu $2p_{3/2}$ and Cu $2p_{1/2}$, respectively, for the film deposited at 200 W (Figure 3.5a). While, the peaks at 932.5 and 952.0 eV correspond to the binding energies of Cu $2p_{3/2}$ and Cu $2p_{1/2}$, respectively, for the film deposited at 250 W (Figure 3.5b). These results are in good agreement with a previous report by Lu *et al.* and Ghijsen *et al.*[12, 38] These energies further clarify the presence of the CuO and Cu_2O phases in films obtained at 200 and 250 W, respectively.

The main peak of CuO is accompanied with a satellite peak (also known as shaken-up satellite) at about 941.1 to 944.2 eV.[39] This is absent in the case of Cu_2O. Shake-up satellite occurs when the outgoing photoelectron simultaneously interacts with a valence electron and excites it (shakes it up) to a higher energy level. The energy of the core electron is then slightly reduced, giving rise to a satellite structure with a few electron volts below the core level position.[39]

For a more precise determination of phase composition of the films, Raman spectra were also obtained and are presented in Figure 3.6. Three peaks located at 292, 341 and 621 cm^{-1} (Figure 3.6a) are observed and are ascribed to CuO.[40] The Cu_2O peaks are shown in Figure 3.6b. Four distinct peaks located at 113, 147, 215 and 631 cm^{-1} are observed and ascribed to Cu_2O.[12, 41, 42] Thus, in terms of sample identification, the results of Raman spectroscopy are in agreement with those obtained from XRD and XPS.

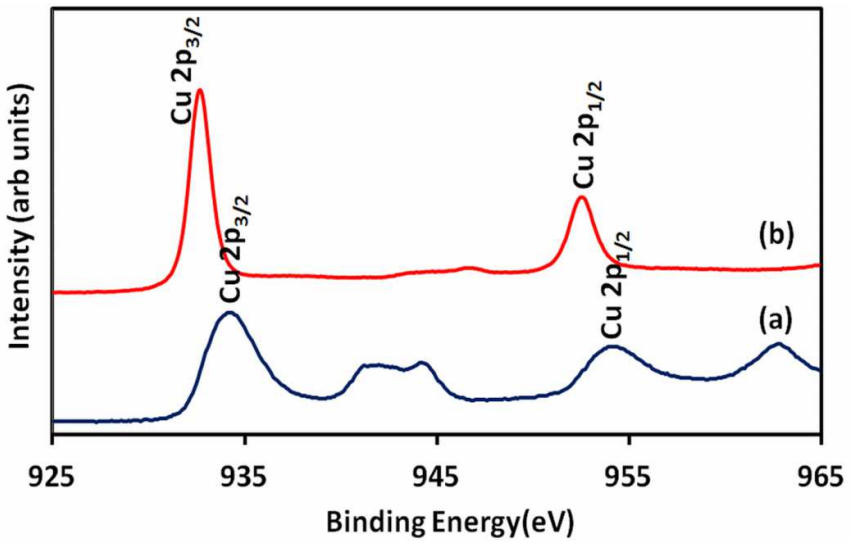

Figure 3.5 The Cu 2p XPS patterns of films obtained at (a) 200 W (which corresponds to CuO) and (b) 250 W (which corresponds to Cu_2O).

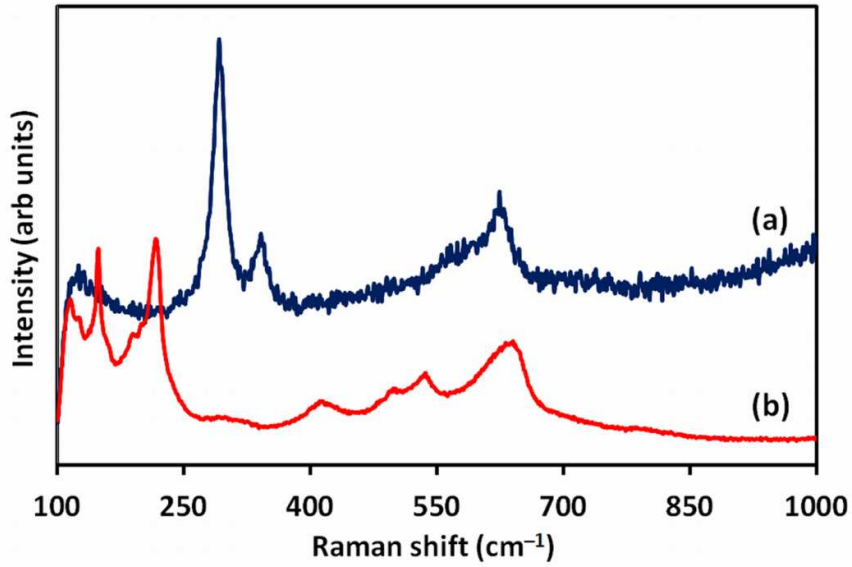

Figure 3.6 Raman spectra of films obtained at (a) 200 W (which corresponds to CuO) and (b) 250 W (which correspond to Cu_2O).

3.3.2 Gas sensing performance

Sensors based on CuO and Cu_2O sensitive layers that were formed at 200 and 250 W, respectively, were used in gas sensing measurements. In order to verify the actual thickness of the films, the author of this thesis fabricated 10 different devices for each type of films obtained at 200 and 250 W. Figure 3.7 shows the average thickness of 200 and 250 W films, which correspond to CuO and Cu_2O, respectively. Both of the films contain highly oriented crystalline, as shown in Figure 3.3. Such highly oriented crystalline films are expected to increase the sensitivity and/or selectivity of the metal oxide gas sensors.[43] It is well-known that the response of any metal oxide based semiconducting gas sensor is greatly influenced by its operating temperature. Generally high thermal energies are required to overcome the energy barrier on the surface of the metal oxide to allow the gas molecule interactions to occur.[44] In order to determine the optimal operating temperature for

the sensors based on Cu_xO to ethanol vapour, they were exposed to 12.5 ppm ethanol (in ambient air) at various operating temperatures between 120 to 320 ºC and the resultant responses are shown in Figure 3.8. The sensors did not exhibit noticeable responses below the operating temperatures of 140 ºC and 180 ºC for CuO and Cu_2O based sensors, respectively. Beyond these temperatures, both sensors showed significant increase in their responses. The highest sensor responses (*R*) obtained were ~2.2 and ~1.2 (defined as R_g/R_a in which R_g is the resistance of the sensor when it is exposed to gas and R_a the resistance of the sensor when exposed to ambient air), which were measured at 180 ºC and 260 °C, for CuO and Cu_2O devices, respectively. However, both of the sensors responses were reduced significantly as the operating temperature was further increased. The author of this thesis also compared XRD patterns of "as–deposited" (formed at 120 °C) and "elevated temperature" devices to investigate the effect of temperature on the composition and crystallinity of the films, as presented in Figures 3.9 and 3.10. From the XRD patterns, one can observe that both of the Cu_xO films retained their composition phase after being kept at elevated temperatures. No mixed crystal phase (Cu_2O together with CuO) was observed in any of the films. Based on these results, one can deduce that the operating temperature used in this work does not alter the Cu_xO stoichiometry.

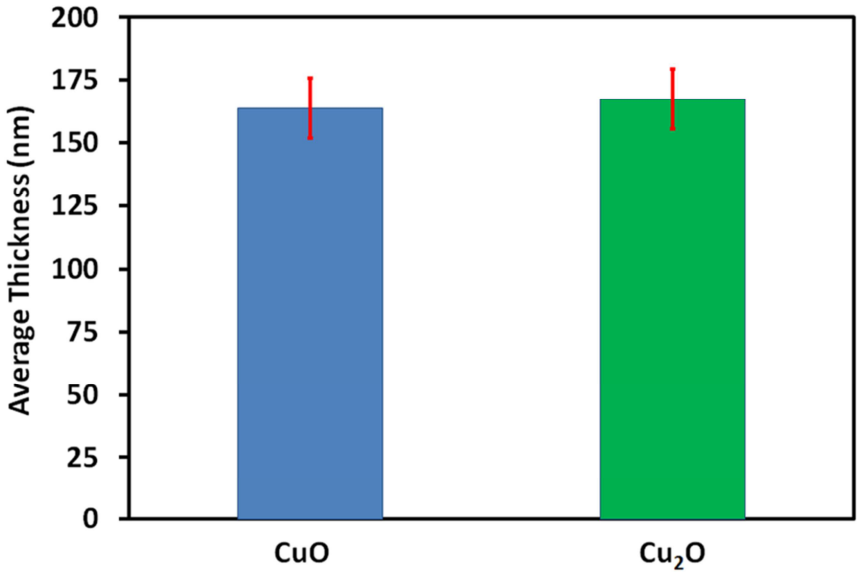

Figure 3.7 Average thickness of CuO and Cu_2O films. The tests were performed on ten similarly deposited films. The film thickness variations were less than ±11%.

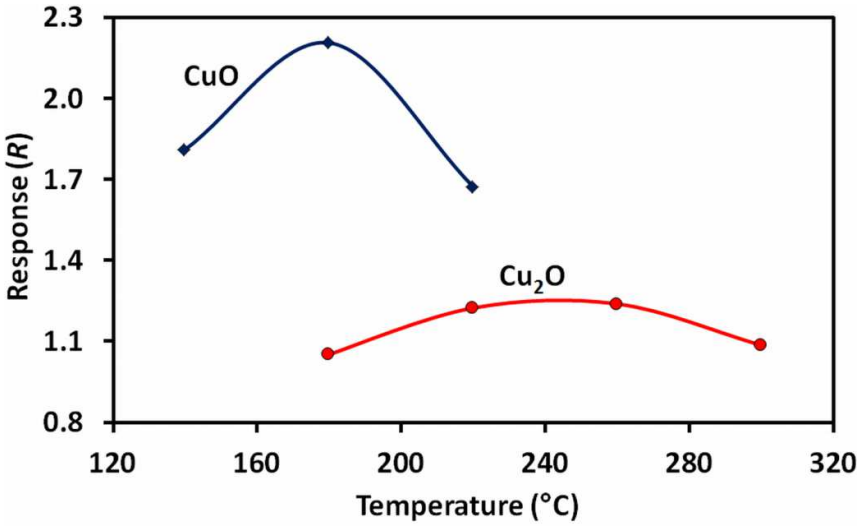

Figure 3.8 Sensor response curves of the CuO and Cu_2O based sensors towards ethanol (12.5 ppm) at different operating temperatures.

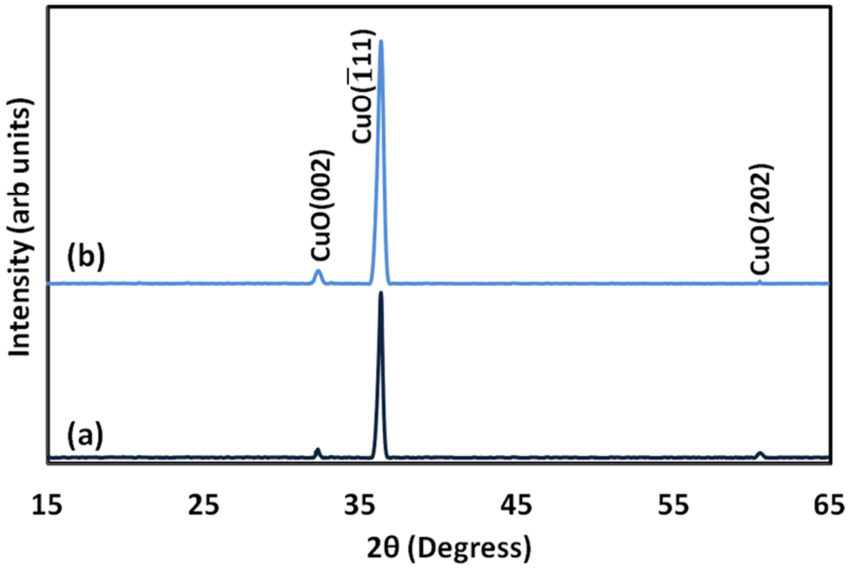

Figure 3.9 XRD patterns of CuO films (a) as–deposited and (b) after exposure at 180 ºC.

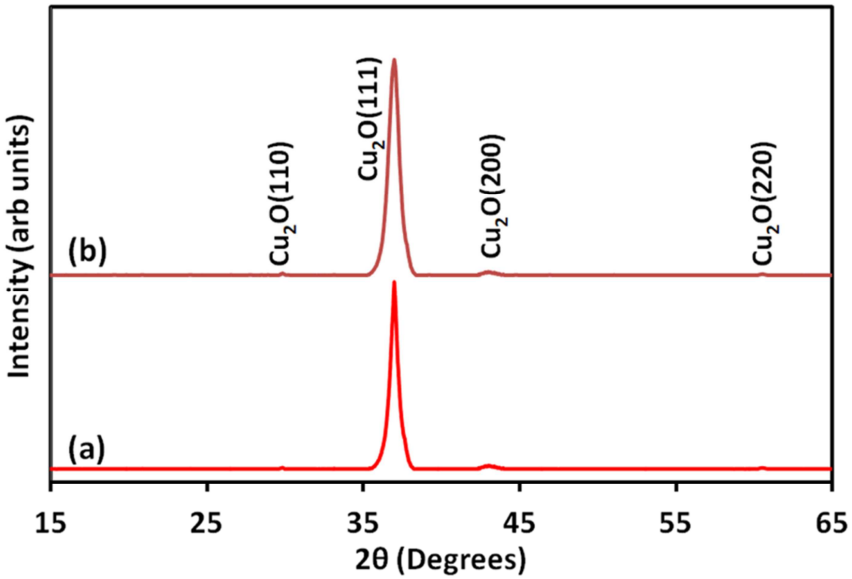

Figure 3.10 XRD patterns of Cu_2O films (a) as–deposited and (b) after exposure at 260 ºC.

The dynamic responses of the CuO and Cu_2O sensors towards various concentrations of ethanol vapour at operating temperatures of 180 ºC and 260 ºC are presented in Figure 3.11. Both sensors showed good sensor response, repeatability and reversibility. The response (τ_{res}) and recovery times (τ_{rec}) (defined as the time that it takes for the response to rises from 10% to 90% of the maximum value and vice versa) of the CuO based sensor towards 12.5 ppm ethanol was 31 and 52 s, while the Cu_2O based sensor exhibited 36 and 76 s responses.

For the sensing performance comparison, CuO and Cu_2O sensor response *vs* ethanol gas concentration graphs are presented in Figure 3.12. Both of the CuO and Cu_2O sensor responses increased proportionally to the ethanol vapour concentration, which is in agreement with a previous report.[9] However, it can be observed that the CuO sensor exhibits higher sensitivity (defined as the slope of the curve given by $S = R/C$, where S is the sensitivity, R is the sensor response, and C is the analyte concentration in ppm) than the Cu_2O sensor. This can be ascribed to the grain size effect. It can be seen clearly from the SEM images as shown in Figure 3.4, that the grain size of CuO is significantly smaller compared to Cu_2O. This leads to an enhanced surface area to volume ratio and the formation of depletion regions comparable in size with the grains' dimensions, enabling a more efficient interaction towards ethanol vapour.[9, 45] In addition, when the grains are smaller than the theoretical penetration length of the depletion region, the energy bands are almost flat throughout the whole grain, the conductivity is fully controlled by the intra-crystallite conductivity, which are the most sensitive areas during the gas molecules interactions with the surface.[45] The sensitivity of a metal oxide gas sensor is mainly determined by the efficient interactions between the target analyte and the surface area of the materials. Greater surface area to volume ratio of the materials

enhance the interaction between adsorbed analyte and the sensor surface, boosting the sensitivity of a sensor.[44] A comprehensive explanation regarding the effect of grain size on the sensitivity of metal oxide gas sensors can be found in the report by Rothschild *et al.* and Tricoli *et al.*[43, 45, 46]

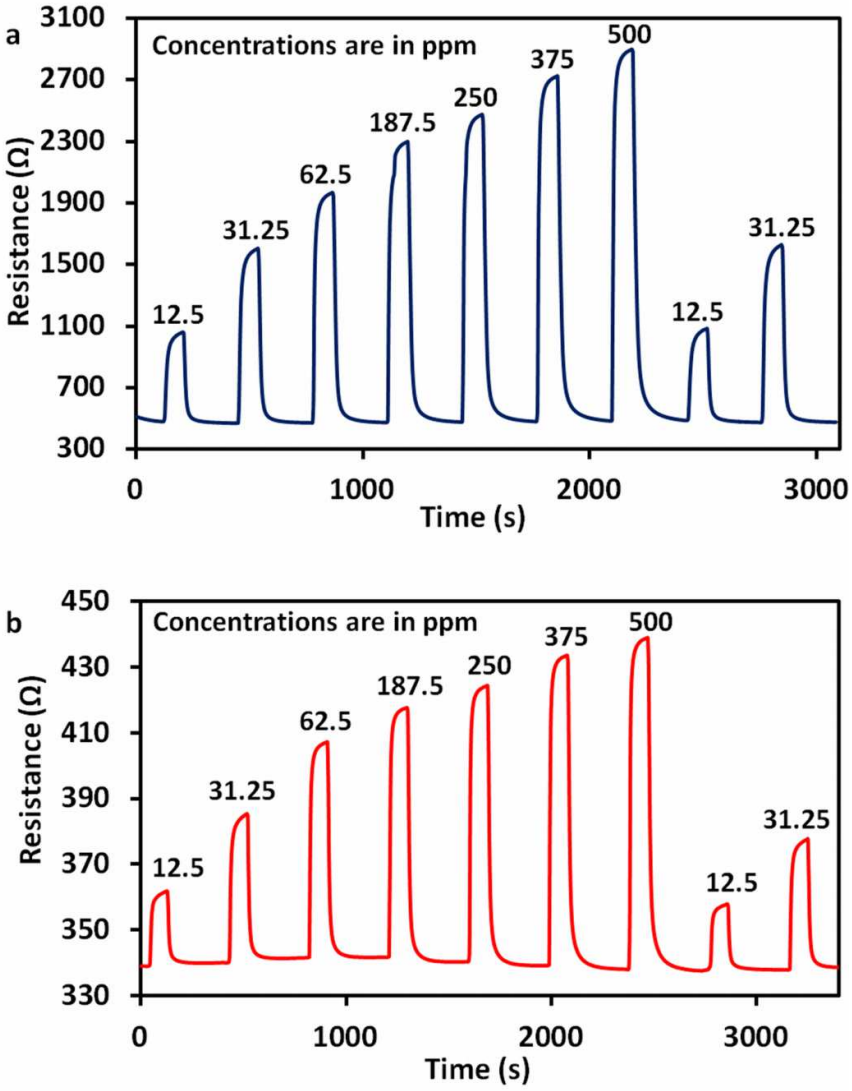

Figure 3.11 Dynamic response of: (a) CuO based sensor towards ethanol at the optimum operating temperature of 180 °C and (b) Cu_2O based sensor towards ethanol at the optimum operating temperature of 260 °C.

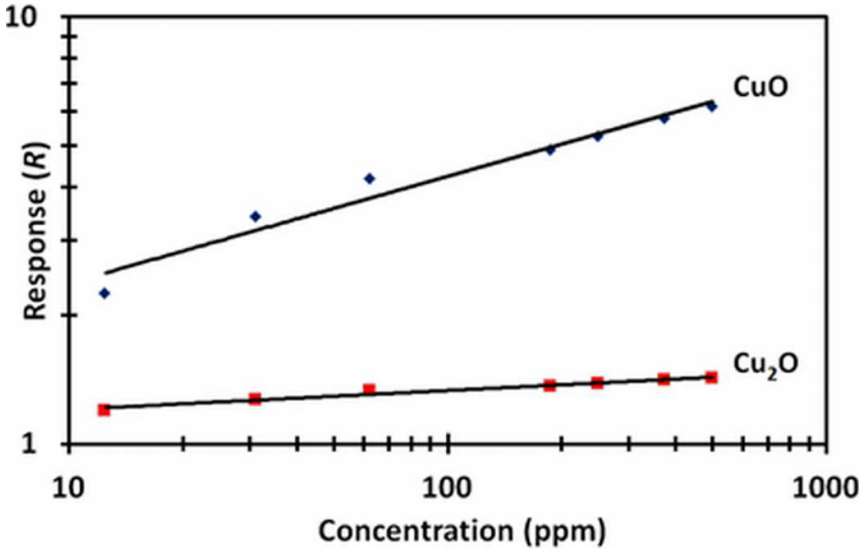

Figure 3.12 Response of the developed CuO and Cu_2O based sensors to ethanol concentration at their optimum operating temperature.

In order to further understand the effects of sensing layers towards sensitivity of the Cu_xO films, the author of this PhD thesis has conducted additional characterization to assess the morphology, adhesion and conductivity properties of the films. By using c–AFM, one can simultaneously obtain topographical image, and adhesion, as well as a current map of the Cu_xO nanostructured surfaces.

Figure 3.13(i) shows the two-dimensional (2D) c–AFM topographical images of the RF sputtered Cu_xO films. The CuO films (Figure 3.13a(i)) have surface roughness with root mean square (RMS) value of ~10 nm. As the sputtering power increased to 250 W, the surface roughness of Cu_2O films decreased with RMS value of ~7 nm (Figure 3.13b(i)). The dependence of gas sensor sensitivity on the surface roughness of metal oxides is well−established knowledge.[47] It was found that the sensitivity increases with the increase of surface roughness, due to the availability of more adsorption surface for the analyte molecules.[47] Therefore, higher sensitivity

of the CuO device in comparison to Cu_2O device was expected. However, a moderate increase in surface roughness (from 7 to 10 nm) does not seem to account for the total increase in the sensitivity. Hence, in order to explain high improvement in sensitivities, the author provides an additional explanation based on adhesion and current maps of the sensing films.

The adhesion map is determined by the contact region difference between tip-approach and tip-retract, while scanning the surface of the films. The adhesion maps of the surfaces of CuO and Cu_2O films are presented in Figure 3.13a(ii) and b(ii), respectively. In these images, the bright areas of the adhesion map correspond to higher adhesion to the surface, relative to other areas of the surface. The highest adhesion intensity is observed at the grain boundaries of the nanostructured Cu_xO films. The CuO films (Figure 3.13a(ii)) clearly reveal relatively higher adhesion areas compared to Cu_2O films (Figure 3.13b(ii)). Highly adhesive surfaces, especially along the boundaries of the grains, possibly promote more interaction between adsorbed analyte and the sensing layers. Possibly the higher adhesive nature of the surface increases the sensing performance of the device which is the case for CuO devices in comparison to Cu_2O devices.

The current map is determined by biasing the AFM tip (made of silicon nitride with a 20 nm coating of platinum/iridium) at a DC voltage of 1.0 V between the tip and the surface. The current map of the CuO and Cu_2O films are presented in Figure 3.13a(iii) and b(iii), respectively. The bright areas of the generated current map correspond to higher conductivities with reference to other areas of the surface. The CuO films (Figure 3.13a(iii)) clearly demonstrate relatively higher conducting areas compared to the Cu_2O films (Figure 3.13b(iii)). The conductivity areas are due to the existence of cation-deficiency *via* copper and/or oxygen vacancy in the Cu_xO films.

[48, 49] Cation-deficiency such as oxygen vacancies play an important role as adsorption sites for gaseous species and highly enhanced gas sensitivity.[50, 51] This is another possibility for the enhancement of the CuO sensitivity in comparison to the Cu_2O based sensor.

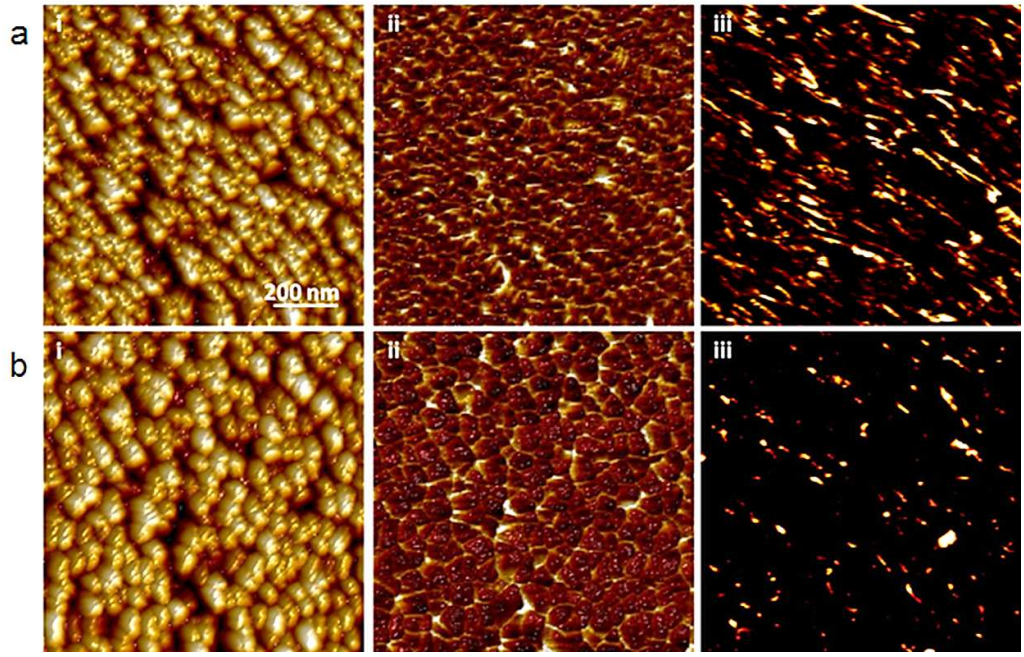

Figure 3.13 c–AFM (arbitrary units) (i) topographical, (ii) adhesion and (iii) current map images of (a) CuO and (b) Cu_2O thin films. Scale bars are similar for all figures.

The behaviour of the Cu_xO gas sensor is based on changes in electrical resistance induced by adsorption/desorption of the target gas molecules on its surface.[52-54] Oxygen molecules adsorbed on the surface of the sensing films lead to the formation of molecular (O_2^-) and atomic (O^-, O^{2-}) ions. In general, below 150 ºC the molecular form dominates, while above this temperature the atomic species are found.[43] Surface acceptor states created by the oxygen adsorption trap electrons from the valence band of *p*-type Cu_xO and in turn increase the accumulation of holes, thus

increasing the electrical carrier concentration.[52] Subsequently, when the sensing films are exposed to a reductive gas such as ethanol, the interaction of ethanol molecules with the surface chemisorbed oxygen species takes place, thereby releasing electrons that recombine with holes to decrease the electrical conductance of the semiconductor. As a result, the resistance of the gas sensor eventually increases.[53] This mechanism is known as the *ionosorption model* [52] and the sensing surface reaction is shown as:

$$C_2H_5OH\ (ads) + 3O_2^-\ (ads) \rightarrow 2CO_2\ (g) + 3H_2O\ (g) + 3e^- \qquad (3.1)$$

Besides the ionosorption model, another possible mechanism is closely related to the decomposition and/or oxidation reaction on the surface of *p*-type Cu_xO. Jinkawa *et al*. reported that the decomposition of ethanol at elevated temperatures depends on the metal oxide catalytic activities that generates acetaldehyde and surface absorbed H^+ ions.[55]

$$C_2H_5OH\ (g) \rightarrow CH_3CHO(g) + 2H^+ + 2e^- \qquad (3.2)$$

The generated electrons recombine with holes and decrease the electrical conductance of the *p-type* materials, as a result the resistance of the sensor eventually increases. In addition, H^+ ions reduced the Cu_xO films with oxygen deficiency in the form of Cu_xO_{1-y}. When the film is exposed to air (oxygen), the reduced film surface reverts back to its original fully oxidized state, which is described by the following reaction:

$$(y/2)O_2 + Cu_xO_{1-y} \rightleftharpoons Cu_xO \qquad (3.3)$$

For comparison with this work, the responses of various nanostructured CuO thin films (without any additional catalytic layers) which have been developed by other

groups using different fabrication techniques, are summarized in Table 3.1. It is observed that the nanostructured CuO based sensor from this work has the lowest operating temperature (180 ºC) as well as the second highest response (~2.2). The superior performance of the CuO sensors is mainly due to the size of the nanocrystallites that form the thin films. In comparison, the dimensions of the base of the nanocrystallites incorporated into the thin films of this work are the smallest, and are in the order of 30 nm (Table 3.1).

Although, the CuO based sensor fabricated by Barecca *et al.*[9] shows a relatively higher sensor response towards 10 ppm ethanol vapour, their operating temperature was 200 °C and also the sensor response and recovery times were 5 and 3 times larger than this work, respectively.

As for the Cu_2O, the sensor response was lower compared to CuO. The developed sensor showed a sensor response of ~1.2 for 12.5 ppm ethanol at a higher operating temperature of 260 °C, which was inferior in comparison to many other reports [9, 24, 25, 56, 57]. This is probably due to the large size of Cu_2O nanopillar crystallites with base dimensions in the order of 85 nm. Although the author was able to sputter thin film Cu_2O at relatively low power, it was still insufficient to produce smaller Cu_2O crystallites compared to the other techniques. In addition, low surface roughness as well as low adhesive properties of the Cu_2O films further deteriorated the sensor's performance by hindering interaction between adsorbed analyte and the sensing material. It was also found that Cu_2O had a lower cation-deficiency compared to CuO films. Lower cation-deficiency such as oxygen vacancies definitely degraded the sensor's performance."

Table 3.1. Sensor response of CuO nanostructures toward ethanol vapour on various fabrication techniques and morphologies.

Fabrication technique (morphology)	Optimum operating temperature (ºC)	Sensor response (R)	Concentration at which the sensor response is measured (ppm)	Minimum grain dimension (nm)	Reference
Thermal oxidation (nanowires)	200	<1.0	100	50	[16]
DC sputtering (nanowires)	300	1.27	1000	50	[23]
Thermal oxidation (nanowires)	240	1.5	1000	80	[17]
Hydrothermal (nanorods)	400	<1.5	100	80	[21]
Chemical vapour deposition (nanocrystallites)	200	3.0	10	80	[9]
RF sputtering (nanocrystallites)	180	2.2	12.5	30	This work

3.4 Summary

In this chapter, the author of this thesis demonstrated an ethanol vapour sensing devices based on nanostructured and highly crystalline CuO and Cu_2O, which are synthesized by RF sputtering at relatively low power of 200 and 250 W, respectively, and at a low substrate temperature of 120 °C. The author adjusted various parameters of the RF sputtered to engineer the CuO and Cu_2O thin films. The relatively small target-to-substrate distance, as well as relatively low power and substrate temperature during the sputtering process provides a means for controlling the dimensions of the Cu_xO nanocrystallites and the accurate stoichiometry of Cu_xO. Sputtering at 200 W

results in smaller CuO nanostructures, with enhanced surface area to volume ratio. The fabricated sensors show fast response and recovery, as well as high sensitivity for the CuO based ethanol sensors. The sensor response of CuO was 2.2 at an optimum operating temperature of 180 °C for 12.5 ppm concentration of ethanol in ambient air. Moreover, the developed sensors exhibited remarkable baseline stability, excellent repeatability and a large and fast response towards ethanol vapour. These characteristics are promising for industrial applications, especially in gas and vapour related chemical sensing.

In the next chapter, the author will present his achievements in producing ZnO-Cu_2O based heterojunction solar cells. The author will discuss in detail, the fabrication process, characterization and the investigation of tuning and engineering ZnO and Cu_2O in improving the quality of the heterointerface to enhance the efficiency of such heterojunction solar cells.

References

[1] C. Wang, L. Yin, L. Zhang, D. Xiang, and R. Gao, "Metal oxide gas sensors: Sensitivity and influencing factors," *Sensors*, vol. 10, pp. 2088-2106, 2010.

[2] G. Eranna, B. C. Joshi, D. P. Runthala, and R. P. Gupta, "Oxide materials for development of integrated gas sensors - A comprehensive review," *Crit. Rev. Solid State*, vol. 29, pp. 111-188, 2004.

[3] N. Barsan, D. Koziej, and U. Weimar, "Metal oxide-based gas sensor research: How to?," *Sensor Actuat. B-Chem.*, vol. 121, pp. 18-35, 2007.

[4] N. Barsan and U. Weimar, "Conduction model of metal oxide gas sensors," *J. Electroceram.*, vol. 7, pp. 143-167, 2001.

[5] E. Comini, "Metal oxide nano-crystals for gas sensing," *Anal. Chim. Acta*, vol. 568, pp. 28-40, 2006.

[6] M. H. Yaacob, M. Breedon, K. Kalantar-zadeh, and W. Wlodarski, "Absorption spectral response of nanotextured WO_3 thin films with Pt catalyst towards H_2," *Sensor Actuat. B-Chem.*, vol. 137, pp. 115-120, 2009.

[7] M. Shafiei, J. Yu, R. Arsat, K. Kalantar-zadeh, E. Comini, M. Ferroni, *et al.*, "Reversed bias Pt/nanostructured ZnO schottky diode with enhanced electric

field for hydrogen sensing," *Sensor Actuat. B-Chem.*, vol. 146, pp. 507-512, 2010.

[8] A. Z. Sadek, V. Bansal, D. G. McCulloch, P. G. Spizzirri, K. Latham, D. W. M. Lau, *et al.*, "Facile, size-controlled deposition of highly dispersed gold nanoparticles on nitrogen carbon nanotubes for hydrogen sensing," *Sensor Actuat. B-Chem.*, vol. 160, pp. 1034-1042, 2011.

[9] D. Barreca, E. Comini, A. Gasparotto, C. Maccato, C. Sada, G. Sberveglieri, *et al.*, "Chemical vapor deposition of copper oxide films and entangled quasi-1D nanoarchitectures as innovative gas sensors," *Sensor Actuat. B-Chem.*, vol. 141, pp. 270-275, 2009.

[10] E. Comini, G. Faglia, G. Sberveglieri, Z. W. Pan, and Z. L. Wang, "Stable and highly sensitive gas sensors based on semiconducting oxide nanobelts," *Appl. Phys. Lett.*, vol. 81, pp. 1869-1871, 2002.

[11] A. E. Rakhshani, "Preparation, characteristic and photovoltaic properties of cuprous oxide - A review," *Solid State Electron.*, vol. 29, pp. 7-17, 1986.

[12] Y. M. Lu, J. Y. Chen, and T. S. Wey, "Nano Cuprous Oxides film Prepared by Magnetron Sputtering," *Mater. Res. Soc. Symp. P*, vol. 822, pp. 55-64, 2004.

[13] E. Comini, G. Faglia, G. Sberveglieri, Y. X. Li, W. Wlodarski, and M. K. Ghantasala, "Sensitivity enhancement towards ethanol and methanol of TiO_2 films doped with Pt and Nb," *Sensor Actuat. B-Chem.*, vol. 64, pp. 169-174, 2000.

[14] P. Hu, G. Du, W. Zhou, J. Cui, J. Lin, H. Liu, *et al.*, "Enhancement of ethanol vapor sensing of TiO_2 nanobelts by surface engineering," *ACS Appl. Mater. Inter.*, vol. 2, pp. 3263-3269, 2010.

[15] M. L. Zhong, D. C. Zeng, Z. W. Liu, H. Y. Yu, X. C. Zhong, and W. Q. Qiu, "Synthesis, growth mechanism and gas-sensing properties of large-scale CuO nanowires," *Acta Materialia*, vol. 58, pp. 5926-5932, 2010.

[16] L. Liao, Z. Zhang, B. Yan, Z. Zheng, Q. L. Bao, T. Wu, *et al.*, "Multifunctional CuO nanowire devices: p-type field effect transistors and CO gas sensors," *Nanotechnology*, vol. 20, 2009.

[17] P. Raksa, A. Gardchareon, T. Chairuangsri, P. Mangkorntong, N. Mangkorntong, and S. Choopun, "Ethanol sensing properties of CuO nanowires prepared by an oxidation reaction," *Ceram. Int.*, vol. 35, pp. 649-652, 2009.

[18] M. Faisal, S. B. Khan, M. M. Rahman, A. Jamal, and A. Umar, "Ethanol chemi-sensor: Evaluation of structural, optical and sensing properties of CuO nanosheets," *Mater. Lett.*, vol. 65, pp. 1400-1403, 2011.

[19] C. Yang, X. Su, F. Xiao, J. Jian, and J. Wang, "Gas Sensing Properties of CuO Nanorods Synthesized by A Microwave-Assisted Hydrothermal Method," *Sens. Actuator B Chem.*, vol. 158, pp. 299-303, 2011.

[20] X. Liu, J. Zhang, Y. Kang, S. Wu, and S. Wang, "Brochantite tabular microspindles and their conversion to wormlike CuO structures for gas sensing," *CrystEngComm*, vol. 14, pp. 620-625, 2012.

[21] C. Wang, X. Q. Fu, X. Y. Xue, Y. G. Wang, and T. H. Wang, "Surface accumulation conduction controlled sensing characteristic of p-type CuO nanorods induced by oxygen adsorption," *Nanotechnology*, vol. 18, 2007.

[22] M. R. Parmar, N. Gokhale, K. Rajanna, and Ieee, "Nanostructured copper(II) oxide thin film for alcohol sensing," in *I2mtc: 2009 Ieee Instrumentation & Measurement Technology Conference, Vols 1-3*, ed, 2009, pp. 327-330.

[23] H. T. Hsueh, S. J. Chang, F. Y. Hung, W. Y. Weng, C. L. Hsu, T. J. Hsueh, *et al.*, "Ethanol Gas Sensor of Crabwise CuO Nanowires Prepared on Glass Substrate," *J. Electrochem. Soc.*, vol. 158, pp. J106-J109, 2011.

[24] L. Guan, H. Pang, J. Wang, Q. Lu, J. Yin, and F. Gao, "Fabrication of novel comb-like Cu_2O nanorod-based structures through an interface etching method and their application as ethanol sensors," *Chem. Commun.*, vol. 46, pp. 7022-7024, 2010.

[25] H. Zhang, Q. Zhu, Y. Zhang, Y. Wang, L. Zhao, and B. Yu, "One-pot synthesis and hierarchical assembly of hollow Cu_2O microspheres with nanocrystals-composed porous multishell and their gas-sensing properties," *Adv. Funct. Mater.*, vol. 17, pp. 2766-2771, 2007.

[26] S. Ishizuka, T. Maruyama, and K. Akimoto, "Thin-film deposition of Cu_2O by reactive radio-frequency magnetron sputtering," *JPN J. Appl. Phys. 2*, vol. 39, 2000.

[27] A. A. Ogwu, E. Bouquerel, O. Ademosu, S. Moh, E. Crossan, and F. Placido, "An investigation of the surface energy and optical transmittance of copper oxide thin films prepared by reactive magnetron sputtering," *Acta Mater.*, vol. 53, pp. 5151-5159, 2005.

[28] J. F. Pierson, A. Thobor-Keck, and A. Billard, "Cuprite, Paramelaconite And Tenorite Films Deposited by Reactive Magnetron Sputtering," *Appl. Surf. Sci.*, vol. 210, pp. 359-367, 2003.

[29] T. Ghodselahi, M. A. Vesaghi, A. Shafiekhani, A. Baghizadeh, and M. Lameii, "XPS Study of The Cu@Cu_2O Core-Shell Nanoparticles," *Appl. Surf. Sci.*, vol. 255, pp. 2730-2734, 2008.

[30] A. S. Zoolfakar, M. Z. Ahmad, R. A. Rani, J. Z. Ou, S. Balendhran, S. Zhuiykov, *et al.*, "Nanostructured Copper Oxides As Ethanol Vapour Sensors," *Sens. Actuator B Chem.*, vol. 185, pp. 620-627, 2013.

[31] R. Cebulla, R. Wendt, and K. Ellmer, "Al-doped zinc oxide films deposited by simultaneous rf and dc excitation of a magnetron plasma: Relationships between plasma parameters and structural and electrical film properties," *J. Appl. Phys.*, vol. 83, pp. 1087-1095, 1998.

[32] A. S. Reddy, H.-H. Park, V. S. Reddy, K. V. S. Reddy, N. S. Sarma, S. Kaleemulla, *et al.*, "Effect of Sputtering Power on The Physical Properties of DC Magnetron Sputtered Copper Oxide Thin Films," *Mater. Chem. Phys.*, vol. 110, pp. 397-401, 2008.

[33] K. H. Chiu, J. H. Chen, H. R. Chenc, and R. S. Huang, "Deposition characterization of reactive magnetron sputtered aluminum nitride thin films for film bulk acoustic wave resonator," *Thin Solid Films*, vol. 515, pp. 4819-4825, 2007.

[34] H. Cheng, Y. Sun, and P. Hing, "The influence of deposition conditions on structure and morphology of aluminum nitride films deposited by radio frequency reactive sputtering," *Thin Solid Films*, vol. 434, pp. 112-120, 2003.

[35] M. H. P. Reddy, P. N. Reddy, and S. Uthanna, "Structural, electrical and optical behaviour of rf magnetron sputtered cuprous oxide films," *Indian J. Pure Ap. Phys.*, vol. 48, pp. 420-424, 2010.

[36] C. Zhong, Y. M. Jiang, D. M. Sun, J. Gong, B. Deng, S. Cao, *et al.*, "Oxidation kinetics of nanoscale copper thin films at low temperature characterized by sheet resistance and optical transmittance," *Chinese J. Phys.*, vol. 47, pp. 253-260, 2009.

[37] X. H. Yu, J. Ma, F. Ji, Y. H. Wang, X. J. Zhang, C. F. Cheng, *et al.*, "Effects of sputtering power on the properties of ZnO : Ga films deposited by rf magnetron-sputtering at low temperature," *J. Cryst. Growth,* vol. 274, pp. 474-479, 2005.

[38] J. Ghijsen, L. H. Tjeng, J. Vanelp, H. Eskes, J. Westerink, G. A. Sawatzky, *et al.*, "Electronic-structure of Cu_2O and CuO," *Phys. Rev. B,* vol. 38, pp. 11322-11330, 1988.

[39] J. F. Watts and J. Wolstenholme, *An introduction to surface analysis by XPS and AES*. West Sussex, England: John Wiley & Sons Limited, 2003.

[40] J. F. Xu, W. Ji, Z. X. Shen, W. S. Li, S. H. Tang, X. R. Ye, *et al.*, "Raman spectra of CuO nanocrystals," *J. Raman Spectrosc.*, vol. 30, pp. 413-415, 1999.

[41] A. Compaan and H. Z. Cummins, "Raman Scattering, Luminescence and Exciton Phonon Coupling in Cu_2O " *Phys. Rev. B,* vol. 6, pp. 4753 - 4757, 1972.

[42] L. Wu, L.-k. Tsui, N. Swami, and G. Zangari, "Photoelectrochemical Stability of Electrodeposited Cu_2O Films," *J. Phys. Chem. C,* vol. 114, pp. 11551-11556, 2010.

[43] A. Tricoli, M. Righettoni, and A. Teleki, "Semiconductor Gas Sensors: Dry Synthesis And Application," *Angew. Chem. Int. Edit.*, vol. 49, pp. 7632-7659, 2010.

[44] J. F. Chang, H. H. Kuo, I. C. Leu, and M. H. Hon, "The effects of thickness and operation temperature on ZnO:Al thin film CO gas sensor," *Sensor Actuat. B-Chem.*, vol. 84, pp. 258-264, 2002.

[45] A. Rothschild and Y. Komem, "The effect of grain size on the sensitivity of nanocrystalline metal-oxide gas sensors," *J. Appl. Phys.*, vol. 95, pp. 6374-6380, 2004.

[46] A. Tricoli, M. Graf, and S. E. Pratsinis, "Optimal doping for enhanced SnO_2 sensitivity and thermal stability," *Adv. Funct. Mater.*, vol. 18, pp. 1969-1976, 2008.

[47] B. K. Min and S. D. Choi, "SnO_2 thin film gas sensor fabricated by ion beam deposition," *Sensor Actuat. B-Chem.*, vol. 98, pp. 239-246, 2004.

[48] H. Raebiger, S. Lany, and A. Zunger, "Origins of the p-type nature and cation deficiency in Cu_2O and related materials," *Phys. Rev. B,* vol. 76, 2007.

[49] B. K. Meyer, A. Polity, D. Reppin, M. Becker, P. Hering, P. J. Klar, *et al.*, "Binary Copper Oxide Semiconductors: From Materials Towards Devices," *Phys. Status Solidi B,* vol. 249, pp. 1487-1509, 2012.

[50] M. Ahsan, M. Z. Ahmad, T. Tesfamichael, J. Bell, W. Wlodarski, and N. Motta, "Low temperature response of nanostructured tungsten oxide thin films toward hydrogen and ethanol," *Sensor Actuat. B-Chem.,* vol. 173, pp. 789-796, 2012.

[51] B.-Z. Sun, W.-K. Chen, J.-D. Zheng, and C.-H. Lu, "Roles of oxygen vacancy in the adsorption properties of CO and NO on $Cu_2O(111)$ surface: Results of a first-principles study," *Appl. Surf. Sci.*, vol. 255, pp. 3141-3148, 2008.

[52] C. Yang, X. Su, F. Xiao, J. Jian, and J. Wang, "Gas sensing properties of CuO nanorods synthesized by a microwave-assisted hydrothermal method," *Sensor Actuat. B-Chem.*, vol. 158, pp. 299-303, 2011.

[53] Y. Sui, Y. Zeng, W. Zheng, B. Liu, B. Zou, and H. Yang, "Synthesis of polyhedron hollow structure Cu_2O and their gas-sensing properties," *Sensor Actuat. B-Chem.*, vol. 171, pp. 135-140, 2012.

[54] A. Gurlo and R. Riedel, "In situ and operando spectroscopy for assessing mechanisms of gas sensing," *Angew. Chem. Int. Edit.*, vol. 46, pp. 3826-3848, 2007.

[55] T. Jinkawa, G. Sakai, J. Tamaki, N. Miura, and N. Yamazoe, "Relationship between ethanol gas sensitivity and surface catalytic property of tin oxide sensors modified with acidic or basic oxides," *J. Mol. Catal. A-Chem.*, vol. 155, pp. 193-200, 2000.

[56] J. T. Zhang, J. F. Liu, Q. Peng, X. Wang, and Y. D. Li, "Nearly Monodisperse Cu_2O and CuO Nanospheres: Preparation And Applications For Sensitive Gas Sensors," *Chem. Mater.*, vol. 18, pp. 867-871, 2006.

[57] J. Liu, S. Wang, Q. Wang, and B. Geng, "Microwave chemical route to self-assembled quasi-spherical Cu_2O microarchitectures and their gas-sensing properties," *Sensor Actuat. B-Chem.*, vol. 143, pp. 253-260, 2009.

Chapter 4

Enhancing the Current Density of Electrodeposited ZnO-Cu_2O based Solar Cells by Engineering their Heterointerfaces

4.1 Introduction

In this Chapter, the PhD candidate presents the outcomes of his investigations on the development of ZnO-Cu_2O based heterojunction solar cells. As presented in Chapter 1, the author chose to use *n*-type ZnO/*p*-type Cu_2O heterojunction as the model for investigating the effect of engineering and nanostructuring of metal oxides films on the solar cell efficiency. For achieving this aims of this section, the author demonstrates an efficient approach by incorporating RF sputtered seed layers to enhance the heterointerface quality of electrodeposited ZnO-Cu_2O solar cells.

As described in chapter 1, thin film photovoltaic devices made of ZnO-Cu_2O heterojunctions are potentially attractive due to their theoretical power conversion efficiency (PCE) of 18% as well as a higher than single crystalline Si absorption coefficient.[1] As described in Chapter 2, the ZnO thin films have favourable characteristics for developing solar cells including their transparency, wide band gap (3.37 eV) and high electron mobility (~120 $cm^2\ V^{-1}\ s^{-1}$).[2, 3] Cu_2O is also a well-known oxide semiconductor for solar cell applications. Cu_2O is a direct band gap material with a band gap of 2.1 eV.[4] It has a high absorption coefficient in the visible region and the minority carrier diffusion length is also suitable for use as a solar cell absorber layer.[5] Overall, both materials are inexpensive and abundant which offer obvious benefits for solar cell technologies.[4, 6, 7] Despite such

advantages, in practice the ZnO-Cu_2O solar systems have never exceeded desirable solar conversion efficiencies.[3, 8, 9] This is due to the fact that theoretically their intrinsic electronic band structure does not allow any open-circuit voltage values larger than 0.7 V.[9] For as-electrodeposited ZnO-Cu_2O bilayer cells, open-circuit voltages no higher than 0.32 V have been reported.[3, 5, 8] By doping the ZnO layer in such heterojunctions, it is possible to increase the efficiency by reducing the internal resistance.[8] Doping also reduces the effect of interface states as a result of a better distribution of charges at the heterointerface. In these cases, an open circuit voltage as large as 0.69 V has been reported.[10]

Though ZnO doping is essential for increasing the efficiency of ZnO-Cu_2O solar cells, it is still imperative to investigate how the crystallinity and heterointerface morphologies can affect such devices. Any improvement in the efficiency, photocurrent or voltage of the as deposited ZnO-Cu_2O offers an excellent pathway, ultimately, for the doped ZnO-Cu_2O systems. The maximum current density ever reported for an undoped electrodeposited bilayer of ZnO-Cu_2O under AM 1.5 illumination has been 8.2 mA cm^{-2} by Cui *et. al*.[11] In the report, the ZnO film had a nanowire morphology and they suggested that this high current density was due to the large surface area of the heterojunction.[11] Based on the literature review, it is suggested that increasing the surface-to-volume ratio, together with high crystallinity of the ZnO and Cu_2O layers, are the most important ways to obtain large current densities for the ZnO-Cu_2O heterojunction devices.[3, 8, 9, 11]

ZnO and Cu_2O can be prepared using different methods such as thermal oxidation, [12] electrodeposition, [11, 13-16] anodic oxidation, [17] pulsed laser deposition, [18] spraying,[19] thermal evaporation [20, 21], nanoparticle inks[22], DC reactive magnetron sputtering [23] and RF reactive magnetron sputtering

deposition.[24-26] Among the aforementioned methods, electrodeposition has several advantages such as control over crystallinity, stoichiometry, nanostructure morphologies and doping concentrations.[14, 27] In addition, post annealing processes can be avoided as the deposited films are highly crystalline.[14] All these factors are important for developing cost-effective and efficient photovoltaic technologies. As a result, ZnO-Cu_2O heterojunction solar cells based on electrodeposition methods have attracted significant attention.[3, 5, 11, 15, 28] However, obtaining rough surfaces that increase the surface-to-volume ratio, hence increasing the heterointerface and solar cell current density, has been a challenge. Many conventional electrodeposition methods of ZnO produce highly crystalline films which is the parameter that is highly sought after in heterojuntion solar cells but often result in low surface roughness.[3, 11] The electrodeposited ZnO crystallites generally follow the topography of the substrates and well-engineered tuning methods are required to modify their morphologies into nanocrystallites with low dimensions.[29-31]

There are also concerns regarding this method as the formation of pin-holes and inhomogeneity of the films can occur due to the solubility of ZnO in high pH electrolytes, which are generally used for the electrodeposition of Cu_2O.[3, 5, 32] During the electrodeposition process, pin-holes can be filled by Cu_2O, forming ohmic contacts with the conductive glass-substrate, which is detrimental, as it degrades the performance of the solar cells.

In this chapter, the author of this PhD thesis introduces seed layers of ZnO deposited by a RF sputtering technique before the electrodeposition process due to two fundamental motivations: (a) to tune the morphology of the electrodeposited ZnO grains to increase the surface-to-volume ratio of the heterojunction and (b) to

tune ZnO and Cu_2O nucleation in order to obtain a highly crystalline phase of ZnO and Cu_2O, for films with excellent homogeneity and no pin-holes. The ZnO seed layers are formed at different deposition conditions to alter their crystallinity, adhesion properties of the interfaces and grain morphologies. By introducing the ZnO seed layer approach, the author shows their effect on the electrodeposited ZnO films and their surface roughnesses, and on ZnO-Cu_2O heterojunctions as well as their photovoltaic performance.

The contents of this chapter were published as a full article in the *Journal of Materials Chemistry*.[33]

4.2 Experimental

4.2.1 Materials

Zinc nitrate ($Zn(NO_3)_2$, Aldrich, 98%), copper(II) sulphate ($CuSO_4$, Aldrich, 99%), lactic acid ($C_3H_6O_6$, Aldrich, 85%), and sodium hydroxide (NaOH, Aldrich, 99%) were used in the experiments. All solvents were of analytical grade and solutions were prepared using Milli-Q water with a resistivity of 18.2 MΩcm. All chemicals and solvents were used without further purification.

4.2.2 Growth and characterisation of ZnO

Commercially available fluorine doped tin oxide (FTO) coated glass-substrates with a sheet resistance of 15 Ω per square were purchased from Dyesol. The substrates were cut into rectangles of 10 mm × 25 mm, sonicated in acetone, and rinsed in isopropanol and deionized water to remove any organic contaminations. Seed layers of ZnO were directly deposited on the substrates using the RF sputtering techniques,

which are described below. Then, thin layers of ZnO films were electrodeposited onto the samples.

In the sputtering process, the target was ZnO of 4 inches diameter and 99.99% purity. The sputtering chamber was pumped to an ultimate background pressure of 10^{-5} Torr and the sputtering pressure increased to 20×10^{-3} Torr. The author goals in this approach was to find the deposition parameters for obtaining an optimum seed layer to enhance the ZnO nucleation, crystal morphology and quality, as well as heterointerface adhesion properties. As a result, during the deposition, the sputtering RF power was set at different values ranging from 60 to 110 W. The argon and oxygen gas concentration ratio in the chamber was kept constant at 60% and 40%, respectively. The substrates' deposition duration and temperature were fixed at 60 minutes and 260 ºC, respectively. The target to substrate distance was set at 65 mm.

Electrodeposited ZnO films were prepared from an acidic aqueous solution containing 0.05 M zinc nitrate. The seed layers were used as the working electrode, in a 3 electrode setup consisting of a Ag/AgCl reference electrode and zinc sheet (99.99% purity) as a counter electrode. The deposition temperature was fixed at 62 ºC by using a water bath heater as suggested by Izaki *et. al*.[34] Cyclic voltammetry (CV) measurements were conducted first to determine the deposition potentials of the thin films. The CV measurements were carried out using a CHI410A electrochemistry workstation (CH Instruments). Then, the ZnO thin films were electrodeposited at a constant potential of −0.7 V *vs* Ag/AgCl without stirring. The deposition time was varied from 300 to 2000 s for finding the optimum thickness for the solar cells.

4.2.3 Growth and characterisation of Electrodeposited Cu_2O on ZnO

Cu_2O films were electrodeposited on ZnO/FTO/glass substrates using an alkaline aqueous solution containing 0.4 M copper (II) sulphate and 3 M lactic acid as a chelating agent. The solution pH was adjusted to 13.5 by adding sodium hydroxide. The electrodeposition process was carried out potentiostatically at −0.55 V *vs* Ag/AgCl and the deposition time was varied from 1000 to 2500 s. During the electrodeposition process, the solution was kept at 40 ºC without stirring, as suggested by Izaki *et. al.*[15] To avoid the etching of ZnO films in the Cu_2O growth solution, the negative potential is applied immediately after immersing the samples in the solution to avoid any possible surface corrosion. A high purity graphite rod was used as a counter electrode and Ag/AgCl was used as the reference electrode.

4.2.4 Materials and device characterisation

The crystallographic properties of the films were studied using an X-ray diffraction (XRD - Bruker D8 DISCOVER) microdiffractometer fitted with a GADDS (General Area Detector Diffraction System) using CuKα radiation (λ = 1.54178 Å) and Raman spectroscopy (Renishaw 1000 micro-Raman system). In addition, scanning electron microscopy (SEM – FEI Nova NanoSEM) and atomic force microscopy (AFM – Bruker MultiMode 8 with PF TUNA) were utilized to analyze the morphology and structural properties of the films. Circular Au contact pads with a diameter of 5.6 mm were sputtered on top of the ZnO-Cu_2O structures. Photovoltaic measurements were recorded employing an ABET technologies solar simulator with an AM 1.5 spectrum distribution. Electrical and photovoltaic property effects were studied using a Keithley 2602 source meter. The incident photon-to-electron conversion efficiency (IPCE) measurements were carried out using a customized Newport IPCE setup with

no light biasing. Measurements were conducted at short-circuit with reference to a calibrated Si photodiode (Peccell Limited, S1337 – 1010BQ).

4.3 Results and Discussions

Figure 4.1(a,c-f) shows the SEM top view images of films resulting from variable sputtering power set to 60, 80, 100 and 110 W, respectively. The thickness of the films ranged from 200 to 300 nm upon increasing the power. The ZnO films were composed of columnar grains in a direction normal to the substrate surface, with the base of the grains changing depending on the sputtering power. The ZnO grains were found to be densely packed in all cases. In addition, all films seem to have coral-like structures composed of irregular facades that enhance the surface roughness of the films.

As can be seen from Figure 4.1(a,c) at a low sputtering power of 60 W, the main grains were made of much smaller sub-grains. Interestingly at 80 W, the dimensions of the main grains became dominant and the sub-grains completely disappeared (Figure 4.1(a,d)). The size of the main grains increased when the power was elevated to 100 W and eventually to 110 W (Figure 4.1(a,e) and 4.1(a,f), respectively). The increase in grain size can be due to the fact that at higher powers, ions obtain more energy prior to collision with the substrate.[35] Such high-energy ions are capable of adjusting their bond direction and length in order to obtain optimum bonding to the adjacent atoms, promoting vigorous nucleation that contributes to the grains dimensions.[35]

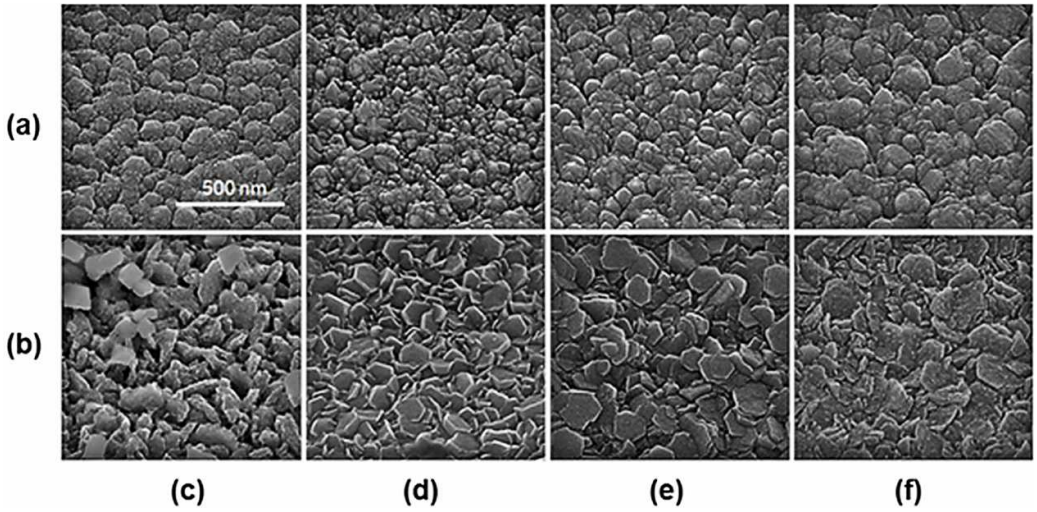

Figure 4.1 SEM images of the surface of ZnO samples (a, c-f) RF sputtered, (b, c-f) electrodeposited under various sputtered powers, (c) 60 W, (d) 80 W, (e) 100 W and (f) 110 W. Scale bars are similar for all figures.

The electrodeposition of ZnO films was conducted as described in the "Experimental" section. The mechanism for the electrodeposition of ZnO films is outlined in equations (4.1)–(4.3). Initially nitrate ions are reduced at the ZnO seed electrode, which raises the electrolyte pH at the solid-solution interface *via* the production of hydroxide ions as shown in equation (4.1). In the presence of zinc ions in the electrolyte $Zn(OH)_4^{2-}$ is formed (equation (4.2)), which converts to ZnO in a dehydration process (equation (4.3)), which occurs rapidly at temperatures greater than 50 ºC.[36, 37]

$$NO_3^- + H_2O + 2e^- \rightarrow NO_2^- + 2OH^- \quad (4.1)$$

$$Zn^{2+} + 2OH^- + 2H_2O \rightarrow Zn(OH)_4^{2-} + 2H^+ \quad (4.2)$$

$$Zn(OH)_4^{2-} + 2H^+ \rightarrow ZnO + 3H_2O \quad (4.3)$$

There are two factors that need to be controlled during the ZnO electrodeposition process: temperature and applied potential.[34, 37] In order to minimise the formation of metallic Zn in the films and promote the process outlined in equations (4.1)–(4.3), the electrodeposition process needs to be carried out at temperatures equal or greater than 50 ºC.[37] In addition, the applied potential must not be too negative so as to avoid hydrogen evolution at the working electrode which would be detrimental to the quality of the electrodeposited film. Therefore, CV experiments were carried out at 62 ºC to elucidate the most appropriate electrodeposition potential for the fabrication of ZnO. Figure 4.2 shows CVs for the electrodeposition of ZnO on five different samples: samples with different seed layers and also blank FTO for comparison. From the current-voltage traces, it is apparent that there is a significant overpotential required for the electrodeposition of ZnO on FTO compared to the seed ZnO layers. Figure 4.3 shows the SEM image of ZnO films electrodeposited onto FTO, demonstrating poor coverage and isolated clusters of ZnO. This shows that the ZnO seed layer is required to increase the adhesion of the ZnO nuclei to the substrate surface. The rougher surface of the seed layer promotes formation of adatoms, which group to form a stable ZnO nucleus.[38]

Figure 4.1(b,c-f) show the SEM images of ZnO films that were electrodeposited on different RF sputtered seed layers. For the film deposited on the 60 W seed layer, the ZnO nanostructures were composed of irregularly shaped grains as shown in Figure 4.1(b,c). The inter-grain spacing was significantly larger than all other samples and many of the grains were loosely placed on the surface. Formation of these loose and isolated ZnO crystals can be observed clearly throughout the films. It is suspected that nucleation is inhibited within the space between the large seed grains and the growth rate of ZnO may be reduced within these areas due to the

diffusion-limited availability of the source materials.[11] For the 80 W seed layer, the electrodeposited grains show uniformly distinctive hexagonal morphologies with clear boundaries (Figure 4.1(b,d)). For the 100 W seed layer, the hexagonal grains size continued to increase but became less dense compared to the 80 W seed layer case as shown in Figure 4.1(b,e). For the 110 W seed layer, the ZnO grains continued to increase in size. However, they significantly deviate from their hexagonal shape and flake like structures with irregular shapes (Figure 4.1(b,f)) appeared. For the films electrodeposited onto 80, 100 and 110 W seed layers, the resultant films consisted of densely packed grains with no evidence of pores. The SEM images clearly show that the morphology of the ZnO seed layers significantly influenced the packing density and shape of the grains in the electrodeposited ZnO films and allowed the crystallinity and morphology of the material to be controlled.

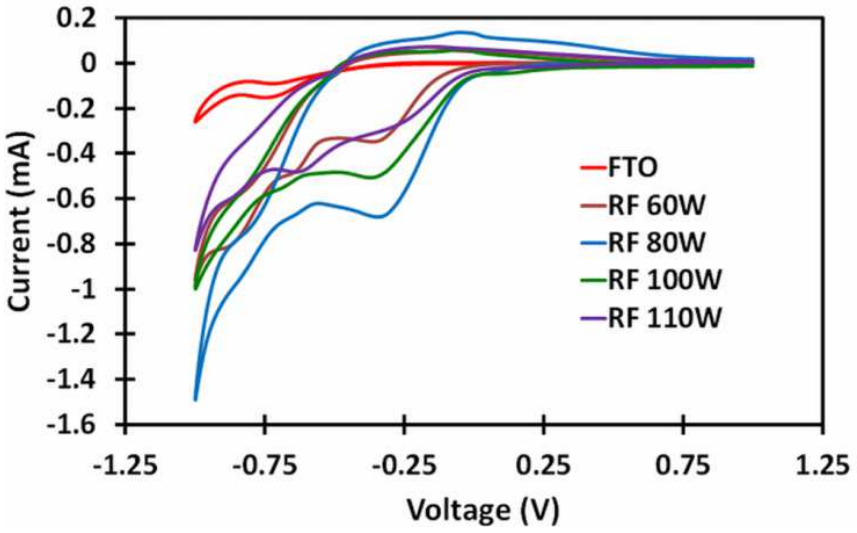

Figure 4.2 Cyclic voltammetry of electrodeposited ZnO layers on different RF sputtered ZnO films on FTO glass substrates as well as a blank FTO for comparison.

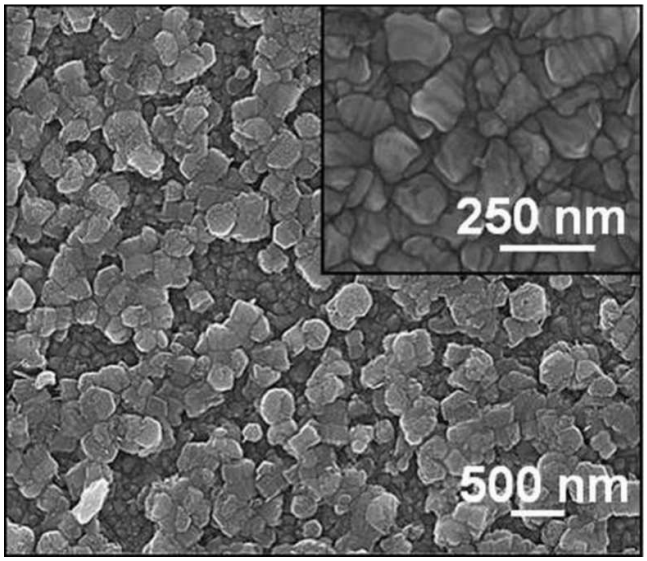

Figure 4.3 Top view SEM image of an electrodeposited ZnO on the FTO glass substrate without a seed layer. Inset: SEM image of the FTO surface.

From the CV data, the electrodeposited film formed onto the 80 W seed layer has the highest reduction peak magnitude at –0.31 V. This cathodic process is due to the reduction of nitrate at the working electrode as stated in equation (4.1). A further rise in cathodic current beyond –0.75 V is most likely due to the direct reduction of Zn^{2+} ions to Zn metal as reported previously.[37, 39] At potentials more negative than −0.90 V a sharp increase in current was detected due to the hydrogen evolution reaction. On the reverse sweep a small anodic peak was observed at –0.50 V, which is due to stripping of Zn metal from the electrode. Here it is clear that the onset potential for ZnO growth is –0.025 V and therefore a potential of –0.70 V was chosen to ensure ZnO growth while avoiding both Zn metal electrodeposition and hydrogen evolution. Interestingly, the magnitude of the reduction peak decreases significantly for the other seed layers of 60, 100, and 110 W respectively, as well as a slight shift to a more negative potential indicating a more inhibited reduction process. This is probably due to the surface morphology and grain sizes of the seed layers.

Smaller grain sizes and increased surface roughness increase both the ease and rate of reduction of the nitrate ions and hence ZnO formation. This suggests defect site driven growth, in particular when compared to the FTO case, which is a much smoother electrode material. Significantly, this results in more densely packed films.

The effect of the seed layers on the surface morphology of the electrodeposited ZnO films were studied using AFM. It has been reported that the morphologies and crystal size of ZnO seed layers affect the quality of the hydrothermally deposited ZnO.[40] Breedon *et. al.* reported that the growth of ZnO nanostructured arrays from HMT assisted solutions on RF sputter coated ZnO substrates is a function of the sputtered crystallite sizes.[41] Wang *et. al.* pointed out that films deposited onto ZnO seeds of (002) preferred orientation led to well-defined hexagonal facets (002) ZnO nanorods grown nearly vertical to the substrates.[42] This work used the same concept but for electrodeposited ZnO films.

Figure 4.4 shows the two-dimension (2D) AFM images of the electrodeposited ZnO films formed onto different seed layers using various sputtering powers. The 60 W seed layer resulted in (Figure 4.4(a)) the smallest surface roughness of the electrodeposited layer with the root mean square (RMS) value of ~12 nm. As the sputtering power increased to 80 W, the surface roughness of the electrodeposited layer increased, showing an RMS value of ~34 nm (Figure 4.4(b)). Further, increasing the sputtering power to 100 and 110 W decreased the surface roughness of the electrodeposited layer to ~28 (Figure 4.4(c)) and ~25 nm (Figure 4.4(d)), respectively. Larger surface roughness are expected to increase the heterointerface area between the *p*-*n* junctions.[43] Therefore, for films with similar crystallinity, the author expects that the electrodeposited film onto the 80 W seed

layer would produce the largest current density. Crystallinity of the films is investigated next.

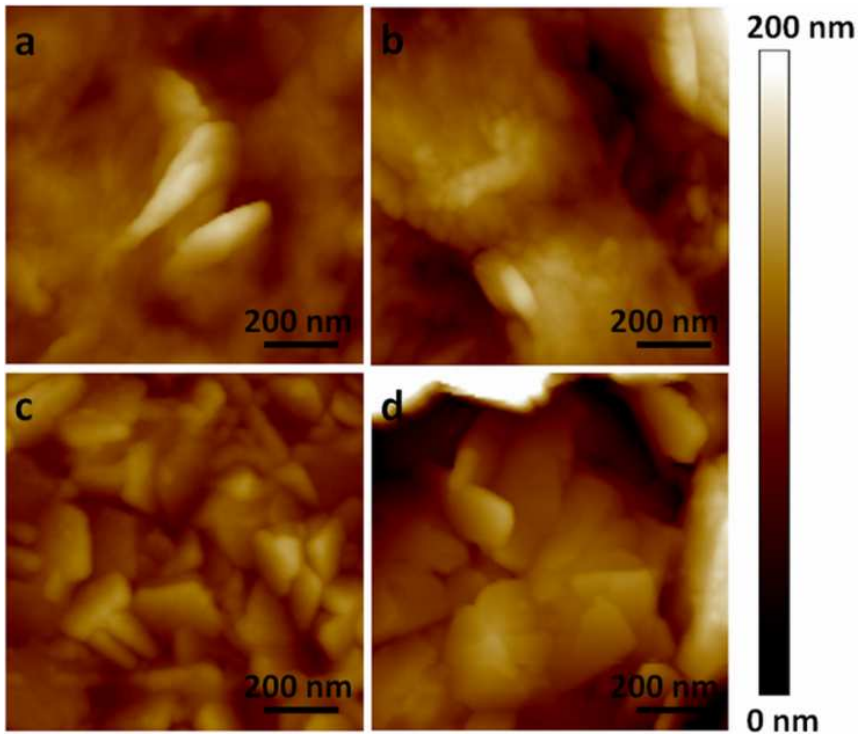

Figure 4.4. AFM images of electrodeposited ZnO thin films grown onto different RF sputtered ZnO seed layers (a) 60 W, (b) 80 W, (c) 100 W and (d) 110 W.

The phases of the obtained ZnO samples were investigated using XRD measurements. Figure 4.5(a) shows the XRD patterns of the seed layers resulting from variable sputtering powers. The films deposited were crystalline in nature with a wurtzite structure which appear in the crystal orientation of (100), (002), (101), (102), (110), (103) and (112) matching ICDD No. [21-1486]. The XRD patterns also show clearly resolved diffraction peaks originating from the FTO substrate noted with asterisks, ICDD No. [41-1445]. At the lower sputtering power of 60 W, the ZnO crystal orientation of (100), (002), (101), (102), (110) and(103) were weak and could

barely resolved. This confirms the SEM observation that the ZnO films were made of smaller sub-grains, which did not receive enough energy to form larger dimensions. Additionally, the films are also the thinnest at this low sputtering power due to smaller growth rates. After increasing the sputtering power to 80 W, the peak intensity, especially for the preferred orientation (002) peak, showed a significant increase compared to the other crystal orientations. By further increasing the power to 100 W, all the wurtzite peaks could be clearly observed, especially the crystal orientation of (103). Interestingly, the preferred orientation (002) peak intensity decreased with the increase of power to 110 W. At high powers, ZnO films became non-stoichiometric due to oxygen deficiency which lead to the growth of less homogeneous films with more crystallographic faults[44] as also observed in the SEM image (Figure 4.1(a,f)).

Figure 4.5(b) show the XRD patterns for the electrodeposited ZnO layers on different ZnO seed layers and blank FTO for comparison. For the ZnO film electrodeposited on blank FTO, the intensity of the ZnO crystal peaks was almost immeasurable and FTO diffraction peaks dominated the pattern. This is due to the poor coverage of ZnO films on the substrate as seen in Figure 4.3. For the electrodeposited film onto the 60 W seed layer, all ZnO crystal orientations of (100), (002), (101), (102), (110), (103) and (112) peaks can be observed. Most of the peaks were weak as the SEM image also revealed that the grains were randomly oriented on the surface. For the higher power seed layer of 80 W, the crystallinity of the electrodeposited ZnO film improved significantly, especially evidenced by the increase in the intensity of (002) peak. In confirmation, uniformly distinctive hexagonal morphologies with clear boundaries could also be observed in the SEM images (Figure 4.1(b,d)). This increase was continued further for the sample with

the 100 W seed layer. Interestingly, the (002) ZnO peak emerged as the dominant peak, indicating the presence of ordered ZnO to a large extent. For the 110 W seed layer, peaks corresponding to the (100) and (101) planes show an increase in their intensities, indicating better crystallinity towards (100) and (101) planes in comparison with the film obtained at lower sputtering powers.

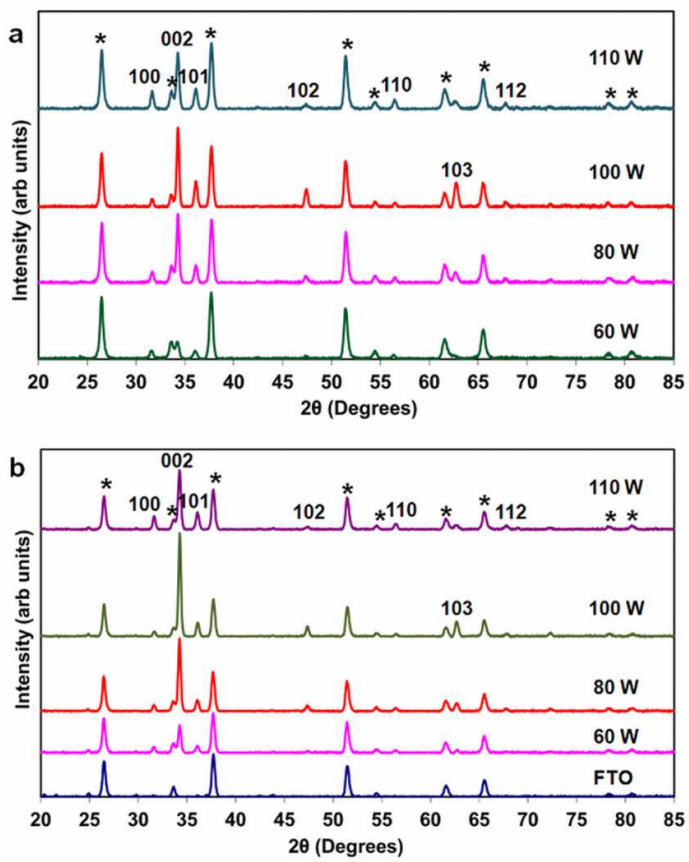

Figure 4.5 XRD patterns of ZnO films (a) RF sputtered at different applied powers and (b) electrodeposited. FTO is indicated with an *.

Figure 4.6 shows SEM micrographs of the ZnO-Cu_2O heterojunction by electrodepositing Cu_2O (of 1.8 μm thickness) on top of the ZnO films (only the sample incorporating the electrodeposited ZnO onto the 80 W seed layer is demonstrated). Cu_2O was formed according to the following electrochemical reaction:[15]

$$2Cu^{2+} + 2e^{-} + 2OH^{-} \rightarrow Cu_2O + H_2O \qquad (4.4)$$

The electrodeposition process was carried out potentiostatically at −0.55 V *vs* Ag/AgCl and the deposition time was varied from 1000 to 2500 s. During the electrodeposition process, the solution was kept at 40 ºC without stirring as suggested by Izaki *et. al*.[15] The Cu_2O film was composed of columnar grains grown in the direction normal to the substrate surface. No defects, such as pores or pin-holes, were observed on the surface or throughout the film thickness. Top and cross-sectional views shown in Figure 4.6(a) and (b) indicate that the ZnO and Cu_2O films clearly establish a rough heterointerface between the films. Figure 4.6(c) and (d) show the crystal grains of ZnO and Cu_2O, respectively.

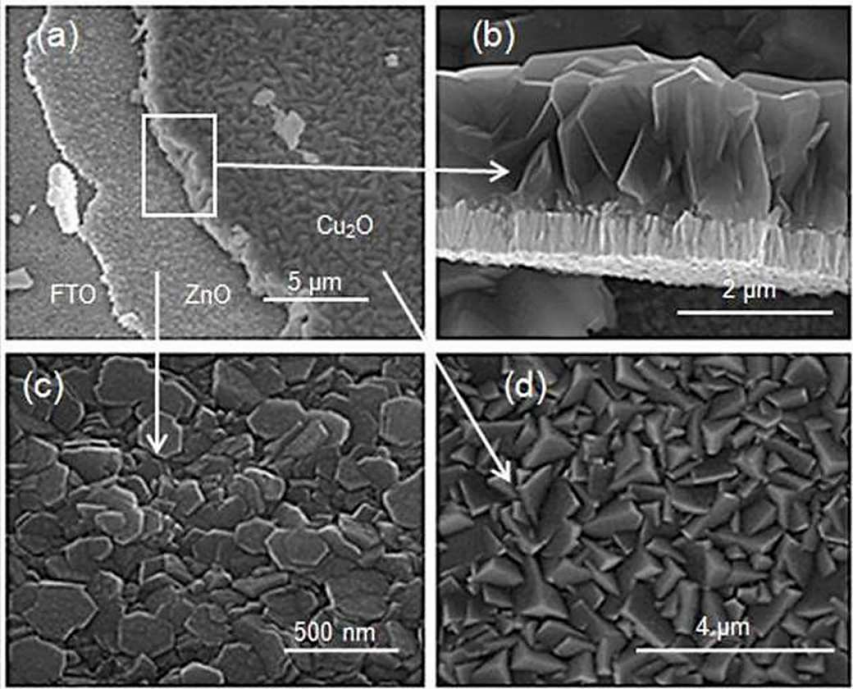

Figure 4.6 SEM images of surface morphology and cross-section (a) top view image of ZnO-Cu_2O on a FTO glass substrate, (b) 45 º tilted image of the ZnO-Cu_2O heterojunction, (c) top view image of electrodeposited ZnO film and (d) top view image of electrodeposited Cu_2O film.

The composition of the electrodeposited ZnO-Cu_2O heterojunction was analyzed using the XRD measurements. Figure 4.7 shows the XRD patterns of films comprising Cu_2O on ZnO electrodeposited onto ZnO seed layers, resulting from sputtering powers of 60, 80, 100, and 110 W and blank FTO. The XRD pattern of ZnO-Cu_2O without a seed layer reflects the dominant peak at 2θ value of 36.5º corresponding to the (111) plane of Cu_2O (ICDD No. [75-1531]). Secondary peaks at 29.6 º, 42.4 º, 52.6 º, 61.5 º, 73.7 º and 77.6 º corresponding to (110), (200), (211), (220), (311) and (222) planes of Cu_2O, respectively, were also observed. Peaks corresponding to ZnO were barely resolved. However, device with seed layers show ZnO peaks at 34.4 º, 47.5 º and 62.9 º corresponding to the (002), (102) and (103) planes of ZnO, respectively. At a low sputtering power of 60 W, strong Cu_2O peaks of (111), (200) and (220) dominated the films. At a higher sputtering power of 80 W and 100 W, the films were dominated by the (111) planes of Cu_2O, indicating the presence of ordered Cu2O to a larger extent. [11, 45] However, at the larger power of 110 W, the (111) Cu_2O crystal plane was no longer dominant as other crystal orientations such as (200) and (220) peaks appeared with intensities significantly larger than achieved when Cu_2O was electrodeposited onto films that had seed layers fabricated at the lower power of 80 and 100 W films. This indicates that Cu_2O in this film is highly crystalline with a random distribution of cuprous oxide crystals. In all measurements, weak ZnO peak intensities were observed due to the presence of ZnO underneath the Cu_2O films.

For a more precise determination of phase composition of the films, Raman spectra were also obtained and presented in Figure 4.8. The Cu_2O peaks were noted with asterisks. Three peaks located at 110, 146 and 217 cm^{-1} are observed and ascribed to Cu_2O.[24, 45, 46] The broad peaks centred at 512 and 626 cm^{-1} are also

believed to be contributed by Cu_2O.[24] A ZnO peak is also observed at 407 cm^{-1} associated with the E_2 vibration of the wurtzite lattice.[37, 47] The Raman spectra of ZnO-Cu_2O films agree well with the XRD results for sample composition identification.

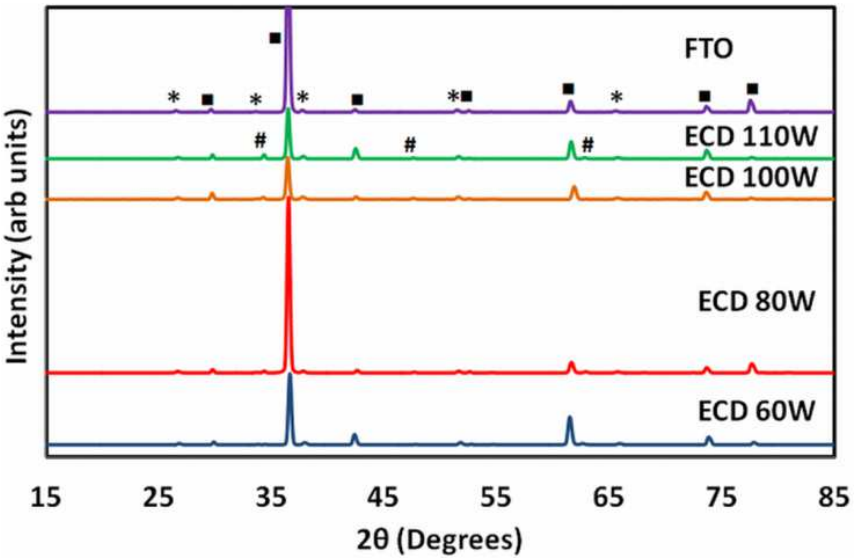

Figure 4.7 XRD patterns for ZnO-Cu_2O films: the ZnO electrodeposited films are formed onto RF sputtered ZnO seed layers, which are deposited onto FTO. For comparison, the XRD pattern of the electrodeposited Cu_2O onto electrodeposited ZnO without any seed layer is also demonstrated. FTO is indicated with an *****, ZnO is indicated with a #, and Cu_2O is indicated with a ■

In order to further understand the effects of ZnO seed layers at the heterointerface of the electrodeposited ZnO-Cu_2O, AFM adhesion mapping was carried out on the electrodeposited ZnO thin films grown onto different RF sputtered ZnO seed layers (Figure 4.9). The adhesion mapping is determined by the contact region difference between tip-approach and tip-retract while scanning the surface of the films. A strong adhesion is clear when a high difference in horizontal (*z*) position of the jump-to-contact and jump-to-off-contact points occurs. The amount of force just before the jump-off-contact gives a measurement of the maximum tip-sample adhesion. The

corresponding sample adhesion, which is measured by this force, is then translated into an image as a function of (x,y) position. The dark areas of the adhesion mapping images correspond to lower adhesion to the surface, relative to other areas of the surface. The films formed using a 60 W seed layer surface (Figure 4.9(a)) show the greatest adhesion compared to the rest of the samples. Interestingly, as the sputtering power increased to 80 W (Figure 4.9(b)) and 100 W (Figure 4.9(c)), the surface adhesion properties of the electrodeposited layer decreased significantly. By further increasing the sputtering power to 110 W, the adhesion of the films increased but was lower than the 60 W sample (Figure 4.9(d)).

The author also carried out direct observation of cross section images of heterointerface electrodeposited ZnO-Cu_2O grown onto different rf sputtered ZnO seed layers (a) 60 W, (b) 80 W, (c) 100 W and (d) 110 W using FEI Nova NanoSEM (Figure 4.10). Based on the SEM images, the author observed that the heterointerface for the 60W (Figure 4.10(a)) sample is the most different from the other three. It seems that the Cu_2O interface for the 60W sample is made of less crystalline materials, and does not have the perfect crystal grain perfection that are specifically seen in the 80 (Figure 4.10(b)) and 100 W (Figure 4.10(c)) samples after cleaving the films. It is found that a highly adhesive surface hinders the formation of highly crystalline Cu_2O, which is also confirmed by the XRD patterns as shown in Figure 4.7.

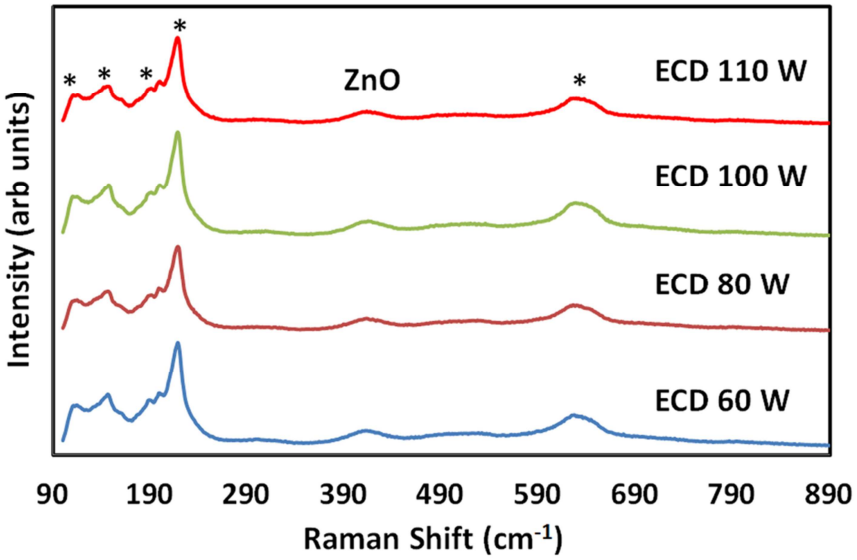

Figure 4.8 Raman spectra of ZnO-Cu_2O films. The ZnO electrodeposited films are formed onto RF sputtered ZnO seed layers, which are deposited onto FTO substrate.

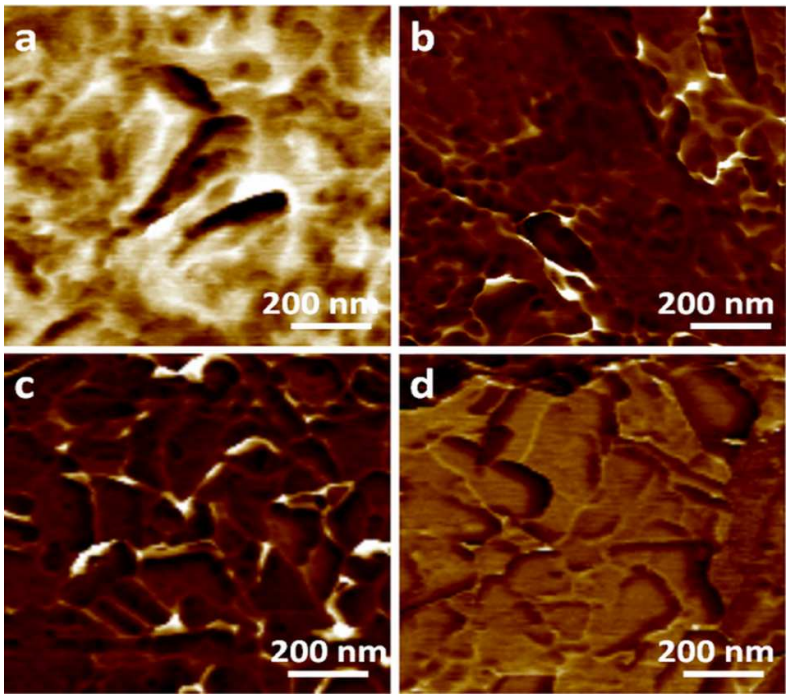

Figure 4.9 AFM adhesion images (arbitrary units) of electrodeposited ZnO thin films grown onto different RF sputtered ZnO seed layers (a) 60 W, (b) 80W, (c) 100 W and (d) 110 W. The dark areas correspond to lower adhesion.

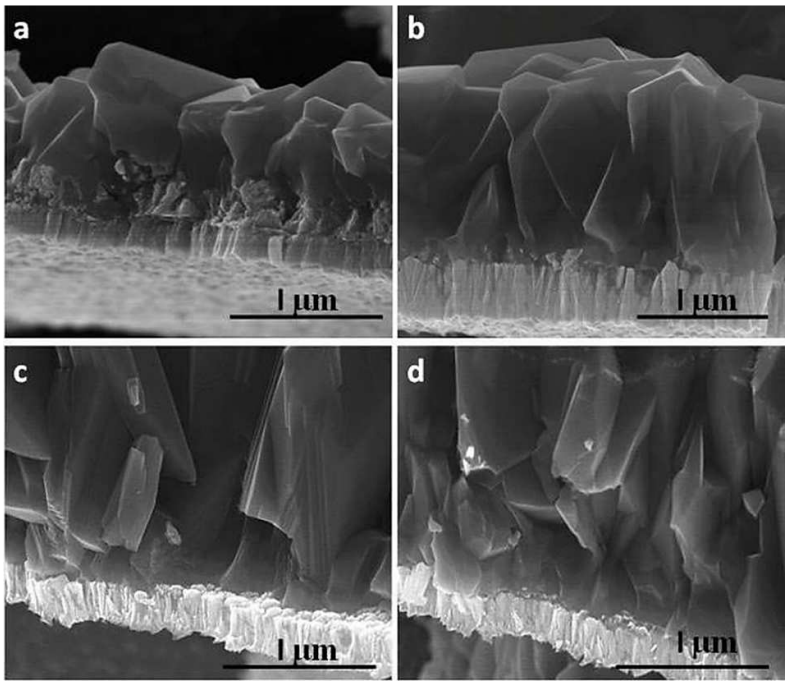

Figure 4.10 SEM cross section image of electrodeposited ZnO-Cu_2O heterojunction grown onto different RF sputtered ZnO seed layers (a) 60 W, (b) 80 W, (c) 100 W and (d) 110 W.

In order to probe the effect of RF sputtered seed layers on interface morphology and material composition and the subsequent effect on electrical conduction, photovoltaic devices were prepared. The photovoltaic power conversion efficiencies (PCEs) of electrodeposited ZnO-Cu_2O devices were studied by measuring the current density-voltage (*J*-*V*) characteristics at simulated AM 1.5 solar illumination (100 mW cm^{-2}). Illumination was through the FTO substrate.

The schematic of the developed ZnO-Cu_2O heterojunction solar cells is illustrated in Figure 4.11(a). The photovoltaic *J*-*V* curves for different ZnO-Cu_2O heterojunctions under AM 1.5 illumination are shown in Figure 4.11(b) and the corresponding parameters of the measured solar cells are summarized in Table 4.1. The author fixed the electrodeposition duration for ZnO and Cu_2O at 1000 s and 2000 s, respectively. The thicknesses of the electrodeposited ZnO films were found

to be consistent even though different seed layers were used. It can be concluded that the ZnO seed layers have less significant influence on the final thickness of the ZnO film compared to morphology or crystallinity of the films.

The ZnO-Cu_2O film heterojunction prepared on a blank FTO (*i.e.* without using any seed layer of ZnO) exhibited the lowest PCE of 0.09% with an open circuit voltage (V_{oc}) of 0.071 V, a short circuit current density (J_{sc}) of 5.25 mA cm^{-2} and a fill factor (FF) of 23.87%. As mentioned previously, on the blank FTO, the ZnO electrodeposition process only produced a poor coverage as shown in Figure 4.3. The effect was even more exacerbated due to the solubility of ZnO in the high pH solution for the deposition of Cu_2O, leading to the formation of pinholes throughout the ZnO layer. These pinholes were then filled by Cu_2O and formed shunted diodes and a short circuit between the FTO glass substrate and the electron conductor layer.

The solar cells performance improved significantly when thin layers incorporating ZnO seed layers were used. The combination of RF sputtered seed layer and electrodeposited ZnO layers promoted the formation of stable ZnO nuclei, resulting in more robust ZnO films. Therefore, pin-hole problems were successfully resolved.

The ZnO-Cu_2O heterojunction device prepared with a seed layer of 60 W produced the lowest photovoltaic properties among the other seed layers with V_{oc}, J_{sc}, *FF* and PCE of 0.161 V, 6.83 mA cm^{-2}, 27.19 %, and 0.30 %, respectively. This is most likely due to the poor crystallinity of the ZnO and Cu_2O films (due to the small intensity of (111) for Cu_2O - a result of higher ZnO surface adhesive properties, Figure 4.9(a) - and (002) for ZnO films) as well as the lower heterointerface surface roughness, as demonstrated by the AFM measurements (Figure 4.4(a)). In addition,

the formation of isolated ZnO crystallites as shown in Figure 4.1(b,c) possibly increased the internal resistance of the films and reduced the current density of the device.

As the author increased the RF power of the seed layer to 80 W, the photovoltaic properties of the device significantly enhanced. V_{oc}, J_{sc}, *FF* and PCE increased to 0.248 V, 12.7 mA cm^{-2}, 32.40 % and 1.02 %, much larger than the device incorporating the 60 W seed layer. As demonstrated using AFM, XRD and SEM characterizations, this can be due to a combination of the increase in the junction interface area, higher surface roughness, lower adhesion at the heterointerface and better crystallinity of both ZnO and Cu_2O films. Figure 4.1(b,d) clearly shows that the ZnO grains have uniformly distinctive and perfect hexagonal morphologies.

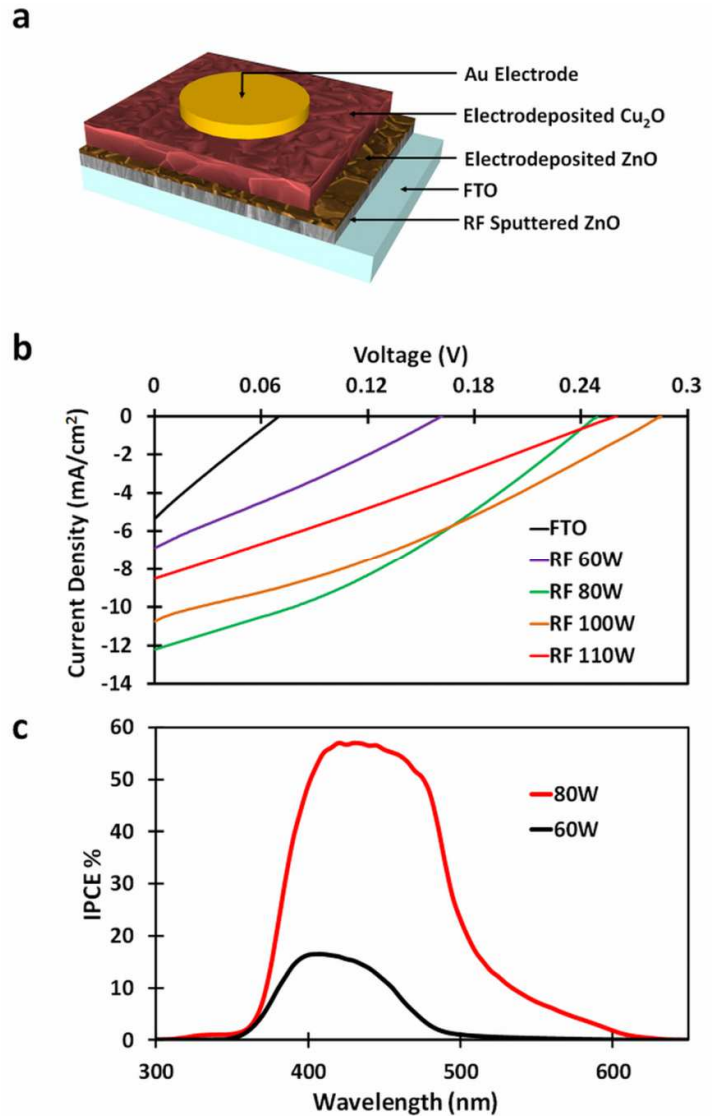

Figure 4.11 Schematic and characteristic of the ZnO-Cu_2O based heterojunction solar cells. (a) The 3D schematic of the electrodeposited ZnO-Cu_2O solar cells incorporating different RF sputtered ZnO seed layers, and (b) *J-V* characteristic curves of four types ZnO-Cu_2O heterojunction solar cells. For comparison the response of the electrodeposited ZnO-Cu_2O without any seed layer is also demonstrated. (c) The IPCE spectra of ZnO-Cu_2O based heterojunction solar cells incorporating 60 and 80 W sputtered seed layers.

Table 4.1. Photovoltaic properties of five types of ZnO–Cu2O solar cells obtained from Figure 4.11

Solar Cell	J_{SC} (mA/cm^2)	V_{OC} (V)	FF (%)	PCE (%)
FTO	5.25	0.071	23.87	0.09
RF 110W	8.51	0.262	26.10	0.58
RF 100W	10.84	0.285	31.35	0.95
RF 80W	12.78	0.248	32.40	1.02
RF 60W	6.83	0.161	27.19	0.30

However, further increasing the sputtering power of the incorporated seed layer to 100 W did not improve the photovoltaic properties any further. Although the hexagonal grains dimensions continued to increase, less densely packed grains were observed compared to the 80 W case as shown in Figure 4.1(b,e).This resulted in a decrease in surface roughness as confirmed by the AFM measurements. This factor may explain the reduction of short circuit current density from 12.7 to 10.8 mA cm^{-2} for devices incorporating 80 and 100 W seed layers, respectively. Interestingly, the open circuit voltage increased slightly from 0.248 to 0.285 V. This can be ascribed to a decrease in the interface states density at the heterointerface due to the reduction of the surface to volume ratio. This limits the unwanted band bending and carrier recombination of the film. A full explanation about the interface states is discussed thoroughly by Musselman *et. al.*[8] To summarize, if a significant number of states exist at the interface of the heterojunction films that act as acceptors, electrons may be removed from the depletion region and bend the energy band of Cu_2O upwards. Upward band bending in Cu_2O near the interface would therefore reduce the open circuit voltage of the device.[8] Interface state density has direct correlation with the

surface to volume ratio between *p-n* junctions. A larger surface-to-volume produces more interface state.[8]

As expected, increasing the sputtering power to 110 W further deteriorated the solar cell performance. J_{sc}, V_{oc} and PCE showed a small decrease in comparison with 100 W but still much higher than 60 W. As the RF power increased to 110 W, the ZnO grains continued to increase in size and lost their hexagonal shape and eventually converted to flake like structures with irregular morphologies (Figure 4.1 (b,f)). As a result, J_{sc} was reduced to 8.51 mA cm^{-2}. Obviously, the decrease of J_{sc} reduces the PCE. The same trend is expected for further increasing the sputtering power. In order to verify the reproducibility of the solar cells performance, the author fabricated six different samples for each type of ZnO-Cu_2O heterojunction solar cells and obtained the average values (Figure 4.12).

The IPCE spectra of solar cells prepared using 60 and 80 W ZnO seed layers are shown in Figure 4.11(c). These two solar cells were chosen as they presented the highest and lowest PCEs. As expected, the peak magnitude of the IPCE spectrum of the device which incorporated the 80 W seed layer was four times larger than its 60 W counterpart, showing a maximum conversion efficiency of 57.2% in comparison to 15.8%. These numbers indicate that the larger surface area between the *p-n* junction and the improved crystallinity of the electrodeposited ZnO films has a positive effect on the IPCE. From the measured IPCE and known solar spectrum, J_{sc} can be predicted ($J_{sc} = q \int \mathrm{AM1.5}(\lambda) \times \mathrm{IPCE}(\lambda) \times d\lambda$). The measured J_{sc} under AM1.5 illumination is higher than the calculated J_{sc} for both of the *J-V* curves that can be ascribed to the charge trapping affect in the low light intensity IPCE measurements.[5, 48, 49]

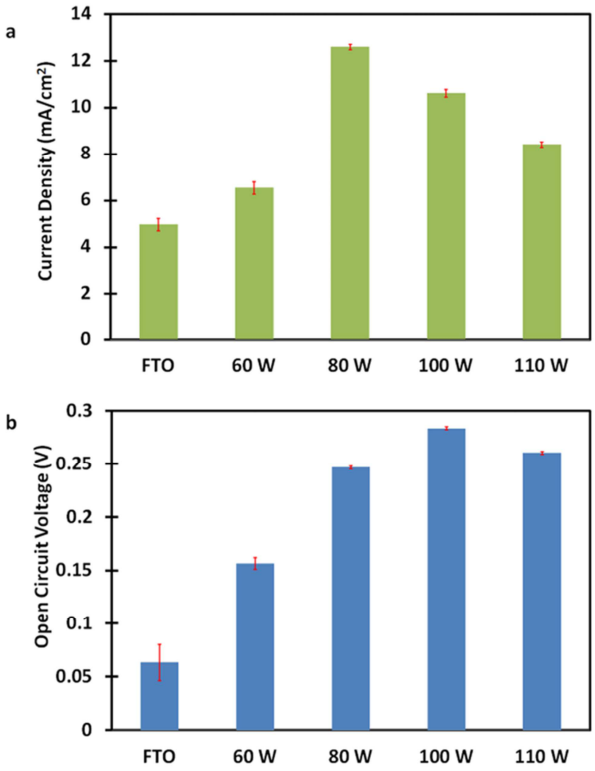

Figure 4.12 Average of short circuit current density and open circuit voltage values for five types of ZnO-Cu_2O heterojunction solar cells. The tests were performed on six similarly fabricated samples.

4.4 Summary

In this chapter, the author of this PhD thesis demonstrated the effect of ZnO seed layers on the electrodeposited ZnO films in ZnO-Cu_2O heterojunctions as well as the photovoltaic performance of such devices. By incorporating RF sputtered ZnO seed layers, the author was able to tune the growth conditions and adhesion properties of the ZnO layer surface as well as the crystal quality, morphology and surface roughness of the interfaces between the electrodeposited ZnO and Cu_2O films in order to produce excellent heterojunctions with large surface-to-volume ratios. The seed layer also proved to be effective in ensuring pinhole-free films. These factors

enabled the as-deposited ZnO-Cu_2O heterojunction solar cells to reach a relatively high photovoltaic performance of 1.02 % using seed layers which were deposited at 80 W. In addition to this, the current density obtained was the largest ever reported (12.7 mA cm^{-2}) for such a heterojunction.

In the next chapter, the author will present his work on memristors based on ZnO thin films. The author will discuss the fabrication process, the methods that he has implemented for tuning their properties, their performance and the mechanism governing the switching of these memristors.

References

[1] S. M. Sze and K. K. Ng, *Physics of Semiconductor Devices*. New Jersey: John Wiley and Sons, 2007.

[2] C. M. Lieber, "One-Dimensional Nanostructures: Chemistry, Physics & Applications," *Solid State Commun.*, vol. 107, pp. 607-616, 1998.

[3] H. Wei, H. Gong, Y. Wang, X. Hu, L. Chen, H. Xu, *et al.*, "Three Kinds of Cu_2O/ZnO Heterostructure Solar Cells Fabricated With Electrochemical Deposition And Their Structure-Related Photovoltaic Properties," *Crystengcomm*, vol. 13, pp. 6065-6070, 2011.

[4] A. E. Rakhshani, "Preparation, characteristic and photovoltaic properties of cuprous oxide - A review," *Solid State Electron.*, vol. 29, pp. 7-17, 1986.

[5] S. S. Jeong, A. Mittiga, E. Salza, A. Masci, and S. Passerini, "Electrodeposited ZnO/Cu_2O Heterojunction Solar Cells," *Electrochim. Acta*, vol. 53, pp. 2226-2231, 2008.

[6] S. Jeong and E. S. Aydil, "Heteroepitaxial growth of Cu_2O thin film on ZnO by metal organic chemical vapor deposition," *J. Cryst. Growth*, vol. 311, pp. 4188-4192, 2009.

[7] J. Katayama, K. Ito, M. Matsuoka, and J. Tamaki, "Performance of Cu_2O/ZnO solar cell prepared by two-step electrodeposition," *J. Appl. Electrochem.*, vol. 34, pp. 687-692, 2004.

[8] K. P. Musselman, A. Marin, A. Wisnet, C. Scheu, J. L. MacManus-Driscoll, and L. Schmidt-Mende, "A Novel Buffering Technique for Aqueous Processing of Zinc Oxide Nanostructures and Interfaces, and Corresponding Improvement of Electrodeposited ZnO-Cu_2O Photovoltaics," *Adv. Funct. Mater.*, vol. 21, pp. 573-582, 2011.

[9] K. P. Musselman, A. Wisnet, D. C. Iza, H. C. Hesse, C. Scheu, J. L. MacManus-Driscoll, *et al.*, "Strong Efficiency Improvements in Ultra-low-

Cost Inorganic Nanowire Solar Cells," *Adv. Mater.*, vol. 22, pp. E254-E285, 2010.

[10] T. Minami, Y. Nishi, T. Miyata, and J. Nomoto, "High-Efficiemcy Oxide Solar Cells with ZnO/Cu_2O Heterjunction Fabricated on Thermally Oxidized Cu_2O sheets," *Appl. Phys. Express*, vol. 4, p. 62301, 2011.

[11] J. B. Cui and U. J. Gibson, "A Simple Two-Step Electrodeposition of Cu_2O/ZnO Nanopillar Solar Cells," *J. Phys. Chem. B,* vol. 114, pp. 6408-6412, 2010.

[12] A. Mittiga, E. Salza, F. Sarto, M. Tucci, and R. Vasanthi, "Heterojunction Solar Cell with 2% Efficiency Based on a Cu_2O Substrate," *Appl. Phys. Lett.*, vol. 88, p. 163502, 2006.

[13] E. W. Bohannan, L. Y. Huang, F. S. Miller, M. G. Shumsky, and J. A. Switzer, "In Situ Electrochemical Quartz Crystal Microbalance Study of Potential Oscillations During the Electrodeposition of Cu/Cu_2O Layered Nanostructures," *Langmuir*, vol. 15, pp. 813-818, 1999.

[14] B. M. Fariza, J. Sasano, T. Shinagawa, H. Nakano, S. Watase, and M. Izaki, "Electrochemical Growth of (0001)-n-ZnO Film on (111)-p-Cu_2O Film and the Characterization of the Heterojunction Diode," *J. Electrochem. Soc.*, vol. 158, pp. 621-625, 2011.

[15] M. Izaki, T. Shinagawa, K.-T. Mizuno, Y. Ida, M. Inaba, and A. Tasaka, "Electrochemically Constructed P-Cu_2O/N-ZnO Heterojunction Diode for Photovoltaic Device," *J. Phys. D Appl. Phys.*, vol. 40, pp. 3326-3329, 2007.

[16] S. Xu and Z. L. Wang, "One-Dimensional ZnO Nanostructures: Solution Growth and Functional Properties," *Nano Res.*, vol. 4, pp. 1013-1098, 2011.

[17] A. Roos and B. Karlsson, "Properties of Oxidized Copper Surfaces for Solar Applications II," *Sol. Energ. Mater.*, vol. 7, pp. 467-480, 1983.

[18] N. Kikuchi and K. Tonooka, "Electrical and Structural Properties of Ni-doped Cu_2O Films Prepared by Pulsed Laser Deposition," *Thin Solid Films,* vol. 486, pp. 33-37, 2005.

[19] D. A. Firmansyah, T. Kim, S. Kim, K. Sullivan, M. R. Zachariah, and D. Lee, "Crystalline Phase Reduction of Cuprous Oxide (Cu_2O) Nanoparticles Accompanied by a Morphology Change during Ethanol-Assisted Spray Pyrolysis," *Langmuir*, vol. 25, pp. 7063-7071, 2009.

[20] A. H. Jayatissa, K. Guo, and A. C. Jayasuriya, "Fabrication of Cuprous and Cupric Oxide Thin Films by Heat Treatment," *Appl. Surf. Sci.*, vol. 255, pp. 9474-9479, 2009.

[21] L. S. Huang, S. G. Yang, T. Li, B. X. Gu, Y. W. Du, Y. N. Lu, *et al.*, "Preparation of Large-Scale Cupric Oxide Nanowires by Thermal Evaporation Method," *J. Cryst. Growth*, vol. 260, pp. 130-135, 2004.

[22] A. J. Morfa, G. Beane, B. Mashford, B. Singh, E. Della Gaspera, A. Martucci, *et al.*, "Fabrication of ZnO Thin Films from Nanocrystal Inks," *J. Phys. Chem. C*, vol. 114, pp. 19815-19821, 2010.

[23] C. L. Chu, H. C. Lu, C. Y. Lo, C. Y. Lai, and Y. H. Wang, "Physical Properties of Copper Oxide Thin Films Prepared by DC Reactive Magnetron Sputtering Under Different Oxygen Partial Pressures," *Physica B,* vol. 404, pp. 4831-4834, 2009.

[24] Y. M. Lu, J. Y. Chen, and T. S. Wey, "Nano Cuprous Oxides film Prepared by Magnetron Sputtering," *Mater. Res. Soc. Symp. P*, vol. 822, pp. 55-64, 2004.

[25] Y. M. Lu, W. S. Hwang, W. Y. Liu, and J. S. Yang, "Effect of RF Power on Optical and Electrical Properties of ZnO Thin Film by Magnetron Sputtering," *Mater. Chem. Phys.*, vol. 72, pp. 269-272, 2001.
[26] J. L. Campbell, M. Breedon, K. Latham, and K. Kalantar-zadeh, "Electrowetting of Superhydrophobic ZnO Nanorods," *Langmuir*, vol. 24, pp. 5091-5098, 2008.
[27] B. J. Plowman, S. K. Bhargava, and A. P. O'Mullane, "Electrochemical Fabrication of Metallic Nanostructured Electrodes for Electroanalytical Applications," *Analyst*, vol. 136, pp. 5107-5119, 2011.
[28] B. M. Fariza, J. Sasano, T. Shinagawa, S. Watase, and M. Izaki, "Light-assisted electrochemical construction of (111)Cu_2O/(0001)ZnO heterojunction," *Thin Solid Films*, pp. 2261-2264, 2011.
[29] V. Donderis, M. A. Hernández-Fenollosa, L. C. Damonte, B. Marí, and J. Cembrero, "Enhancement of Surface Morphology and Optical Properties of Nanocolumnar ZnO films," *Superlattice. Micros.*, vol. 42, pp. 461-467, 2007.
[30] X. J. Huang, O. Yarimaga, J. H. Kim, and Y. K. Choi, "Substrate Surface Roughness-Dependent 3-D Complex Nanoarchitectures of Gold Particles from Directed Electrodeposition," *J. Mater. Chem.*, vol. 19, pp. 478-483, 2009.
[31] A. I. Inamdar, S. H. Mujawar, S. B. Sadale, A. C. Sonavane, M. B. Shelar, P. S. Shinde, *et al.*, "Electrodeposited zinc oxide thin films: Nucleation and growth mechanism," *Sol. Energ. Mater. Sol. C.*, vol. 91, pp. 864-870, 2007.
[32] S. J. Limmer, E. A. Kulp, and J. A. Switzer, "Epitaxial electrodeposition of ZnO on Au(111) from alkaline solution: Exploiting amphoterism in Zn(II)," *Langmuir*, vol. 22, pp. 10535-10539, 2006.
[33] A. S. Zoolfakar, R. A. Rani, A. J. Morfa, S. Balendhran, A. P. O'Mullane, S. Zhuiykov, *et al.*, "Enhancing The Current Density of Electrodeposited ZnO-Cu_2O Solar Cells by Engineering Their Heterointerfaces," *J. Mater. Chem.*, vol. 22, pp. 21767-21775, 2012.
[34] M. Izaki and T. Omi, "Transparent zinc oxide films prepared by electrochemical reaction," *Appl. Phys. Lett.*, vol. 68, pp. 2439-2440, 1996.
[35] X. H. Yu, J. Ma, F. Ji, Y. H. Wang, X. J. Zhang, C. F. Cheng, *et al.*, "Effects of sputtering power on the properties of ZnO : Ga films deposited by r.f. magnetron-sputtering at low temperature," *J. Cryst. Growth*, vol. 274, pp. 474-479, 2005.
[36] C. V. Manzano, D. Alegre, O. Caballero-Calero, B. Alen, and M. S. Martin-Gonzalez, "Synthesis and luminescence properties of electrodeposited ZnO films," *J. Appl. Phys.*, vol. 110, p. 043538, 2011.
[37] A. Chatterjee and J. Foord, "Electrochemical Deposition of Nanocrystalline Zinc Oxide at Conductive Diamond Electrodes," *Diam. Relat. Mater.*, vol. 15, pp. 664-667, 2006.
[38] J. Cembrero and D. Busquets-Mataix, "ZnO Crystals Obtained by Electrodeposition: Statistical Analysis of Most Important Process Variables," *Thin Solid Films*, vol. 517, pp. 2859-2864, 2009.
[39] A. I. Inamdar, S. H. Mujawar, S. R. Barman, P. N. Bhosale, and P. S. Patil, "The effect of bath temperature on the electrodeposition of zinc oxide thin films via an acetate medium," *Semicond. Sci. Tech.*, vol. 23, pp. 1-6, 2008.
[40] B. Weintraub, Z. Zhou, Y. Li, and Y. Deng, "Solution synthesis of one-dimensional ZnO nanomaterials and their applications," *Nanoscale*, vol. 2, pp. 1573-1587, 2010.

[41] M. Breedon, J. Yu, W. Wlodarski, and K. Kalantar-Zadeh, "ZnO Nanostructured Arrays Grown from Aqueous Solutions on Different Substrates," presented at the 2008 International Conference on Nanoscience and Nanotechnology, 2008.

[42] S. F. Wang, T. Y. Tseng, Y. R. Wang, C. Y. Wang, and H. C. Lu, "Effect of ZnO seed layers on the solution chemical growth of ZnO nanorod arrays," *Ceram. Int.*, vol. 35, pp. 1255-1260, 2009.

[43] Y.-M. Shen, C.-S. Chen, P.-C. Yang, S.-Y. Ma, and C.-F. Lin, "Improvement of surface morphology of thin films and performance by applying electric field on P3HT:PCBM based solar cells," *Sol. Energ. Mater. Sol. C.*, vol. 99, pp. 263-267, 2012.

[44] S.-S. Lin, J.-L. Huang, and D.-F. Lii, "The effects of r.f. power and substrate temperature on the properties of ZnO films," *Surf. Coat. Tech.*, vol. 176, pp. 173-181, 2004.

[45] L. Wu, L.-k. Tsui, N. Swami, and G. Zangari, "Photoelectrochemical Stability of Electrodeposited Cu_2O Films," *J. Phys. Chem. C*, vol. 114, pp. 11551-11556, 2010.

[46] A. Compaan and H. Z. Cummins, "Raman Scattering, Luminescence and Exciton Phonon Coupling in Cu_2O " *Phys. Rev. B*, vol. 6, pp. 4753 - 4757, 1972.

[47] K. A. Alim, V. A. Fonoberov, M. Shamsa, and A. A. Balandin, "Micro-Raman investigation of optical phonons in ZnO nanocrystals," *J. Appl. Phys.*, vol. 97, p. 124313, 2005.

[48] P. E. de Jongh and D. Vanmaekelbergh, "Investigation of the electronic transport properties of nanocrystalline particulate TiO2 electrodes by intensity-modulated photocurrent spectroscopy," *J. Phys. Chem. B*, vol. 101, pp. 2716-2722, 1997.

[49] T. Trupke, P. Wurfel, and I. Uhlendorf, "Dependence of the photocurrent conversion efficiency of dye-sensitized solar cells on the incident light intensity," *J. Phys. Chem. B*, vol. 104, pp. 11484-11488, 2000.

Chapter 5

Engineering Electrodeposited ZnO Films and Their Memristive Switching Performance

5.1 Introduction

In this Chapter, the PhD candidate presents the outcomes of his investigation on the development of ZnO memristors. Based on the knowledge achieved regarding the tuning and engineering of electrodeposited ZnO films *via* seed layers approach, as described in Chapter 4, the author draws his attention to employ a similar concept for developing high performance of electrodeposited ZnO based memristive switches.

Memristive switching involves a "switch" from a high resistance state (HRS, or "OFF" state) to a low resistance state (LRS, or "ON" state) and *vice versa*. Generally, such a switching mechanism can be classified according to the dominant contribution to this effect including thermal, electronic or ionic effect during the ON/OFF process. [1, 2] Transition metal oxide based memristive devices have attracted considerable attention due to their electronics and electrical structural simplicity, low power consumption, fast switching, high density integration and process compatibility with CMOS technologies. [3-7] Transition metal oxides such as TiO_2 [5, 8, 9], NiO [10, 11], Al_2O_3 [12], HfO_2 [13], ZrO_2 [14], Ta_2O_5 [15], SnO_2 [16] and ZnO [7, 17, 18] are some of the promising materials for memristive applications.

Amongst the various transition metal oxides being investigated for memristor applications, ZnO possesses several advantages. As described in Chapters 2 and 4,

ZnO has favourable properties including a wide band gap (3.37 eV), high electron mobility (~120 $cm^2\ V^{-1}\ s^{-1}$), and large excitation binding energy (60 meV). [19-21] It is also inexpensive and abundant. For memristive devices, a wide band gap metal oxide is favourable due to its susceptibility to doping by incorporating a variety of defects and impurities. Typically, as synthesized ZnO is intrinsically "self-doped" by native interstitial, vacancy point defects, and substituting cations of various valence states which introduce oxygen vacancies into the crystal lattice. [1, 5, 22]

ZnO-based memristors can be prepared using several techniques such as pulsed laser deposition [17], sputtering [7, 23-26], electrodeposition [27], metal organic chemical vapour deposition [28] and spin coating [29]. However, among these methods, electrodeposition has several advantages, including control over crystallinity, stoichiometry, nanostructure morphologies and doping concentrations, which are all favourable for this PhD research. So far there has been no report on ZnO thin film based memristive switching devices formed using an electrodeposition approach. One of the goals of this PhD research is to demonstrate that electrodeposition can be applied as a highly tuneable deposition process for fabricating ZnO based memristive switching devices and investigate their operation.

In this chapter, the author of this PhD thesis synthesizes and characterises the behaviour of electrodeposited ZnO thin film based memristive switching devices in the presence and absence of seed layers. The seed layers were prepared by forming thin layers of ZnO using the RF sputtering technique. The application of the seed layer is due to two fundamental motivations: (a) to tune the morphology of the electrodeposited ZnO films in order to increase the grain boundary density as well as construct a highly ordered arrangement of grain boundaries and (b) to optimise the oxygen vacancy concentrations of the films. The resulting ZnO thin films are then

characterized using scanning electron microscopy (SEM), X–ray diffraction (XRD), conductive AFM and X–ray photoelectron spectroscopy (XPS). Variation of electrodeposition duration has been applied to ensure excellent coverage of ZnO films on the substrate as well as to investigate the effect of thickness on their switching behaviour. The author shows the effect of the seed layer on the surface morphology, crystallographic and structural properties of the electrodeposited ZnO as well as the switching performance of the devices based on such films.

The contents of this chapter were published, as a full article, in the journal *Physical Chemistry Chemical Physics*.[30]

5.2 Materials and Methods

5.2.1 RF sputtered ZnO films as seed layers

Memristor devices were fabricated on Pt (50 nm)/Ti (10 nm)/SiO_2 (300 nm)/Si substrates. The substrates were diced into rectangular shapes with dimension of 27 mm × 10 mm. They were then sonicated in acetone and rinsed in isopropanol and deionized water to remove any organic contaminants. Seed layers of ZnO were directly deposited on the substrates using RF magnetron sputtering. In the sputtering process, the target was ZnO of 100 mm diameter and 99.999% purity. The sputtering chamber was pumped to an ultimate base pressure of 1×10^{-5} Torr and the sputtering pressure increased to 2×10^{-2} Torr. During the deposition, the sputtering RF power was set at 100 W. The argon and oxygen gas concentrations in the chamber were kept constant at 60% and 40%, respectively. The deposition duration of the substrates and temperature were fixed at 30 minutes and 260 ºC, respectively. The target to substrate distance was set at 65 mm. As a result, a ~20 nm thick ZnO layer was formed as the seed layer.

5.2.2 Electrodeposited ZnO films

Thin layers of ZnO films were electrodeposited onto the seed layers. For comparison, devices without RF sputtered seed layers were also fabricated. Zinc nitrate [$Zn(NO_3)_2$, Aldrich, 98%], was used in the experiments. The electrolyte solution was prepared using Milli-Q water with resistivity of 18.2 MΩ.cm. Electrodeposited ZnO films were prepared from an aqueous solution containing 0.05 M zinc nitrate with a pH value of about 5.4, as suggested by Izaki *et al*.[31] The substrate (with or without any seed layer) was used as the working electrode, in a 3 electrode setup consisting of a Ag/AgCl reference electrode and a zinc sheet (99.99% purity) as the counter electrode.

It is reported that the electrodeposition of ZnO films occurs based on equations which are presented as (5.1) to (5.3) below.[32, 33] Initially nitrate ions are reduced at the ZnO seed electrode. This produces hydroxide ions and the process raises the electrolyte pH at the solid-solution interface. In the presence of zinc ions in the electrolyte, $Zn(OH)_4^{2-}$ is formed that is eventually converted to ZnO in a dehydration process. This process takes place rapidly at temperatures greater than 50 ºC.

$$NO_3^- + H_2O + 2e^- \rightarrow NO_2^- + 2OH^- \quad (5.1)$$

$$Zn^{2+} + 2OH^- + 2H_2O \rightarrow Zn(OH)_4^{2-} + 2H^+ \quad (5.2)$$

$$Zn(OH)_4^{2-} + 2H^+ \rightarrow ZnO + 3H_2O \quad (5.3)$$

Both temperature and applied potential can be used for controlling the ZnO electrodeposition process.[33] In order to ensure the formation of ZnO, the electrodeposition process needs to be carried out at temperatures equal to or greater than 50 ºC.[34] Additionally, hydrogen evolution, which is detrimental to the quality

of the electrodeposited films, can be avoided by choosing the right voltage. As a result, cyclic voltammetry (CV) experiments were carried out at 62 ºC to elucidate the most appropriate electrodeposition potential for the fabrication of ZnO. Figure 5.1 shows the CV response for the electrodeposition of ZnO on two different samples: samples with and without seed layers. From the CV, it is apparent that there is a significant overpotential required for the electrodeposition of ZnO on a platinum substrate (i.e. without seed layer) compared to the seed ZnO layers. This is reflected in the onset potential for nitrate reduction of ca. −0.30 V at the seed layer compared to ca. −0.65 V at the Pt substrate. The rougher surface of the seed layer as well as a lower energy barrier may promote the formation of adatoms which enable stable ZnO nucleation centres to form and subsequently allow growth of ZnO. [35-37]

From the CV data, a peak maximum is observed at –0.74 V for the electrodeposition of ZnO on the seed layer. This cathodic process is due to the reduction of nitrate at the working electrode as stated in equation (5.1). At potentials more negative than –0.82 V, a sharp increase in current was detected due to the hydrogen evolution reaction. During the reverse sweep, no anodic current peak was observed, which indicates that Zn metal was not formed within the film during the deposition process. Therefore, a deposition potential of –0.60 V *vs* Ag/AgCl was chosen for the samples to avoid both hydrogen evolution and Zn metal deposition. The deposition durations and their corresponding thicknesses are shown in Table 5.1.

Table 5.1. ZnO electrodeposition durations and their corresponding thicknesses.

Sample ID		***Electrodeposition duration (s)***	***Thickness (nm)***
Absence of seed layers	ECD 500s	500	Poor coverage
	ECD 1000s	1000	250
	ECD 3000s	3000	400
Presence of seed layers	SL & ECD 500s	500	150
	SL & ECD 1000s	1000	170

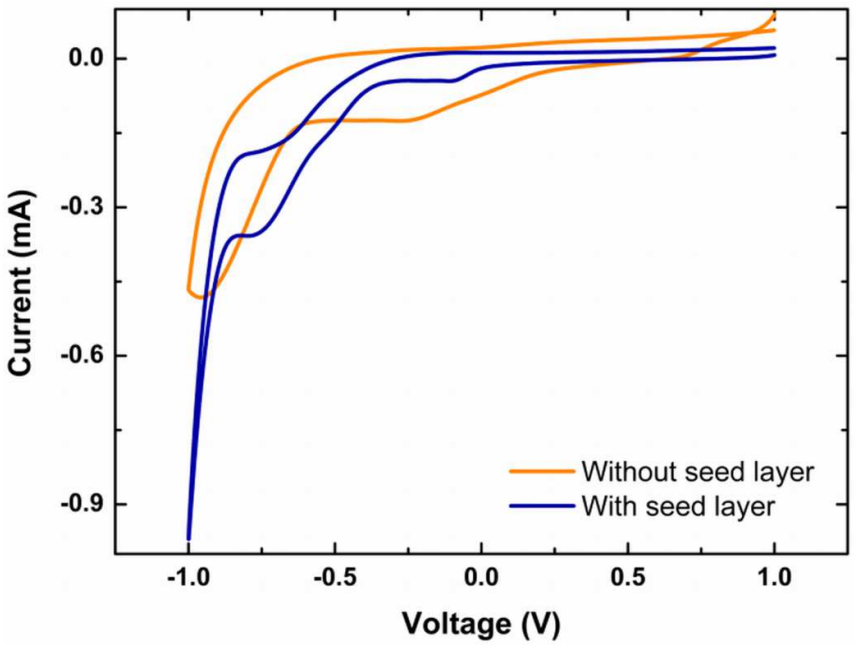

Figure 5.1 Cyclic voltammetry of electrodeposited ZnO layers onto surfaces with and without RF sputtered ZnO seed films.

5.2.3 Materials and device characterisation

Surface characterization was carried out using SEM (FEI Nova NanoSEM), atomic force microscopy (AFM – Bruker Multimode 8 with PF TUNA) and XPS (Thermo Scientific *K*–alpha of Al–*K*α X–ray source (1486.7 eV) with a pass energy of 50 eV).

Depth profiles were performed by lightly etching the surface with an Ar^+ ion beam of energy. The crystallographic properties of the films were studied *via* XRD using a Bruker D8 DISCOVER microdiffractometer fitted with a GADDS (General Area Detector Diffraction System) that accommodates Cu-*K*α radiation (λ = 1.54178 Å). By applying controlled volume silver paste droplets, circular Ag contact pads with a diameter of 1.5 mm were formed on ZnO films and acted as top electrodes whereas the platinum layers of the substrates acted as the bottom electrodes. Effects of electrical properties were measured using a CHI413A electrochemistry workstation (CH Instruments). The schematic of the developed Ag/ZnO/Pt based memristor devices is illustrated in Figure 5.2.

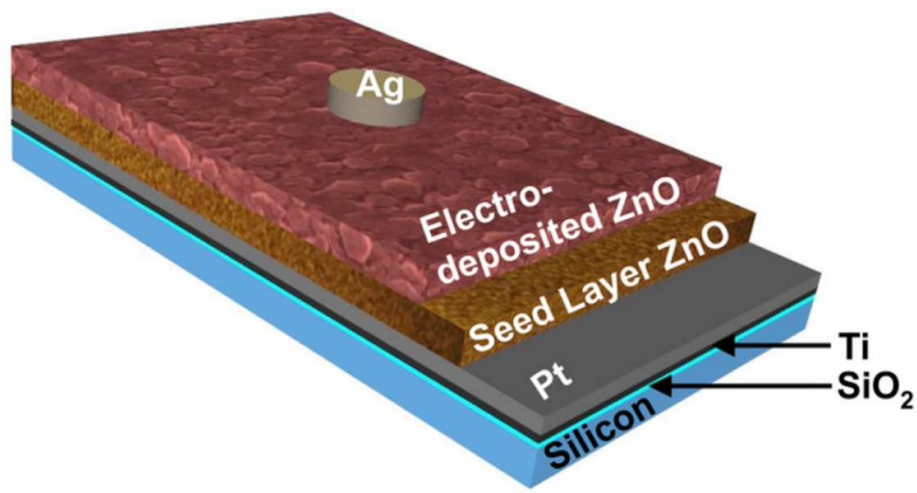

Figure 5.2 The 3D schematic of the Ag/ZnO/Pt based resistor switching incorporating the RF sputtered ZnO seed layer.

5.3 Results and Discussions

5.3.1 Morphology and structural properties

Figure 5.3(a) shows the SEM top view image of a ZnO film that was electrodeposited on a RF sputtered ZnO seed layer. The ZnO film is comprised of columnar hexagonal grains in the *c* axis direction (normal to the substrate surface) with clear boundaries and grains dimensions in the order of ~130 nm.

In addition, the resultant film consisted of densely packed grains with no evidence of pores. Figure 5.3(b) shows the cross section view of the electrodeposited ZnO film formed onto the RF sputtered ZnO seed layer (Figure 5.3(c)). An organised grain distribution is observed with nano-sized grains ranging from 10 to 30 nm for the seed layer. A magnified version of Figure 5.3(b) is presented in Figure 5.3(d). It can be seen that the electrodeposited ZnO film uniformly covers the seed layer.

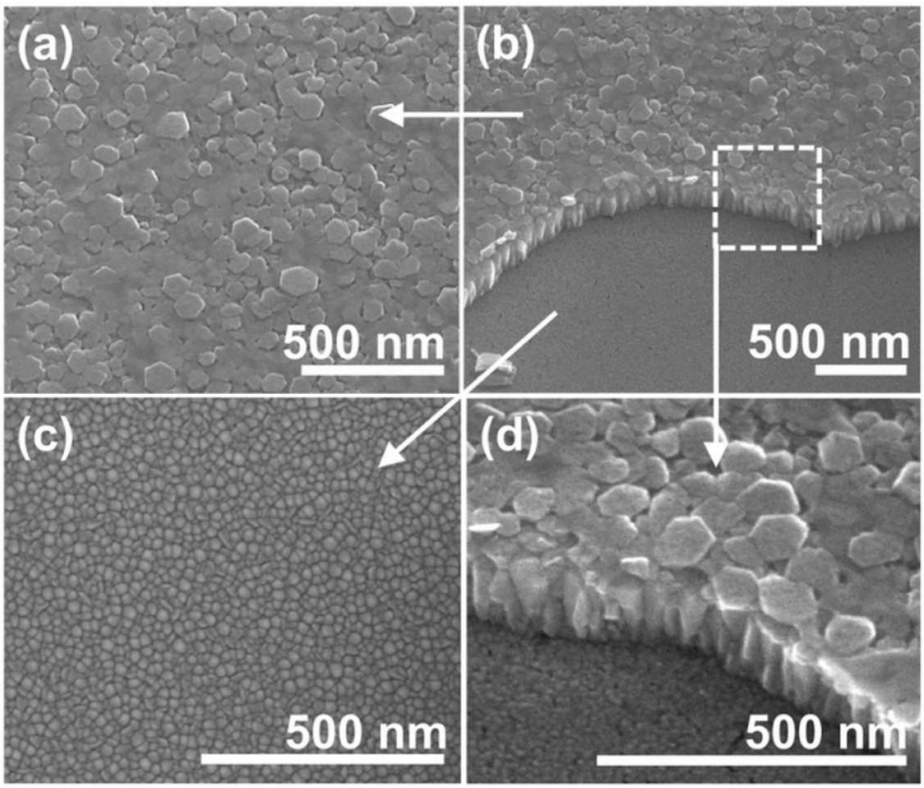

Figure 5.3 SEM images of the surface microstructure of electrodeposited ZnO for 1000 s onto RF sputtered ZnO seed layers, (a) top down view, (b) cross section view, (c) RF sputtered ZnO seed layer and (d) a magnified image of the interface in (b).

In Figure 5.4, the surface morphology of ZnO film electrodeposited directly on a platinum substrate without any seed layer is compared for different deposition durations. The ZnO film deposited for 1000 s (Figure 5.4(a)) is composed of hexagonal grains with relatively large inter-grain spacing. By increasing the electrodeposition duration to 3000 s (Figure 5.4(b)), the electrodeposited film grains became denser with grain sizes of ~350 nm. For comparison, a sample with a RF sputtered seed layer and subsequent electrodeposition for 1000 s is shown in Figure 5.4(c). It can be observed that, the film incorporating seed layers contain more densely packed grains with smaller grain dimensions. This results in a higher grain boundary density in these films, in comparison to samples without any seed layer.

This increase in grain density is driven by the nature of the nucleation site, which is strongly dependent on the growth conditions and structural morphology of the seed layer.[21, 38-40] Higher grain boundaries density and thinner films are expected to increase the memristive switching ratio of the device. [41, 42] Therefore, the author expects that the device with the seed layer would produce better memristive switching performance.

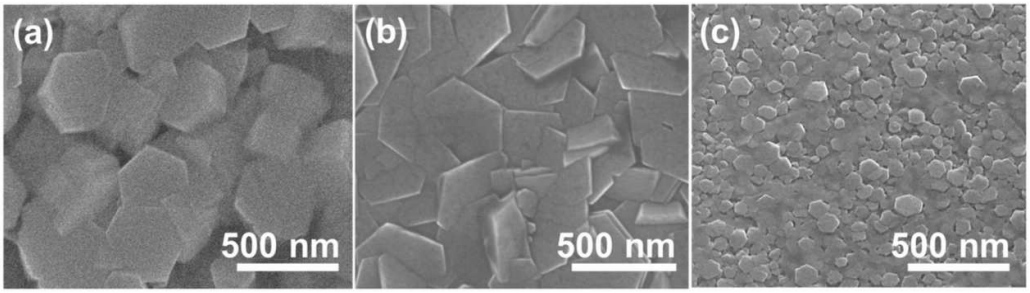

Figure 5.4 SEM top view images of the surface microstructure of electrodeposited ZnO on platinum without the ZnO seed layer at (a) 1000s, (b) 3000s durations, and (c) electrodeposited on the seed layer for 1000 s.

The crystallographic phases of the obtained ZnO samples were investigated using XRD. Figure 5.5 shows the XRD patterns for three types of ZnO films: the RF sputtered ZnO seed layer, electrodeposited ZnO on platinum (without seed layer), and electrodeposited ZnO with a seed layer. The electrodeposited films were crystalline in nature with a wurtzite structure which appear in the preferred crystal orientation of (002), matching ICDD No. [89-1397]. Secondary peaks are observed at 31.74º and 36.21º, corresponding to the (100) and (101) planes of ZnO, respectively. In addition, the XRD patterns also show clearly-resolved diffraction peaks originating from the platinum substrate matching ICDD No. [87-0647]. A strong platinum (111) peak can be observed for all films. By comparing the three

types of ZnO films, RF sputtered ZnO films had the weakest peak intensities associated with the preferred wurtzite orientation (002). This was mainly due to the thickness of the films which is in the range of 20 nm. A weak ZnO (002) peak was also observed for electrodeposited ZnO on platinum at 1000 s (i.e. without the seed layer). For electrodeposited films with a seed layer, a significant increase of (002) peak intensity was measured, which is associated with higher crystallinity. This supports the hypothesis of the seed layers enhancing ZnO nucleation during the electrodeposition process, which resulted in a highly crystalline phase of ZnO with the preferred (002) orientation.[21] The same trends were observed for longer electrodeposition times.

XPS analysis was carried out to study the composition variations in the ZnO thin films deposited on different substrates and durations. Peaks for zinc and oxygen are expected at 1022 eV and 531 eV, respectively, and are observed in Figure 5.6(a). A XPS analysis of a standard ZnO target [ZnO, target materials, >99%] was carried out as a reference. Figure 5.6(b) shows XPS analysis focusing on the oxygen (O1s) peak. It can be seen that the concentration of oxygen in the electrodeposited ZnO films is lower compared to the 99.999% pure ZnO target reference (Table 5.2). This suggests the presence of oxygen vacancies in the films. It has been reported that the electrodeposition technique has a relatively high tendency to promote oxygen vacancies or interstitial Zn centers especially when the deposition is carried out at high current density.[35] This resulted in an increase in the electrodeposition rate, which leads to the formation of oxygen vacancies.[35] Therefore, it is clear that the electrodeposited ZnO films contain oxygen vacancies, and such vacancies of appropriate concentration are desirable for memristive characteristics. In order to verify the reproducibility of the Zn and O composition as a function of film

processing, the author fabricated five different samples for each type of ZnO films (SL, ECD 1000s, ECD 3000s, SL & ECD 500s, SL & ECD 1000s). Figure 5.7 shows the average of Zn and O elemental composition. The tests were performed on five times.

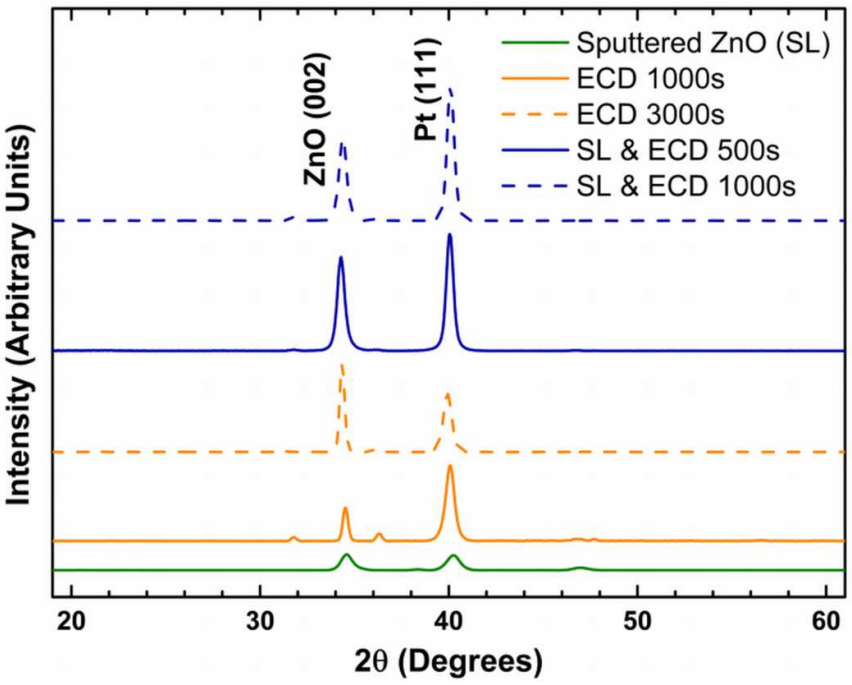

Figure 5.5. XRD patterns of ZnO thin films: RF sputtered ZnO as the seed layer and two samples of electrodeposited ZnO directly on platinum (without the seed layer), and onto seed layers at different durations.

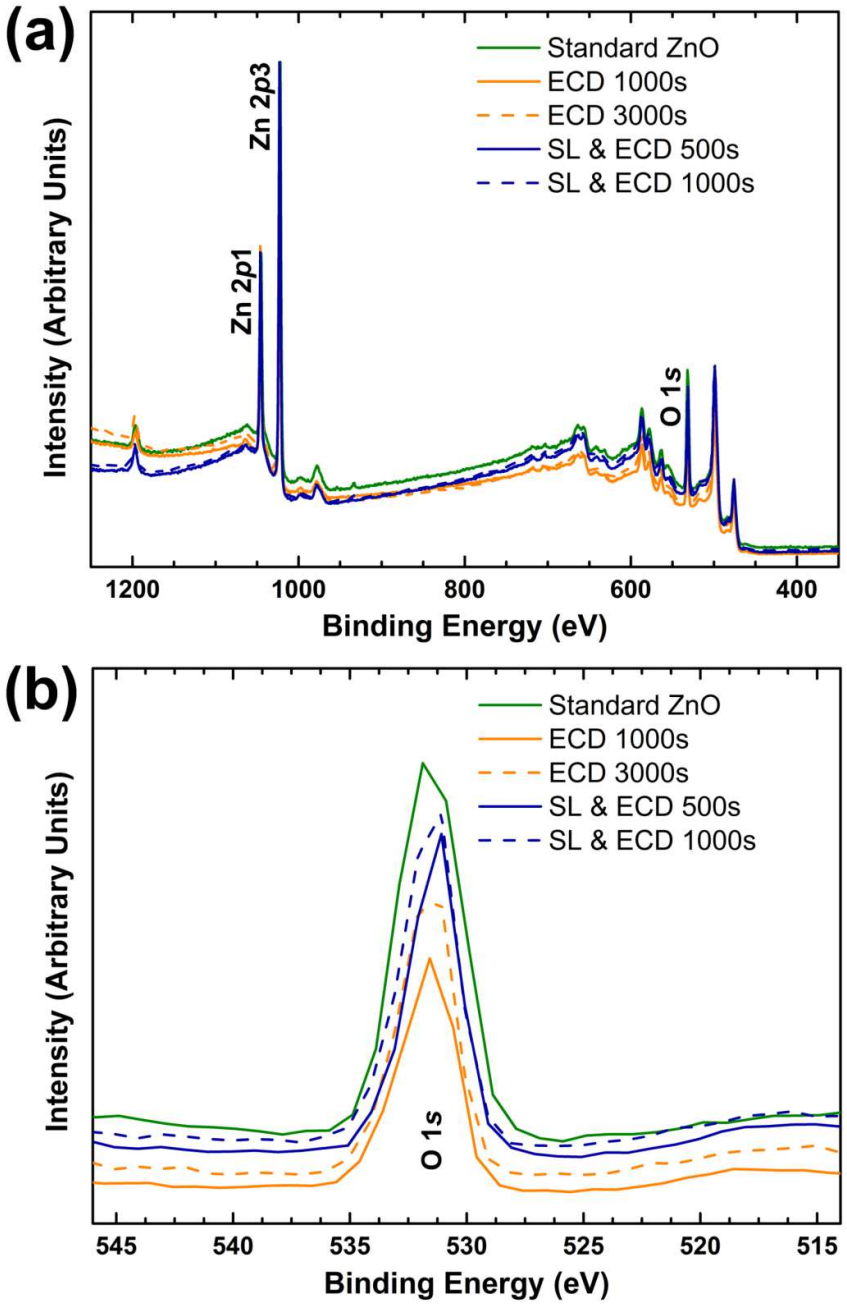

Figure 5.6. XPS spectra of ZnO thin films; RF sputtered ZnO as the seed layer and two samples of ZnO electrodeposited with and without seed layers at different durations for (a) survey scan and (b) O1s. For reference, the XPS spectrum of 99.999% the ZnO target is also presented.

Table 5.2. Average variation of elements in ZnO thin films

Samples	Elemental Composition (%)	
	Zn	O
99.99% ZnO target	49.39	50.62
ZnO seed layer	49.56	50.44
ECD 1000s	57.61	42.39
ECD 3000s	55.43	44.57
SL & ECD 500s	53.19	46.81
SL & ECD 1000s	51.83	48.17

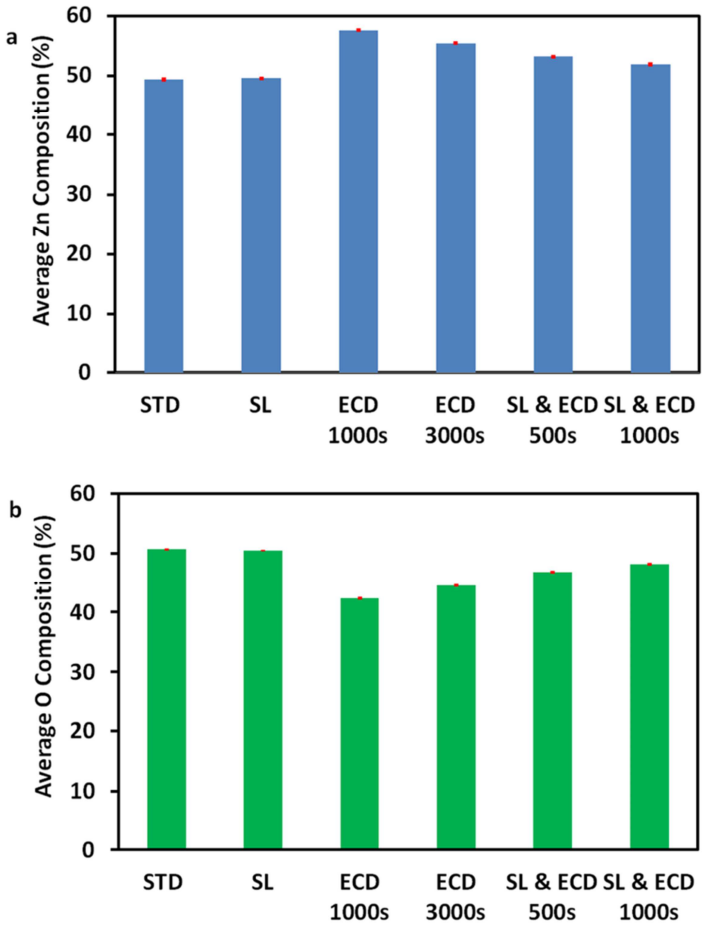

Figure 5.7 Average of Zn and O elemental compositions for six different types of ZnO (standard ZnO target and films). The tests were performed on five similarly fabricated samples. The standard deviation was < 10%.

5.3.2 Memristive switching performance

The current-voltage (*I-V*) characteristics of the ZnO memristive devices were conducted at room temperature and each sample was characterized by sweeping the bias voltage in the sequence of 0 → 1 → 0 → –1 → 0. Figure 5.8(a) and (b) shows the *I-V* characteristics of devices electrodeposited without seed layers at 1000 and 3000 s, while Figure 5.8(c) and (d) shows devices electrodeposited with seed layers at 500 and 1000 s. The electrodeposited ZnO was found to be in a high resistance state (HRS) of ~20 kΩ (without the seed layer) and ~1.6 MΩ (with the seed layer) and did not show any resistance switching characteristic until a significant increase of current was recorded when the applied bias voltage reached +1 V.

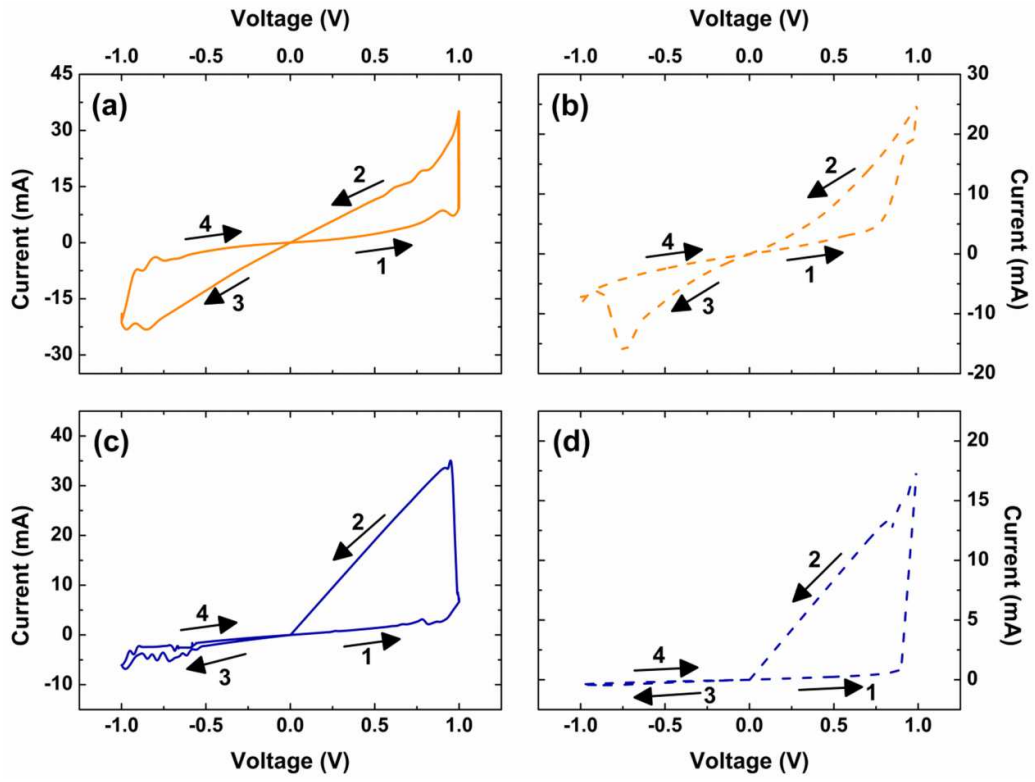

Figure 5.8 ZnO memristive switching curves of the device (a) ECD 1000s, (b) ECD 3000s, (c) SL & ECD 500s and (d) SL & ECD 1000s.

At this moment, the resistance was ~30 Ω for the device without the seed layer and ~35 kΩ for the device with the seed layer indicating the achievement of a low resistance state (LRS). This conversion is known as "SET". As the voltage sweeps back from 1 to –0.5 V, the device remains in the LRS with the *I-V* curve passing through the origin. As the device continues its negative sweep to –1 V, the current suddenly reduced resulting in a transition from the LRS back to a HRS and is known as "RESET". From Figure 5.8, one can observe that ZnO devices without the seed layer exhibit a symmetrical pinched hysteresis loop while ZnO devices with a seed layer demonstrate an asymmetrical hysteresis loop. The asymmetrical *I-V* curve during negative polarity sweeping for devices with a seed layer is due to a large resistance of ~1.6 MΩ which causes the switching effect to reduce significantly.[18, 43-45] The low quantity of oxygen vacancies (as shown in Table 2) for seed layer devices would increase the bulk resistance and cause the depletion layer to be wider, which results in large initial resistance values. [46] As a result, low hysteresis switching at negative polarity can be observed for the devices with seed layers compared to those without seed layer devices.

Figure 5.9 shows the semi-logarithmic *I-V* characteristics of the devices. The ON/OFF ratio between the HRS and LRS were calculated at 0.5 V and the memristive switching ratio were 5 and 3 for devices without seed layer electrodeposited for 1000 and 3000 s, respectively. Significantly, for devices with a seed layer, memristive switching ratios of 10 and 40 were measured for electrodeposition duration of 500 and 1000s, respectively.

The hysteresis loops for the 10^{th}, 20^{th} and 30^{th} cycles, electrodeposited on a seed layer at 500 s are shown in Figure 5.10. The device shows good repeatability

without significant deterioration. The resistance values at HRS were high for the initial cycles and then stabilized to lower values after more switching cycles. On the other hand, the values at the LRS are quite stable over the course of 30 switching cycles. The inset shows the endurance data, where one can observes a significant difference between LRS and HRS to distinguish two memory states.

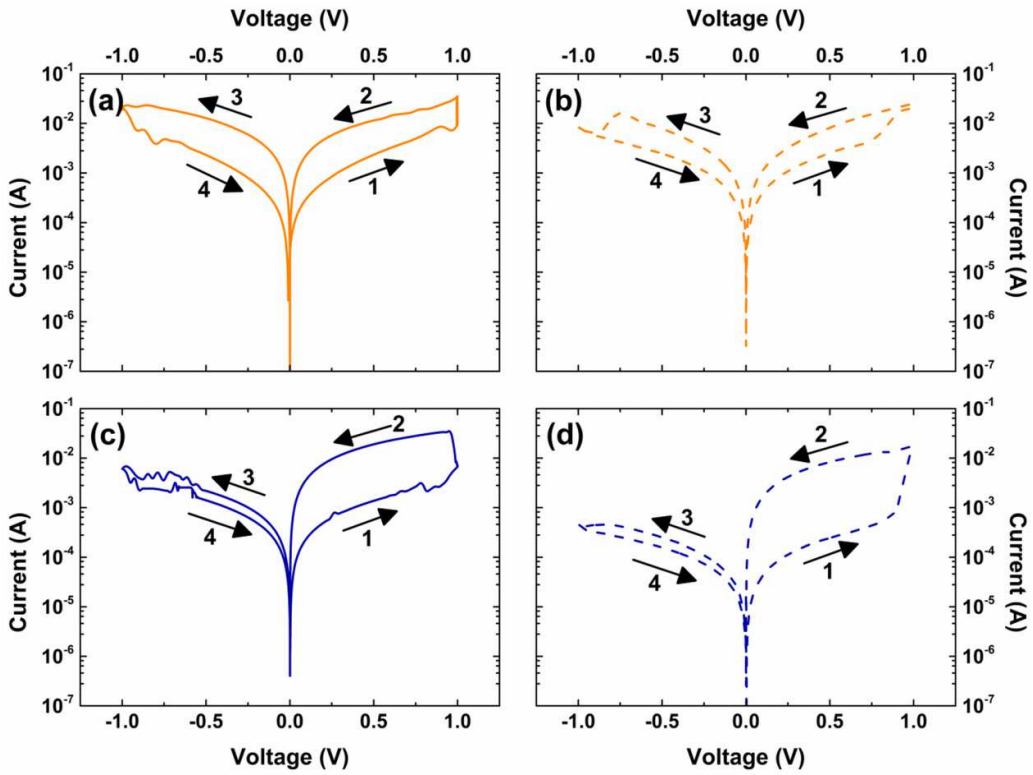

Figure 5.9 Semi-log plots of current-voltage (*I-V*) characteristics of ZnO memristor (a) ECD 1000 s, (b) ECD 3000 s, (c) SL & ECD 500 s and (d) SL & ECD 1000s.

5.3.3 Memristive switching mechanism

The observation of memristive switching can be attributed to the valence change mechanism usually taking place in transition metal oxides.[6] It is reported that ZnO

prepared by electrodeposition at high current density (similar to the current densities used in this work), comprise of a large amount of oxygen vacancies or interstitial Zn. [35] The oxygen vacancies of the films generally occur at the surface of the grains which form the boundaries between them [47] and the conductive filaments that are formed at the grain boundaries enables the switching effect. [48-51] These native defects have a very strong effect on the electronic transport and directly influence the switching properties of the devices. [52] XPS analysis in Figure 5.6 and Table 5.2 confirmed that the electrodeposited ZnO films contain relatively high oxygen vacancies in comparison with the standard ZnO target. Interestingly, the RF sputtered ZnO seed layers have a similar Zn and O elemental composition to the standard ZnO target.

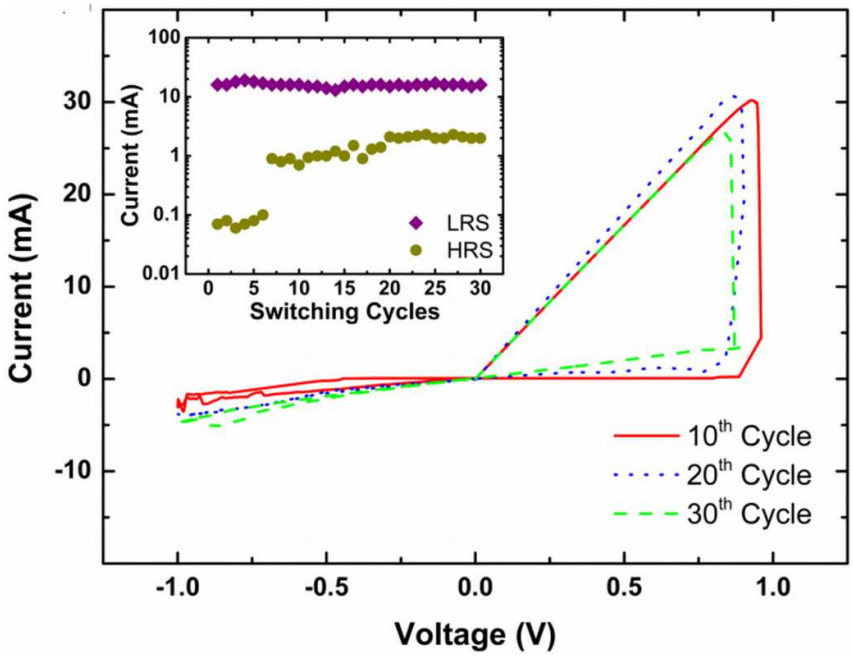

Figure 5.10 Hysteresis loop of ZnO films on the seed layer at 10th, 20th and 30th cycles. Inset: resistance changes of the HRS and LRS with the number of switching cycles.

The conductive filaments created by oxygen vacancies at the grain boundaries, which act as positive charge carriers, are proposed to explain the memristive effect of the devices. Based on the Kröger-Vink equation, ZnO defects are formed as follows [53]:

$$ZnO + O_O^x \Leftrightarrow V_{Zn}'' + 2V_O^{\bullet} + \frac{1}{2}O_2(g) + ZnO\ (surface) \tag{5.4}$$

$$ZnO \Leftrightarrow V_{Zn}'' + 2V_O^{\bullet\bullet} + ZnO\ (surface) \tag{5.5}$$

$$O_o^x \Leftrightarrow \frac{1}{2}O_2(g) + V_O^{\bullet} + e' \tag{5.6}$$

$$O_o^x \Leftrightarrow \frac{1}{2}O_2(g) + 2V_O^{\bullet\bullet} + 2e' \tag{5.7}$$

where $V_O^{\bullet}$ and $V_O^{\bullet\bullet}$ are the oxygen vacancies with single and double positive charges, respectively, while O_O^x, V_{Zn}'' and e' indicate the neutral oxygen ion in the lattice site, a zinc vacancy with a double negative charge and an electron with a single negative charge, respectively.

By applying positive voltage at the Ag top electrode (TE), the oxygen ions (O_O^x) migrate to the TE and oxygen vacancies are created close to the Ag/ZnO interface. The oxygen ions are finally absorbed by the TE or released as O_2 gas according to equation (5.6). The abundant oxygen vacancies on the surface of ZnO grains would be driven towards the Pt bottom electrode (BE) and assemble a conducting channel through the grain boundaries of the device when a sufficiently positive bias voltage is applied. The injected electrons are simultaneously transported from the TE to the BE and the device switches from the OFF state to the ON state (Figure 5.11(a)). By applying a negative bias, oxygen ions absorbed by the TE would be released back to the ZnO region from the Ag/ZnO interface and neutralize the

oxygen vacancies, so the conducting filaments would break near the Ag/ZnO interface. As the process continues, more oxygen vacancies are neutralized and the filaments would finally rupture and the resistance of the device would then increase. This results in switching to the OFF state (Figure 5.11(b)).

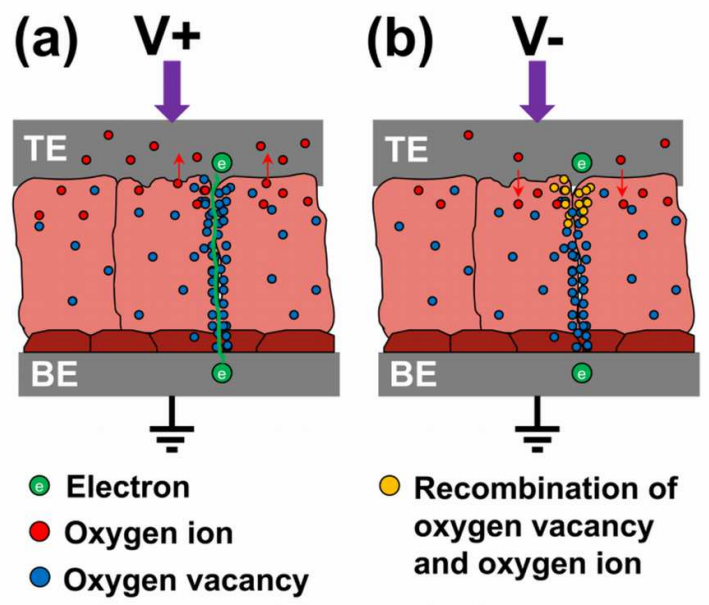

Figure 5.11 Schematic depictions of oxygen vacancies driven conduction in memristive devices (a) positive voltage drives the SET condition and (b) negative voltage drives the RESET condition.

The improvement of resistance change ratios for devices fabricated with a ZnO seed layer can be related to the variation of grain boundary density. It is observed that the films prepared with seed layers result in densely packed nano-sized grains ranging from 90 to 130 nm (as seen in Figure 5.3b) where an increase in the grain boundary density of the films with the seed layer can be observed. The density is approximately 20 × higher than the films without the seed layer as depicted in Figure 5.4(a) and (b) (calculated using the ImageJ software package). The seed layer also promotes a highly ordered arrangement of grain boundaries. Therefore, it is

postulated that straight rather than branched filaments are more likely to form along the flat grain boundaries in the highly (002) oriented and columnar-hexagonal structured ZnO films. Hence, formation of many conducting channels for electron migration is possible. On the other hand, for devices deposited without the seed layer, the grain boundaries of the films were not perfectly arranged. The scattered grain boundaries in devices without the seed layer create many paths where the boundaries could be exposed to air and as a result any oxygen vacancies will be quickly replenished by the surrounding oxygen molecules. Consequently, the switching ratio for the devices without the seed layer is much lower as compared to devices with the seed layer. A similar increase in the ON/OFF ratio has also been reported for memristors based on CuS films, where the grains of the films are transformed to highly oriented (001) after high temperature annealing. [41]

In order to verify the existence of conducting channels through the grain boundaries of the ZnO films and understand their effect on the resistance change ratios of the devices, conductive AFM (c–AFM) measurements were carried out on the ZnO seed layer and the films deposited in the presence and absence of seed layers. By using c–AFM, one can simultaneously obtain topographical image (Figure 5.12(i)) as well as the current map (Figure 5.12(ii)) of the ZnO nanostructured surfaces. The current map is determined by biasing the AFM tip (made of silicon nitride with a 20 nm coating of platinum/iridium) at a dc voltage of 1.0 V between the tip and the surface. The bright areas of the generated current map correspond to higher conductivities with reference to the other areas of the surface. The electrodeposited ZnO films formed onto seed layers at different durations of 500 and 1000 s (Figure 5.12(a) and 5.12(b)) clearly reveal relatively higher conducting areas compared to the electrodeposited ZnO without seed layers, ECD 1000s (Figure 5.12

(c)) or the seed layer itself (Figure 5.12(d)). Obviously the highest current intensity is seen in Figure 5.12(b). This enhancement is due to the formation of many well-dispersed conducting channels resulting from higher grain boundary densities, as discussed in the previous section.

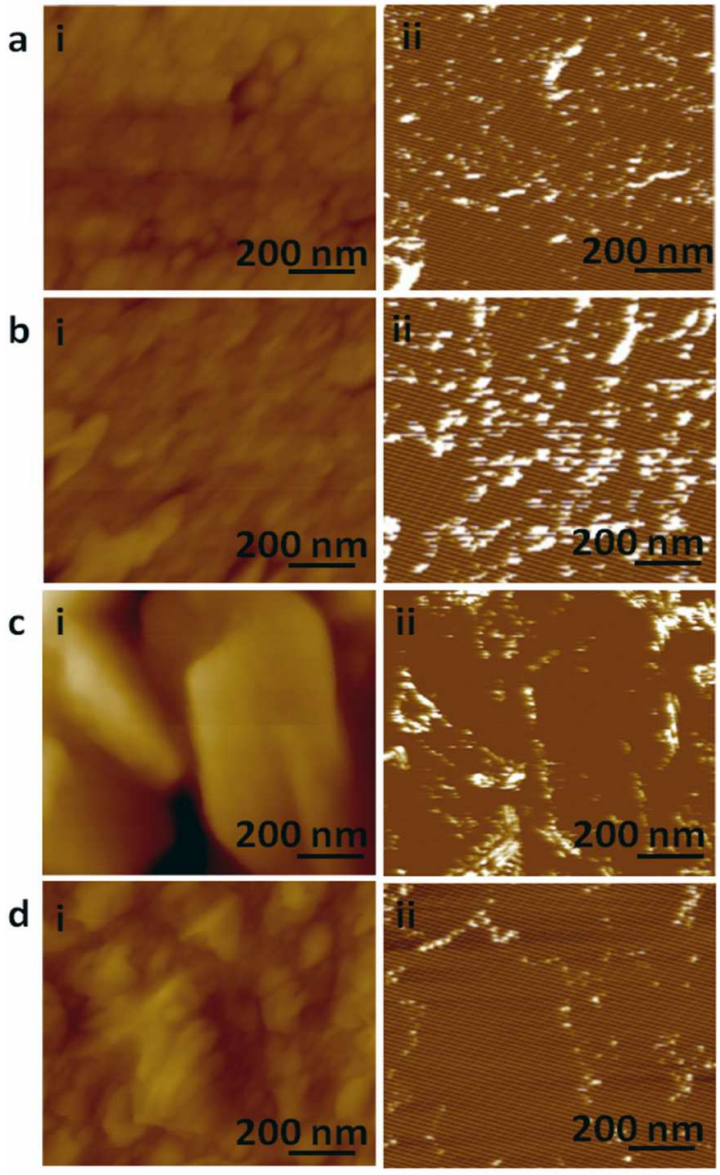

Figure 5.12 c–AFM (arbitrary units) (i) topographical and (ii) current map images of ZnO thin film, (a) SL & ECD 500s, (b) SL & ECD 1000s, (c) ECD 1000s and (d) RF sputtered seed layer. The bright areas correspond to higher conductive region relative to other areas.

This observation strongly supports the hypothesis that the conductive channels created by the oxygen vacancies are highly localised at the grain boundaries of the ZnO films as illustrated in Figure 5.11. Even if the filament current at the ZnO boundaries is not considered, the change in the content of oxygen vacancies in the films electrodeposited with and without seed layers can be responsible for the alteration of the switching quality. Xu *et al.* have reported the dependence of memristive switching on the number of oxygen vacancies in memristor devices. It was found that the memristive switching characteristics become more prominent by increasing the number of oxygen vacancies.[54] However, too many oxygen vacancies in their $LaMnO_3$ films reduced the switching ratio due to excessive structural distortion. Thus it is also possible that by introducing ZnO seed layers, the concentration of oxygen vacancies in the electrodeposited ZnO thin films can be controlled. As can be seen in Table 5.2, the elemental composition of the ZnO seed layer is very close to the ZnO target. Interestingly, the presence of this seed layer assists in optimizing the oxygen vacancy concentration of the subsequently electrodeposited ZnO films to form ZnO_{1-x}, where x relates to the percentage of oxygen vacancies. Based on the XPS measurements, the author can concludes that ZnO_{1-x} of $0.05 < x < 0.08$ was the optimum condition for better switching characteristics.

Besides anion migration, another possible mechanism for memristive switching of a Ag/ZnO/Pt device can be cation migration.[23, 55, 56] As the Ag TE is an electrochemically active material, when a positive voltage is applied, oxidation occurs and Ag ions (Ag^+) are generated. The mobile Ag^+ cations can migrate towards the Pt BE through the ZnO layer and be reduced by electrons flowing from the cathode to form Ag metal atoms. The successive precipitations of Ag metal atoms at

the cathode lead to a growth of the Ag protrusion, which finally reaches the TE to form conducting filaments which results in a device in the ON state. On changing the polarity of the bias voltage, Ag metal atoms dissolve at the edge of the conductive filaments which eventually annihilate the filament and turn the device to the RESET state. [1, 23] In order to check for the concept of this cation migration in the Ag/ZnO/Pt device, the author has carried out XPS analysis on the device in the SET state (Figure 5.13). However, no Ag element was detected in the ZnO films thus proving that the mechanism of the devices solely relies on the presence of oxygen vacancies.

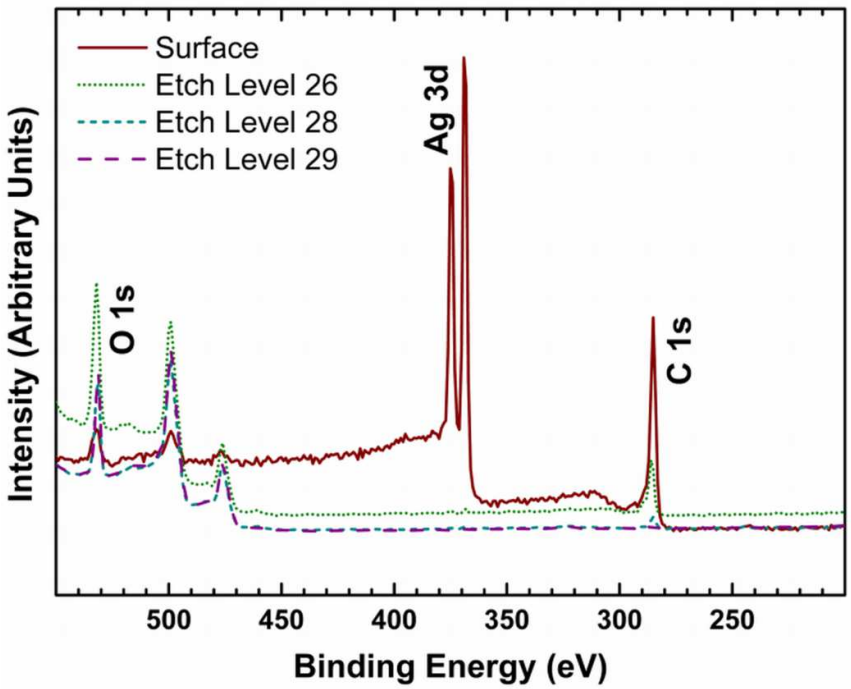

Figure 5.13 Respective XPS spectra of the Ag 3d obtained after continuous depth profile etch on the Ag electrode.

5.4 Summary

In this chapter, the author of this PhD thesis demonstrated the effect of ZnO seed layers on electrodeposited ZnO films towards their memristive switching performances. By incorporating RF sputtered ZnO seed layers, the author was able to tune the composition and the grain boundary densities of the deposited films. The memristive switching behaviour of the devices corresponds to oxygen-vacancy density at the grain boundaries interface. The seed layers controlled the growth of electrodeposited ZnO, where ZnO films with smaller grain size and higher grain boundary densities were obtained, which promoted the facile formation of straight conducting filaments. Consequently, ZnO memristive devices incorporating seed layers have higher switching ratios than devices without a seed layer. Devices with an incorporated seed layer showed stable and reliable memristive switching behaviours under continuous cycling conditions. This work clearly show the importance of the seed layer effect in engineering the electrodeposited films for fabricating memristive devices and provide a pathway for further improving their performance.

In the next chapter, the author will present the summary and concluding remarks of this PhD thesis. In addition, the author will highlight his achievements and elaborate on the future outlooks of this research work.

References

[1] R. Waser and M. Aono, "Nanoionics-based Resistive Switching Memories," *Nat. Mater.,* vol. 6, pp. 833-840, 2007.

[2] L. Chua, "Resistance Switching Memories are Memristors," *Appl. Phys. A-Mater.,* vol. 102, pp. 765-783, 2011.

[3] K. Szot, W. Speier, G. Bihlmayer, and R. Waser, "Switching the Electrical Resistance of Individual Dislocations in Single-Crystalline $SrTiO_3$," *Nat. Mater.,* vol. 5, pp. 312-320, 2006.

[4] Y. Watanabe, "Review of Resistance Switching of Ferroelectrics and Oxides in Quest for Unconventional Electronic Mechanisms," *Ferroelectrics,* vol. 349, pp. 190-209, 2007.

[5] J. J. Yang, M. D. Pickett, X. Li, D. A. A. Ohlberg, D. R. Stewart, and R. S. Williams, "Memristive Switching Mechanism for Metal/Oxide/Metal Nanodevices," *Nat. Nanotechnol.,* vol. 3, pp. 429-433, 2008.

[6] R. Waser, R. Dittmann, G. Staikov, and K. Szot, "Redox-Based Resistive Switching Memories - Nanoionic Mechanisms, Prospects, and Challenges," *Adv. Mater.,* vol. 21, pp. 2632-2663, 2009.

[7] N. Xu, L. F. Liu, X. Sun, C. Chen, Y. Wang, D. D. Han, *et al.,* "Bipolar Switching Behavior in TiN/ZnO/Pt Resistive Nonvolatile Memory With Fast Switching And Long Retention," *Semicon. Sci. Tech.,* vol. 23, p. 075019, 2008.

[8] N. Duraisamy, N. M. Muhammad, H.-C. Kim, J.-D. Jo, and K.-H. Choi, "Fabrication of TiO_2 Thin Film Memristor Device using Electrohydrodynamic Inkjet Printing," *Thin Solid Films,* vol. 520, pp. 5070-5074, 2012.

[9] J. J. Yang, F. Miao, M. D. Pickett, D. A. A. Ohlberg, D. R. Stewart, C. N. Lau, *et al.,* "The Mechanism of Electroforming of Metal Oxide Memristive Switches," *Nanotechnology,* vol. 20, p. 215201, 2009.

[10] M.-J. Lee, S. I. Kim, C. B. Lee, H. Yin, S.-E. Ahn, B. S. Kang, *et al.,* "Low-Temperature-Grown Transition Metal Oxide Based Storage Materials and Oxide Transistors for High-Density Non-volatile Memory," *Adv. Func. Mater.,* vol. 19, pp. 1587-1593, 2009.

[11] S. Seo, M. J. Lee, D. H. Seo, S. K. Choi, D. S. Suh, Y. S. Joung, *et al.,* "Conductivity Switching Characteristics and Reset Currents in NiO Films," *Appl. Phys. Lett.,* vol. 86, p. 093509, 2005.

[12] K. M. Kim, B. J. Choi, B. W. Koo, S. Choi, D. S. Jeong, and C. S. Hwang, "Resistive Switching in $Pt/Al_2O_3/TiO_2/Ru$ Stacked Structures," *Electrochem. Solid St.,* vol. 9, pp. G343-G346, 2006.

[13] S. Lee, W.-G. Kim, S.-W. Rhee, and K. Yong, "Resistance Switching Behaviors of Hafnium Oxide Films Grown by MOCVD for Nonvolatile Memory Applications," *J. Electrochem. Soc.,* vol. 155, pp. H92-H96, 2008.

[14] S.-Y. Wang, D.-Y. Lee, T.-Y. Huang, J.-W. Wu, and T.-Y. Tseng, "Controllable Oxygen Vacancies to Enhance Resistive Switching Performance in a ZrO_2-Based RRAM with Embedded Mo Layer," *Nanotechnology,* vol. 21, p. 495201, 2010.

[15] T. Tsuruoka, K. Terabe, T. Hasegawa, and M. Aono, "Forming and Switching Mechanisms of a Cation-Migration-Based Oxide Resistive Memory," *Nanotechnology,* vol. 21, p. 425205, 2010.

[16] K. Nagashima, T. Yanagida, K. Oka, and T. Kawai, "Unipolar Resistive Switching Characteristics of Room Temperature Grown SnO_2 Thin Films," *Appl. Phys. Lett.,* vol. 94, p. 242902, 2009.

[17] L. M. Kukreja, A. K. Das, and P. Misra, "Studies on Nonvolatile Resistance Memory Switching in ZnO Thin Films," *B. Mater. Sci.,* vol. 32, pp. 247-252, 2009.

[18] A. Shih, W. Zhou, J. Qiu, H.-J. Yang, S. Chen, Z. Mi, *et al.*, "Highly Stable Resistive Switching on Monocrystalline ZnO," *Nanotechnology*, vol. 21, p. 125201, 2010.

[19] C. M. Lieber, "One-Dimensional Nanostructures: Chemistry, Physics & Applications," *Solid State Commun.*, vol. 107, pp. 607-616, 1998.

[20] H. Wei, H. Gong, Y. Wang, X. Hu, L. Chen, H. Xu, *et al.*, "Three Kinds of Cu_2O/ZnO Heterostructure Solar Cells Fabricated With Electrochemical Deposition And Their Structure-Related Photovoltaic Properties," *Crystengcomm*, vol. 13, pp. 6065-6070, 2011.

[21] A. S. Zoolfakar, R. A. Rani, A. J. Morfa, S. Balendhran, A. P. O'Mullane, S. Zhuiykov, *et al.*, "Enhancing The Current Density of Electrodeposited ZnO-Cu_2O Solar Cells by Engineering Their Heterointerfaces," *J. Mater. Chem.*, vol. 22, pp. 21767-21775, 2012.

[22] M. Janousch, G. I. Meijer, U. Staub, B. Delley, S. F. Karg, and B. P. Andreasson, "Role of Oxygen Vacancies in Cr-doped $SrTiO_3$ for Resistance-Change Memory," *Adv. Mater.*, vol. 19, pp. 2232-2235, 2007.

[23] Y. C. Yang, F. Pan, Q. Liu, M. Liu, and F. Zeng, "Fully Room-Temperature-Fabricated Nonvolatile Resistive Memory for Ultrafast and High-Density Memory Application," *Nano Lett.*, vol. 9, pp. 1636-1643, 2009.

[24] W.-Y. Chang, Y.-C. Lai, T.-B. Wu, S.-F. Wang, F. Chen, and M.-J. Tsai, "Unipolar Resistive Switching Characteristics of ZnO Thin Films for Nonvolatile Memory Applications," *Appl. Phys. Lett.*, vol. 92, p. 022110, 2008.

[25] Z. Ji, Q. Mao, and W. Ke, "Effects of Oxygen Partial Pressure on Resistive Switching Characteristics of ZnO Thin Films by DC Reactive Magnetron Sputtering," *Solid State Commun.*, vol. 150, pp. 1919-1922, 2010.

[26] S. Lee, H. Kim, D.-J. Yun, S.-W. Rhee, and K. Yong, "Resistive Switching Characteristics of ZnO Thin Film Grown on Stainless Steel for Flexible Nonvolatile Memory Devices," *Appl. Phys. Lett.*, vol. 95, p. 262113, 2009.

[27] P. Liu, G. She, W. Shi, and D. Chen, "Electric-Pulse-Induced Resistance Switching Observed in ZnO Nanotube Point Contact System," *Physica E*, vol. 42, pp. 791-794, 2010.

[28] J. W. Seo, J.-W. Park, K. S. Lim, J.-H. Yang, and S. J. Kang, "Transparent Resistive Random Access Memory and Its Characteristics for Nonvolatile Resistive Switching," *Appl. Phys. Lett.*, vol. 93, p. 223505, 2008.

[29] S. Kim, H. Moon, D. Gupta, S. Yoo, and Y.-K. Choi, "Resistive, Switching Characteristics of Sol-Gel Zinc Oxide Films for Flexible Memory Applications," *IEEE T. Electron Dev.*, vol. 56, pp. 696-699, 2009.

[30] A. S. Zoolfakar, R. Ab Kadir, R. A. Rani, S. Balendhran, X. Liu, E. Kats, *et al.*, "Engineering electrodeposited ZnO films and their memristive switching performance," *Phys. Chem. Chem. Phys.*, vol. 15, pp. 10376-10384, 2013.

[31] M. Izaki, T. Shinagawa, K.-T. Mizuno, Y. Ida, M. Inaba, and A. Tasaka, "Electrochemically Constructed P-Cu_2O/N-ZnO Heterojunction Diode for Photovoltaic Device," *J. Phys. D Appl. Phys.*, vol. 40, pp. 3326-3329, 2007.

[32] M. Izaki and T. Omi, "Transparent Zinc Oxide films Prepared by Electrochemical Reaction," *Appl. Phys. Lett.*, vol. 68, pp. 2439-2440, 1996.

[33] A. Chatterjee and J. Foord, "Electrochemical Deposition of Nanocrystalline Zinc Oxide at Conductive Diamond Electrodes," *Diam. Relat. Mater.*, vol. 15, pp. 664-667, 2006.

[34] J. Cembrero and D. Busquets-Mataix, "ZnO Crystals Obtained by Electrodeposition: Statistical Analysis of Most Important Process Variables," *Thin Solid Films,* vol. 517, pp. 2859-2864, 2009.

[35] G.-R. Li, C.-R. Dawa, Q. Bu, X.-H. Lu, Z.-H. Ke, H.-E. Hong, *et al.*, "Electrochemical Self-Assembly of ZnO Nanoporous Structures," *J. Phys. Chem. C,* vol. 111, pp. 1919-1923, 2007.

[36] S. Xu and Z. L. Wang, "One-Dimensional ZnO Nanostructures: Solution Growth and Functional Properties," *Nano Res.,* vol. 4, pp. 1013-1098, 2011.

[37] R. B. Peterson, C. L. Fields, and B. A. Gregg, "Epitaxial chemical deposition of ZnO nanocolumns from NaOH," *Langmuir,* vol. 20, pp. 5114-5118, 2004.

[38] S. Guillemin, V. Consonni, E. Appert, E. Puyoo, L. Rapenne, and H. Roussel, "Critical Nucleation Effects on the Structural Relationship Between ZnO Seed Layer and Nanowires," *J. Phys. Chem. C,* vol. 116, pp. 25106-25111, 2012.

[39] M. Breedon, J. Yu, W. Wlodarski, and K. Kalantar-Zadeh, "ZnO Nanostructured Arrays Grown from Aqueous Solutions on Different Substrates," presented at the 2008 International Conference on Nanoscience and Nanotechnology, 2008.

[40] M. Breedon, M. B. Rahmani, S.-H. Keshmiri, W. Wlodarski, and K. Kalantar-zadeh, "Aqueous Synthesis of Interconnected ZnO Nanowires using Spray Pyrolysis Deposited Seed Layers," *Mater. Lett.,* vol. 64, pp. 291-294, 2010.

[41] B. Yang, H. X. Guo, K. B. Yin, Y. D. Xia, L. Chen, J. Yin, *et al.*, "The < 00l >-Oriented Growth of Cu_2S Films and Its Switching Properties," *J. Electroceram,* vol. 22, pp. 87-90, 2009.

[42] T. S. Herng, A. Kumar, C. S. Ong, Y. P. Feng, Y. H. Lu, K. Y. Zeng, *et al.*, "Investigation of the Non-Volatile Resistance Change in Noncentrosymmetric Compounds," *Sci. Rep.,* vol. 2, pp. 587-595, 2012.

[43] S. H. Jo, K.-H. Kim, and W. Lu, "High-Density Crossbar Arrays Based on a Si Memristive System," *Nano Lett,* vol. 9, pp. 870-874, 2009.

[44] D. B. Strukov, G. S. Snider, D. R. Stewart, and R. S. Williams, "The Missing Memristor Found," *Nature,* vol. 453, pp. 80-83, 2008.

[45] Y. Dong, G. Yu, M. C. McAlpine, W. Lu, and C. M. Lieber, "Si/a-Si Core/Shell Nanowires as Nonvolatile Crossbar Switches," *Nano Lett.,* vol. 8, pp. 386-391, 2008.

[46] F. Zhang, X. Li, X. Gao, L. Wu, F. Zhuge, Q. Wang, *et al.*, "Effect of Defect Content on the Unipolar Resistive Switching Characteristics of ZnO Thin Film Memory Devices," *Solid State Commun.,* vol. 152, pp. 1630-1634, 2012.

[47] K. McKenna and A. Shluger, "The Interaction of Oxygen Vacancies with Grain Boundaries in Monoclinic HfO_2," *Appl. Phys. Lett.,* vol. 95, p. 222111, 2009.

[48] M. Lanza, K. Zhang, M. Porti, M. Nafria, Z. Y. Shen, L. F. Liu, *et al.*, "Grain Boundaries as Preferential Sites for Resistive Switching in the HfO_2 Resistive Random Access Memory Structures," *Appl. Phys. Lett.,* vol. 100, p. 123508, 2012.

[49] J. Y. Son and Y. H. Shin, "Direct Observation of Conducting Filaments on Resistive Switching of NiO Thin Films," *Appl. Phys. Lett.,* vol. 92, p. 222106, 2008.

[50] K. Yin, M. Li, Y. Liu, C. He, F. Zhuge, B. Chen, *et al.*, "Resistance Switching in Polycrystalline $BiFeO_3$ Thin Films," *Appl. Phys. Lett.*, vol. 97, p. 042101, 2010.
[51] C. Kalkert, J.-O. Krisponeit, M. Esseling, O. I. Lebedev, V. Moshnyaga, B. Damaschke, *et al.*, "Resistive Switching at Manganite/Manganite Interfaces," *Appl. Phys. Lett.*, vol. 99, p. 132512, 2011.
[52] D. B. Strukov and R. S. Williams, "Exponential Ionic Drift: Fast Switching and Low Volatility of Thin-Film Memristors," *Appl. Phys. A-Mater.*, vol. 94, pp. 515-519, 2009.
[53] F. A. Kröger and H. J. Vink, "Relations Between the Concentrations of Imperfections in Solids," *J. Phys. Chem. Solids*, vol. 5, pp. 208-223, 1958.
[54] Z.-t. Xu, K.-j. Jin, L. Gu, Y.-l. Jin, C. Ge, C. Wang, *et al.*, "Evidence for a Crucial Role Played by Oxygen Vacancies in $LaMnO_3$ Resistive Switching Memories," *Small*, vol. 8, pp. 1279-1284, 2012.
[55] C. Y. Dong, D. S. Shang, L. Shi, J. R. Sun, B. G. Shen, F. Zhuge, *et al.*, "Roles of Silver Oxide in the Bipolar Resistance Switching Devices with Silver Electrode," *Appl. Phys. Lett.*, vol. 98, p. 072107, 2011.
[56] J. Zhao, F. Liu, J. Sun, H. Huang, Z. Hu, and X. Zhang, "Low Power Consumption Bipolar Resistive Switching Characteristics of ZnO-Based Memory Devices," *Chin. Opt. Lett.*, vol. 10, p. 013102, 2012.

Chapter 6

Conclusions and Future Works

6.1 Concluding Remarks

The author vision for this PhD involved in engineering and tuning of transition metal oxides with foci on copper oxides (Cu_xO) and zinc oxide (ZnO) into desired nano−architectures that provide remarkable enhancement for developing advanced sensing, energy conversion and memory devices.

In the course of conducting this research, the author thoroughly investigated literature on Cu_xO and ZnO. Through this, it was realized that a comprehensive review on the properties, method of synthesis and applications of nanostructured Cu_xO was lacking, while plenty of great reviews are available on different aspects of nanostructured ZnO. As a result, the author prepared a review article which presented a comprehensive analysis of the fundamental properties, synthesis approaches and applications of nanostructured Cu_xO. Based on the literature reviews the author identified the possibilities and advancements that could be achieved *via* engineering and tuning the Cu_xO and ZnO. As such, the author's research was organized and pursued in three major models in order to achieve the proposed research outcomes and to target the gaps in the current knowledge.

In the first model, the author demonstrated ethanol vapour sensing devices based on nanostructured CuO and Cu_2O, which are synthesized by RF sputtering technique. The author adjusted various parameters of the RF sputtered to alter the

stoichiometry of the Cu_xO with the aim of producing nanostructures with well-engineered morphological sizes as well as investigated their sensing performance.

In the second model, the author investigated the effect of RF sputtered ZnO seed layers on the electrodeposited ZnO films in ZnO-Cu_2O heterojunctions. He successfully demonstrated that the incorporation of seed layers allowed the growth conditions tuning and the adjustment of the adhesion properties of the ZnO layer surface as well as the engineering of the crystal quality, morphology and surface roughness of the interfaces between the electrodeposited ZnO and Cu_2O films. As a result, he was able to produce excellent heterojunctions with large surface-to-volume ratios and desirable stoichiometry and crystallinity. By adopting such methods, he successfully demonstrated the enhanced performance for such devices.

In the third and final model of this PhD research, the author explored the idea of incorporating seed layers for developing high performance of electrodeposited ZnO based memristive switches. He successfully demonstrated that the ZnO seed layers were able to tune the morphology of the electrodeposited ZnO films in order to increase the grain boundary density as well as construct highly ordered arrangements of grain boundaries. Additionally, the seed layer also assisted in optimizing the concentration of oxygen vacancies in the films.

As such, the major achievements in each model of this research work are summarized as follows:

6.1.1 Model 1

- As presented in Chapter 3, at the time that his research commenced, the number of reports on the sensing properties of *p*-type metal oxide

semiconductor was significantly lower than their *n*-type counterparts. The author's effort to tackle such an issue resulted in the development of nanostructured Cu_xO based ethanol vapour sensors. To the best of the author's knowledge, this was the first research to develop nanostructured CuO and Cu_2O films for ethanol vapour sensing formed using RF magnetron sputtering approach. The author adjusted various parameters of the RF sputtered to engineer the CuO and Cu_2O thin films.

- The author deposited nanostructured Cu_xO at relatively low temperature and power conditions. At 120 °C, single stoichiometry CuO and Cu_2O films were deposited using the sputtering power of 200 and 250 W, respectively. At such sputtering conditions CuO films exhibited smaller nanocrystallite base dimensions (~30 nm), in comparison to Cu_2O films (~85 nm), which significantly enhanced surface area-to-volume ratio of the sensitive layers.
- The author thoroughly characterization the obtained nanostructured Cu_xO films including conductive atomic force microscopy (c−AFM). Based on these results, he proposed a detailed reaction mechanism and investigated the effect of morphology, adhesion and conductivity properties of sensing layers.
- Both nanostructured CuO and Cu_2O gas sensors were able to detect ethanol vapour as low as several ppm and at relatively low operating temperatures of 180 and 260 ºC, respectively. The sensors showed high sensitivity and repeatability, as well as fast response and recovery towards ethanol vapour. The sensor response of CuO and Cu_2O were 2.2 and 1.2 for 12.5 ppm concentration of ethanol in ambient air, respectively. Additionally, the response (τ_{res}) and recovery times (τ_{rec}) of the CuO based sensor towards

12.5 ppm ethanol was 31 and 52 s, while the Cu_2O based sensor exhibited 36 and 76 s response and recovery times, respectively. These characteristics are promising for industrial applications, especially for gas and vapour related chemical sensing.

6.1.2 Model 2

- In this model, the author introduced sputtered ZnO seed layers followed by the sequential electrodeposition of ZnO and Cu_2O films. The author thoroughly characterized the seed layers and successfully demonstrated that these seed layers were able to control the growth and crystallinity as well as to augment the surface area of the electrodeposited ZnO films, thereby tuning the quality of the ZnO-Cu_2O heterointerface. Additionally, the seed layers also assisted in forming high quality ZnO films, with no pin-holes, in the high pH electrolyte solution that was used for the electrodeposition.
- In order to investigate the effects of the seed layers, the author deposited these layers using different sputtering powers including 60, 80, 100 and 110 W to obtain thicknesses in the range of 200 to 300 nm. The author also compared the photovoltaic performance of such devices in the presence and absence of the seed layers. It was shown that the performance improved significantly in the presence of the seed layers. The combination of seed layers and electrodeposited ZnO layers promoted the formation of stable ZnO nuclei, resulted in ZnO films with desired properties.
- Characterization techniques including AFM adhesion mapping were employed to assess the heterointerface quality of the electrodeposited ZnO-Cu_2O films. It was found that a highly adhesive surface hindered the

formation of crystalline Cu_2O which deteriorated the performance of ZnO-Cu_2O heterojunction based devices.

- The seed layer proved to be effective in enabling the ZnO−Cu_2O heterojunction solar cells to reach a relatively high photovoltaic conversion efficiency of 1.02 % for seed layers which were deposited at 80 W and the current density obtained was the largest ever reported (12.7 mA cm^{-2}) for such a heterojunction.

6.1.3 Model 3

- In this final model of the PhD research, the author demonstrated the influence of ZnO seed layers on the performance of ZnO-based memristive devices fabricated using an electrodeposition approach. To the best of author's knowledge, no report on ZnO thin films based memristive switching devices formed using an electrodeposition approach, had been published prior to the proposed research.
- The author observed that the film incorporating seed layers contained more densely packed grains with fairly small grain dimensions of ~ 130 nm. This resulted in a relatively high grain boundary density.
- The seed layer also promoted a highly ordered arrangement of grain boundaries. Hence, formation of many conducting channels for electron migration was possible, which enhanced the memristive switching ratios significantly.
- The author demonstrated that the seed layers assisted in optimizing the oxygen vacancy concentration of the subsequently electrodeposited ZnO films to form ZnO_{1-x} where x relates to the percentage of oxygen vacancies.

He concluded that ZnO_{1-x} of $0.05 < x < 0.08$ was the optimum condition for better switching characteristics.

- The ZnO memristive devices incorporating seed layers had higher switching ratios than devices without a seed layer. Devices with an incorporated seed layer showed stable and reliable memristive switching behaviours under continuous cycling conditions. This PhD work clearly showed the importance of the seed layer's effect in engineering the electrodeposited films for fabricating memristive devices and provided pathways for further improving their performance.

6.2 Journal Publications

The work conducted by the author of this dissertation during his PhD candidature, resulted in eighteen journal publications (four as the first author). The list of author's scientific manuscripts is as follows:

- **A. S. Zoolfakar**, R. A. Rani, A. J. Morfa, S. Balendhran, A. P. O'Mullane, S. Zhuiykov and K. Kalantar-zadeh, "Enhancing the current density of electrodeposited ZnO-Cu_2O solar cells by engineering their heterointerfaces", *Journal of Materials Chemistry*, 2012, 22, 21767-21775.
- **A. S. Zoolfakar**, R. Ab Kadir, R. A. Rani, S. Balendhran, X. Liu, E. Kats, S. K. Bhargava, M. Bhaskaran, S. Sriram, S. Zhuiykov, A. P. O'Mullane and K. Kalantar-zadeh, "Engineering electrodeposited ZnO films and their memristive switching performance", *Physical Chemistry Chemical Physics*, 2013, 15, 10376-10384.

- **A. S. Zoolfakar**, M. Z. Ahmad, R. A. Rani, J. Z. Ou, S. Balendhran, S. Zhuiykov, K. Latham, W. Wlodarski and K. Kalantar-zadeh, "Nanostructured copper oxides as ethanol vapour sensors", *Sensors and Actuators B: Chemical*, 2013, 185, 620-627.
- **A.S. Zoolfakar**, R. A. Rani, A. J. Morfa, A.P. O'Mullane and K. Kalantar-zadeh, "Nanostructured copper oxide semiconductors: a perspective on materials, synthesis methods and applications", *Journal of Materials Chemistry C*, 2014, Under review
- J. Z. Ou, S. Balendhran, M. R. Field, D. G. McCulloch, **A. S. Zoolfakar**, R. A. Rani, S. Zhuiykov, A. P. O'Mullane and K. Kalantar-zadeh, "The anodized crystalline WO_3 nanoporous network with enhanced electrochromic properties", *Nanoscale*, 2012, 4, 5980-5988.
- J. Z. Ou, R. A. Rani, S. Balendhran, **A. S. Zoolfakar**, M. R. Field, S. Zhuiykov, A. P. O'Mullane and K. Kalantar-zadeh, "Anodic formation of a thick three-dimensional nanoporous WO_3 film and its photocatalytic property", *Electrochemistry Communications*, 2013, 27, 128-132.
- R. A. Rani, **A. S. Zoolfakar**, J. Z. Ou, M. R. Field, M. Austin and K. Kalantar-zadeh, "Nanoporous Nb_2O_5 hydrogen gas sensor", *Sensors and Actuators B: Chemical*, 2013, 176, 149-156.
- R. A. Rani, **A. S. Zoolfakar**, J. Z. Ou, R. Ab. Kadir, H. Nili, K. Latham, S. Sriram, M. Bhaskaran, S. Zhuiykov, R. B. Kaner and K. Kalantar-zadeh, "Reduced impurity-driven defect states in anodized nanoporous Nb_2O_5: the possibility of improving performance of photoanodes", *Chemical Communications*, 2013, 49, 6349-6351.

- M. M. Rahman, R. A. Rani, A. Z. Sadek, **A. S. Zoolfakar**, M. R. Field, T. Ramireddy, K. Kalantar-zadeh and Y. Chen, "A vein-like nanoporous network of Nb_2O_5 with a higher lithium intercalation discharge cut-off voltage", *Journal of Materials Chemistry A*, 2013, 1, 11019-11025.
- P. Gutruf, C. M Shah, S. Walia, H. Nili, **A. S Zoolfakar**, C. Karnutsch, K. Kalantar-zadeh, S. Sriram and M. Bhaskaran, "Transparent functional oxide stretchable electronics: micro-tectonics enabled high strain electrodes", *NPG Asia Materials*, 2013, **5**, e62.
- M. Z. Ahmad, A. Wisitsoraat, **A. S. Zoolfakar**, R. A. Kadir and W. Wlodarski, "Investigation of RF sputtered tungsten trioxide nanorod thin film gas sensors prepared with a glancing angle deposition method toward reductive and oxidative analytes", *Sensors and Actuators B: Chemical*, 2013, **183**, 364-371.
- M. Z. Ahmad, J. Kang, **A. S. Zoolfakar**, A. Z. Sadek and W. Wlodarski, "Gas sensing studies of pulsed laser deposition: deposited WO_3 nanorod based thin films", *Journal of Nanoscience and Nanotechnology*, 2013, **13**, 8315-8319.
- P. Pimpang, **A. S. Zoolfakar**, D. Wongratanaphisan, A. Gardchareon, E. P. Nguyen, S. Zhuiykov, S. Choopun and K. Kalantar-zadeh, "Atomic force microscopy adhesion mapping: revealing assembly process in inorganic systems", *The Journal of Physical Chemistry C*, 2013, **117**, 19984-19990.
- S. Walia, S. Balendhran, Y. Wang, R. Ab Kadir, **A. S. Zoolfakar**, P. Atkin, J. Z. Ou, S. Sriram, K. Kalantar-zadeh and M. Bhaskaran, "Characterization of metal contacts for two-dimensional MoS_2 nanoflakes", *Applied Physics Letters*, 2013, **103**, 232105.

- R. Ab Kadir, R. A. Rani, **A. S. Zoolfakar**, J. Z. Ou, A.F. Chrimes, A. Z. Sadek and K. Kalantar-zadeh, "Electrospun granular hollow SnO_2 nanofibers hydrogen gas sensors operating at low temperatures", *The Journal of Physical Chemistry C*, 2014, **118**, 3129-3139.
- R. A. Rani, **A. S. Zoolfakar**, J. Subbiah, J. Z. Ou and K. Kalantar-zadeh, "Highly ordered anodized Nb_2O_5 nanochannels for dye-sensitized solar cells", *Electrochemistry Communications*, 2014, **40**, 20-23.
- R. Ab Kadir, R. A. Rani, **A. S. Zoolfakar**, J. Z. Ou, M. Shafiei, W. Wlodarski and K. Kalantar-zadeh, "Nb_2O_5 Schottky based ethanol vapour sensors: effect of metallic catalysts", *Sensors and Actuators B: Chemical*, 2014 (Minor correction).
- M. Nour, K. Berean, A.F. Chrimes, **A. S. Zoolfakar**, K. Latham, C. Mcsweeney, M. R. Field, S. Sriram, J. Z. Ou and K. Kalantar-zadeh, "Silver nanoparticle/PDMS nanocomposite membranes for H_2S gas separation", *Nanoscale*, 2014 (Under review).

6.3 Presentations at International Conferences

In addition to the journal publications, the author also had the opportunity to present his work in several prestigious international conferences. The list of the conferences is as follows:

- **A. S. Zoolfakar**, H. Zheng, M. Z. Ahmad, R. A. Rani, K. Latham and K. Kalantar-zadeh, "Synthesization and characterizations of Cu_2O films by RF Magnetron sputtering", Australia-India Joint Symposium on Smart Nanomaterials in Victoria 2011, November 2011, Melbourne, Australia

- R. A. Rani, J. Z. Ou, Y. Zhang, M. Bhaskaran, S. Sriram, **A. S. Zoolfakar**, K. Latham and K. Kalantar-zadeh, "Synthesize of highly-ordered porous niobium oxide films by chemical anodization technique", Australia-India Joint Symposium on Smart Nanomaterials in Victoria 2011, November 2011, Melbourne, Australia
- **A. S. Zoolfakar**, R. A. Rani, A. J. Morfa, S. Balendhran, A. P. O'Mullane, S. Zhuiykov and K. Kalantar-zadeh, "Effect of Sputtered ZnO Seed Layer on the Performance of Electrodeposited ZnO/Cu_2O Heterojunction Solar Cells", International Conference on Electronic Materials (IUMRS-ICEM 2012) September, 2012, Yokohama, Japan
- **A.S. Zoolfakar**, R. A. Rani, A. J. Morfa, A.P. O'Mullane and K. Kalantar-zadeh, "Nanostructured copper oxides as ethanol vapour sensors", 7^{th} International Conference on Advanced Materials Technologies (ICMAT 2013), June 2013, Singapore

6.4 Recommendations for Future Work

Significant progress has been achieved in the development of advanced sensing, energy conversion and memory devices *via* tuning and engineering transition metal oxides *via* this PhD research. As there are still numerous opportunities for expending the research in alignment with the outcomes presented in this thesis, the author presents the following as the future outlook of this dissertation:

- As mentioned in Chapter 3, the sensor response of Cu_2O was not as impressive as CuO. This is probably due to the large size of Cu_2O nanopillar crystallites with base dimensions in the order of 85 nm. Although, the author was able to sputter thin films of Cu_2O at relatively low powers, it was still

insufficient to produce smaller Cu_2O crystallites. Therefore, further investigation is needed to be carried out by tuning other sputtering parameters including substrate temperature and target-to-substrate distance in order to produce smaller grains as to increase to surface-to-area volume ratios.

- Surface modifications of the gas sensing layers by incorporating catalytic metal including palladium and gold can improve gas sensitivity of the nanostructured metal oxide based conductometric devices. The catalytic metals can enhance the target gas dissociation onto the gas sensitive layers. Such catalysts should be incorporated in future investigations.
- Application of different materials for forming interdigital transducers, such as platinum and palladium, can alter the vapour sensor performance and their contact behaviour, which shall be investigated for comparison.
- Development of two and three dimensional theoretical models to describe the behaviour/characteristics of seed layers towards *p–n* heterojunction solar cells and memristive switches to predict the effects of the materials' stoichiometry and grain boundaries.
- The open circuit voltage is still low for the developed ZnO-Cu_2O heterojunctions in this PhD thesis. It is possible to increase the open circuit voltage by doping the ZnO layer in such heterojunctions with the aims to reduce the internal resistance. Doping also reduces the effect of interface states and as a result better distribution of charges at the heterointerfaces.
- For the measurement of ZnO-Cu_2O based heterojunction solar cells and ZnO based memristive switching, it is highly desirable to conduct impedance spectroscopy to determine the internal resistance of the devices.

- It will be beneficial to investigate the effects of different types of metal electrodes such as aluminium and gold on the electrodeposited ZnO memristive switches.